THE FIRST REPORTED MUTATIONS OF THE PROTO-ONCOGENE PITUITARY TUMOR TRANSFORMING GENE 1 - BINDING FACTOR (PBF); CHARACTERISING THEIR FUNCTIONAL SIGNIFICANCE

by

WARAPORN IMRUETAICHAROENCHOKE

UNIVERSITY OF BIRMINGHAM

A thesis submitted to

The University of Birmingham

for the degree of

DOCTOR OF PHILOSOPHY

Institute of Metabolism and Systems Research

School of Clinical and Experimental Medicine

University of Birmingham

2016

Abstract

Pituitary tumor transforming gene 1 (PTTG1) - binding factor (PBF) is a ubiquitously expressed transmembrane glycoprotein that is significantly upregulated in a variety of human tumours, including those of the thyroid, breast and colon. In thyroid cancer, PBF is implicated in early tumour recurrence, distant metastasis and poor oncological outcome. Indeed, PBF induces cell transformation *in vitro* and tumourigenesis *in vivo*. PBF interacts with multiple protein-binding partners and modulates their activities and functions, including cortactin (CTTN), the tyrosine kinase Src, the sodium iodide symporter (NIS) and p53. According to the COSMIC (Catalogue of Somatic Mutations in Cancer) and TCGA (The Cancer Genome Atlas) databases, 27 PBF mutations have now been reported in human cancer. The studies in this thesis aimed to establish the basic biochemical characteristics of the first 10 reported missense PBF mutations, including protein glycosylation, dimerisation and stability. Following initial functional studies, the impact of two specific mutations discovered *in vivo*, C51R and R140W, upon WT PBF function in modulating cellular proliferation, cell invasion, cell migration, radioiodine uptake and transforming ability were investigated in more depth. The data in this thesis demonstrate that although the reported mutations identified *in vivo* preserve some critical functions of PBF such as cellular proliferation and radioiodine uptake, it is unlikely that PBF mutations represent distinct driver events, and that upregulation of PBF expression in human cancer may be more important in terms of driving tumourigenesis than sequence changes.

Dedication

I would like to dedicate the thesis for my parents, Ussavachai and Sauvanee,

and my sister, Arinporn, for their endless support.

Acknowledgements

I would like to acknowledge my supervisors, Professor Chris McCabe, Professor Jayne Franklyn and Dr Kristien Boelaert for their admirable supervision of this thesis, and for their invaluable encouragement. I also acknowledge Mr John Watkinson for providing me the great contingency to study here, and for his meaningful advice. I also thank Dr Vicki Smith and Dr Read Martin for their time to teach and support me. I am thankful to every member in my group for helping me all time as well as everyone on the 2nd floor IBR for being my friends.

This research was funded by the Faculty of Medicine Siriraj Hospital, Mahidol University in Thailand.

Table of Contents

List of Figures

List of Tables

List of Abbreviations

°C	Degrees Centigrade
^{125}I	Radioactive Iodine 125
^{131}I	Radioactive Iodine 131
3Rs	Replacement, Reduction and Refinement
Ab	Antibody
AJCC	American Joint Committee on Cancer
AKT	Protein Kinase B
Amp	Ampicillin
AQP7	Aquaporin-7
Arp2/3	Actin – Related Protein 2 and 3
BCA	Bicinchoninic Acid
bp	Base Pair
BRAF	V-Raf Murine Sarcoma Viral Oncogene Homolog B or B-type Raf Kinase
BrdU	Bromodeoxyuridine
BSA	Bovine Serum Albumin
Cdc42	Cell Division Cycle 42
cDNA	Complementary Deoxyribonucleic Acid
CHEK1	Checkpoint Kinase 1
CO_2	Carbon Dioxide

COSMIC	Catalogue of Somatic Mutation in Cancer
Co-IP	Co-immunoprecipitation
CTTN	Cortactin
cpm	Counts Per Minute
ct	Cycle Threshold Value
DES	Diethylstilbestrol
DMEM	Dulbecco's Modified Eagle's medium
DNA	Deoxyribonucleic Acid
DPX	Distyrene Plasticizer Xylene
DTC	Differentiated Thyroid Carcinoma
ECL	Electrochemiluminescence
ECM	Extracellular Matrix
EDTA	Ethylenediaminetetraacetic Acid
EGTA	Ethyleneglycol Bis(2-Aminoethyl Ether)-N,N,N',N' Tetraacetic Acid
EMG1	Essential for Mitotic Growth 1
ER	Endoplasmic Reticulum
ERE	Estrogen Receptor Elements
ERK	Extracellular Signal-Regulated Kinase
EST	Estradiol
FAK	Focal Adhesion Kinases
FAM	6-Carboxyfluorescein
FANCG	Fanconi Anemia of Complementation Group G

FBS	Foetal Bovine Serum
FCS	Foetal Calf Serum
FFPE	Formalin-fixed, Paraffin-embedded
FOXO3a	Forkhead Box O3
g	Gram
GBM	Glioblastoma
GFR	Growth Factor Receptors
GST	Glutathione-S-Transferase
GTPase	Guanosine Triphosphate Phosphohydrolase
HA	Haemagglutinin
HBSS	Hank's Balanced Salt Solution
HDM2	Human Homolog of MDM2
HER-2	Human Epidermal Growth Factor Receptor-2
hNUE	Human Sodium Iodide Symporter Upstream Enhancer
HPRT1	Hypoxanthine Gaunine Phosphoribosyltransferase 1
hr	Hour
HRAS	V-Ha-Ras Harvey Rat Sarcoma Viral Oncogene Homolog
HRP	Horseradish Peroxidise
I^-	Iodine
IF	Immunofluorescence
IGF-1	Insulin-Like Growth Factor 1

IgG	Immunoglobulin
I-TASSER	Iterative Threading Assembly Refinement
KRAS	V-Ki-ras2 Kirsten rat sarcoma viral oncogene homolog
kDa	Kilodalton
LB	Laemmli buffer
LB	Lysogeny Broth
LDHA	Lactate Dehydrogenase A
M	Molar
mA	Milliamp
MAPK	Mitogen-Activated Protein Kinases
µCi	Microcurie
MCT8	Monocarboxylate Transporter 8
MDM2	Mouse Double Minute 2 Homolog
MEK	Mitogen-Activated Protein/Extracellular Signal-Regulated Kinase Kinase
mg	Milligram
µg	Microgram
MGMT	O(6)-Methylguanine-DNA Methyltransferase gene
min	Minute
miR	MicroRNA
ml	Millilitre
µl	Microlitre

mM	Millimolar
mm	Millimetre
MMPs	Matrix Metalloproteinases
μM	Micromolar
μm	Micrometre
MMP14	Matrix Metallopeptidase 14
MNG	Multinodular Goitres
mRNA	Messenger Ribonucleic Acid
miRNA	Micro Ribonucleic Acid
MTS	3-(4,5-Dimethylthiazol-2-yl)-5-(3-Carboxymethoxyphenyl)-2-(4-Sulfophenyl)-2H-Tetrazolium
MUTYH	MutY Homolog (E. coli)
NADPH	Reduced Form of Nicotinamide Adenine Dinucleotide Phosphate
NCI	National Cancer Institute
NCK1	Non-Catalytic Region of Tyrosine Kinase Adaptor Protein
NCS	Newborn Calf Serum
Neo	Neomycin
ng	Nanogram
NGF	Nerve Growth Factor
NHGRI	National Human Genome Research Institute

NIS	Sodium Iodide Symporter
nM	Nanomolar
NLS	Nuclear Localisation Signal
NRAS	Neuroblastoma RAS Viral Oncogene Homolog
NTRK1	Neurotrophic Tyrosine Receptor Kinase Type 1
OCT4	Octamer-Binding Transcription Factor 4
Ori	Origin of Replication
pAKT	Phosphorylated Protein Kinase B
PAX	Paired Box Family
PBF	The Pituitary Tumour Transforming Gene 1 (PTTG1) - Binding Factor
PBS	Phosphate Buffered Saline
PCR	Polymerase Chain Reaction
PES	Phenazine Ethosulfate
PFA	Paraformaldehyde
PI3K	Phosphatidylinositol-3-Kinase
PIK3CA	Phosphatidylinositol-4,5-Bisphosphate 3-Kinase Catalytic Subunit Alpha
PI3K	Phosphatidylinositol-3-Kinase
PLA2G3	Phospholipase A2 Group III
PM	Plasma Membrane
pmol	Picomole
PPARϒ	Peroxisome Proliferator Activated Receptor Gamma

PPIA	Peptidylprolyl Isomerase A (Cyclophilin A)
PP1	4-Amino-5-(4-Methylphenyl)-7-(*t*-butyl)Pyrazolol[3,4-d]Pyrimidine
PSI	Plexin Semaphorin Integrin
PTTG	The Pituitary Tumor Transforming Gene
PVDF	Polyvinylidene Fluoride
qPCR	Real-Time Polymerase Chain Reaction
Rac	Ras-related C3 Botulinum Toxin Substrate 1
RAD51	A Member of the RecA-like Gene
RAF	Rapidly Accelerated Fibrosarcoma
RAI	Radioactive Iodine Ablation
RAS	Rat Sarcoma
RB1	Retinoblastoma
RET	Rearranged During Transfection
Rho	Rhodopsin Gene
RIN	RNA Integrity Number
RIPA	Radioimmunoprecipitation Assay
RNA	Ribonucleic Acid
rpm	Revolutions Per Minute
RT-PCR	Reverse Transcription Polymerase Chain Reaction
RYR2	Ryanodine Receptor 2
SCC	Squamous Cell Carcinoma
SDS	Sodium Dodecyl Sulfate

SEM	Standard Error of Mean
SEER	The Surveillance, Epidemiology, and End Results Program
SIFT	Sorting Intolerant From Tolerant
siRNA	Small Interfering Ribonucleic Acid
SNP	Single Nucleotide Polymorphism
SOX2	Sex Determining Region Y – Box 2
SPR	Surface Plasmon Resonance
SRC	V-src Avian Sarcoma (Schmidt-Ruppin A-2) Viral Oncogene Homolog
SSEA4	Stage Specific Embryonic Antigen 4
T_3	Triiodothyronine
T_4	Thyroxine
TAMRA	Tetramethylrhodamine
TBS-T	Tris-buffered Saline with Tween
TCGA	The Cancer Genome Atlas
TFG	Tyrosine Receptor Kinase Fused Gene
Tg	Thyroglobulin
TGF	Transforming Growth Factor
TGFβ	Transforming Growth Factor Beta
T_M	Melting Temperature
TPR	Translocated Promoter Region
TRK	Tropomyosin Receptor Kinase

TSHR	Thyroid Stimulating Hormone Receptor
UCSC	University of California Santa Cruz
USF1	Upstream Transcription Factor 1
VO	Vector Only
WT	Wild Type
XRCC3	X-ray Repair Complementing Defective Repair in Chinese Hamster Cells

CHAPTER 1 - GENERAL INTRODUCTION

1.1 Pituitary Tumor Transforming Gene 1 - Binding Factor (PBF)

1.1.1 Overall

Pituitary tumor transforming gene 1 (PTTG1) - binding factor (PBF), also known as PTTG1IP, was first identified through investigations into PTTG (pituitary tumor transforming gene) functions via yeast two-hybrid assays, where it was found to be a binding partner of PTTG (Chien, Pei 2000). PTTG functions as the human securin, suppressing separase activity and prohibiting the premature separation of sister chromatids during mitotic anaphase (Zou et al. 1999). Although initial DNA sequencing errors in the publication of Chien and Pei (2000) suggested it to be a new and unreported gene, PBF was later found to be a formerly cloned gene, c21orf3 (Yaspo et al. 1998).

PBF remains a poorly characterised proto-oncogene located on the long arm of chromosome 21 at 21q22.3 (Yaspo et al. 1998). It shares no significant homology with other human proteins, suggesting potentially unique function, but it is highly conserved across a range of animal species (Figure 1.1) (Smith, Franklyn & McCabe 2011).

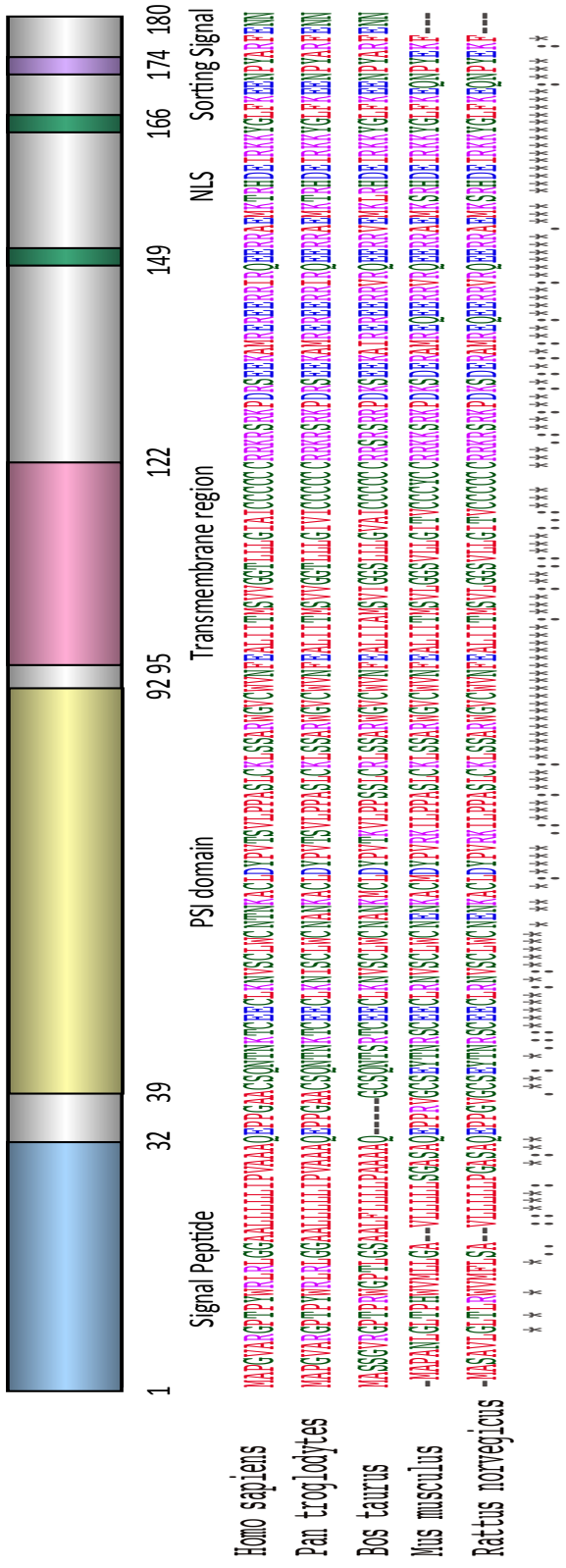

Figure 1.1: PBF is highly conserved across different species. *Representative amino acid sequences of PBF among various animal species compared to human PBF. PBF schematic illustrates an N-terminal signal peptide (blue colour), a plexin semaphorin*

integrin (PSI) domain (yellow), a transmembrane region (pink), a bipartite nuclear localization signal (NLS, green) and a sorting signal (purple). The colours of amino acid residues were classified according to their physicochemical properties; Red -hydrophobic group, Blue - acidic group, Magenta - basic group, Green – hydroxyl, sulfhydryl, amine and glycine (G) amino acids, Grey - unusual amino acids. An asterisk (*) denotes an amino acid which is fully conserved. A colon (:) indicates a conservation site with amino acids havingf strongly similar properties, while a period (.) indicates conservation between amino acids with weakly similar properties. Adapted from https://ebi.ac.uk/Tools/msa/clustalo/.

PBF is ubiquitously expressed as determined through Northern blotting in multiple human tissues, including thyroid, adrenal gland, stomach, lymph node, trachea and bone marrow (Chien, Pei 2000, Yaspo et al. 1998). PBF is predicted to be a type 1a transmembrane glycoprotein (Yaspo et al. 1998) consisting of 6 exons which give rise to 180 amino acids, and spanning 24.23 kb with a protein molecular mass of around 22 kDa (Chien, Pei 2000). PBF contains several functional domains, with a putative cleaved N-terminal signal peptide (1-32), a plexin semaphorin integrin (PSI) domain (39-92) comprised of 8 cysteine residues and implicated in cellular signaling and protein-protein interactions (Kozlov et al. 2004, Bork et al. 1999), a transmembrane region (95-122) and a C-terminal 30 amino acids containing a bipartite nuclear localisation signal (NLS) situated between amino acid residues 149 and 166, and a putative motif for rapid protein internalisation through coated-pit-mediated endocytosis (Yaspo et al. 1998) (Figure 1.2). PBF also has two putative N-glycosylation sites at asparagine residue 45 and 54 (Figure 1.2) (Yaspo et al. 1998).

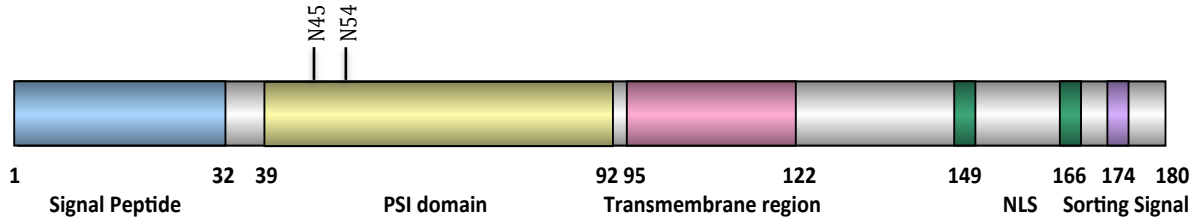

Figure 1.2: Schematic diagram of the PBF. *Representative PBF structure illustrating an N-terminal signal peptide (residue 1-32, blue colour), a PSI domain (residue 39-92, yellow), a transmembrane region (residue 95-122, pink), a bipartite NLS (residue 149-166, green), a putative sorting signal (residue 174, purple) and two putative sites of N-linked glycosylation at asparagine residues 45 and 54 (N45 and N54).*

In terms of subcellular localisation, PBF is located in both the nucleus and the cytoplasm (Chien, Pei 2000); deletion of the NLS of PBF interrupts nuclear translocation, resulting in shifting of PBF to the perinuclear and cytoplasmic compartments (Chien, Pei 2000). In immunofluorescence microscopy, PBF is predominantly observed in specific vesicles within cells, and co-localises with the marker for late endosomes, tetraspanin CD63 (Smith et al. 2009). In keeping with the presence of a putative endocytosis motif, a mutant with a truncated C-terminus was mainly apparent at the plasma membrane (Smith et al. 2009).

PBF also has amino acid sequences that are predicted to be sites of post-translational modification such as glycosylation and phosphorylation. Indeed, asparagine (N) amino acids situated at residue 45 (N45) and 54 (N54) are likely to be potential sites of N-linked glycosylation. Furthermore, putative phosphorylation residues, including serine, threonine and tyrosine, are predicted via the NetPhos 2.0 Server (http;//www.cbs.dtu.dk/services/NetPhos/). Putative phosphoserine sites were determined at S85, S126 and S132, while T10 and Y174 were predicted for phosphothreonine and phosphotyrosine, respectively (Figure 1.3).

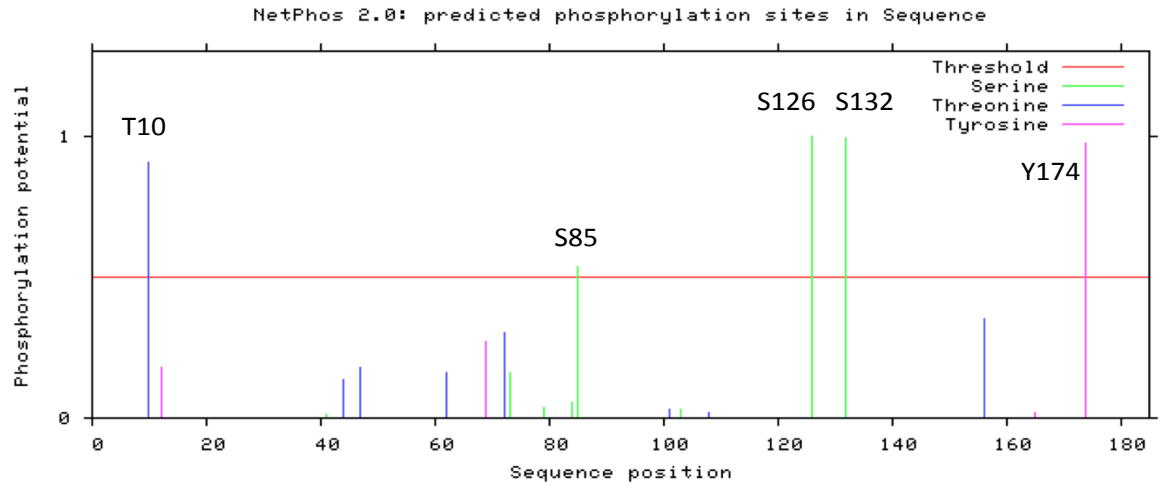

Figure 1.3: Putative phosphorylation sites of PBF. *Potential sites of PBF phosphorylation. Red line indicates threshold = 0.500. Scores above the threshold set at 0.5 indicate predicted phosphorylation sites for threonine (blue), serine (green) and tyrosine (pink). Adapted from the NetPhos 2.0 Server.*

PhosphoSitePlus® is another available website (http://www.phosphosite.org/) supplying biological data related to post-translational modifications, especially phosphorylation (Hornbeck et al. 2015). In human PBF, tyrosine residue 174 (Y174) is the most common phospho-protein site of PBF studied in approximately 2,000 publications (Table 1.1) (Hornbeck et al. 2015), and is the same residue as predicted to be a putative phosphorylated site through the NetPhos 2.0 Server (Figure 1.3), suggesting that Y174 is a critical residue for PBF phosphorylation.

HTP	Amino Acid Residue	Human
1984	Y174	LFKEENPyARFENN_
144	Y165	HDEIRKKyGLFKEEN
1	T156	ERRAEMKtRHDEIRK

Table 1.1: Phospho-protein sites of PBF determined via PhosphoSitePlus®. *Putative phosphorylated sites of human PBF. HTP = number of hits that each modification site was*

identified through mass spectrometry. Human = amino acid sequences in human PBF. Y = Tyrosine residue; T = Threonine residue. The red lower case characteristics denote phospho-protein sites of PBF. Adapted from PhosphoSitePlus®.

PBF is both transforming *in vitro* and tumourigenic *in vivo* (Stratford et al. 2005). It is significantly upregulated in a variety of human cancer types such as pituitary, thyroid, colon and breast (McCabe et al. 2003, Stratford et al. 2005, Watkins et al. 2010, Read et al. 2016), and independently associated with poorer oncological outcome. For instance, patients diagnosed with papillary thyroid cancer who have high PBF expression are more likely to develop early loco-regional recurrence and distant metastasis, and have decreased disease specific survival compared to those who carry low thyroidal PBF expression levels (Hsueh et al. 2013, Stratford et al. 2005). Moreover, high PBF expression in colorectal samples correlates with the presence of extramural vascular invasion (EMVI) (Read et al. 2016). Patients who have high PBF promoter activity also have increased breast cancer risk (Xiang et al. 2012). PBF interacts with and modifies the subcellular localisation of various important proteins such as NIS (sodium iodide symporter), regulating radioiodine uptake in thyroid cancer (Smith et al. 2013, Smith, Franklyn & McCabe 2011, Smith et al. 2010) and MCT8, controlling thyroid hormone secretion (Smith et al. 2012, Smith et al. 2010).

As PBF action has mainly been characterised in 3 human neoplasias - thyroid, colon and breast - PBF expression and function is now described in these settings:

1.1.2 PBF in Thyroid Cancer

1.1.2.1 Overview of Thyroid Cancer

Thyroid cancer comprises around 1% of all new cancer cases, approximately 3,200 patients, diagnosed each year in the United Kingdom, making it the 18th most common cancer in females and 20th most common cancer in males in 2011 (http://www.cancerresearchuk.org/cancerinfo/cancerstats/types/thyroid/incidence/uk-thyroid-cancer-incidence-statistic) (most recent UK data available), and approximately 3.8% in the United States, where it is estimated to be the 8th most common cancer in the United States in 2016 (http://seer.cancer.gov/statfacts/html/thyro.html). The incidence of new thyroid cancer cases in females is higher than that of males, with a ratio of 2.5:1, and in the UK the crude incidence rate was 6 for every 100,000 women in 2011 (Figure 1.4). The proportion of new cases in the UK is significantly lower than that of the United States in 2011 (most recent UK data available in 2011), which demonstrated an incidence of 4 and 13.5 per 100,000, respectively. In addition, based on 2010-2012 data from the SEER (Surveillance, Epidemiology, and End Results) database, 1.1% of the American population may be diagnosed with thyroid cancer at some stage during their lifespan. Although there has been a notable increase in thyroid cancer incidence due to a significant increase in use of ultrasound scanning worldwide, the death rate remains stable, which is approximately 0.5 per 100,000 men and women per year (SEER 18 2009-2013, http://seer.cancer.gov/statfacts/html/thyro.html), and the 5-year survival rate is around 98.1% (SEER 18 2006-2012, http://seer.cancer.gov/statfacts/html/thyro.html), depending on the staging and subtypes of the cancer.

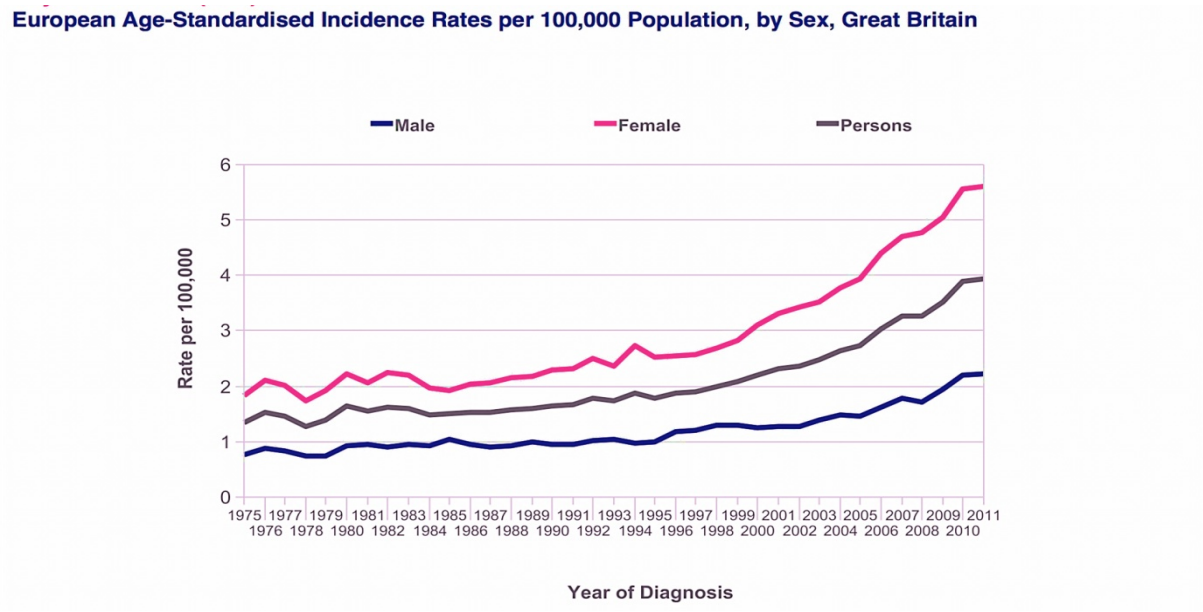

Figure 1.4: Incidence of thyroid cancer. *European age-standardised incidence rates, 1975-2011. Taken from http://www.cancerresearchuk.org/.*

Thyroid cancers are classified into four categories depending on histopathology, which consists of papillary (including follicular variant of papillary carcinoma), follicular (including Hürthle cell carcinoma), medullary and anaplastic thyroid cancer. Papillary thyroid cancer is the most common, and accounts for around 80% of all thyroid cancer cases, while follicular cancer are found in 10% of all cases. Anaplastic cancer is the least common tumour type (1% of thyroid cancers), but carries the poorest prognosis, with a 5-year survival rate of around 7%, (http://www.cancer.org/cancer/thyroidcancer/detailedguide/thyroid-cancer-survival-rates) compared with 98.1% overall in patients having any type of thyroid cancer (http:// seer.cancer.gov/statfacts/html/thyro.html). However, the precise prognosis of papillary thyroid cancer depends on post-operative tumour staging (Table 1.2).

Staging	TNM staging	5-year relative survival rate
I	Tumour ≤ 2 cm, no nodal nor distant metastases (T1 N0 M0)	Near 100%
II	Tumour > 2 cm but ≤ 4 cm, no nodal nor distant metastases (T2 N0 M0)	Near 100%
III	Tumour > 4 cm, no nodal nor distant metastases (T3 N0 M0) or Tumour of any size but limited to thyroid with level 6 lymph node metastases but no distant metastases (T1-3 N1a M0)	93%
IV	Tumour of any size extending beyond the thyroid capsules to invade subcutaneous tissue, larynx, trachea, oesophagus or recurrent laryngeal nerve with/without regional lymph node metastases but no distant metastases (T4a N0-1a M0) or Tumour of any size extending beyond the thyroid capsules to invade subcutaneous tissue, larynx, trachea, oesophagus or recurrent laryngeal nerve with lateral cervical lymph node metastases but no distant metastases (T1-4 N1b M0) or Tumour of any size invading prevertebral fascia or encasing carotid artery or mediastinal vessel with/without lymph node metastases but no distant metastases (T4b AnyN M0) or Tumour of any size with/without lymph node metastases but having distant metastases (AnyT AnyN M1)	51%

Table 1.2: 5-year relative survival rate of patients diagnosed with papillary thyroid cancer, classified by 7th edition of American Joint Committee on Cancer (AJCC) TNM staging for thyroid cancer. *Adapted from http://www.cancer.org/cancer/.*

Treatment of thyroid cancer consists of two major modalities: surgery and radioiodine ablation (RAI). Nevertheless, the minority of cases which have refractory disease with poor radioiodine uptake may gain some benefit from obtaining external beam radiation or targeted therapy, but still carry a significantly worse prognosis. Even though RAI is one of the main treatments and 68-80% of thyroid cancers have some sodium iodide symporter (NIS) activity and are capable of accumulating iodine (Castro et al. 2001), thyroid cancer cells can uptake only 20% iodine compared with normal cells and the uptake is significantly lower in poorly differentiated papillary thyroid cancers and anaplastic thyroid cancers. Additionally, although thyroid cancer has a relatively good prognosis, up to 30% of patients still develop loco-regional recurrence (Jonklaas et al. 2006, Desforges, Mazzaferri 1993). These findings may be explained by multiple biological mechanisms. For instance, expression levels of some microRNAs (miR) such as human miR-27b and miR-96 were significantly increased in human papillary thyroid tumours compared to normal thyroid (Lakshmanan et al. 2015). The same was also observed in breast cancer compared to normal breast tissue (Wang et al. 2009, Lin et al. 2010). Indeed, exogenous expression of miR-27b also promoted cell proliferation, cell invasion and cell migration in breast cancer cells *in vitro* (Wang et al. 2009). Moreover, overexpressed miR-96 in breast cancer cell lines downregulated tumour suppressor FOXO3a (forkhead box O3) expression by directly interacting with 3'-untranslated region of FOXO3a mRNA, resulting in significantly increased cellular proliferation and anchorage independent cell growth (Lin et al. 2010). Therefore, both miR-27b and miR-96 may play a vital role in tumourigenesis of breast cancer (Wang et

al. 2009, Lin et al. 2010). In addition, Lakshmanan et al. reported that miR-339-5p was able to directly interact with the 3'UTR of the human NIS (hNIS) mRNA, and overexpression of this miR noticeably reduced NIS mRNA levels and radioiodine uptake in both HEK293 human embryonic kidney cells transfected with NIS and MCF7 breast cancer cells treated with transretinoic acid and hydrocortisone (Lakshmanan et al. 2015). TGFβ_1 (transforming growth factor beta 1) also decreased TSH-stimulated NIS mRNA and protein expression, resulting in abolished radioiodine uptake ability in FRTL-5 thyroid cells (Kawaguchi et al. 1997). Moreover, PBF expression, which is upregulated in thyroid cancer compared to normal tissue (Stratford et al. 2005), has a negative correlation with NIS mRNA expression levels (Read et al. 2011), leading to poor radioiodine uptake in thyroid cancer. Overexpression of PBF reduces the human NIS upstream enhancer element (hNUE) activity in the NIS promoter (Boelaert et al. 2007), and also alters subcellular localisation of NIS from the plasma membrane to late endosomes (Smith et al. 2009), resulting in decreased functional NIS activity that is associated with tumour recurrence and distant metastasis in thyroid cancer (Boelaert et al. 2007). Overall then, a reduction in the capability to uptake radioiodine into thyroid cells leads to a decreased ability to destroy residual microscopic thyroid disease, potentially causing thyroid cancer recurrence, a process PBF is intimately involved in.

1.1.2.2 Clinical Importance of PBF Expression in Thyroid Cancer

With respect to PBF in thyroid cancer, there is wide-ranging evidence supporting the importance of PBF in tumour development, progression and prognosis of this tumour type. Hsueh et al. recently reported that 61.4% of DTC (differentiated thyroid carcinoma) patients had high PBF expression, which was associated with significantly

increased loco-regional recurrence and distant metastasis at the time of diagnosis, and independently reduced disease specific survival (Hsueh et al. 2013). These findings also supported the initial finding of Stratford et al. that PBF was upregulated in human well-differentiated thyroid cancer (DTC) compared to normal thyroid tissue (Figure 1.5A) (Stratford et al. 2005), and that higher PBF mRNA expression was an independent prognostic marker for early recurrence in DTC patients (Figure 1.5B) (Stratford et al. 2005).

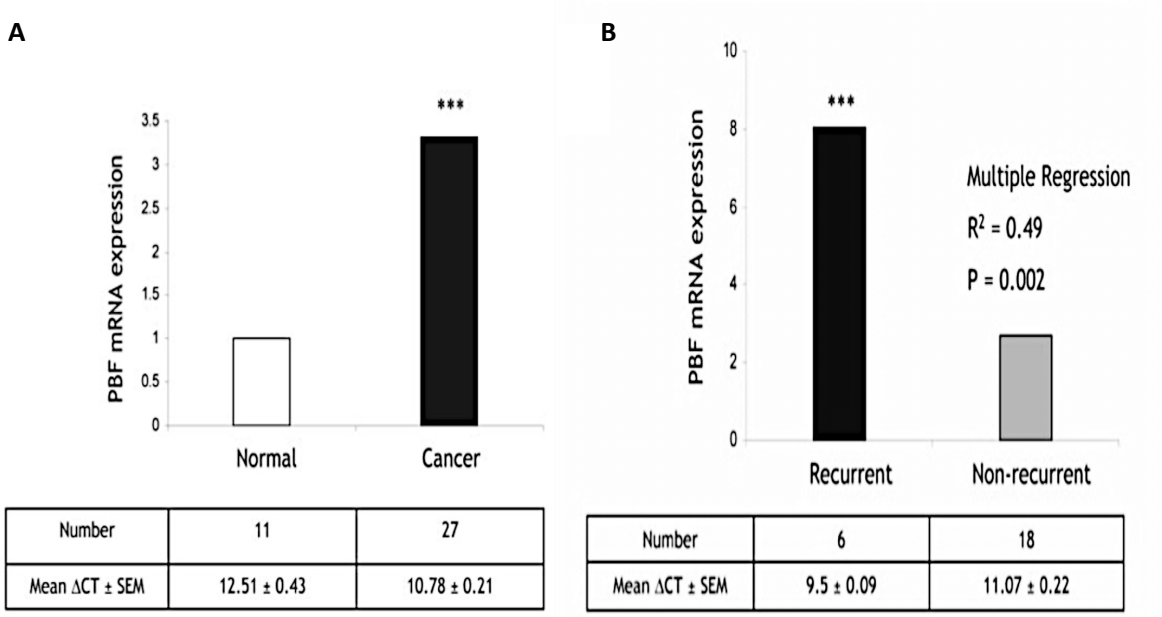

Number	11	27
Mean ΔCT ± SEM	12.51 ± 0.43	10.78 ± 0.21

Number	6	18
Mean ΔCT ± SEM	9.5 ± 0.09	11.07 ± 0.22

Figure 1.5: PBF expression is significantly higher in DTC, especially in recurrent samples. *A, PBF mRNA expression in thyroid cancer compared to normal samples. B, PBF mRNA expression comparing between recurrent and non-recurrent thyroid tumours. ΔCT = cycle threshold (Ct) of PBF subtracted from the Ct of the internal reference gene. SEM = standard error of mean. ***P<0.001. Taken from Stratford et al. 2005.*

Stable overexpression of PBF in murine NIH 3T3 fibroblast cells significantly induced colony formation in soft agar assays compared to VO (vector only) controls, demonstrating the ability of PBF to transform cells *in vitro* (Stratford et al. 2005). When injected into the subcutaneous tissue of nude mice, these NIH 3T3 cells stably

overexpressing PBF induced aggressive high-grade carcinomas (Figure 1.6), while control cells stably expressing empty vector did not (Figure 1.6), implying tumourigenic capability of PBF *in vivo* (Stratford et al. 2005).

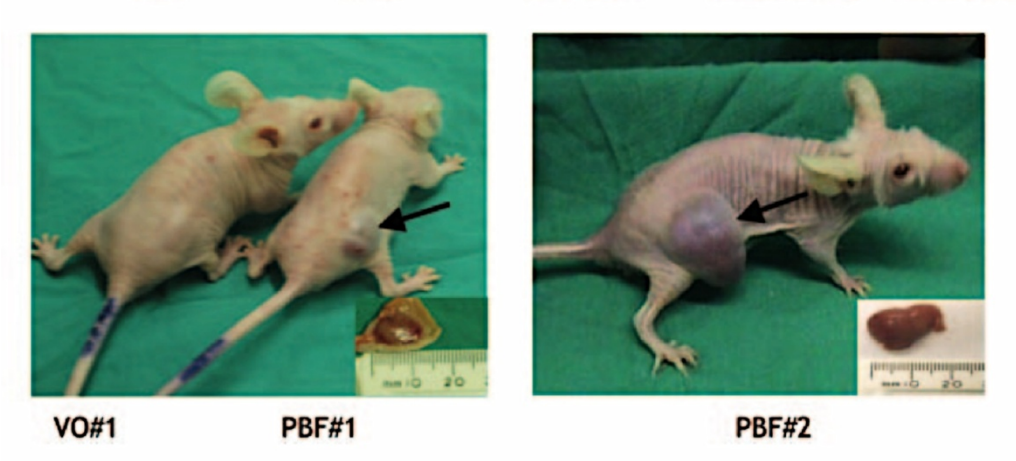

Figure 1.6: PBF is tumourigenic in vitro. *Tumour development (black arrows) in nude mice injected with NIH 3T3 cells stably overexpressing PBF (PBF#1 and PBF#2) compared to VO control (VO#1). Taken from Stratford et al. 2005.*

To investigate this potential effect in a more physiological setting, Read et al. generated a transgenic mouse model carrying thyroid specific PBF overexpression using the Tg (thyroglobulin) promoter (PBF-Tg) (Read et al. 2011). PBF-Tg mice had significantly increased sizes and weights of thyroid glands compared to litter-matched WT mice (Figure 1.7A and 1.7B) (Read et al. 2011). Interestingly, the histology of thyroid glands in PBF-Tg mice exhibited hyperplasia and macrofollicular lesions (Figure 1.7C and 1.7D), and had significantly increased pAKT (phosphorylated protein kinase B), TSHR (thyroid stimulating hormone receptor) and cyclin D1 expression levels compared to WT controls, whilst demonstrating relatively unchanged thyroid hormone levels compared to WT mice (Read et al. 2011).

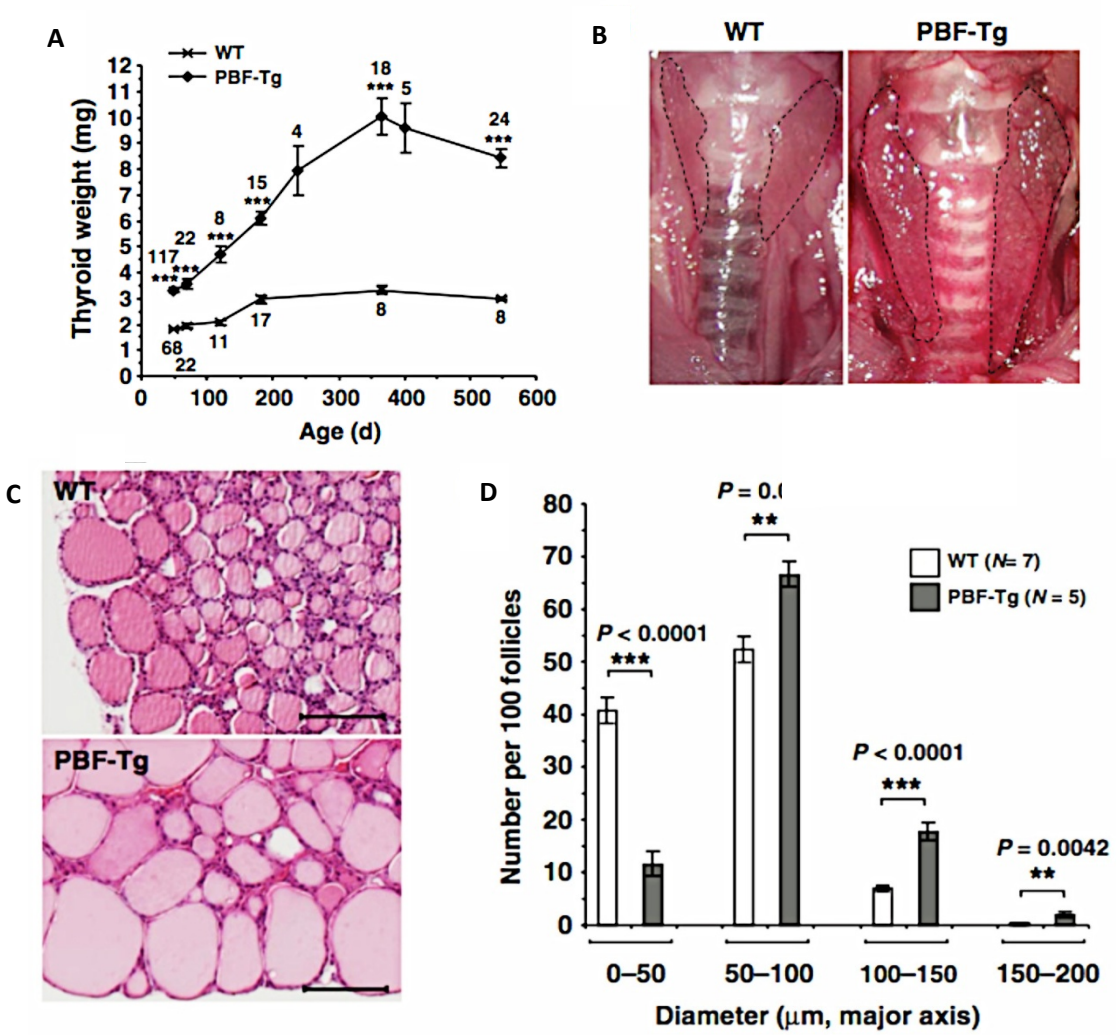

Figure 1.7: Overexpressed PBF induces thyroid gland enlargement in PBF-Tg mice. *A, thyroid weight of PBF-Tg mice compared with age-matched WT mice. Numbers of mice analysed are illustrated. B, representative images of thyroid glands of PBF-Tg and WT litter mates at 52-weeks old. Dashed lines illustrate the outline of thyroid glands. C, representative H&E microscopic figures of thyroid glands comparing WT and PBF-Tg mice. Scale bars, 100 mm. D, Quantification of follicular diameter in thyroid glands of PBF-Tg (N=5) and WT litter mates (N=7) at age 26 weeks. Scale bars = 100 μm. Data showed as mean ± SEM. SEM = standard error of mean. **P<0.01; ***P<0.001. Taken from Read et al. 2011.*

However, even though thyroid glands were enlarged, no obvious cancer induction was found in this study (Read et al. 2011). Furthermore, in human

multinodular goitres (MNG), PBF mRNA and protein expression were significantly induced compared to normal samples, by approximately 2.2-2.3 fold (Read et al. 2011), and TSHR protein expression was also increased (Read et al. 2011). Thus although overexpression of PBF causes thyroid cell proliferation and thyroid gland enlargement through an increase of TSHR expression and stimulation of the AKT pathway in PBF-Tg mice and human MNG, this situation does not affect circulating thyroid hormone levels (Read et al. 2011).

1.1.2.3 PBF and Sodium Iodide Symporter (NIS)

As PBF is up-regulated in human thyroid cancer and PBF overexpression correlates with poorer oncological consequences (Hsueh et al. 2013, Stratford et al. 2005), several studies have investigated the relationship between PBF and the efficacy of radioiodine (RAI) treatment in thyroid cancer. In human primary thyrocytes, overexpressed PBF significantly decreased NIS mRNA expression, leading to a significant reduction in radioiodine uptake by 68% compared to VO transfected cell *in vitro* (Boelaert et al. 2007). NIS mRNA expression was also decreased in thyroid cancer, especially in cancers exhibiting recurrence, nodal positive status or distant metastatic disease (Boelaert et al. 2007). Boelaert et al. also defined a mechanism of how PBF reduced NIS expression and they found that overexpression of PBF significantly reduced specific activity of the NIS promoter, including the human NIS upstream enhancer (hNUE) through PAX8/USF1 (pair-box8/upstream stimulatory factor1) sites (Boelaert et al. 2007). Although there is evidence that PBF represses the NIS enhancer (hNUE) via the PAX8/USF1 binding site, the actual mechanism is unknown.

In addition, co-immunoprecipitation and GST (glutathione-S-transferase) pull-down assays confirmed a specific interaction between PBF and NIS (Smith et al. 2009). Immunofluorescence (IF) microscopy revealed that overexpressed PBF modified the subcellular localisation of NIS, from the plasma membrane (PM) where NIS functions to late endosomes (Figure 1.8A and 1.8B) (Smith et al. 2009). Thus high PBF expression was associated with low NIS function due to internalisation of NIS by PBF (Figure 1.8) as well as secondary to transcriptional repression.

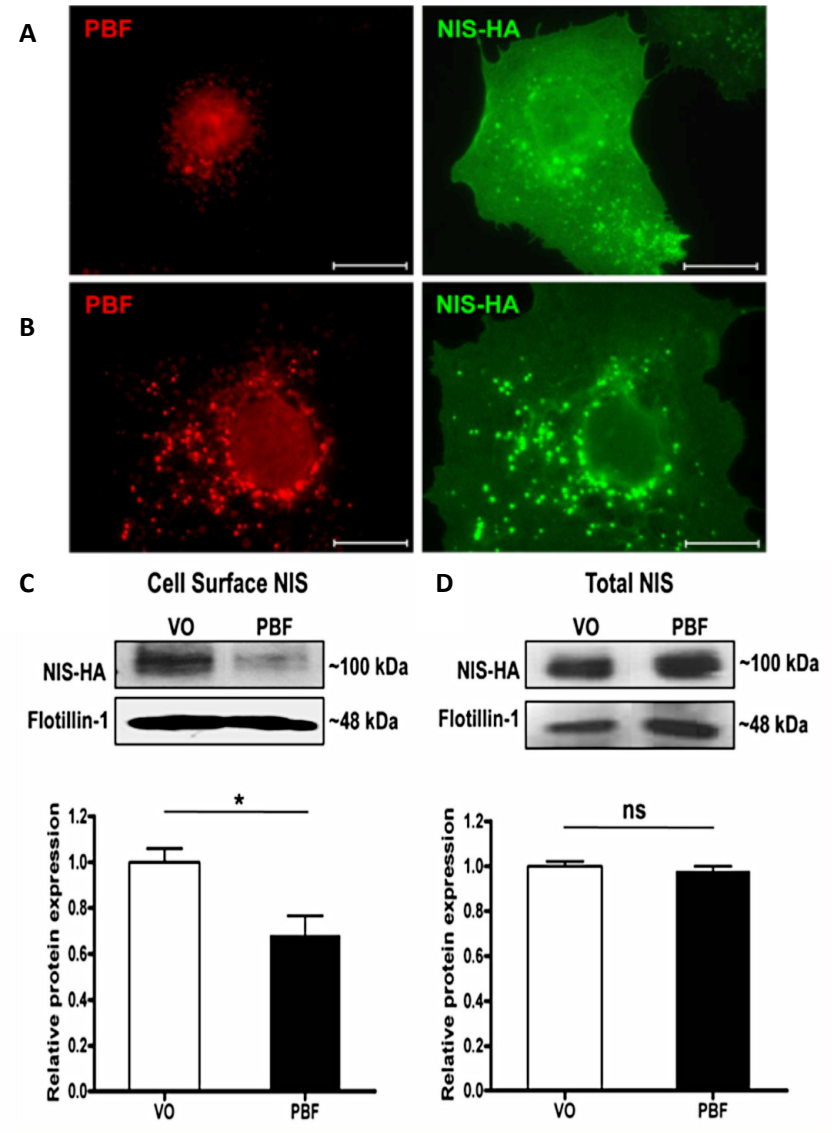

Figure 1.8: PBF modulates subcellular localisation of NIS and co-localises within intracellular vesicles. *A, representative immunofluorescent microscopy showing*

*endogenous PBF (red) and NIS (green) in COS7 cells transfected with VO and HA-tagged NIS (NIS-HA). B, representative immunofluorescent figures demonstrating exogenously transfected PBF (red) and NIS (green) in COS7 cells co-transfected with PBF and NIS-HA. Magnification = 100X. Scale bars = 20 µm. C and D, representative Western blots showing cell surface NIS (C) compared to total NIS (D) from cell surface biotinylation assays in COS7 cells transfected with VO or PBF-HA. Graphs illustrate mean of cell-surface and total NIS protein expression levels relative to the cell surface marker protein Flotillin-1. *P<0.05; ns = not significant. Taken from Smith et al. 2009.*

Furthermore, PBF expression, which was significantly increased in human MNG, was associated with a significant decrease in NIS mRNA expression compared to normal thyroid tissue (Figure 1.9) (Read et al. 2011). In PBF-Tg mice, NIS staining demonstrated through immunohistochemistry showed a distinct reduction in PBF-Tg mice compared to control WT mice (Figure 1.10), and there was also a significant decrease in thyroidal NIS mRNA expression apparent in the PBF-Tg model (Read et al. 2011).

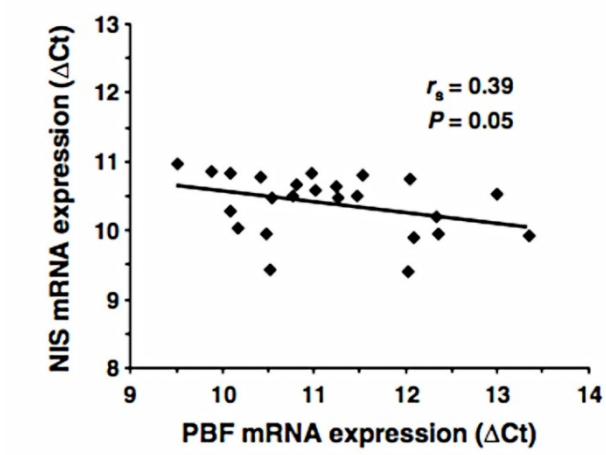

Figure 1.9: Reverse correlation between PBF and NIS mRNA expression in human multinodular goitres. *Representative scatterplot demonstrating correlation between PBF and NIS mRNA expression in human MNG. Data were analysed using Spearman's rank*

correlation. ΔCT = cycle threshold (Ct) of PBF subtracted from the Ct of the internal reference gene. r_s = rho score, indicating relationship between 2 genes via Spearman's rank correlation coefficient. P=0.05. Taken from Read et al. 2011.

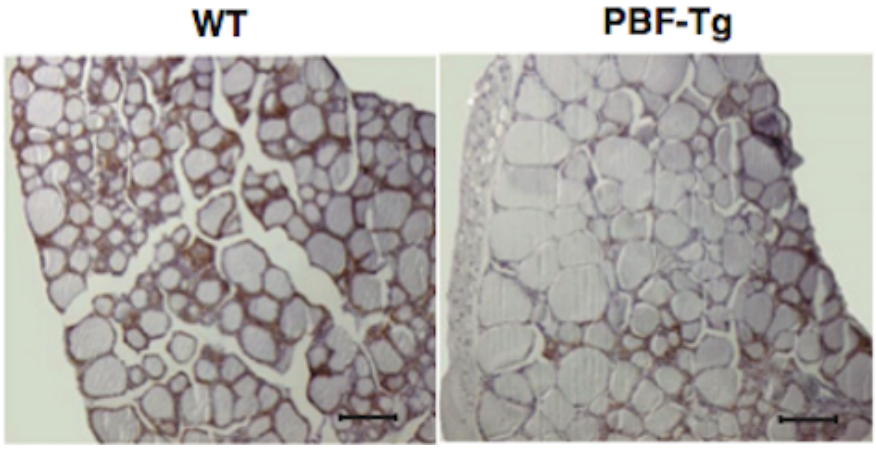

Figure 1.10: NIS protein expression is reduced in PBF-Tg mice compared to WT littermates. *Representative detected NIS staining through immunohistochemistry comparing thyroid glands of WT and PBF-Tg mice. The 10% goat serum was used for negative control (data not shown in the original publication). Scale bars = 100 μm. Taken from Read et al. 2011.*

Importantly, knocking down PBF using specific siRNAs (small interfering ribonucleic acids) in primary thyroid cells from PBF-Tg mice significantly rescued radioiodine uptake, while scrambled siRNA transfected cells did not (Read et al. 2011). Moreover, de-phosphorylation of PBF using PP1 administration (Src family-selective tyrosine kinase inhibitor, 4-amino-5-(4-methylphenyl)-7-(*t*-butyl)pyrazolo[3,4-d]-pyrimidine) or artificial mutation of tyrosine 174 residue of PBF (Y174A) caused a significant increase in plasma membrane retention of PBF, and ameliorated binding to NIS, leading to a significant increase in iodine uptake (Smith et al. 2013). Taken together, PBF overexpression significantly represses radioiodine uptake through NIS functional modulation, a characteristic that can be reversed by downregulation of PBF.

1.1.2.4 PBF and Monocarboxylate 8 (MCT8) in Thyroid Cells

Monocarboxylate transporter 8 (MCT8) is encoded in humans by the SLC16A2 gene and functions as an active transporter for thyroid hormone secretion from the thyroid gland (Friesema et al. 2003). Co-IP and GST pull-down assays demonstrated that PBF and MCT8 specifically bound *in vitro* (Smith et al. 2012). In IF microscopy, when COS7 cells were transfected with MCT8-HA, MCT8 was mainly located at the plasma membrane as previously shown in our group (James et al. 2009) (Figure 1.11A). However, when co-overexpressed with PBF, MCT8 noticeably shifted to the intracellular compartment, and co-localised with PBF within intracellular vesicles, resulting in decreased PM staining (Figure 1.11B and 1.11C) (Smith et al. 2012). Cell surface biotinylation assays also affirmed a significant decrease in MCT8 expression at the PM when cells transfected with PBF compared to VO controls (Smith et al. 2012).

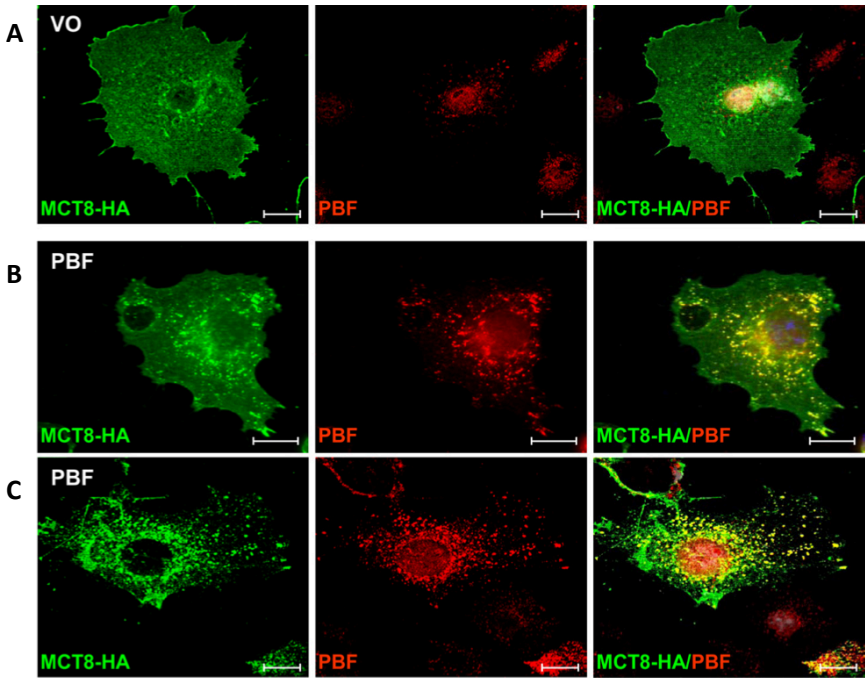

Figure 1.11: PBF modifies the subcellular localisation of MCT8 from the plasma membrane to cytoplasmic vesicles. *A, representative confocal images in COS7 cells*

transfected with VO and MCT8-HA. B and C, representative epifluorescent (B) and confocal (C) microscopy in COS7 cells co-transfected with PBF and MCT8-HA. All images showing PBF (red), MCT8-HA (green) and co-localisation (yellow). Scale bars = 20 μm. Taken from Smith et al. 2012.

In the *in vivo* setting, thyroidal MCT8 mRNA and protein expression were not changed between PBF-Tg mice and controls (Smith et al. 2012). However, there was a significant increase in the accumulation of intrathyroidal thyroid hormone content, including non-Tg and Tg bound T_3 and T_4, in the thyroid glands of PBF-Tg mice compared to WT litter mates, while serum thyroid hormones were similar in both groups (Smith et al. 2012). Taken together, PBF acts as a protein-binding partner of MCT8, in common with its role for NIS, resulting in significant induction of thyroid hormone accumulation in the thyroid gland through alteration in the subcellular localisation of the specific thyroid hormone transporter MCT8.

1.1.2.5 PBF and p53 in Thyroid Cancer

The tumour suppressor p53 is a critical protein in mediating genetic stability. GST pull-down assays illustrated that p53 specifically bound to PBF, with potential binding sites at residues 100-160 and 318-393 of p53 (Figure 1.12) (Read et al. 2014). Co-IPs and proximity ligation assays (PLA) in TPC1 and K1 papillary thyroid cancer cells also validated the interaction between two proteins in the presence and absence of ionising radiation (Figure 1.13) (Read et al. 2014).

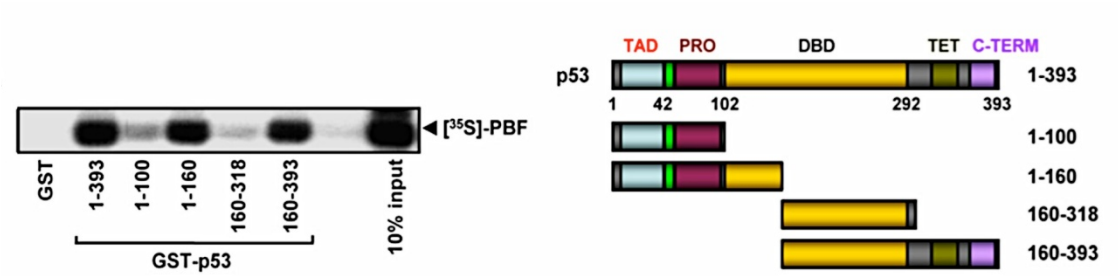

Figure 1.12: PBF binds p53 via GST pull-down assays. *Representative Western blot showing binding between L-α-(^{35}S) methionine labelled PBF and GST tagged p53, including WT and its mutants as demonstrated in schematic diagram of p53 structure. TAD = transcriptional activation domain; PRO = proline rich domain; DBD = DNA- binding domain; TET = tetramerisation domain and C-TERM = C-terminal. Taken from Read et al. 2014.*

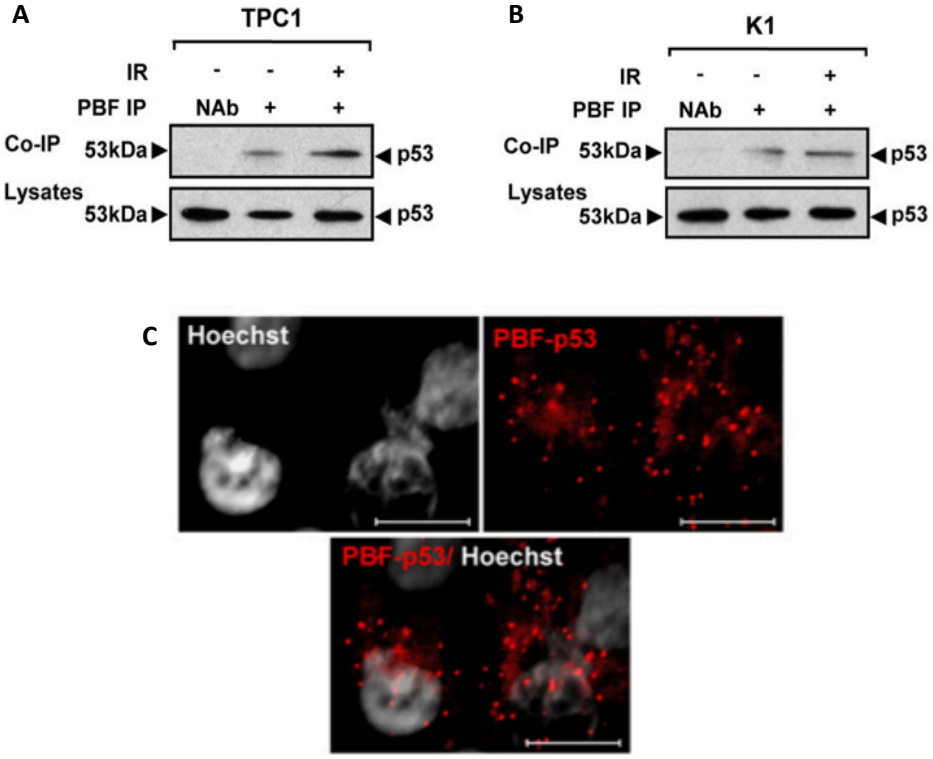

Figure 1.13: PBF specifically binds p53 through co-IP and PLA assays*. A and B, representative co-IP assays of PBF and p53 in TPC1 (A) and K1 (B) cells with either non-irradiated (–IR) or irradiated (+IR) conditions. Nab = no antibody control samples. C,*

representative PLA images of PBF and p53 in TPC1 cells. Red dots indicate a specific interaction between 2 proteins. Scale bars = 10 μm. Taken from Read et al. 2014.

PBF overexpression reduced p53 stability through two mechanisms. Firstly, half-life studies in both TPC1 and K1 cells revealed that overexpressed PBF significantly enhanced p53 turnover compared to controls after 120 minutes as demonstrated in Figure 1.14 (Read et al. 2014). Secondly, overexpression of PBF also significantly induced p53 ubiquitination compared to VO (Read et al. 2014).

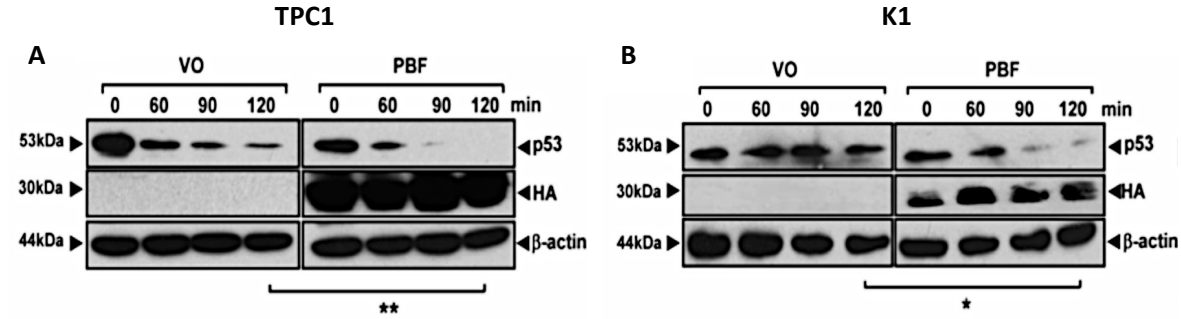

Figure 1.14: Overexpression of PBF induces turnover of p53 in vitro. *Representative Western blots of p53 protein relative to β-actin in TPC1 (A) and K1 (B) cells transfected with VO or PBF, and treated with 100 μM Anisomycin before being harvested at 0, 60, 90 and 120 minutes. *P<0.05; **P<0.01. Taken from Read et al. 2014.*

In contrast, depletion of PBF using specific siRNAs in both TPC1 and K1 cells significantly increased p53 stability compared to scrambled controls after 120 minutes, supporting the capability of PBF to regulate p53 stability in thyroid cancer cells *in vitro* (Read et al. 2014). Moreover, PBF-Tg mice suggested impaired p53 function via significantly increased genetic instability compared to WT control mice as demonstrated via fluorescent inter simple sequence repeat (FISSR) PCR analysis (Read et al. 2014). In primary thyroid cultures from transgenic mice, 12 out of 27 (40%) DNA repair genes such as Mgmt (O(6)-methylguanine-DNA methyltransferase gene), Xrcc3

(X-ray repair complementing defective repair in Chinese hamster cells 3) and Rad51 (a member of the RecA-like gene), were significantly reduced (Read et al. 2014).

In terms of apoptosis, an absence of PBF using specific siRNAs (short interfering ribonucleic acids) treatment in thyroid cancer cells enhanced their response to irradiation with a marked rise in caspase-3/7 level and a significant reduction in cell survival (Read et al. 2014). However, when SW1736 anaplastic thyroid cancer cells, having no p53 expression, were transfected with PBF, there was no alteration in cell viability, suggesting that any cell survival mechanism of PBF is likely to be p53 dependent (Read et al. 2014). Taken together, PBF functions as a dysregulator of p53 activity in thyroid cells.

1.1.3 PBF in Colon Cancer

1.1.3.1 Epidemiology of Colon Cancer

Colorectal cancer is the 4th most common cancer in both men and women, and is estimated to comprise approximately 8% of all new cancer cases in the United States in 2016 (http://seer.cancer.gov/statfacts/html/colorect.html). Based on 2009-2013 data from the SEER (Surveillance, Epidemiology, and End Results) database, the incidence of new colorectal cancer cases in males has been slightly higher than that of females, with a ratio of 1.3:1, and a crude incidence rate of 47.1 for every 100,000 American men in all races (http://seer.cancer.gov/statfacts/html/colorect.html). Additionally, around 4.5 percent of the population may develop colorectal cancer at some period during their lifespan, based on SEER 2010-2012 data.

The death rate remains quite stable, which is approximately 20-30 per 100,000 persons per year in the last 4 decades (SEER 9 Incidence & U.S. Mortality 1975-2013, http://seer.cancer.gov/statfacts/html/colorect.html). The 5-year survival rate is around 65.1%, varying between 60-68% in the last 30 years (SEER 18 2006-2012, http://seer.cancer.gov/statfacts/html/colorect.html), and it is significantly decreased to 13.5% in patients who have distant metastasis.

The understanding of genetic alterations involved in colorectal tumour initiation such as APC (adenomatous polyposis coli) and BRAF (V-Raf Murine Sarcoma Viral Oncogene Homolog B) is well-characterised (Davies et al. 2002), whereas the potential effects of genes related to the progression of tumours in late stages such as TP53 and KRAS (V-Ki-ras2 Kirsten rat sarcoma viral oncogene homolog) remain less well defined (Fearon 2011).

1.1.3.2 PBF and p53 in Colon Cancer

Functional inactivation of p53 due to genetic mutation is identified in approximately 35-45% of colorectal cancers, and correlates with lymphatic invasion and overall survival (Russo et al. 2005). The frequency of mutations also escalates with more advanced tumour stage (Russo et al. 2005). Additionally, PTTG is upregulated in all colon cancers compared with normal tissues (N=48), and higher PTTG expression is also associated with invasion of surrounding lymph nodes presumably being another marker for invasive colorectal cancer (Heaney et al. 2000). Moreover, a specific interaction between PTTG and p53 was determined in transformed cells (Kim et al. 2007); however, the precise mechanism of how PTTG regulates p53 function is not

known.

As PBF is a binding partner of PTTG, and PBF also acts as a negative regulator of p53 function in thyroid cancer, Read et al. investigated the relationship between PBF and p53 in colon cancer (Read et al. 2016). There was a significant increase in PBF expression in colorectal cancers compared to matched normal samples (Read et al. 2016). The TCGA data suggest that this is unlikely to be due to an increase in copy number and in fact revealed a deletion of PBF in around 3% of colorectal tumours (http://www.cbioportal.org). GST pull-down and co-IP assays in HCT116 colon cancer cells also confirmed the interaction between PBF and p53. Indeed, GST pull-down assays revealed that GST tagged WT-PBF and a c-terminal deletion PBF mutant (Δ149-180) still bound with L-α-(^{35}S) methionine labelled p53, but that deletion of amino acids 94-149 (Δ94-149) abrogated the ability of PBF to interact with p53 (Figure 1.15) (Read et al. 2016).

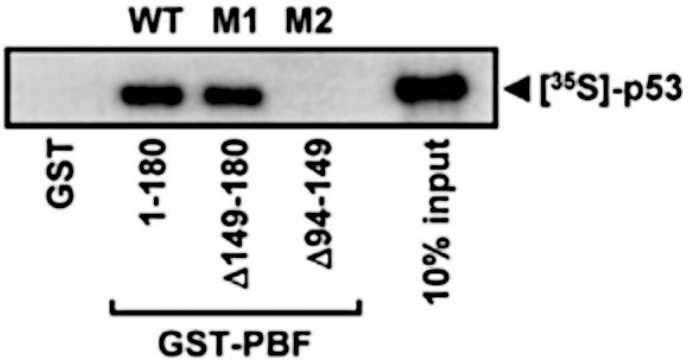

Figure 1.15: PBF binds p53 via a specific region of PBF. *Representative Western blot demonstrating binding between L-α-(^{35}S) methionine labelled p53 and GST tagged PBF, including WT and two mutants as indicated. Taken from Read et al. 2016.*

In keeping with the data described above for thyroid cells, upregulation of PBF significantly induced p53 turnover in HCT116 colon cancer cells as demonstrated in half-life assays (Figure 1.16A), and also increased p53 ubiquitination compared to VO

cells as shown in Figure 1.16B (Read et al. 2016). Both mechanisms lead to reduction in p53 stability of HCT116 cells transfected with PBF compared to controls (Read et al. 2016).

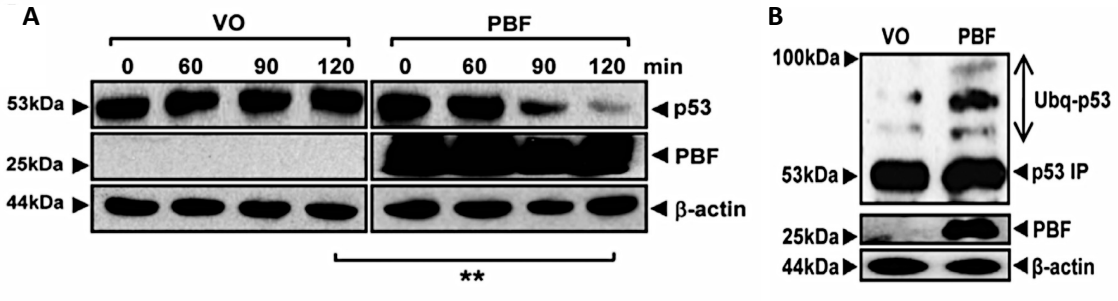

Figure 1.16: PBF overexpression decreases p53 stability and induces p53 ubiquitination in colon cancer cells. *A, representative Western blotting of p53 relative to β-actin in HCT116 cells transfected with either VO or PBF, and treated with 100 μM Anisomycin before being harvested at 0, 60, 90 and 120 minutes. N=4 individual experiments. Data presented as mean ± SEM. SEM = standard error of mean. B, representative Western blot showing high molecular weight of p53 conjugates which represent ubiquitinated p53 (Ubq-p53) in HCT116 cells transfected with the same conditions as in Fig. 16A and treated with the proteasomal inhibitor MG132. **P<0.01. Taken from Read et al. 2016.*

1.1.3.3 PBF and Cell Migration in Colon Cancer

In tumours harbouring WT TP53, high expression of PBF was also associated with the presence of extramural vascular invasion (EMVI) in tissue samples (Read et al. 2016), which is independent prognostic marker for local recurrence and decreased overall survival (Smith et al. 2008), compared to those having no invasion (Read et al. 2016). *In vitro*, overexpressed PBF in HCT116 colon cancer cells significantly promoted cell migration by 60% compared to VO control cells (Figure 1.17).

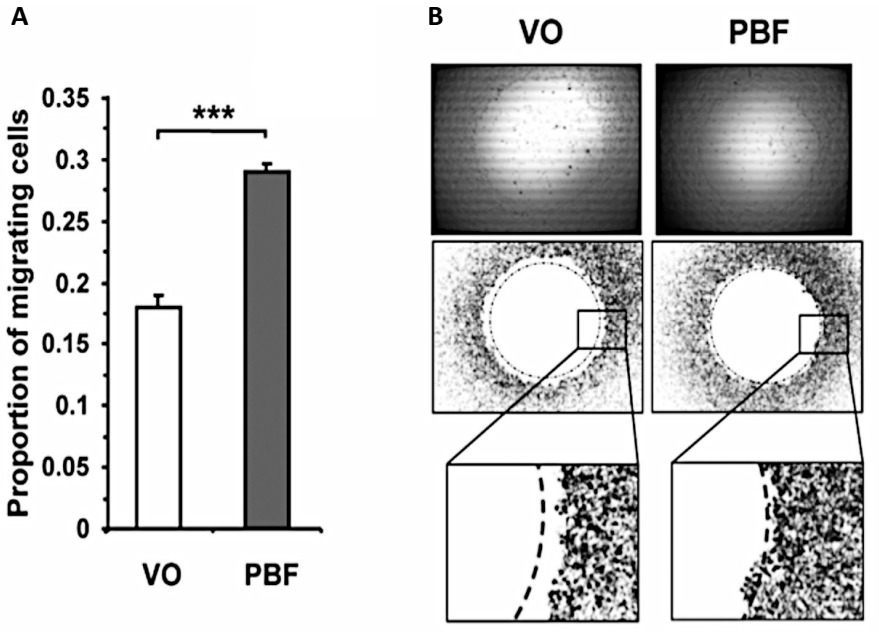

Figure 1.17: PBF has a pro-migratory characteristic in colon cancer cells in vitro. *A, graph demonstrating relative proportion of migrating HCT116 cells transfected with VO or PBF at 24 hours. N=8. Data presented as mean ± SEM. SEM = standard error of mean. B, representative microscopic images of migrating regions, with magnified images in lower panel. Dashed lines of same diameter are labeled to highlight and compare the area of migration. ***P<0.001. Taken from Read et al. 2016.*

Taken together, PBF is over-expressed in colorectal cancer and correlates with extramural vascular invasion. *In vitro*, and in common with thyroid cell findings, PBF binds p53 and inhibits its functions. Furthermore, over-expression of PBF induces increased cell migration. Additional insights into PBF's precise roles in colorectal cancer are required to fully understand its mechanisms of action.

1.1.4 PBF in Breast Cancer

1.1.4.1 Epidemiology of Breast Cancer

Breast cancer is the most common cancer in females, and is estimated to represent around 14.6% of all new cancer cases in the United States in 2016 (http://seer.cancer.gov/statfacts/html/breast.html). Based on SEER 2010-2012 data, around 12.3 percent of the female population may be diagnosed with breast cancer at some time during their lifespan. Indeed, the number of new breast cancer cases in women was 125 for every 100,000 in the USA across all races, based on SEER 18 2009-2013 data (http://seer.cancer.gov/statfacts/html/breast.html).

As for thyroid and colorectal cancer, the death rate remains quite stable, being approximately 20-30 per 100,000 persons per year over the last 4 decades (http://seer.cancer.gov/statfacts/html/breast.html, SEER 9 Incidence & U.S. Mortality 1975-2013). The 5-year survival rate is also relatively stable at approximately 90% across the last 2 decades (http://seer.cancer.gov/statfacts/html/breast.html, SEER 18 2006-2012), and is significantly reduced to less than 30% in patients who carry distant metastasis.

Generally, the induction of breast cancer demands multiple genetic alterations. However, the precise mechanisms involved in tumour development and progression are still not fully recognised, especially in triple negative breast cancer (tumours negative for estrogen receptor, progesterone receptor and HER-2 (human epidermal growth factor receptor-2)).

1.1.4.2 PBF Functions in Breast Cancer

The binding partner of PBF, PTTG, was initially shown to be upregulated in breast cancer, and to correlate with invasive ductal carcinoma and breast tumour recurrent disease (Solbach et al. 2004). Watkins et al. then investigated the role of PBF in breast cancer.

The PBF promoter contains putative estrogen receptor elements (ERE), and treatment with oestrogen analogues such as 17β-estradiol (EST) and diethylstilbestrol (DES) in MCF7 ERα positive breast cancer cells significantly induced PBF mRNA and protein expression, suggesting that PBF is an oestrogen regulated gene (Figure 1.18A and 1.18B) (Watkins et al. 2010). ICI 182780, an anti-oestrogen drug, blocked oestrogen induction of PBF protein expression as demonstrated in Figure 1.18C (Watkins et al. 2010).

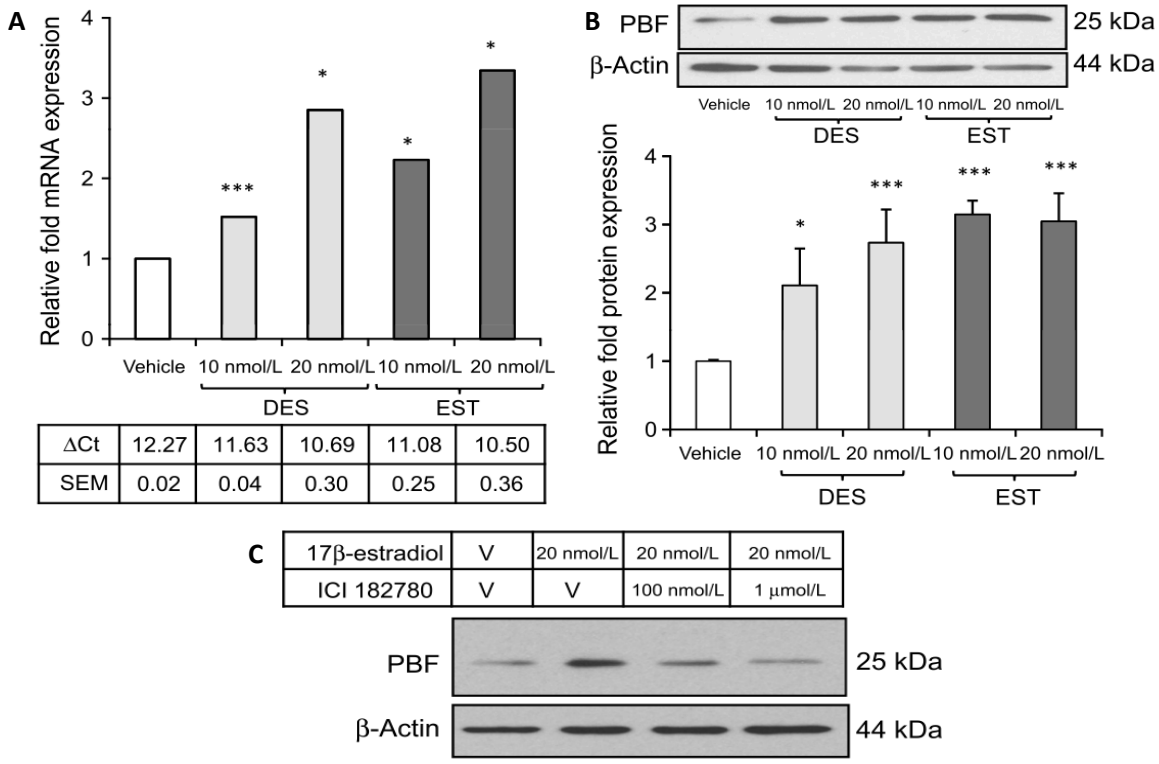

Figure 1.18: Oestrogen treatment induces PBF expression in breast cancer cells in vitro. *A, relative PBF mRNA expression in MCF7 cells treated with diethylstilbestrol (DES)*

*or 17β-estradiol (EST) for 48 hours in different concentrations compared to VO cells. Data presented as ΔCT ± SEM. ΔCT = cycle threshold (Ct) of the PBF subtracted from the Ct of the internal reference gene. SEM = standard error of mean. B, scanning densitometry of PBF protein expression levels relative to β-actin in MCF7 cells treated with the same conditions as in Fig. 18A. N=3 individual experiments. Inset – Western blotting of PBF and β-actin expression levels. C, Western blotting of PBF and β-actin expression levels in MCF7 cells treated with either 17β-estradiol or anti-oestrogen, ICI 182780, for 48 hours compared to vehicle cells. *P<0.05; **P<0.01; ***P<0.001. Taken from Watkins et al. 2010.*

Additionally, EREs in the proximal PBF promoter bind directly with ERα as demonstrated in oligonucleotide pull-down assays (Watkins et al. 2010). In human breast cancer, PBF mRNA and protein expression were significantly upregulated compared to normal breast samples (Watkins et al. 2010), and breast cancer tissue having higher numbers of ERE repeats carried greater PBF mRNA expression compared to those with low ERE repeat numbers (Watkins et al. 2010). Moreover, an escalation in the variable numbers of tandem repeats in the PBF promoter is significantly associated with an increased risk of ER positive breast cancer (Xiang et al. 2012).

In common with the findings for HCT116 colorectal cells (Figure 1.17), PBF overexpression significantly enhanced cellular invasion in MCF7 breast cancer cells compared to VO controls (Figure 1.19). However, this invasive effect was entirely abolished using specific PBF siRNA treatment (Watkins et al. 2010).

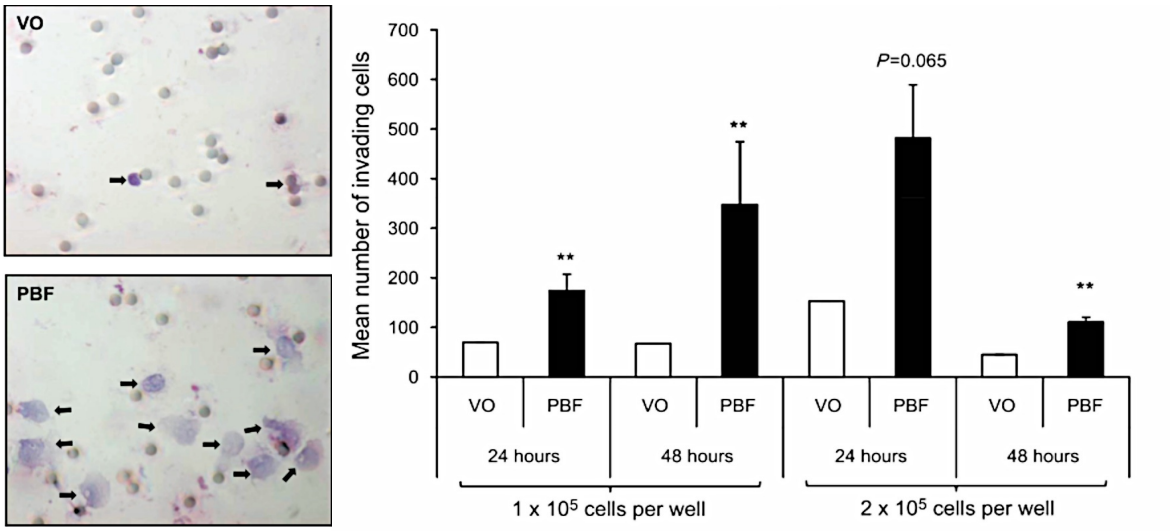

Figure 1.19: PBF has pro-invasive properties in breast cancer cells in vitro. *Representative graph demonstrating average numbers of invading cells in cell invasion assays in MCF7 cells transfected with either VO or PBF at 24 and 48 hours, with different cell density. Data presented as mean ± SEM. SEM = standard error of mean. **P<0.01. N=3 individual experiments. Inset - representative microscopic images of H&E staining of invading cells (arrows). Taken from Watkins et al. 2010.*

Taken together, the functions of PBF have been determined almost exclusively in thyroid (Section 1.1.2), colon (Section 1.1.3) and breast (Section 1.1.4) cancer models. PBF is able to bind NIS and MCT8, altering their subcellular localisation, and hence their function (Figure 1.20). Through interaction with p53, which has been studied particularly in thyroid and colorectal models, PBF over-expression is associated with altered DNA repair response (Figure 1.20). PBF induces cell invasion and migration in colorectal and breast cancer cells. A transgenic thyroid line demonstrated that PBF is mildly pro-proliferative *in vivo*, and soft agar assays showed that PBF induces anchorage independent growth *in vitro*, and tumours in xenograft models. However, despite being over-expressed in thyroid, colorectal and breast tumours, to date there

have been fewer than 20 publications addressing PBF function, and its exact role in tumourigenesis requires further clarification.

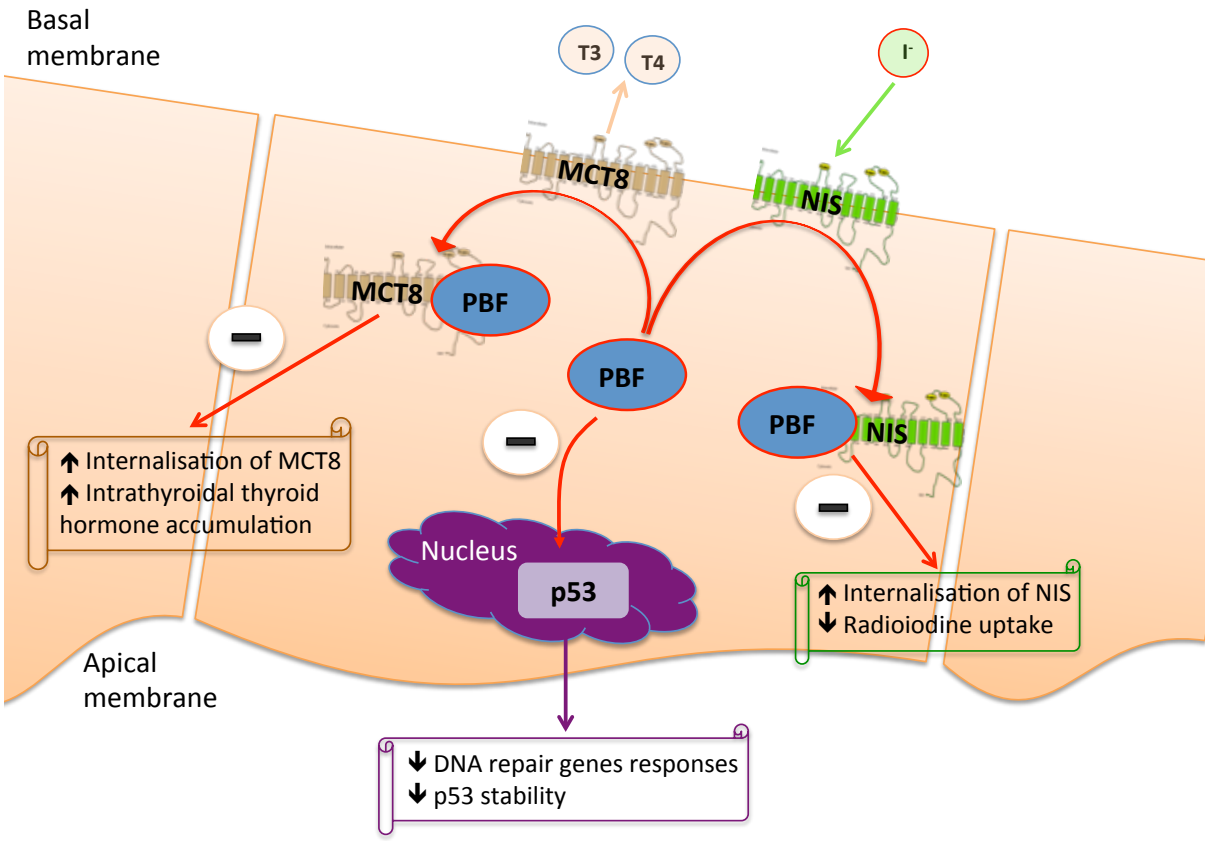

Figure 1.20: Schematic diagram of the interactions between PBF and its binding partners. *Representative diagram illustrating the specific interactions between PBF and its binding partners NIS, MCT8 and p53. T_3 and T_4 denote triiodothyronine and thyroxine, which are actively transported by MCT8, while I^- indicates iodine incorporated into the thyroid gland via NIS. A minus sign (-) shows negative regulation of the other protein function by PBF.*

1.1.5 Genetic Mutations in Human Cancer

1.1.5.1 Catalogue of Somatic Mutations in Cancer (COSMIC) Database

The COSMIC database was initiated in 2004 to collect and describe information on somatic mutations and related data detailing human cancer (http://cancer.sanger.ac.uk). This database has recruited genomic data relating to mutations discovered in all pre-malignant and cancerous lesions from both the scientific literature and from the cancer genome project at the Sanger Institute. The main aim of this project is to analyse the frequencies and specifics of somatic mutations in various human cancers. At the time of PhD submission, the COSMIC website has provided more than 2 million point mutations, 10,000 fusion mutations, nearly 30,000 gene transcripts, 60,000 genetic rearrangements, 700,000 copy number aberrations and 60 million gene expression variants (Forbes et al. 2015). The information, including an overview of each gene, a schematic diagram of the gene view, complex phenotype-specific mutations, tissue discovered mutations, copy number variations and details of drug sensitivity, are displayed on the website in a format for easy understanding and interpretation (http://cancer.sanger.ac.uk).

For instance, data from the COSMIC database reveal the high frequency of point missense substitutions in BRAF (V-Raf Murine Sarcoma Viral Oncogene Homolog B gene) (Figure 1.21). These mutations are discovered from a variety of human tissues such as thyroid, skin, lung, oesophagus, stomach and large intestine. One of the most common BRAF genetic alterations is the $BRAF^{V600E}$ missense substitution (http://cancer.sanger.ac.uk/cosmic/gene/analysis?ln=BRAF). The information from this database leads to the identification of predictive and prognostic markers, development of early diagnostic tools, and targeted therapy in particular cancers, such as melanoma and thyroid cancer (Ascierto et al. 2012, Kebebew et al. 2007).

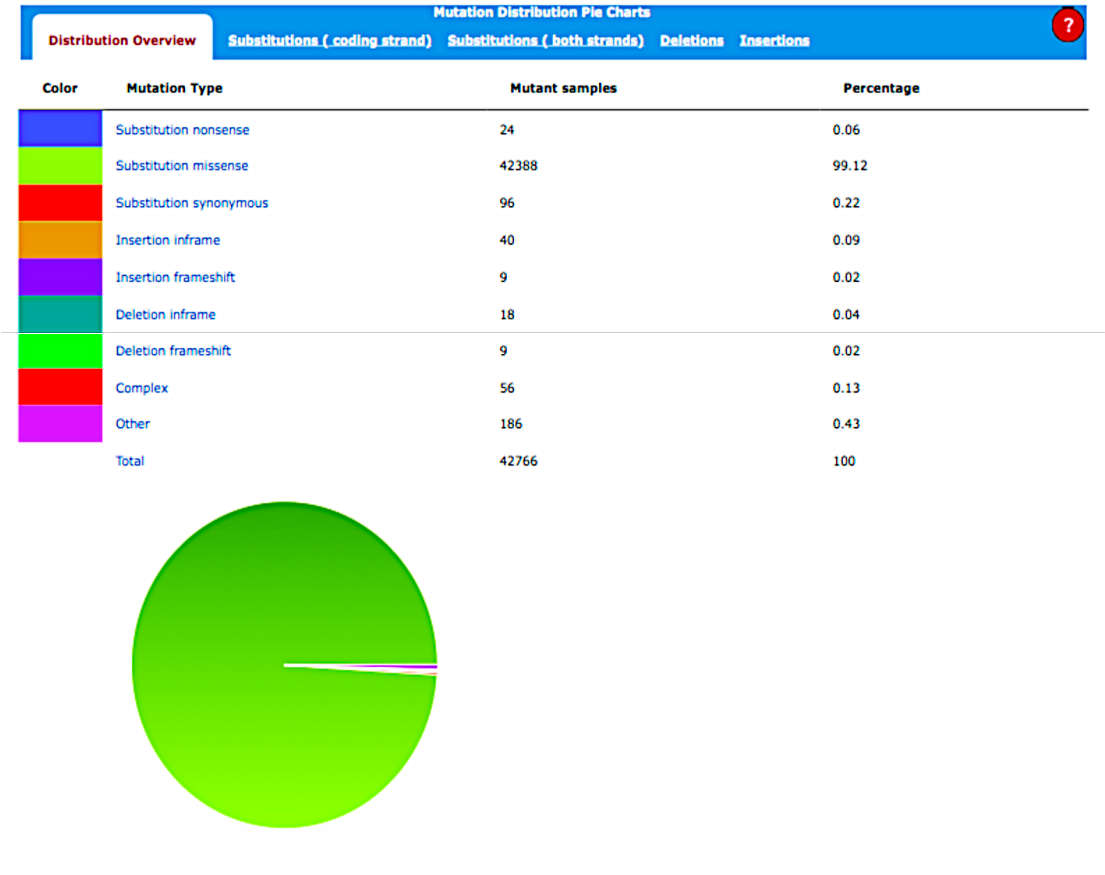

Figure 1.21: Example of mutation distribution in the BRAF gene from the COSMIC database. *Representative diagram showing distribution of BRAF mutations, including number of samples and percentages of each mutation type, retrieved from the COSMIC database.*

Loi et al. investigated a relationship between mutations of PIK3CA (phosphatidylinositol-4,5-bisphosphate 3-kinase catalytic subunit alpha) and the effectiveness of trastuzumab treatment in patients diagnosed with breast cancers (Loi et al. 2013). This study started the project by using the COSMIC database to retrieve data related to a variety of genes such as PIK3CA, BRAF, TP53 and KRAS and their recurrent hotspot mutations, before the samples in this project were sequenced to ensure the coverage of all significant substitutions in these genes rather than restriction to only well known mutated areas (Loi et al. 2013). The genetic alterations were then

correlated with tumour prognosis and trastuzumab administration (Loi et al. 2013). The result showed that most of the PIK3CA mutations were linked to small, well differentiated breast cancers with estrogen receptor positive status, while they carried a potential resistance to trastuzumab treatment (Loi et al. 2013). Thus information from the COSMIC database can be, as well as cataloguing tumour mutational status, used to drive the direction of translational research. Thus this joined up bioinformatic approach is rapidly becoming an essential preliminary step to identify driver somatic mutations of interest in human cancer; however, most mutations identified through large scale untargetted next generation sequencing are likely to be passenger mutations that do not directly affect tumour progression. Therefore, further biological experiments are needed to validate driver genetic mutations.

1.1.5.2 The Cancer Genome Atlas (TCGA) Database

The pilot project of the TCGA database started in 2006 is a joint collaboration between the National Cancer Institute (NCI) and the National Human Genome Research Institute (NHGRI), which are institutes of the National Institutes of Health in the United States. This database is an attempt to unite genome analysis technologies, including microarrays and large-scale whole genome sequencing, as well as bioinformatic data to generate statistically significant conclusions, thereby improving the knowledge of the molecular basis of human cancer (Tomczak, Czerwińska & Wiznerowicz 2015). The central remit of TCGA is creating an outline of key genetic alterations in major cancer types including papillary thyroid cancer, breast carcinoma, colorectal adenocarcinoma and liver hepatocellular carcinoma. The TCGA project also establishes a freely available website (https://tcga-data.nci.nih.gov) for any researchers to access the genetic

information and validate critical discoveries, in turn helping in the development of diagnostic procedures, treatment and cancer prevention (Tomczak, Czerwińska & Wiznerowicz 2015). At the time of submission, the TCGA has processed tissue collections from more than 25,000 patients, including tumour and matched normal samples and sequences through large-scale whole genome sequencing, focusing particularly on 33 main tumour types (Table 1.3).

Available Cancer Types	No. cases with Data	Date Last Updated (mm/dd/yy)
Acute Myeloid Leukemia	200	05/02/16
Adrenocortical Carcinoma	80	04/27/16
Bladder Urothelial Carcinoma	412	04/29/16
Brain Lower Grade Glioma	516	05/02/16
Breast Invasive Carcinoma	1097	04/08/16
Cervical Squamous Cell Carcinoma and Endocervical Adenocarcinoma	307	05/05/16
Cholangiocarcinoma	36	04/29/16
Colon Adenocarcinoma	461	04/28/16
Esophageal Carcinoma	185	05/03/16
Glioblastoma Multiforme	528	05/02/16
Head and Neck Squamous Cell Carcinoma	528	05/03/16
Kidney Chromophobe	66	05/02/16
Kidney Renal Clear Cell Carcinoma	536	04/08/16
Kidney Renal Papillary Cell Carcinoma	291	04/08/16
Liver Hepatocellular Carcinoma	377	04/27/16
Lung Adenocarcinoma	521	04/08/16
Lung Squamous Cell Carcinoma	504	05/02/16
Lymphoid Neoplasm Diffuse Large B-cell Lymphoma	48	04/08/16
Mesothelioma	87	04/08/16
Ovarian Serous Cystadenocarcinoma	586	05/02/16
Pancreatic Adenocarcinoma	185	05/06/16
Pheochromocytoma and Paraganglioma	179	05/03/16
Prostate Adenocarcinoma	498	05/02/16
Rectum Adenocarcinoma	171	04/28/16
Sarcoma	261	05/02/16
Skin Cutaneous Melanoma	470	04/08/16
Stomach Adenocarcinoma	443	05/02/16
Testicular Germ Cell Tumours	150	05/03/16
Thymoma	124	05/03/16
Thyroid Carcinoma	507	05/05/16
Uterine Carcinosarcoma	57	04/29/16
Uterine Corpus Endometrial Carcinoma	548	04/28/16
Uveal Melanoma	80	04/29/16

Table 1.3: Human tumour types collected in the TCGA project. *Representative*

available cancer types sequenced through large-scale whole genome sequencing and collected via the TCGA database. Adapted from https://tcga-data.nci.nih.gov.

The cBioPortal for Cancer Genomics (http://www.cbioportal.org) is an example of the output of the TCGA database. It is an open website evolved by the Memorial Sloan-Kettering Cancer Centre, MSKCC, for public access, analysis and downloading of genetic datasets from the scientific literature and the TCGA database itself. This website provides a panel of genomic information such as genetic mutations, gene expression, DNA copy number variants, DNA methylation as well as related clinical data and patient survival.

As one example, the TCGA project has to date collected and finalised 511 thyroid cancer samples from 507 patients. The results reveal that BRAF, NRAS (neuroblastoma rat sarcoma viral oncogene homolog) and HRAS (V-Ha-Ras harvey rat sarcoma viral oncogene homolog) are the three most commonly mutated genes in thyroid cancer (https://tcga-data.nci.nih.gov). It also provides clinical data related to each patient, copy number alterations and oncological outcome such as disease specific survival and overall survival (https://tcga-data.nci.nih.gov). In turn, this has yielded bioinformatic platforms to assimilate the data. For example, the DOTS-Finder (Driver Oncogene and Tumor Suppressor Finder) has utilised data from the TCGA to identify potential driver genes through computational approaches (Melloni et al. 2014).

Glioblastoma or GBM was the first tumour type clarified in the TCGA project. Brennan et al. used the data from the TCGA database combined with some computational analysis programmes, including MutSig (Mutational Significance) run by the Cancer Genome Analysis (CGA) group (www.broadinstitute.org/cancer/CGA), to develop a directory of genetic modifications and to determine driver genes in GBM

(Brennan et al. 2013). The outcome demonstrated a panel of well-known genes harbouring significant mutations such as TP53, PIK3CA and RB1 (retinoblastoma) (Brennan et al. 2013). They also identified the $BRAF^{V600E}$ substitution in the GBM dataset, which is the same mutation determined in melanoma patients (Brennan et al. 2013). As vemurafenib is a drug used for treatment in some melanoma patients (Chapman et al. 2011), studies using this drug in GBM patients carrying this mutation may subsequently determine the potential of targeted therapies.

The TCGA Pan-Cancer analysis is another example using information from the TCGA database integrated with the other genomic tools such as the UCSC (University of California Santa Cruz) Cancer Genomics Browser (https://genome-cancer.ucsc.edu) and cbioportal data (http://www.cbioportal.org) to establish genetic correlation between different tumour types and to identify the prognosis of cancer (Cline et al. 2013). To illustrate, this analysis linked genetic clusters to the clinical outcome of patients with acute myeloid leukemia (Cline et al. 2013). They demonstrated that tumours were essentially categorised by the origin of tissue (Cline et al. 2013). Thus, whilst squamous cell carcinoma (SCC) of lung was grouped with other SCC (for example, head and neck SCC and bladder cell carcinoma), lung adenocarcinoma had unique characteristics and different overall survival compared to lung SCC, driving distinct patient treatment regimens (Cline et al. 2013).

Taken together, the COSMIC and the TCGA initiatives have rapidly revolutionised the genetic and epigenetic information available to researchers for human tumours. Previously, sequencing initiatives were based on relatively small scale and disparate approaches in single tumour types. Now, through unifying sequence data, new mechanisms and insights are emerging into the processes which initiate and drive

tumourigenesis, and which can be targeted for treatment.

1.1.5.3 *In Vivo* PBF Mutations

In 2013, the first 11 PBF mutations, with 10 missense substitutions and 1 synonymous substitution, were reported by the COSMIC database, as demonstrated in Figure 1.22. However, further substitutions of the protein have subsequently been discovered in both the COSMIC and the TCGA databases. Currently, the data from whole exome sequencing through the Wellcome Trust COSMIC database, which was updated in May 2016, has revealed 27 PBF mutations in various human cancers, with 20 missense substitutions, four synonymous substitutions, two inframe deletions and one inframe insertion (Figure 1.22). These mutations are distributed across all functional domains of PBF, especially the PSI domain, transmembrane region and proximal to NLS, and they are also found in various tumour types, such as lung, colon, stomach, breast, ovary and prostate.

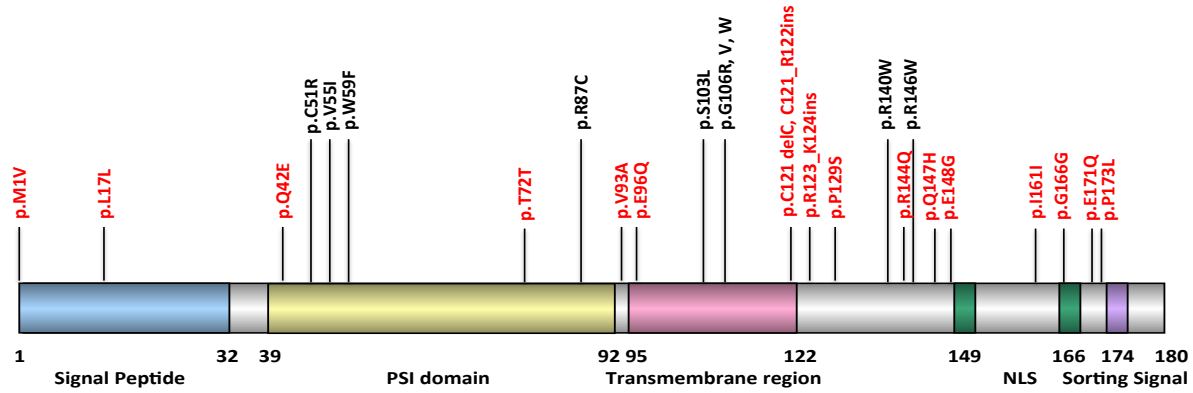

Figure 1.22: Schematic diagram of PBF with its in vivo mutations discovered in the COSMIC database. *PBF schematic with all 27 reported amino acid residue changes in COSMIC. The first 10 nonsynonymous PBF mutations that were discovered in April 2013 and investigated through this thesis are denoted in black. Ins denotes insertional*

mutagenesis, while del illustrates deletion mutation. Adapted from COSMIC database, May 2016.

According to the TCGA database (http://www.cbioportal.org), there are numerous genetic abnormalities of PBF found in multiple human cancers. However, most of them are amplifications of PBF, while fewer than 0.5% represented overall mutations in the gene. There are also additional substitutions, such as A57V, P88L, G94R, G101S and P129S, found in different domains, especially the transmembrane region, suggesting that mutations in some critical domains may influence specific protein functions. Nevertheless, 511 papillary thyroid cancer samples were sequenced but analysis of the data reveal that there were no mutations in PBF. In addition, our group also sequenced the entire PBF coding region in 24 well-differentiated thyroid cancer samples, and failed to find any PBF mutations (Stratford et al. 2005). Thus, whilst PBF has an integral role in regulating thyroid cell function (Read et al. 2011), it is not commonly mutated in thyroid cancer. However, PBF mutations are more apparent in other endocrine and non-endocrine tumour types, and study of these mutations may reveal novel mechanisms of human cancer.

1.2 Approaches to Identify Potentially Oncogenic Mutations

1.2.1 Bioinformatic Approaches

As discussed above, there has been a dramatic increase in the numbers of genetic mutations discovered across various cancer types due to the worldwide application of next generation sequencing. However, only a minority of them are likely to confer a

specific growth advantage, resulting in clonal expansion and development of tumour (driver mutations), whilst the majority of the substitutions are predicted to be passenger mutations, which have no direct effect on tumour development and progression (Torkamani, Schork 2008, Greenman et al. 2007). The critical reason to clarify the drivers is to gain translational information from research to the clinic, including applying specific genes as being potentially diagnostic, prognostic or therapeutic markers for particular types of human cancer and also understanding the precise molecular mechanism responsible for tumour formation.

For instance, one of the most well-known driver genes implicated in human cancer pathways is BRAF. The BRAF V600E point mutation is observed across different kinases, predicting an established role in oncogenesis (Torkamani, Schork 2008), and this knowledge has been applied in the use of the BRAF inhibitor vemurafenib as a specific targeted therapy for treatment of melanoma patients who harbour the mutation (Ravnan, Matalka 2012). Moreover, the NRAS mutation is also a biomarker for melanoma, and patients having NRAS mutant-tumours derive sensitivity to MEK (mitogen-activated protein/extracellular signal-regulated kinase kinase) inhibitors (Flaherty, Hodi & Fisher 2012).

In parallel to the rapid increase in the number of discovered somatic mutations in human cancer, a variety of statistical approaches based on bioinformatic data analysis have been adopted in an attempt to verify driver genes and mutations. There are 4 main computational approaches, which are based on protein functional changes due to mutational effect, frequency of mutations, pattern of mutations within genes and pathway-based analysis (Melloni et al. 2014). Firstly, protein functional approaches can be used to predict the risk of functional changes caused by point substitutions (Reva,

Antipin & Sander 2011, Ng, Henikoff 2006, Ng, Henikoff 2003). For example, Sorting Intolerance From Tolerance (SIFT) is one of the protein functional approaches based on the physical property of amino acids and sequence homology to predict whether an amino acid substitution is likely to alter protein function (Ng, Henikoff 2006, Ng, Henikoff 2003). Secondly, the frequentist procedure is another statistical strategy based on the frequency of the particular mutations compared to background mutation rate for a specific DNA region. However, this approach has a critical drawback due to the requirement of the potentially unavailable background mutation rate in the whole human genome. Thirdly, the pattern-based method is a statistical programme used to apply mutational details such as location of mutations found in the gene, and types of mutation such as missense or silent substitutions to determine the probability of being driver mutations, and can be applied to tumour suppressor genes as well as oncogenes (Vogelstein et al. 2013). Indeed, typical genetic alterations in oncogenes are usually concentrated in specific protein domains, and consist of missense substitutions that are located on key amino acid residues and do not cause a stop codon, and insertion or deletion mutations having an unchanged reading frame (Melloni et al. 2014). In contrast, mutations in tumour suppressor genes are generally truncating and initiate a stop codon in a non-specific mutational pattern such as the mutation of APC in colorectal cancer (Melloni et al. 2014). The fourth procedure is pathway-oriented which is the analysis of a group of mutations in a specific pathway (Leiserson et al. 2013), but this procedure is more difficult for rare genetic mutations, where pathways may be more obscure.

To illustrate, Vogelstein et al. used the pattern-based analysis to define driver genes in human cancer using the “20/20 rule” (Vogelstein et al. 2013). In this study, the

driver genes were identified and classified into 2 categories, oncogenes and tumour suppressor genes (Vogelstein et al. 2013). Indeed, a driver oncogene was a gene containing more than 20% of reported mutations at the same amino acid position, such as missense substitutions in the LDHA (Lactate Dehydrogenase A) and PIK3CA genes, whilst a driver tumour suppressor gene carried 20% inactive mutations or more, such as in RB1 and VHL (Von Hippel-Lindau) (Vogelstein et al. 2013).

OncodriveCLUST is another computational programme based on patterns of genetic alterations, and provides freely accessible via http://bg.upf.edu/oncodriveclust (Tamborero, Gonzalez-Perez & Lopez-Bigas 2013). This analysis focuses on somatic mutations that assemble in particular region of genes, especially clustered groups within 5 amino acid residues or less, before calculating a score used to predict potential driver genes (Tamborero, Gonzalez-Perez & Lopez-Bigas 2013). This approach was applied to some TCGA datasets, including breast, ovary and uterus, and novel driver genes which were not identified using other strategies were determined with the OncodriveCLUST programme, such as MMP14 (matrix metallopeptidase 14), involving in disruption of extracellular matrix, and PLA2G3 (phospholipase A2 group III), relating to cell death (Tamborero, Gonzalez-Perez & Lopez-Bigas 2013). Nevertheless, each statistical strategy has advantages and disadvantages, and there is no single programme that can accurately determine all driver genes.

Another such statistical approach is the DOTS-Finder, a computational programme based on 3 statistical steps, including protein function, frequentist and pattern-based principles, for the prediction of potential driver genes in human cancer (Melloni et al. 2014). This tool can be utilised with either the large-scale information from the TCGA database or with the data of tumours from smaller studies to estimate

the driver status. The DOTS-Finder has been applied to 34 individual cancer types such as breast and thyroid carcinoma to identify driver genes and then analyse the results compared to predicted mutations from other projects such as the TCGA database or the TUSON (Tumor Suppressor and Oncogene) Explorer (Melloni et al. 2014).

When the DOTS-Finder was applied to breast cancer samples, a poor correlation was found between the results from this approach and the TCGA database. Indeed, the DOTS-Finder had an ability to discriminate and eliminate any mutated genes that did not correlate with human cancer such as RYR2 (Ryanodine receptor 2) (Melloni et al. 2014). The DOTS-Finder also discovered novel putative driver genes such as AQP7 (Aquaporin-7) (Melloni et al. 2014), involving in cellular proliferation and cell migration *in vitro* and local invasion and metastasis of the tumour *in vivo* (Verkman, Hara-Chikuma & Papadopoulos 2008).

The DOTS-Finder strategy was also applied to 326 thyroid tumour samples from the TCGA dataset. When compared with the results from the TUSON Explorer, some genes such as BRAF and TG were identified in both approaches. Nevertheless, the DOTS-Finder also revealed more putative driver genes such as EMG1 (essential for mitotic growth 1) and IGF-1 (insulin-like growth factor 1) (McMahon et al. 2010). In addition, the DOTS-Finder also predicted that PBF may be one of 12 putative genes driving thyroid carcinogenesis in tumour samples from the TCGA database (Melloni et al. 2014). Cifola et al. also applied the DOTS-Finder programme to primary plasma cell leukemia samples and identified 14 new potential driver genes playing critical roles in this malignancy (Cifola et al. 2015).

However, although statistical strategies such as these can be readily applied to large-scale genetic information and may predict rare driver mutations among all somatic mutations, there is no current bioinformatic approach that can guarantee definitive driver gene status. Therefore, conventional functional studies are still needed to appraise potential driver mutations identified through bioinformatic screening of mass sequencing data.

1.2.2 Laboratory Approaches

As driver genes are important for tumour formation and can be applied as potential predictive and prognostic biomarkers for early diagnostic methods and targeted therapy in human cancer, confirmation of these driver genes and mutations are needed before the knowledge can be used. An oncogenic driver genes is a gene that provides tumour growth benefit and induces clonal development of cancer (Stratton, Campbell & Futreal 2009, Haber, Settleman 2007). These genes or mutations generally promote their oncogenic functions such as cellular invasion and metastasis, carry a high recurrence rate in cancer samples and probably cluster in specific amino acid residues or in particular domains (Sakoparnig, Fried & Beerenwinkel 2015, Melloni et al. 2014, Stratton, Campbell & Futreal 2009). In addition, the driver genes or driver mutations are likely to retain the capability to transform benign to malignant cells *in vitro*, and induce tumourigenicity *in vivo* (Hanahan, Weinberg 2011, Hanahan, Weinberg 2000).

As driver genes or mutations frequently have selective growth advantage, cellular proliferation assessments such as MTS (3-(4,5-Dimethylthiazol-2-yl)-5-(3-Carboxymethoxyphenyl)-2-(4-Sulfophenyl)-2H-Tetrazolium) or BrdU

(Bromodeoxyuridine) assays are commonly used to determine the impact of genes or mutations on the proliferative phenotype. If the cell turnover rate is significantly increased, the investigated gene or mutation is potentially a driver. Other standard biological measures such as cellular invasion and cell migration are useful, as are gene function-specific measures. Anchorage-independent growth remains a crucial feature suggesting malignant transformational ability *in vitro*. Finally, the capacity for inducing tumours *in vivo* through xenograft or transgenic models is the ultimate test to establish driver gene status.

As an example, BRAF governs the MAPK/ERK pathway (mitogen-activated protein kinases/extracellular signal-regulated kinases), involved in cellular division, cell growth and differentiation. Perhaps unsuprisingly, BRAF was predicted through the bioinformatic approach of Melloni et al. to be a driver oncogene in thyroid carcinoma (Melloni et al. 2014). The $BRAF^{V600E}$ substitution, identified in both the COSMIC and the TCGA databases, is the most common genetic mutation found in the BRAF gene, and is apparent in a variety of human cancers, especially thyroid and melanoma (Liu et al. 2007, Garnett, Marais 2004). Overexpression of $BRAF^{V600E}$ in the thyroid gland of a mouse model induced papillary thyroid cancer (Knauf et al. 2005). Depletion of BRAF protein expression using specific BRAF siRNAs in cells carrying the $BRAF^{V600E}$ mutation significantly reduced cellular proliferation, colony formation and tumour growth in nude mice (Liu et al. 2007). Thus, bioinformatic and laboratory data were in complete agreement for BRAF (Melloni et al. 2014).

NRAS is another gene predicted through the DOTS-Finder to be a potential driver gene in acute myeloid leukemia and thyroid cancer (Melloni et al. 2014). This gene interacts with PI3K (Phosphatidylinositol-3-Kinase), regulating the MAPK and

PI3K/AKT (Phosphatidylinositol-3-Kinase/Protein Kinase B) pathways, and influencing cell cycle, differentiation and apoptosis (Eisfeld et al. 2014). The amino acid G12 residue is also the recurrent hot spot of mutations occurring in the NRAS gene, and $NRAS^{G12D}$ is one of the most common substitutions established in the COSMIC and the TCGA datasets in multiple human tumours such as leukemia, lymphoma, colorectal carcinoma, breast cancer and anaplastic thyroid cancer. Human skin fibroblast cells stably transfected with the $NRAS^{G12D}$ mutant showed significantly induced cellular proliferation via BrdU assays (Eisfeld et al. 2014). Moreover, NIH 3T3 murine fibroblast cells stably transfected with this mutation demonstrated enhanced cell transformation ability through soft agar assays compared to controls (Eisfeld et al. 2014). Therefore, the $NRAS^{G12D}$ mutation is a clear driver mutation both from bioinformatic prediction and standard cell biological assays (Melloni et al. 2014).

By contrast, KRAS (V-Ki-ras2 Kirsten rat sarcoma viral oncogene homolog) is also a member of RAS (rat sarcoma) subfamily, but is not anticipated to be a driver gene in thyroid cancer through computational analysis (Melloni et al. 2014). However, multiple somatic KRAS mutations in a variety of human cancers have been identified in the COSMIC and the TCGA databases, and the G12 residue also has highly mutated recurrence rate in this gene. Furthermore, $KRAS^{G12V}$ substitution correlates with a high mortality rate and aggressive phenotype in human colorectal tumours (Andreyev et al. 1998), and Caco-2 colon cancer cells overexpressing $KRAS^{G12V}$ showed enhanced cell transformation in soft agar assays (Oikonomou et al. 2009). Thus, although KRAS is not a predicted driver oncogene in thyroid cancer (Melloni et al. 2014), the laboratory results suggest that this gene does has specific growth enhancement and is indeed likely to be a driver.

In conclusion, laboratory experiments remain necessary for the confirmation of driver gene status and may occasionally contradict bioinformatic approaches.

1.3 Hypothesis and Aims

I hypothesise that PBF, being previously classified as a proto-oncogene, may in fact be an oncogene, with rare amino acid substitutions in some residues affecting its mechanisms of action. The main aim of this study is to analyse the functional effect of the first 10 discovered nonsynonymous mutations in PBF, particularly those occurring in the critical PSI domain, transmembrane region and proximal to the NLS. Further, the aim of this thesis is to study the effect of amino acid substitutions on protein structure, subcellular localisation of PBF, glycosylation, dimerisation, stability and known functions of the protein, such as proliferation, invasion, migration, radioiodine uptake ability, transforming ability and binding partner interaction. Thus the overall objectives are to determine whether mutations in PBF are aetiological, and in doing this, to gain new insight into the mechanisms of action of this under-characterised gene.

CHAPTER 2 - MATERIALS AND METHODS

2.1 Cell Culture and Transfection

2.1.1 Cell Lines

TPC1 and SW1736 are thyroid cancer cell lines that were kindly supplied by Dr Rebecca Schweppe (Division of Endocrinology, Metabolism, & Diabetes, University of Colorado Denver, Aurora, Colorado). The TPC1 cell line is derived from human papillary thyroid carcinoma which expresses wild type of BRAF, HRAS, KRAS, NRAS, PTEN and p53, but contains the *RET/PTC1* re-arrangement (Saiselet et al. 2012, Ribeiro et al. 2008). The SW1736 cell is originated from anaplastic thyroid cancer, with high expression of several cancer stem markers, including SOX2 (sex determining region Y - box 2), OCT4 (octamer-binding transcription factor 4) and SSEA4 (stage specific embryonic antigen 4) (Carina et al. 2013). Both cell lines were cultured in RPMI media (Invitrogen, UK) containing 10% (v/v) heat-inactivated foetal calf serum (FCS; Invitrogen, UK) and 1% Penicillin (10^5 U/l)/Streptomycin (100 mg/l).

MCF7 breast adenocarcinoma cancer cells were obtained from the European Collection of Cell Cultures (ECACC). This cell line was first isolated from the malignant pleural effusion of a female patient having adenocarcinoma of breast. MCF7 cells are able to respond to estradiol via estrogen receptors and also contain progesterone receptors. However, these cells have no amplification of ERBB2 or erb-b2 receptor tyrosine-protein kinase 2 gene amplification and no TP53 mutation (Ross, Perou 2001, Soule et al. 1973). MCF7s were routinely maintained with complete RPMI containing 10% (v/v) heat-inactivated foetal calf serum (FCS; Invitrogen, UK) and 1% Penicillin (10^5 U/l)/Streptomycin (100 mg/l) as described for TPC1 and SW1736 cells.

HeLa cells, a malignant epithelial cell line derived from a cervical carcinoma (Scherer, Syverton & Gey 1953), were utilised as a human cell line which shows highly efficient transfection. Cells were cultured in Dulbecco Modified Eagle's Media DMEM (Sigma, UK) supplemented with 10% (v/v) heat-inactivated foetal calf serum (FCS; Invitrogen, UK), 1% Penicillin (10^5 U/l)/Streptomycin (100 mg/l) and 1% L-glutamine (Invitrogen, UK). Cells were incubated and then passaged twice weekly.

NIH 3T3 cells are mouse embryonic fibroblast cells originating in 1962 at New York University School of Medicine Department of Pathology. These cells were acquired from the American Type Culture Collection (ATCC). Cells were maintained in DMEM (Sigma, UK) supplemented with 10% (v/v) calf serum (ATCC, USA), 1% Penicillin (10^5 U/l)/Streptomycin (100 mg/l) and 1% L-glutamine (Invitrogen, UK).

All cell lines were seeded in sterile T75 tissue culture flasks and incubated in a humidified incubator at 37°C and 5% CO_2 atmosphere. The appropriate seeding cell-density of all cell lines was determined by cell growing rate but they were usually passaged twice weekly as required.

2.1.2 Plasmid Purification

2.1.2.1 Vector (VO)

Overexpression of proteins of interest was accomplished via transfection with mammalian expression vectors carrying specific coding sequence cDNAs. Plasmids used were pcDNA3.1(+) (Invitrogen, UK), pCI-Neo (Promega, USA) and pCMV6-Entry (Origene, USA) as illustrated in Figure 2.1A, 2.1B and 2.1C, respectively. All vectors

consist of the origin of replication, the cytomegalovirus promoter and sites for specific antibiotic resistance.

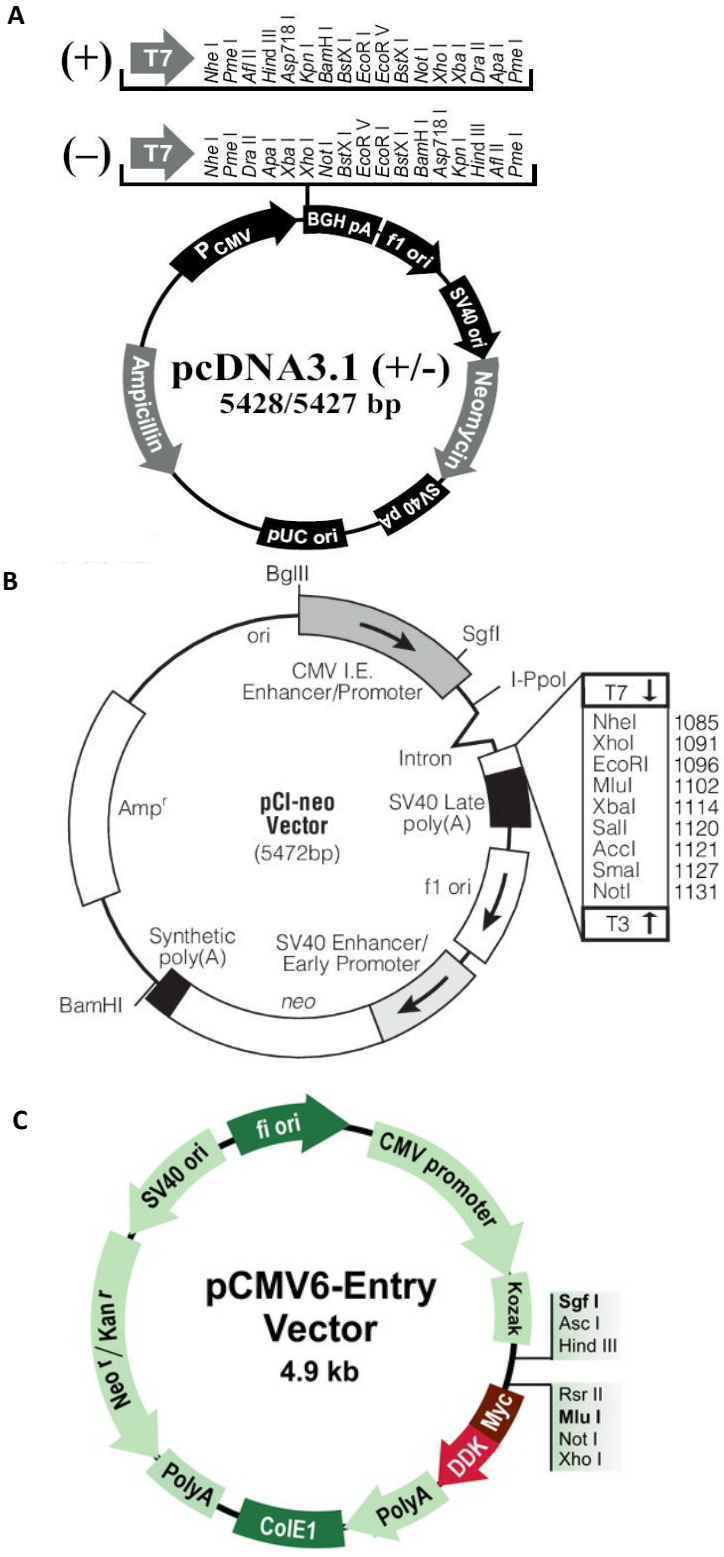

Figure 2.1: Schematic diagram of pcDNA3.1(+/-), pCI-neo and pCMV6-Entry vectors.

The figures illustrate diagrams of three vectors consisting of pcDNA3.1(+/-) (A), pCI-neo

(B) and pCMV6-Entry vectors (C), with origin of replication (Ori), Cytomegalovirus (CMV) promoter and antibiotic resistance genes, including Ampicillin (Amp), Neomycin (Neo) and Kanamycin (Kan) resistance. The restriction enzymes sites are also noted.

2.1.2.2 Mutagenesis

Mutagenesis was performed using the Quick Change II XL site directed mutagenesis kit (Agilent Technologies, UK). The first step was to design individually mutagenic oligonucleotide primers (Sigma, UK) based on information from the COSMIC database. Following the manufacturer's suggestions, the desired substitutions were in the middle of the primer with 10–15 bases of normal sequence on both sides, and a length of 25-45 bases, with a melting temperature (T_M) more than 78°C (T_M = 81.5+0.41(%GC)−(675/N)−%mismatch; N is the primer length in bases). In addition, primers were designed to have a minimum GC content of 40% and to terminate in one or more C or G bases.

2.1.2.3 Bacterial Transformation

Bacterial transformation was performed after construction of mutated plasmids. Lysogeny broth (LB) solution was prepared in concentration 20 g/l, and LB agar was assembled with a proportion of 4 g LB powder, 3 g agar and 200 ml water. Then, after being warmed until melted, LB agar was supplemented with 100 μg/ml of Ampicillin or 50 μg/ml of Kanamycin, and poured into a plate. The plate was left at room temperature until set, and then incubated at 37°C at least 1 hour before used. The next process was implemented using Subcloning EfficiencyTM DH5αTM Competent E.Coli Cells

(Invitrogen, UK) according to the manufacturer's instructions. 6 ng of plasmid DNA were added to 50 µl DH5αTM cells in a 1.5 ml Eppendorf tube. The tube was then swirled gently to mix them together and incubated on ice for 30 minutes, before the DH5αTM cells were heat shocked at 42°C for 20 seconds and left on ice for the next 2 minutes. 950 µl of prepared LB solution were added into the tube and the sample was incubated at 37°C for 1 hour in a shaking incubator. After the solution was centrifuged at 13,000 rpm for 3 minutes at room temperature to form the cell pellet and to get rid of the supernatant, the cells were re-suspended in 50 µl of LB solution and then aliquoted onto 2 warmed LB plates. The plates were incubated at 37°C for 16 hours to let them form colonies used for the next steps which are DNA purification (Miniprep) and DNA amplification (Maxiprep).

2.1.2.4 Deoxyribonucleic Acid (DNA) Purification (Miniprep) and Sequencing

DNA purification was accomplished using the Wizard® Plus SV Miniprep DNA Purification System (Promega, USA) according to the manufacturer's instructions. After a 16-hour incubation period in the bacterial transformation step, a single colony was obtained and added into 5 ml LB solution containing suitable antibiotics as previously described. The sample was then incubated at 37 °C for 16 hours in a shaking incubator, before the purification process was performed at room temperature. Firstly, the suspension solution was centrifuged at 10,000 g for 5 minutes to form the pellet, and the supernatant was discarded. The pellet was next re-suspended thoroughly in Cell Resuspension Solution (Promega, USA), before the cells were lysed using Cell Lysis Solution (Promega, USA). Next, the sample was mixed and then incubated until the

suspension became cleared. After adding Alkaline Protease Solution (Promega, USA) into the tube and mixing to inactivate any endonucleases released during cell lysis, the lysate was incubated on the bench for 5 minutes, and Neutralisation Solution (Promega, USA) was then supplemented. The tube was centrifuged at 14,000 g for 10 minutes. All further steps were carried out in a spin column combined with a collection tube provided in the kit. After insertion of a spin column into a collection tube, the clear supernatant was decanted into the column, and then centrifuged at 14,000 g for 1 minute, before the flowthrough was subsequently discarded. The plasmid was washed twice by using Washing Solution (Promega, USA), and centrifuged at 14,000 g for 1 minute and 2 minutes, respectively, before discarded the flowthrough. After the spin column was transferred to a new collection tube, nuclease free water was added into the column and the sample was centrifuged at 14,000 g for 1 minute to elute the plasmid DNA. The DNA concentration was quantified using the NanoDrop© ND-1000 Spectrophotometer (NanoDrop) and accompanying ND-1000 software on the DNA-50 setting. The plasmid was kept at -20°C.

To sequence the plasmid, 250-500 ng of the plasmid DNA were added with 3.2 pmol of forward or reverse primers, and made up to 10 µl in total volume with nuclease free water. Primers for the pCI-neo vector were T7 for forward (TAATACGACTCACTATAGGG) and T3 (ATTAACCCTCACTAAAGGGA) for reverse, while primers for the pcDNA3.1(+) were T7 forward (TAATACGACTCACTATAGGG) but BGH (bovine growth hormone terminator) reverse (TAGAAGGCACAGTCGAGG). For the pCMV6-Entry vector, primers were forward primer VP1.5 (GGACTTTCCAAAATGTCG) and reverse primer XL39 (ATTAGGACAAGGCTGGTGGG).

2.1.2.5 DNA Amplification (Maxiprep)

After sequencing of the plasmid DNA, DNA amplification was carried out using the GenEluteTM HP Plasmid Maxiprep Kit (Sigma, USA) according to the manufacturer's instructions. 5 ml LB solution were used to inoculate a starter culture with a pipette dipped of selected glycerol stock, and incubated at 37°C for 8 hours in shaking incubator at 250-300 rpm. Next, the starter culture was diluted with LB medium (1:500) with appropriate antibiotics, and the sample was then cultured at 37 °C for 12-16 hours in orbital shaker at 250-300 rpm to gain good plasmid yields. The processes after this step were carried out at room temperature. After incubation overnight, the suspension was centrifuged at 5,000 g for 10 minutes to create the pellet and discard the supernatant. After the bacterial pellet was further re-suspended thoroughly with chilled Resuspension/RNase A Solution (Sigma, USA), lysing the cells was performed with Lysis solution (Sigma, USA). The suspension was left for 3-5 minutes until it became clear and viscous. The samples was next neutralised by using chilled Neutralization Solution to form a white aggregate, and Binding Solution was added to bind the plasmid DNA, before the sample was immediately poured into the prepared syringe and let to stand for 5 minutes. While waiting, a GenElute HP Maxiprep Binding Column was placed into a 50 ml collection tube provided in the kit, and washed by Column Preparation Solution, before being spun at 3,000 g for 2 minutes and the eluate was discarded. Subsequently, the plunger was placed into the filter syringe placed over the binding column, and then gently applied to squeeze the cleared lysate to pass through the filter and go to the binding column. The solution was centrifuged at 3,000 g for 2 minutes and the flowthrough was discarded, before the DNA was washed twice with Wash Solution 1 and Wash Solution 2, and centrifuged at 3,000 g for 2 minutes and 5 minutes, respectively. Finally, after the column was transferred to a new collection tube, and

Elution solution was added to elute the plasmid, the sample was centrifuged at 3,000 g for 5 minutes. The eluate DNA was transferred to a new Eppendorf and kept at -20°C. The concentration of DNA was measured and the sequencing was performed as described in section 2.1.2.4.

2.1.3 Transfections of Plasmids

TPC1 cells were seeded at 75,000 cells per well of 6-well plates, while the other cells, including SW1736, MCF7, HeLa and HCT116, were seeded into 6 well plates at 150,000 cells each well. After being seeded in 6-well plates and incubated at 37°C and 5% CO_2 condition for 24 hours, cells were transfected at 70-80% confluence with TransIT®-LT1 reagent (Mirus, USA). Prior to transfection, 2 μg of plasmid DNA were added into 200 μl of Opti-MEM serum-free media (Invitrogen, UK) and left for 5 minutes at room temperature, before being incubated with 6 μl of transfection reagent for the next 20 minutes to allow complex formation. After the desired solution was added to each well containing cells and incubated for further 24-48 hours, experiments were performed. No media change was done for all cell lines.

2.1.4 Short Interfering (siRNA) Transfection

Cells were seeded in 6-well plates as described in section 2.1.3 and incubated at 37°C and 5% CO_2 condition for 24 hours. Cells were transfected at 70-80% confluence with siPORT™ NeoFX™ (Invitrogen, UK). Prior to transfection, 10 μl of silencer cortactin siRNA 4666 and 4667 (concentration 10 μM, Invitrogen, UK) or 2.5 μl of negative

control siRNA or scramble siRNA (concentration 40 μM, Invitrogen, UK) were added into 100 μl of Opti-MEM serum-free media (Invitrogen, UK) to make the final concentration 50 nM. In the meantime, 5 μl of siPORT™ NeoFX™ were diluted into 100 μl of Opti-MEM serum-free media (Invitrogen, UK), and left for 10 minutes at room temperature, before being combined and incubated at room temperature for the next 10 minutes for allowing complex formation. The 200 μl of transfection solution were then dispensed in each well and incubated for a further 24 hours before overexpression experiments were performed.

2.2 Protein Extraction and Quantification (Bicinchoninic Acid Assay or BCA)

After cells were washed with phosphate buffered saline (PBS), proteins were harvested with RIPA buffer (50 mM Tris-HCl, pH 7.4, 150 mM NaCl, 1% (v/v) Igepal CA-630, 6 mM sodium deoxycholate and 1 mM ethylenediaminetetraacetic acid or EDTA) or modified RIPA buffer (50 mM Tris-HCl, pH 7.4, 150 mM NaCl, 1% (v/v) Igepal CA-630, 6 mM Sodium deoxycholate and 1 mM ethyleneglycol bis(2-aminoethyl ether)-N,N,N',N' tetraacetic acid or EGTA) combined with a protease inhibitor (Sigma, USA) and two phosphatase inhibitor cocktails (Sigma, USA) in proportion of 1 ml: 60 μl: 10 μl: 10 μl, respectively. For the phosphoprotein study, the cells were treated with pervanadate (100 μM) at 37°C for 20 minutes before being harvested with modified RIPA as described above. The samples were then incubated at -20°C for 20-30 minutes. Once thawed, the plates were scraped and samples were centrifuged at 13,200 rpm, at 4°C for 20 minutes before cell debris was discarded.

Subsequently, the Bicinchoninic Acid (BCA) assay was carried out by adding 80 μl of BCA reagents, combining BCA reagent A and reagent B (Fisher Scientific, UK) in the ratio of 50:1, in 4 μl of each protein sample, before protein concentration was determined by measuring absorbance at 560 nm with a Wallac Victor^3 plate reader (Perkin-Elmer, USA). This value was used to calculate the quantity of protein applied in Western blotting analysis.

2.3 Protein Homogenisation

After weighing the frozen human tissues, the master mix containing modified RIPA (50 mM Tris-HCl, pH 7.4, 150 mM NaCl, 1% (v/v) Igepal CA-630, 6 mM Sodium deoxycholate and 1 mM EGTA), a protease inhibitor (Sigma, USA) and two phosphatase inhibitor cocktails (Sigma, USA) was made in the proportion of 1 ml: 60 μl: 10 μl: 10 μl, respectively. Then, 350 μl of the master mix were aliquoted into the polyethelene tube containing tissue before homogenisation. After the samples were centrifuged at 1,000 rpm for 1 minute to get rid of air bubbles and transferred to new Eppendorf tubes, they were centrifuged again at 13,200 rpm at 4 °C for 20 minutes to get rid of debris and the supernatant was next transferred to new Eppendorf tubes. The Bicinchoninic Acid (BCA) assay was then carried out as described in section 2.2.

2.4 RNA (Ribonucleic Acid) Extraction in Cell Lines

After cells were seeded at an appropriate cell density in a 6-well plate and transfected for 24-48 hour, cells were washed with 1 ml phosphate buffered saline

(PBS), before being harvested with 500 µl Tri-reagent (Sigma, USA) in each well of 6-well plate. Cells were next scraped and the content was transferred to new Eppendorf tubes and frozen at -80°C overnight. Once thawed, 100 µl (200 µl/ml Tri-reagent) Chloroform (Sigma, USA) were aliquoted into each Eppendorf tube and samples were shaken vigorously for 15 seconds, before being left to stand at room temperature for 15 minutes. Subsequently, the samples were centrifuged at 12,000 g for 15 minutes at 4°C to separate RNA content from protein and DNA. The clear aqueous layer was transferred to new Eppendorf tubes before 250 µl (500 µl/ml Tri-reagent) isopropanol (Sigma, USA) were added and mixed gently. The samples were then left to stand at room temperature for 10 minutes before being centrifuged at 12,000 g for 10 minutes at 4°C. Supernatant was removed and the pellet was washed with 500 µl (1 ml/ml Tri-reagent) of 75% ethanol and vortexed vigorously, before the Eppendorfs were centrifuged at 9,000 g for 5 minutes at 4°C. After the ethanol was all discarded and the pellet was left to air dry at room temperature for 10 minutes, 30 µl of nuclease free water were applied to resuspend the pellet. The concentration of RNA samples were quantified using the NanoDrop Spectrometer (NanoDrop Products, USA) and the extracted RNA products were stored at -80°C.

2.5 Western Blotting

After protein extraction, samples were prepared for Western blotting by combining the proteins with 4 times Laemmli buffer (Biorad, USA), containing 2-Mercaptoethanol (Sigma, USA), and then they were incubated at 37°C for 30 minutes, allowing them to be denatured.

12% and 15% sodium dodecyl sulphate-polyacrylamide gels were used, with or without 5% stacking gels. Samples were loaded into each well alongside 5 μl of Precision Plus protein standards dual colour (Biorad, USA), used as protein ladder marker, in the first lane of each gel. Different sizes of protein were run and separated by electrophoresis at 70 V, until protein markers passed through the stacking gel, before increasing the voltage to 140 V, leading them to run through the bottom of the resolving gels. Proteins were transferred from resolving gels to Polyvinylidene Fluoride (PVDF) membranes (Fisher Scientific, UK) in wet transferred apparatus at 360 mA for 1 hour 15 minutes, before blocking membranes were performed with 5% non-fat milk in Tris-Buffered Saline with Tween (TBS-T; 50 ml of 1 M Tris pH 7.6, 20 gm sodium chloride, 0.625 ml of Tween 80 and 2447.5 ml of distilled water) or 5% bovine serum albumin (BSA) in TBS-T, depending on the primary antibodies, for 1 hour at room temperature to reduce non-specific protein binding. After being probed with primary antibodies in 5% non-fat milk or 5% BSA in TBS-T (ranging from 1:500 to 1:10000 concentration) at 4°C overnight, the membranes were washed in TBS-T for ten minutes, three times, and then incubated with appropriate horseradish peroxidise conjugated secondary antibodies in 5% non-fat milk in TBS-T (1:2000) at room temperature for one hour before being washed for additional three times of TBS-T. Finally, ECL-2 (Thermo Scientific, UK) or Supersignal West Pico Chemiluminescent Substrate (Thermo Scientific, UK) was applied onto the membranes to visualise protein bands on films.

The primary antibodies used for Western blotting were mouse anti-flag (1:500, Sigma, USA), mouse anti-HA (1:1000, Cambridge, UK), rabbit anti-NIS (1:500, Abcam, USA), rabbit anti-PBF (1:500, In-house), mouse anti-cortactin (1:500, Merck and

Millipore, Germany), mouse anti-Myc Tag 9B11 (1:1000, Cell Signaling Technology, USA) and mouse anti-β-actin AC-15 (1:10000, Sigma, USA).

2.6 Immunofluorescence Microscopy

After 48 hours of transfection, cells on coverslips were washed with phosphate buffered saline (PBS) and then incubated with fixing solution (0.1M phosphate buffer Na_2HPO_4 (pH 7.4), 2% paraformaldehyde (PFA), 2% glucose, 0.02% sodium azide) for 20 minutes at room temperature. After rinsing twice with PBS, cells were permeabilised by placing the coverslips in chilled 100% methanol for 10 minutes. Next, cells were briefly washed with PBS two times before being blocked in 10% newborn calf serum (NCS) (Invitrogen, UK) in PBS for further 30 minutes. Primary antibodies, including mouse anti-flag (1:200, Sigma, USA), mouse anti-HA (1:200, Cambridge, UK), rabbit anti-HA (1:200, Santa Cruz Biotechnology, UK), mouse anti-cortactin (1:100, Merck and Millipore, Germany), mouse anti-Myc Tag 9B11 (1:500, Cell Signaling Technology, USA), rabbit anti-NIS (1:500, Abcam, USA), rabbit anti-PBF (1:100, In-house) and rabbit anti-phosphoPBF (Y174, 1:50, In-house), were added into 1% bovine serum albumin (BSA) (Jackson Immunoresearch, USA) in PBS. The coverslips were lowered onto the antibody solutions for one hour and then rinsed three times with PBS, before further incubated in secondary antibody diluted in 1% NCS in 1% BSA for an hour at room temperature. The secondary antibodies comprised Alexa-Fluor-594-conjugated goat anti-rabbit IgG (1:250, Invitrogen, UK), Alexa-Fluor-488-conjugated goat anti-mouse IgG (1:250, Invitrogen, UK) and Hoechst (1:1000, Invitrogen, UK). The coverslips were returned into the wells and washed three times with PBS, before mounted onto slides with Dako Fluorescent Mounting Solution (Dako, Denmark) and allowed to dry. Finally, the cells

were visualised using a Zeiss Axioplan fluorescence microscope (Zeiss, Germany) with 10x and 100x objectives.

2.7 Protein Half-life Studies

MCF7 and SW1736 cells were transfected with vector only (VO), HA tagged or FLAG-tagged wild-type PBF and PBF mutants, and then incubated for 48 hours at 37°C, 5% CO_2. 1 ml of Opti-MEM serum-free media (Invitrogen, UK), containing 5 μl of Anisomycin (Sigma, USA), was added into each well of 6-well plate and then incubated for 0, 12 and 24 hours. Subsequently, protein samples were harvested as above before Western blotting was performed with mouse anti-HA, 1:1000 (Covance, USA), mouse anti-FLAG, 1:500 (Sigma, USA) and mouse anti-β-actin, 1:10000 (Sigma, USA) as primary antibodies, while the secondary antibody was rabbit anti-mouse, 1:2000 (Dako, UK). Densitometry was measured with Image J software to quantify the interested bands taken from Western blotting and then the half-life of each mutation was calculated as a ratio to β-actin to assess protein stability, compared with wild-type PBF.

2.8 Cell Proliferation Assays

2.8.1 3-(4,5-Dimethylthiazol-2-yl)-5-(3-Carboxymethoxyphenyl)-2-(4-Sulfophenyl)-2H-Tetrazolium (MTS) Proliferation Assays

The CellTiter 96® AQ_{ueous} One Solution Cell Proliferation Assays (Promega, UK) contains a tetrazolium compound (3-(4,5-Dimethylthiazol-2-yl)-5-(3-Carboxymethoxyphenyl)-2-(4-Sulfophenyl)-2H-Tetrazolium, inner salt; MTS) and an electron coupling reagent (Phenazine Ethosulfate; PES), being combined with MTS to form a stable complex solution. The MTS reagent is converted by NADPH in metabolically active cells into a formazan product that is soluble in culture medium. This conversion results in a colorimetric method for quantifying the number of viable cells in proliferation assays comparing between wild-type PBF and all mutations.

After 24 hours of transfection in 6-well plates, transfected TPC1 and SW1736 cells were reseeded into a 96-well plate with six replicates in each experiment and incubated at 37°C for 24 hours. Subsequently, 20 μl of the reagent solution were pipetted into each well and the samples were incubated at 37°C for 4 hours, before the absorbance of the samples was measured with a plate reader (Perkin-Elmer, USA) at absorbance 490 nm and then analysed with Sigma Stat software to determine statistical significance.

2.8.2 Cell Proliferation ELISA, Bromodeoxyuridine (BrdU) Colorimetric Assays

The cell proliferation ELISA BrdU (colorimetric) assay (Roche, USA) is a non-radioactive method to determine cell proliferation based on the measurement of BrdU incorporation during DNA synthesis. This results in a colorimetric method used to quantify the number of viable cells in proliferation assays comparing between wild-type PBF and all mutations.

After 24 hours of transfection in 6-well plates, the TPC1 and MCF7 cells were reseeded into 96-well plates with eight replicates in each experiment and incubated at 37°C for 24 hours. Subsequently, 10 μl of the BrdU labelling solution were pipetted into each well and the cells were next incubated for 4 hours at 37°C, before 200 μl of the fixation reagent were added to the well and left for 30 minutes. Next, the fixing solution was removed and then 100 μl of the anti-BrdU-POD working solution were aliquoted in to the wells and the samples were incubated at room temperature for 90 minutes. After washing off the antibody conjugate, 100 μl of the substrate solution were added, and the samples were then incubated at room temperature for 30 minutes. Finally, absorbance of the samples was measured with a plate reader (Perkin-Elmer, USA) at absorbance 405 nm and then analysed with Sigma Stat software to determine statistical significance.

2.9 Cell Invasion Assays

After transfection for 24-48 hours, the complete media containing 10% FCS (Invitrogen, UK) were changed to be complete media containing 2% FCS (Invitrogen, UK) to be chemoattractant to drive cell invasion. After being incubated for 16 hours, the cells were trypsinised with 0.25% trypsin and resuspended in complete media containing 2% FCS. Next, they were reseeded into 8 μm growth reducing invasive chambers (BD bioscience, UK) depending on the appropriate cell-density in each cell line, and incubated at 37°C and 5% CO_2 for the next 24 hours before starting membrane staining. After being washed with PBS, the cells were fixed in 95% ethanol for 5 minutes and incubated for the next 10 minutes with Haematoxylin solution (Sigma, USA). Then,

the membranes were briefly rinsed with tap water, before being placed in Scott tap water (3.5 gm $NaHCO_3$, 20 gm $MgSO_4$ in 1 litre of water) for 5 minutes and incubated in 95% ethanol for the next 2 minutes. After Eosin was applied to the cells for 5 minutes and the cells were quickly washed in tap water, they were placed for 2 minutes in 70% and 95% ethanol, respectively. The cells were left to be dry before being mounted with Distyrene Plasticizer Xylene (DPX) (Sigma, USA) with the cells facing up. The images were captured and the cells were counted with Image J software.

2.10 Co-immunoprecipitation (Co-IP)

After 48 hours of transfection, cells were washed with PBS, and proteins were harvested with 500 μl of RIPA buffer (50 mM Tris-HCl, pH 7.4, 150 mM NaCl, 1% (v/v) Igepal CA-630, 6 mM sodium deoxycholate and 1 mM EDTA) combined with a protease inhibitor (Sigma, USA) and two phosphatase inhibitor cocktails (Sigma, USA) in the proportion of 1 ml: 60 μl: 10 μl: 10 μl, respectively and incubated on a rocker at 4°C for 30 minutes. Then the flasks were scraped and samples were sonicated twice at a medium speed setting for 30 seconds, before being incubated on a rotator at 4°C for an hour. The samples were next centrifuged at 13,200 rpm, at 4°C for 20 minutes before cell debris was discarded. Subsequently, 50 μl of protein samples were aliquoted into new Eppendorfs for Western blotting analysis as whole cell lysate samples. The remaining samples were incubated with 2.5 μl of primary antibodies, including mouse anti-flag (Sigma, UK), mouse anti-HA (Cambridge, UK), rabbit anti-HA (Santa Cruz Biotechnology, UK), mouse anti-cortactin (Merck and Millipore, Germany) and mouse anti-Myc (Cell Signaling Technology, USA), at 4°C overnight. After that, 50 μl of protein G

Sepharose™ 4 Fast Flow beads (GE Healthcare, USA) per sample were centrifuged at 2,000 g, 4°C for 1 minute to remove ethanol, before being washed with 500 μl of RIPA buffer at the same speed, for one minute, three times and then resuspended in 50 μl of RIPA per sample. Subsequently, after being added into the protein samples and incubated on a rotator at 4°C for 2 hours, the beads were rinsed with 500 μl of RIPA at 2,000 g for one minute three times. The protein was then denatured in 2x Laemmli buffer (LB) containing β-mercaptoethanol (0.72 mM) at 37°C for 30 minutes before being centrifuged to discard the beads. The bound protein samples were transferred to new Eppendorfs and used for Western blotting analysis alongside the whole cell lysate samples.

2.11 Reverse Transcription (RT)

After obtaining RNA samples, reverse transcription is required to obtain cDNA for the quantitative polymerase chain reaction (qPCR) assay. 500 ng of RNA samples were aliquoted into each Eppendorf tube and nuclease free water was added to make a total volume of 4.9 μl. The samples were incubated at 70°C for 10 minutes before placing them on ice, while preparing a master mix of the reverse transcription assay (Promega, USA). The master mix contained 2 μl 25 mM $MgCl_2$, 1 μl 10x RT reaction buffer, 1 μl 10 mM dNTP (deoxynucleotide triphosphate), 0.25 μl RNasin (ribonuclease inhibitor), 0.3125 μl AMV RT (Avian Myeloblastosis Virus reverse transcriptase) buffer and 0.5 μl random hexamer primers for each sample, and 5 μl of the master mix were then aliquoted to each Eppendorf tube. After leaving to stand at room temperature for 10 minutes, the samples were heated at 42°C for 1 hour, 95°C for 5 minutes and 4°C for

5 minutes. Finally, 10 µl of nuclease free water were added to achieve the final concentration of 25 ng/µl of cDNA before stored at -20°C.

2.12 Quantitative Real-time Polymerase Chain Reaction (qPCR)

Quantitative real-time polymerase chain reaction or qPCR was used to determine the mRNA expression of specific genes of interest compared to those for internal reference genes. These experiments were performed using an ABI 7500 Sequence Detection System.

Pre-optimised Taqman probes consisted of a quencher, TAMRA (6-carboxy-tetramethyl-rhodamine) at the 3' end, and a reporter fluorophore FAM (6-carboxy-fluorescein) or VIC (full chemical name patent protected) at the 5' end. Basically, the quencher suppresses the emission of fluorescence from the fluorophore. However, 5' to 3' exonuclease activity of the Taq polymerase, due to PCR amplification, extends the primers and degrades the probes, resulting in breaking down the probes' close proximity to the quencher, releasing the fluorophore, and thereby instigating a fluorescence signal. The level of detected fluorescence is directly proportional to the amount of cDNA or RNA present in the reaction.

The PCR assay was carried out in 20 µl volumes on 96-well plates, with 2 µl (10 ng/µl) cDNA, 1 µl specific target gene expression assay (Fisher Scientific, UK), 10 µl 2x GoldStar Taqman PCR master mix (Eurogentec, UK) and 7 µl nuclease free water in each reaction. All specific target genes were labelled with FAM and the housekeeping gene,

18S, with VIC. The thermal cycle steps were as follows: 50°C for 2 minutes, 95°C for 10 minutes, 40 cycles 95°C for 15 seconds and 60°C for 1 minute.

The end data were derived from ΔCt values, which is the cycle threshold (Ct) of the target gene subtracted from the Ct of the internal reference gene. A ΔΔCt value was calculated (ΔΔCt = ΔCt of an experimental group – ΔCT of a control group), and used to ascertain a fold change with an equation: $2^{-(\Delta Ct \text{ of an experimental group} - \Delta CT \text{ of a control group})}$ or $2^{-\Delta\Delta Ct}$.

2.13 Stable Cell Line Generation

The lowest passage number of TPC1 thyroid cancer and NIH 3T3 murine fibroblast cell lines was selected to produce stable cell lines used in cell migration, colony formation and soft agar assays. These cells were cultured and passaged in specific media as described in section 2.1.1. TPC1 cells were transfected with pcDNA3.1(+) vectors containing VO, WT-PBF, C51R and R140W plasmids, while NIH 3T3 cells were transfected with pCI-neo carrying the same plasmid DNA using TransIT®-LT1 reagent (Mirus, USA) as described in section 2.1.3. After 24 hours of transfection, the appropriate antibiotic, G418 (1mg/ml), was applied into the media to select transfected cells. The cells were supplemented with fresh media containing ATB twice a week, and continuously cultured for 2 weeks, to kill untransfected cells. The transfected cells were then diluted and re-seeded in a 60 mm Petri dish with a single cell suspension, and maintained until noticeable colonies developed. Distinct colonies were selected and re-seeded in individual wells, and next cultured in normal fashion

until the cells filled T75 flasks. The protein and mRNA PBF expression of individual colonies were determined using Western blotting and TaqMan RT-PCR, respectively.

2.14 Statistical Analysis

Statistical analysis was only calculated on data sets with a minimum of 3 independent replicates carried out on 2 separate occasions. The normality of the data was determined using the Kolmogorov-Smirnov test. Data were statistically analysed using the student's *t* test and Mann-Whitney *U* test for comparison between two groups of parametric and nonparametric data, respectively. Analysis of variance and Kruskal-Wallis tests were used for between-group comparisons of multiple groups of parametric and nonparametric data, respectively. Significance was taken as $P<0.05$.

CHAPTER 3 - *IN VIVO* PBF MUTATIONS AND PREDICTION OF STRUCTURAL CHANGES AND PROTEIN DAMAGE

3.1 Introduction

Only a minority of genetic mutations are likely to be driver mutations, conferring a specific growth advantage *in vivo*, and resulting in clonal expansion and tumour development. Indeed, the majority of substitutions reported via recent sequencing strategies such as the Catalogue of Somatic Mutations in Cancer (COSMIC) and the Cancer Genome Atlas (TCGA) are likely to be passenger mutations (Torkamani, Schork 2008, Greenman et al. 2007). Functional clarification is now urgently needed to discern the driver mutations which may represent new or refined diagnostic, prognostic or therapeutic markers for particular types of cancer, and to more fully understand the mechanisms responsible for tumour formation.

We previously characterised PBF as a proto-oncogene, based on oncogenic expression inducing tumours in xenograft models (Stratford et al. 2005). We and others have demonstrated that PBF is overexpressed in pituitary, colon, breast, and thyroid tumours (McCabe et al. 2003, Read et al. 2016, Watkins et al. 2010, Stratford et al. 2005), and that upregulation of the gene is significantly associated with poorer oncological outcome in a range of tumours. For instance, papillary thyroid cancer patients with high PBF expression at the time of diagnosis show decreased disease-specific survival compared to those who have low PBF expression (Hsueh et al. 2013). Colorectal tumours which show extramural vascular invasion have significantly higher PBF expression (Read et al. 2016), and high PBF promoter activity is associated with poorer clinical outcome and increased metastatic risk in breast cancer (Xiang et al. 2012). However, whilst transgenic PBF mice demonstrated increased Akt phosphorylation, thyroid gland enlargement, hyperplasia and macrofollicular lesions,

they did not routinely develop tumours (Read et al. 2011). The role of PBF in tumourigenesis is therefore unclear.

PBF is ubiquitously expressed across a broad range of cell types and is highly conserved between diverse species (Smith, Franklyn & McCabe 2011). It interacts with a range of proteins impacting on intracellular signalling. For instance, PBF binds to the sodium iodide symporter (NIS) and the monocarboxylate transporter 8 (MCT8), modulating their subcellular localisation, and regulating radioiodine uptake and thyroid hormone efflux, respectively (Read et al. 2011, Smith et al. 2009, Smith et al. 2012). Furthermore, overexpression of PBF increases p53 ubiquitination, resulting in dysregulated p53 cellular function (Read et al. 2014). Recent in silico efforts to identify driver genes amongst next generation sequencing data identified PBF as a putative oncogene (Melloni et al. 2014).

Classically, proto-oncogenes are oncogenic through over-expression of the wild type form of the gene. The TCGA and the COSMIC are now revealing mutational changes in proto-oncogenes, opening the possibility that proto-oncogenes may, in rare cases, also act as oncogenes through disrupted function, rather than simply enhanced expression. Utilising PBF as a paradigm of this idea, the first 10 reported non-synonymous mutations of PBF in the COSMIC were assessed to determine whether they might have oncogenic gain of function. The predicted influence of these 10 *in vivo* missense substitutions of PBF was screened using Iterative Threading Assembly Refinement (I-TASSER) server and Sorting Intolerant From Tolerant or SIFT assessment. The work presented in Chapter 3 therefore initially addresses the hypothesis that the first ten PBF missense substitutions in human cancer might be oncogenic.

3.2 Materials and Methods

3.2.1 Catalogue of Somatic Mutations in Cancer (COSMIC)

The COSMIC database, started in 2004, is designed to exhibit somatic mutation information and contains clinical details relating to human cancers. There are two ways that this database collects data, consisting of getting data either from scientific literature reviews or from the Cancer Genome project at the Sanger Institute.

This website currently contains information on more than 19,000 publications. It also displays the data of complex phenotype-specific mutations in a graph format for easy understanding and interpretation (http://cancer.sanger.ac.uk) (Forbes et al. 2015, Forbes et al. 2011, Forbes et al. 2008).

3.2.2 The Cancer Genome Atlas (TCGA)

The TCGA database was launched in 2006 and is supervised by the National Cancer Institute (NCI) and the National Human Genome Research Institute (NHGRI). This project uses genetic sequencing and bioinformatic data to display mutations apparent in human cancers and also to generate statistically significant conclusions from information generated (https://tcga-data.nci.nih.gov) (Cline et al. 2013, Guo et al. 2013).

3.2.3 Predicted 3-dimensional (3D) Modeling (Iterative Threading Assembly Refinement (I-TASSER) Server)

This program, an online website begun in the Yang Zhang lab at University of Michigan, is a method used for the prediction of the three-dimensional structure of proteins originating from the sequence of amino acid residues, allowing them to be estimated in terms of protein damage (http://zhanglab.ccmb.med.umich.edu) (Yang, Zhang 2015, Zhang 2008).

3.2.4 Prediction of Protein Damage (Sorting Intolerant From Tolerant or SIFT)

SIFT is a program used to predict whether an amino acid substitution impacts upon protein function and may be responsible for phenotypic differences. Based on this principle, if there is a substitution in an amino acid residue that does not impact on the subtype of amino acid, such as a change from a hydrophobic to another hydrophobic amino acid, this alteration is predicted to be a tolerated protein. Nevertheless, if a mutation causes a considerable adaptation in alignment to another amino acid character (such as polar type), it is expected to be a 'damaged protein', with a SIFT calculated score of less than 0.05. A genetic substitution with a SIFT score more than 0.05 is predicted to be a 'tolerated protein' (http://sift.bii.a-star.edu.sg) (Ng, Henikoff 2006, Ng, Henikoff 2003).

3.3 Results

3.3.1 Discovered Mutations

3.3.1.1 Catalogue of Somatic Mutations in Cancer (COSMIC)

At the outset of this PhD study (April 2013), whole exome sequencing through the Wellcome Trust COSMIC database initially identified ten missense PBF substitutions in human cancers (Figure 3.1). The mutations occurred across all functional domains of PBF, with no obvious 'hot-spots' other than 3 substitutions at residue G106, within the transmembrane region (Figure 3.1). The 8 mutated amino acid residues were highly conserved across various species as demonstrated in Figure 3.1. The multiple substitutions in this protein were also found in various tumour types, such as colon, breast, ovary and prostate, suggesting that PBF may potentially be oncogenic *in vivo*, and that substitutions in some domains may affect functions of the protein and prognosis of cancers. These first reported 10 non-synonymous mutations discovered in the COSMIC in April 2013 which occurred at 8 different amino acid residues within PBF were chosen as the panel of mutations to pursue throughout this PhD.

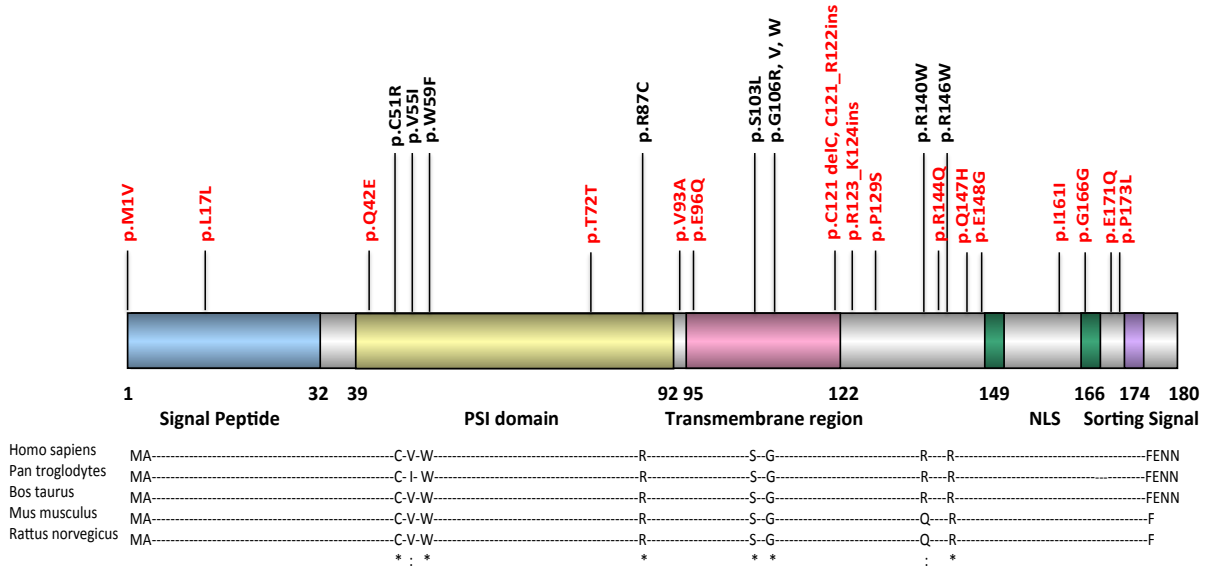

Figure 3.1: Schematic diagram of PBF. *The first 10 reported missense amino acid residue changes denoted in black with amino acid conservation at each site in 5 different*

species. An asterisk (*) denotes amino acid which is fully conserved residue, while a colon (:) indicates a conservation site between amino acids with strongly similar properties. There are four mutations in the PSI domain, consisting of C51R, V55I, W59F and R87C, while substitutions of S103L, G106R, G106V and G106W are present in the transmembrane region. In addition, mutations being proximal to the NLS (nuclear localisation signal) are R140W and R146W. The other 17 PBF mutations discovered in the COSMIC database after April 2013 are highlighted in red. Ins denotes insertional mutagenesis, while del illustrates deletion mutation. Adapted from https://ebi.ac.uk/Tools/msa/clustalo/ and the COSMIC database, May 2016.

The most common cancer harbouring *in vivo* PBF mutations was colon cancer (Table 3.1). There were 7 PBF mutations (8 patients) identified in colon cancer, while the other mutations were found in prostate, lung and ovary tumours (Table 3.1). However, there was no obvious correlation between clinicopathological data, such as gender, age, tumour differentiation, staging or vascular invasion, and the specific PBF mutations (Table 3.1).

PBF mutations	Gender	Age	Organ	Histology	TNM	Vascular invasion	Zygosity
C51R	F	66	Colon	Adenocarcinoma, poorly diff.	T4bN0M0	-	Heterozygous
V55I	M	54	Prostate	Carcinoma	Unknown	Unknown	Unknown
W59F	F	71	Lung	Adenocarcinoma, acinar type	T2aN0M0	Unknown	Unknown
R87C	F	58	Colon	Adenocarcinoma, moderately diff.	T3N0M0	-	Heterozygous
S103L	M	70	Colon	Adenocarcinoma, moderately diff.	T3N2aM0	+	Heterozygous
G106R	F	63	Ovary	Serous carcinoma	Unknown	Unknown	Heterozygous
G106V1	M	68	Colon	Adenocarcinoma, moderately diff.	TxN1bM0	-	Heterozygous
G106V2	M	45	Colon	Adenocarcinoma, moderately diff.	T3N0M0	-	Heterozygous
G106W	F	45	Colon	Adenocarcinoma, well diff.	T3N0M0	+	Heterozygous
R140W	F	58	Colon	Adenocarcinoma, moderately diff.	T3N0M0	-	Heterozygous
R146W	M	78	Colon	Adenocarcinoma, moderately to poorly diff.	T2N0M0	-	Heterozygous

Table 3.1: Clinical and histological data of patients having PBF mutations discovered in various human cancers. *M = male, F = female. T = tumour, N = node, M = metastasis.*

3.3.1.2 The Cancer Genome Atlas (TCGA)

Whilst the first 10 missense mutations in PBF were described via the COSMIC in 2013, subsequent sequencing via the TCGA initiative has revealed other numerous genetic abnormalities of PBF in multiple human cancers. Most of these are genetic amplifications of PBF, while fewer than 0.5% of reported changes represented overall mutations in this gene (Figure 3.2).

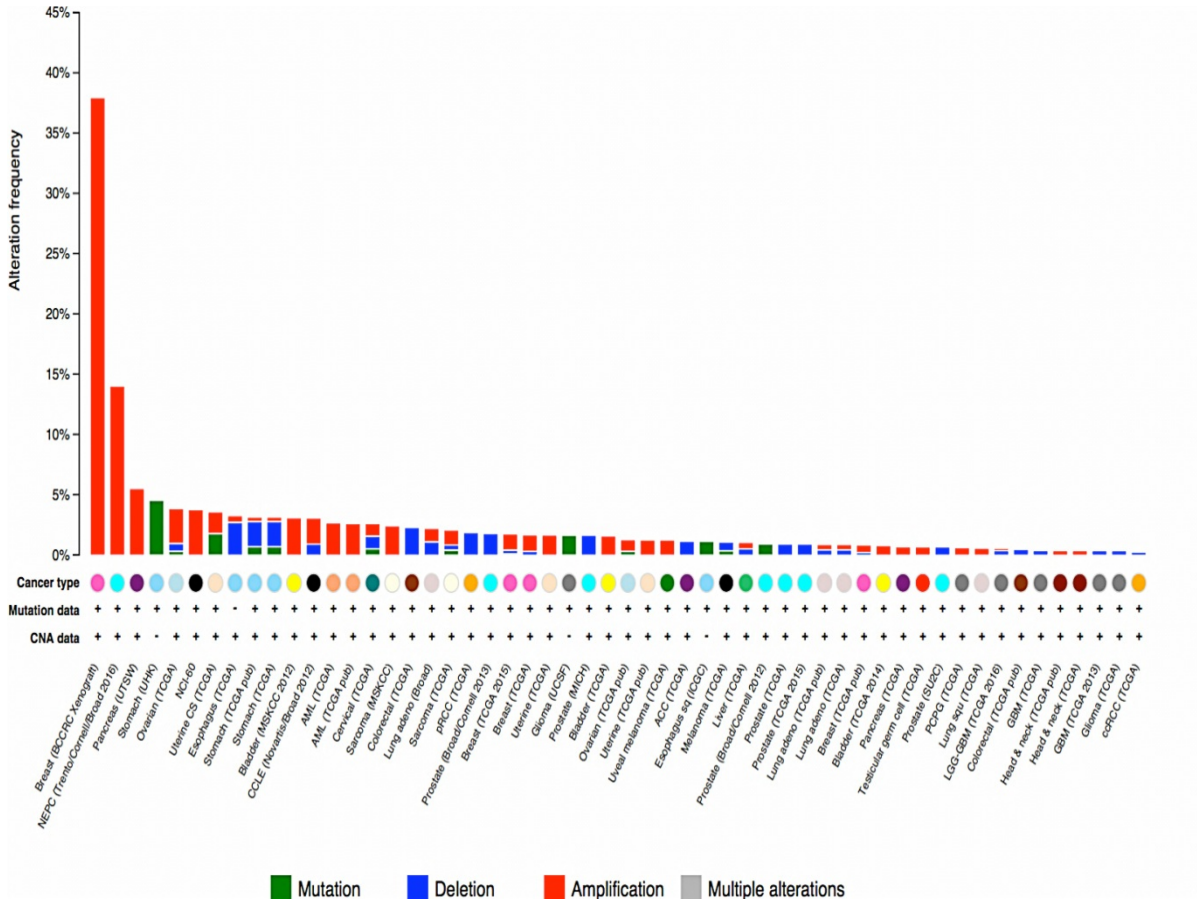

Figure 3.2: The percentages of cross cancer alterations of the PBF gene in various human tumours. *The figure was taken from http://www.cbioportal.org/public-portal/cross_cancer.do?cancer_study_id. Data was adapted in May 2016.*

Some substitutions, such as Q42E, C121del, P129S, R140Q, R144Q and E171Q, were additionally identified in this database (Table 3.2). Nevertheless, in May 2016, 511 papillary thyroid cancer samples and 117 poorly differentiated and anaplastic thyroid cancers were sequenced but there were no mutations in PBF (www.cbioportal.org). Thus, whilst PBF has an integral role in regulating thyroid cell function (Read et al. 2011), it is not commonly mutated in thyroid cancer. However, mutations are more common in other endocrine and non-endocrine tumour types.

Sample ID	Cancer Study	AA change	Type	COSMIC	MS	VS	Mutation Assessor	Allele Freq (T)	#Mut in Sample
TCGA-N9-A4Q1-01	Uterine CS	*C121del*	IF del	1	S	U		0.05	48
TCGA-JW-A5VL-01	Cervical	*Q42E*	Missense		S	U	Neutral	NA	1762
TCGA-EE-A29R-06	Melanoma	*P129S*	Missense	1	S	U	Low	0.60	535
TCGA-DX-A7EF-01	Sarcoma	*N94Mfs*4*	FS del		S	U		NA	55
TCGA-BR-8382-01	Stomach	*K164Nfs*89*	FS del		S	U		0.16	747
TCGA-BR-8382-01	Stomach	*K164Nfs*89*	FS del		S	U		NA	744
TCGA-BR-6452-01	Stomach	*R140Q*	Missense	2	U	U	Low	0.25	6437
TCGA-BR-6452-01	Stomach	*R140Q*	Missense	2	S	U	Low	NA	6415
TCGA-A8-A0A7-01	Breast	*E153K*	Missense		U	U	Medium	0.06	119
TCGA-13-0760-01	Ovarian	*G106R*	Missense	4	S	V	Medium	NA	147
TCGA-13-0760-01	Ovarian	*G106R*	Missense	4	S	V	Medium	NA	149
PR-00-1165	Prostate	*V55I*	Missense	1	S	U	Medium	NA	707
pfg011T	Stomach	*R144Q*	Missense	2	U	U	Medium	NA	84
P01_Rec	Glioma	*A114T*	Missense		U	U	Neutral	0.45	1200
ESCC-153T	Esophagus SCC	*E171Q*	Missense	1	S	U	Neutral	0.22	143

Table 3.2: The in vivo substitutions of amino acid residues of PBF found in various cancers, reported by the TCGA database. *COSMIC = number of occurrences in*

overlapping mutations with the COSMIC database, MS = mutational status; U-unknown and S-somatic, VS = validation status; U-unknown and V-valid, Mutation assessor = predicted impact score from www.mutationaassessor.org; low or neutral - predicted non-functional mutations and medium or high - predicted functional mutations, Allele Freq = variant allele frequency in the tumour sample, #Mut in Sample = total number of nonsynonymous mutations in the sample. The figure was adapted in May 2016 from http://www.cbioportal.org/public-portal/cross_cancer.do?cancer_study_id.

Thus, whilst subsequent TCGA sequencing has recently revealed further mutations in PBF, some of which overlap with the COSMIC initiative, all data presented in this thesis relate to the first 10 missense mutations reported via the COSMIC.

3.3.2 Predicted 3-dimensional (3D) Modeling

Analysis of the 10 amino acid changes via the I-TASSER server yielded predicted 3-dimensional protein structures of wild-type PBF, compared with the mutated proteins (Figure 3.3).

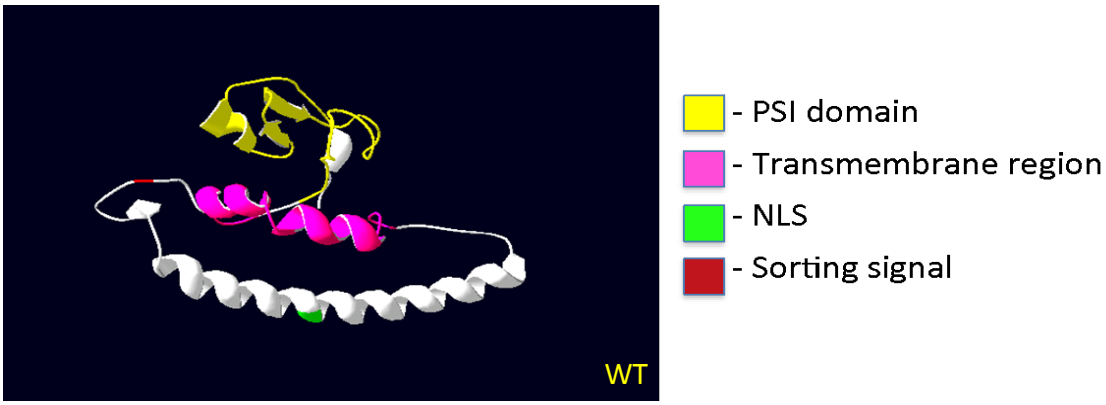

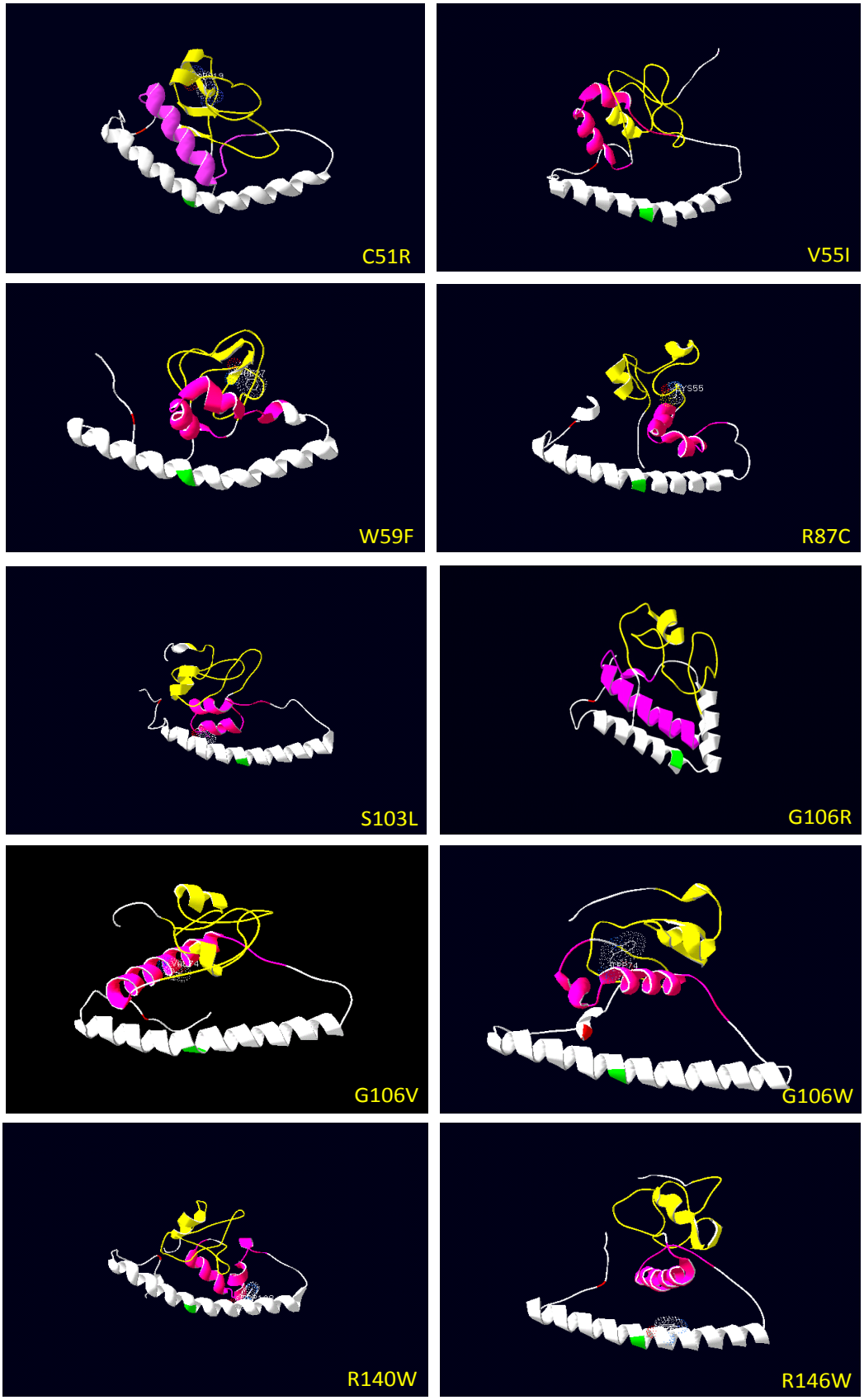

Figure 3.3: 3-dimentional structures of WT-PBF and all 10 in vivo mutations, based on the physical properties of amino acid changes. *For this analysis, the N-terminal*

signal peptide (amino acids 1-32), which is predicted to be cleaved off during PBF processing (Stratford et al. 2005), was omitted to clarify the putative structure of fully processed PBF. For most mutations, substitution of one residue within PBF often implied a considerable change in another part of the protein. The PSI domain, the transmembrane region, the NLS and the sorting signal were denoted with yellow, pink, green and red, respectively.

Overall, missense-substitution of only one amino acid residue caused significant predicted changes in 3-dimensional protein structure, suggesting that these modifications may impact on protein function. Indeed, mutant G106R showed the biggest effect on 3D structure of PBF with a predicted transition of a long helix (shown in white in Figure 3.3) to a helix-loop-helix structure. This helix is part of a putative coiled coil domain, which may therefore impact on the ability of PBF to dimerise and /or interact with other proteins. In addition, access to the C-terminus of PBF may be altered affecting the potential binding of proteins within this region. Given the C-terminal location of the NLS and the sorting signal at tyrosine 174, this may result in aberrant nuclear translocation, endocytosis and phosphorylation of PBF.

3.3.3 Prediction of Protein Damage (Sorting Intolerant From Tolerant or SIFT)

SIFT assessment, based on sequence homology and physical properties of amino acids, was applied for all missense PBF mutations to predict whether specific amino acid substitutions might alter protein function (Table 3.3).

User Input	Position	Reference	Substitution	Prediction	SIFT score
ENSP00000328325,C51R	51	C	R	DAMAGING	0
ENSP00000328325,V55I	55	V	I	DAMAGING	0.05
ENSP00000328325,W59F	59	W	F	DAMAGING	0.02
ENSP00000328325,R87C	87	R	C	DAMAGING	0
ENSP00000328325,S103L	103	S	L	DAMAGING	0.01
ENSP00000328325,G106R	106	G	R	DAMAGING	0.01
ENSP00000328325,G106V	106	G	V	TOLERATED	0.12
ENSP00000328325,G106W	106	G	W	DAMAGING	0
ENSP00000328325,R140W	140	R	W	DAMAGING	0
ENSP00000328325,R146W	146	R	W	DAMAGING	0

Table 3.3: SIFT scores taken from the SIFT prediction of potential protein damage for all substitutions. *Scores less than 0.05 are expected to affect protein function. User input = protein ID plus name of mutation, ESPN = protein ID, Pos = position of amino acid change, Ref = amino acid reference, Subst = amino acid substitution, Prediction = results of predicted protein damage; tolerated = a predicted tolerated protein and damaging = a predicted damaged protein, SIFT score = score predicted potential protein damage in each substitution, with range from 0-1.*

According to SIFT analysis, all mutations except G106V were predicted to elicit protein damage. However, the 3-dimensional predicted G106V structure illustrated considerable changes in the PSI domain and transmembrane region, and so all ten substitutions were considered as candidate changes to investigate *in vitro* in subsequent Chapters.

3.4 Discussion

Recent initiatives such as the COSMIC and the TCGA are unearthing myriad mutational events in thousands of human tumours. However, only a minority of these will confer selective growth advantage and clonal expansion of the cells in which they are found. The silent majority, passenger mutations, are likely to represent the product of the unstable genetic environments which generally develop during cancer progression, and are unlikely to significantly impact upon protein function.

A number of statistical approaches have been utilised to help predict driver mutations and driver genes, based largely on protein function, mutational frequency, pathway-oriented and pattern-based principles. One such statistical approach, the Driver Oncogene and Tumor Suppressor Finder, developed a computational program to identify driver genes based on statistical approaches including pattern-based, protein function and frequentist methods (Melloni et al. 2014). This strategy predicted that PBF may be one of 12 genes driving thyroid carcinogenesis in 326 tumour samples from the TCGA database (Melloni et al. 2014). The McCabe lab has previously appraised the oncogenic function of PBF in numerous studies (Read et al. 2014, Read et al. 2011, Watkins et al. 2010), and has reported significantly induced expression of the gene in thyroid, breast, pituitary, and colorectal tumours (Smith, Franklyn & McCabe 2010, Read et al. 2011, Watkins et al. 2010, McCabe et al. 2003, Read et al. 2016).

PBF is a widely expressed glycoprotein with a 180 amino acid sequence possessing an N-terminal signal peptide, a, PSI domain, a transmembrane region, a bipartite nuclear localisation signal and a putative tyrosine sorting signal. PBF shares no significant homology to any other human proteins but is well-conserved among a diverse range of animal species. In addition, PBF expression is significantly correlated

with poorer oncological outcomes in thyroid, breast and colon cancers (Hsueh et al. 2013, Xing et al. 2005, Read et al. 2016).

According to the COSMIC and the TCGA, the reported PBF mutations were apparent across all domains of PBF at specific residues which are highly conserved in various animal species, such as pongo abelii, pan troglodytes, canis lupus, bos taurus and macaca fascicularis, suggesting that these amino acid residues are functionally important (Figure 3.1). However, there has been a recent increase in the number of identified PBF substitutions due to further sequencing initiatives since the start of this project. Currently, there are 27 reported PBF mutations in the COSMIC database, the vast majority being single amino acid substitutions. The overall incidence of PBF mutations across all cancers sequenced to date via the TCGA is less than 0.5%. No PBF mutations have been reported in thyroid cancer; indeed the majority in this study were apparent in colorectal cancer. In this Chapter, we also found no correlation between PBF mutation status and clinical outcome in colorectal cancer. This is in contrast to previously published clinical associations in colorectal cancer, as well as in thyroid and breast neoplasias, where PBF expression significantly correlated with tumour grade and/or patient outcome as mentioned above. Nevertheless, even though a range of genetic mutations has been reported, only a few of them are likely to impact on cancer cell initiation and development (Melloni et al. 2014). Therefore, in this study, we focused on the first 10 discovered non-synonymous PBF mutations in the COSMIC database.

The I-TASSER results were applied to amino acid sequences of WT-PBF and all 10 *in vivo* missense PBF mutants, and revealed that all amino acid substitutions were predicted to modify 3D protein structure compared to wild-type. Moreover, the SIFT

assessment, a programme used to predict altered protein function, affirmed that most mutations were predicted to cause protein damage, except G106V. There are further ways to assess for prediction of the functional protein impact of amino acid substitutions in proteins, such as Mutation assessor or PolyPhen approaches. However, there is still no definitive computational programme for the confirmation of driver mutation status. It therefore remains necessary to carry out a range of experiments, as described in the subsequent Chapters, to clarify whether the PBF *in vivo* substitutions are driver genetic mutations or not.

CHAPTER 4 - EFFECT OF AMINO ACID SUBSTITUTIONS IDENTIFIED *IN VIVO* ON SUBCELLULAR LOCALISATION, GLYCOSYLATION, DIMERISATION, PBF STABILITY AND CELLULAR PROLIFERATION

4.1 Introduction

Several previous studies have revealed that a monomeric band of PBF is usually observed ranging between 22-30 kDa in Western blotting (Smith et al. 2012, Boelaert et al. 2007, Chien, Pei 2000), with the size range presumably reflecting differential glycosylation (Smith et al. 2010). PBF also appears as a putative oligomer in Western blotting, running at approximately 50 and 75 kDa for dimeric or trimeric bands, respectively. However, the functional importance of PBF glycosylation and dimerisation remain inconclusive. Broadly, glycosylation is one of the most common post-translational alterations of multiple proteins (Lisowska, Jaskiewicz 2012), and also has a tendency to impact on various protein configurations and their stability (Arey 2012, Shental-Bechor, Levy 2008). This process is also vital for some secreted proteins in modulating their activity when they bind to protein ligands or receptors, and may play an important role in protein-protein interaction (Arey 2012).

Furthermore, oligomerisation is another mechanism which may influence protein stabilisation and the ability of proteins to bind to other molecules (Mei et al. 2005, Monod, Wyman & Changeux 1965). Changes in protein structure also generally contribute to alteration of protein stability, modulating protein functions in various models (Ng, Henikoff 2006, Bromberg, Rost 2009). Multiple factors impact on the stabilisation of proteins, including amino acid substitutions, hydrophobic binding, hydrogen bonds and polar interactions (Gromiha 2003, Vogt, Woell & Argos 1997, Menéndez-Arias, Argosf 1989, Imanaka, Shibazaki & Takagi 1986). Regarding genetic mutations, publications from multiple groups have demonstrated that most amino acid substitutions cause significant modifications to protein stability (DePristo, Weinreich & Hartl 2005, Ponnuswamy, Muthusamy & Manavalan 1982) as well as protein

biochemistry, including glycosylation and dimerisation. Consequently, the effect of PBF mutations identified *in vivo* on these characteristics needs to be determined.

In terms of cellular proliferation, we previously discovered that PBF overexpression induced cell turnover in various models, including thyroid, breast and colon (Read et al. 2011, Watkins et al. 2010, Read et al. 2016). PBF is transforming *in vitro* and tumourigenic *in vivo*: stable overexpression of PBF in NIH 3T3 murine fibroblast cells significantly induced colony formation in soft agar assays compared to VO control cells, reflecting anchorage independent growth or transforming ability of the transfected cells (Stratford et al. 2005). In parallel *in vivo* studies, subcutaneous injection of cells stably overexpressing PBF stimulated large and aggressive tumours in nude mice, with histopathological evaluation showing high-grade malignant cancers invading skeletal muscle and adipose tissue (Stratford et al. 2005). Read et al. also investigated a role of PBF upregulation on cellular proliferation by using a murine transgenic model and targeting PBF overexpression to thyroid gland (PBF-Tg mice) (Read et al. 2011). PBF-Tg mice showed a significant increase in the size of their thyroid glands which contained hyperplastic and macrofollicular lesions (Read et al. 2011). The immunostaining of histopathologic specimens also revealed an increase in markers of thyroid cell (thyrocyte) proliferation such as cyclin D1 (Read et al. 2011). Moreover, the study demonstrated a significant upregulation of TSHR (thyroid stimulating hormone receptor) and phosphorylated AKT (protein kinase B) in PBF-Tg mice, while total AKT was not changed (Read et al. 2011). The data in human multinodular goitre (MNG) also exhibited a strongly significant induction of PBF and TSHR protein levels compared to normal thyroid tissue (Read et al. 2011). However, PBF-Tg mice had unchanged thyroid function tests, including T3, T4 and TSH, and also no significant alteration in mRNA

levels of growth factors, such as VEGF (vascular epidermal growth factor), TGFβ (transforming growth factor beta) or IGF-1 (insulin-like growth factor-1) (Read et al. 2011). It is likely therefore that PBF induces cellular proliferation and independently governs cell growth through the TSHR and PI3K/AKT pathways in thyroid cells (Read et al. 2011).

Chapter 3 revealed that most amino acid substitutions of PBF determined *in vivo* were predicted to elicit protein damage. This Chapter therefore determined the basic functional consequences of PBF induced by these mutations, including alterations in subcellular localisation of PBF, glycosylation, dimerisation, protein stability and cellular proliferation, and sought to narrow down from 10 initial mutations to a smaller number of mutants for further studies.

4.2 Materials and Methods

4.2.1 Mutagenesis, DNA Purification (Miniprep), DNA Amplification (Maxiprep) and Sequencing

According to the results from the I-TASSER server and the SIFT assessment in Chapter 3, ten amino acid substitutions were made in the wild-type PBF plasmid with pcDNA3.1(+) backbone, and were labelled with or without an HA tag at the C-terminus or with a FLAG tag at the N-terminus, as described in section 2.1.2.2. All plasmids were transformed into Subcloning EfficiencyTM DH5αTM Competent E.Coli Cells (Invitrogen), before Minipreps were performed to purify the plasmids as mentioned in sections 2.1.2.3 and 2.1.2.4, respectively. After sequencing to confirm the correct substitutions,

the DNA plasmids were amplified and sequenced to use in subsequent experiments as described in section 2.1.2.5.

4.2.2 Cell Culture and Transfection

PBF functions have previously best been characterised in thyroid, breast and colorectal cell models (Read et al. 2016, Read et al. 2014, Smith et al. 2013, Smith et al. 2012, Smith, Franklyn & McCabe 2011, Watkins et al. 2010, Smith et al. 2009). Throughout the results chapters of this thesis, PBF is therefore examined predominantly in these models, but also occasionally in COS7 and HeLa cells, where for example immunofluorescent detail is required.

TPC1, SW1736, MCF7, HeLa and COS7 cells were employed in the experiments in this Chapter. HeLa and COS7 cells were maintained in DMEM containing 10% FCS while TPC1, SW1736 and MCF7 cells were supplemented with RPMI containing 10% FCS as described in section 2.1.1. These cells were transfected with VO and HA-tagged or untagged WT-PBF and all PBF mutations as described in section 2.1.3. Transfection of FLAG-tagged WT-PBF, C51R-PBF and R140W-PBF was also carried out for half-life studies and immunofluorescence microscopy.

4.2.3 Immunofluorescence Microscopy

HeLa and MCF7 cells were plated on coverslips and then transfected with VO, HA-tagged WT and all PBF mutations or FLAG-tagged WT-PBF, C51R-PBF and R140W-PBF as described in section 2.1.3. They were then processed as described in section 2.6.

Primary antibodies were mouse monoclonal anti-HA (1:200, Covance, USA), mouse monoclonal anti-FLAG (1:200, Sigma, USA), rabbit polyclonal anti-PDI (1:200, Cell Signaling Technology, USA) and rabbit monoclonal anti-Golgin-97 (1:200, Cell Signaling Technology, USA).

4.2.4 Protein Extraction and Quantification (Bicinchoninic Acid Assay or BCA)

After harvesting proteins in RIPA solution, absorbances were measured using the bicinchoninic acid (BCA) assay kit as described in section 2.2, with cell lysates compared to bovine serum albumin (BSA) standards of 0, 0.125, 0.25, 0.5, 0.75, 1, 1.5, 2, 2.5 and 5 mg/ml in RIPA solution. The Wallac gamma counter was used as mentioned in section 2.2 to measure the absorbance. Finally, protein concentration was determined using the standard curve from the BSA standards and then applied to calculate the protein volume used in subsequent Western blotting.

4.2.5 Western Blotting

Western blotting for half-life studies and for confirmation of transfection was carried out as described in Section 2.5. The primary antibodies used in this Chapter were mouse monoclonal anti-FLAG (1:500, Sigma, USA), mouse monoclonal anti-HA (1:1000, Covance, USA), rabbit polyclonal anti-PBF (1:500, In-house) and mouse monoclonal anti-β-actin AC-15 (1:10000, Sigma, USA).

4.2.6 Half-life Studies

MCF7 and SW1736 were utilised for half-life studies and protein samples were harvested at 0, 12 and 24 hours after adding Anisomycin as described in section 2.7.

4.2.7 Cellular Proliferation Assays

4.2.7.1 3-(4,5-Dimethylthiazol-2-yl)-5-(3-Carboxymethoxyphenyl)-2-(4-Sulfophenyl)-2H-Tetrazolium (MTS) Proliferation Assays

TPC1, MCF7 and SW1736 cells were used in MTS assays to determine cellular proliferation as mentioned in section 2.8.1. After being seeded into 6-well plates for 24 hours, cells were transfected with VO, WT-PBF, C51R, G106R, G106V, G106W and R140W for 24 hours as in section 2.1.3, before re-seeding into 96-well plates, and then MTS assays were performed 24 hours later.

4.2.7.2 Cell Proliferation ELISA, Bromodeoxyuridine (BrdU) Colorimetric Assays

TPC1 and MCF7 cells were seeded into 6-well plates and then transfected with VO, WT-PBF, C51R, V55I, R140W and R146W for 24 hours as explained in section 2.1.3. After re-seeding into 96-well plates for 24 hours, BrdU assays were applied as described in section 2.8.2.

4.3 Results

4.3.1 The Subcellular Localisation of 10 PBF Mutations Identified *in Vivo*

After the plasmids were sequenced to confirm the correct substitutions as illustrated in Figure 4.1, all ten mutations were examined for subcellular localisation of each HA-tagged mutant (green) within HeLa cells (Figure 4.2). However, HA-tagged R140W was difficult to detect through immunofluorescent microscopy, and a FLAG-tagged R140W version was therefore used and compared to wild type-FLAG (Figure 4.3).

```
Seq_1   120   CGCTGCTCCTGCTGCTCATCCCGGTGGCCGCCGCGCAGGAGCCTCCCGGAGCTGCTTGTT   179
              ||||||||||||||||||||||||||||||||||||||||||||||||||||||||||||
Seq_2   62    CGCTGCTCCTGCTGCTCATCCCGGTGGCCGCCGCGCAGGAGCCTCCCGGAGCTGCTTGTT   121

Seq_1   180   CTCAGAACACAAACAAAACCTGTGAAGAGCGCCTGAAGAACGTCTCCTGTCTTTGGTGCA   239
              |||||||||||||||||||||||||||| ||||||||||||||||||||||||||||||
Seq_2   122   CTCAGAACACAAACAAAACCTGTGAAGAGTGCCTGAAGAACGTCTCCTGTCTTTGGTGCA   181

Seq_1   240   ACACTAACAAGGCTTGTCTGGACTACCCAGTTACAAGCGTCTTGCCACCGGCTTCCCTTT   299
              ||||||||||||||||||||||||||||||||||||||||||||||||||||||||||||
Seq_2   182   ACACTAACAAGGCTTGTCTGGACTACCCAGTTACAAGCGTCTTGCCACCGGCTTCCCTTT   241

Seq_1   300   GTAAATTGAGCTCTGCACGCTGGGGAGTTTGTTGGGTGAACTTTGAGGCGCTGATCATCA   359
              ||||||||||||||||||||||||||||||||||||||||||||||||||||||||||||
Seq_2   242   GTAAATTGAGCTCTGCACGCTGGGGAGTTTGTTGGGTGAACTTTGAGGCGCTGATCATCA   301

Seq_1   360   CCATGTCGGTAGTCGGGGGAACCCTCCTCCTGGGCATTGCCATCTGCTGCTGCTGCTGCT   419
              ||||||||||||||||||||||||||||||||||||||||||||||||||||||||||||
Seq_2   302   CCATGTCGGTAGTCGGGGGAACCCTCCTCCTGGGCATTGCCATCTGCTGCTGCTGCTGCT   361

Seq_1   420   GCAGGAGGAAGAGGAGCCGGAAGCCGGACAGGAGTGAGGAGAAGGCCATGCGTGAGCGGG   479
              ||||||||||||||||||||||||||||||||||||||||||||||||||||||||||||
Seq_2   362   GCAGGAGGAAGAGGAGCCGGAAGCCGGACAGGAGTGAGGAGAAGGCCATGCGTGAGCGGG   421

Seq_1   480   AGGAGAGGCGGATACGGCAGGAGGAACGGAGAGCAGAGATGAAGACAAGACATGATGAAA   539
              ||||||||||||||||||||||||||||||||||||||||||||||||||||||||||||
Seq_2   422   AGGAGAGGCGGATACGGCAGGAGGAACGGAGAGCAGAGATGAAGACAAGACATGATGAAA   481

Seq_1   540   TCAGAAAAAAAATATGGCCTGTTTAAAGAAGAAAACCCGTATGCTAGATTTGAAAACAACT   599
              ||||||||||||||||||||||||||||||||||||||||||||||||||||||||||||
Seq_2   482   TCAGAAAAAAAATATGGCCTGTTTAAAGAAGAAAACCCGTATGCTAGATTTGAAAACAACT   541

Seq_1   600   AAAGCGCTCCAGCTCTAGAGGGCCCGTTTAAACCCGCTGATCAGCCTCGACTGTGCCTTC   659
              ||
Seq_2   542   AA------------------------------------------------------------   543
```

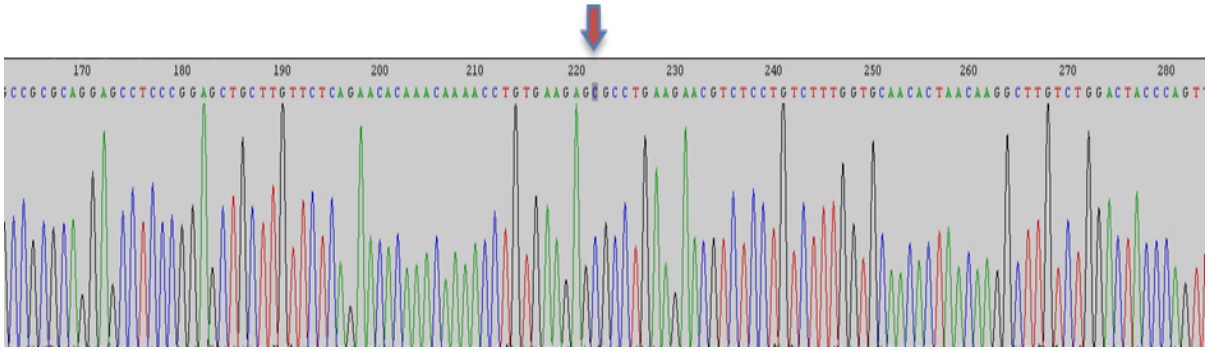

Figure 4.1: Example of sequencing result of C51R mutation. *The illustrations reveal that there was only one substitution of a nucleotide at position 151 from T to C in the PBF nucleotide sequence, as denoted by the red arrow.*

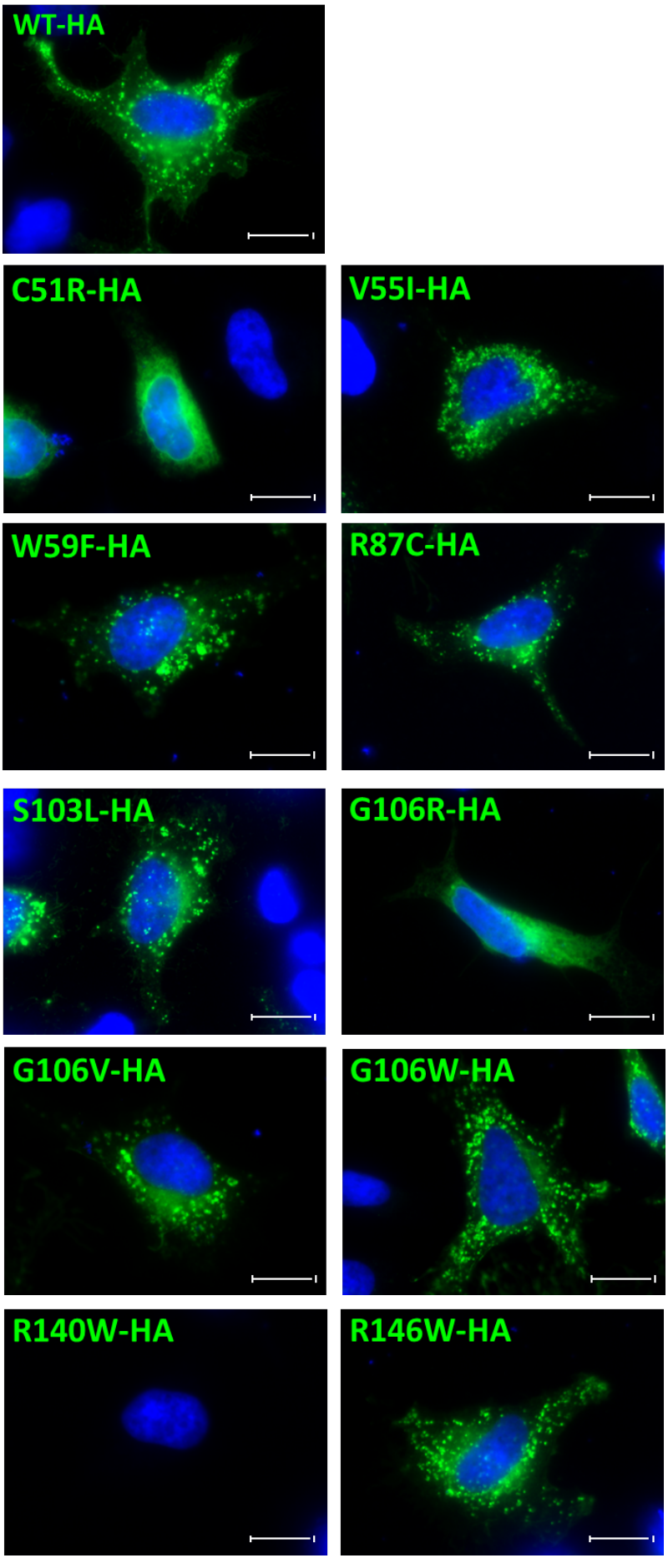
WT-HA
C51R-HA
V55I-HA
W59F-HA
R87C-HA
S103L-HA
G106R-HA
G106V-HA
G106W-HA
R140W-HA
R146W-HA

Figure 4.2: The effect of PBF substitutions on subcellular localisation. *Representative immunofluorescent microscopy of PBF-HA (mouse, anti-HA, green) and DAPI (blue) in HeLa cells transfected with HA-tagged WT-PBF and all 10 PBF mutants. Magnification = 100x. Scale bars = 20 µm.*

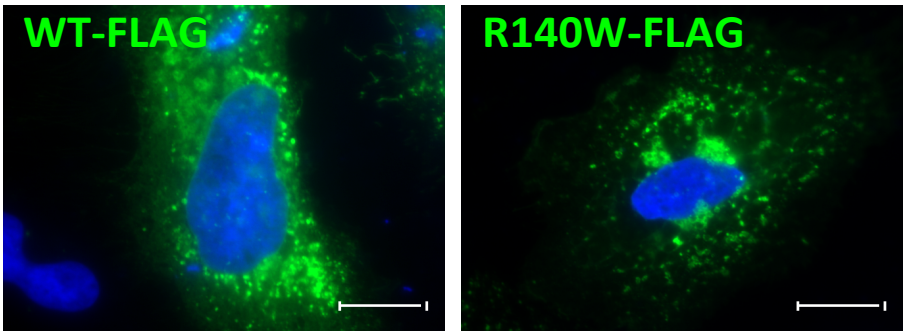

Figure 4.3: R140W substitution detected through FLAG tagging shows altered subcellular localisation compared to WT-PBF-FLAG. *Representative immunofluorescent microscopy of PBF-FLAG (mouse, anti-FLAG, green) and DAPI (blue) in HeLa cells transfected with FLAG-tagged WT-PBF and R140W mutant. Magnification = 100x. Scale bars = 20 µm.*

Overall, wild type PBF was predominantly localised in late endosomes and at the plasma membrane, as reported previously (Smith et al. 2009). Most mutants retained a wild type vesicular subcellular localisation, apart from C51R and G106R, which appeared to be localised predominantly to the endoplasmic reticulum (Figure 4.2), and R140W, which appeared to be mainly confined to the Golgi apparatus (Figure 4.3). The precise subcellular localisations of C51R and R140W are defined in further detail later within this Chapter.

4.3.2 The Influence of Amino Acid Substitutions on Glycosylation and Dimerisation

In the previous Chapter, we revealed that most amino acid substitutions were speculated to modify the predicted 3-dimensional protein structures and protein function compared to WT-PBF. Therefore, we next determined the effect of the PBF mutations on the basic biochemical glycosylation and dimerisation of the protein using Western blotting analysis (Figure 4.4).

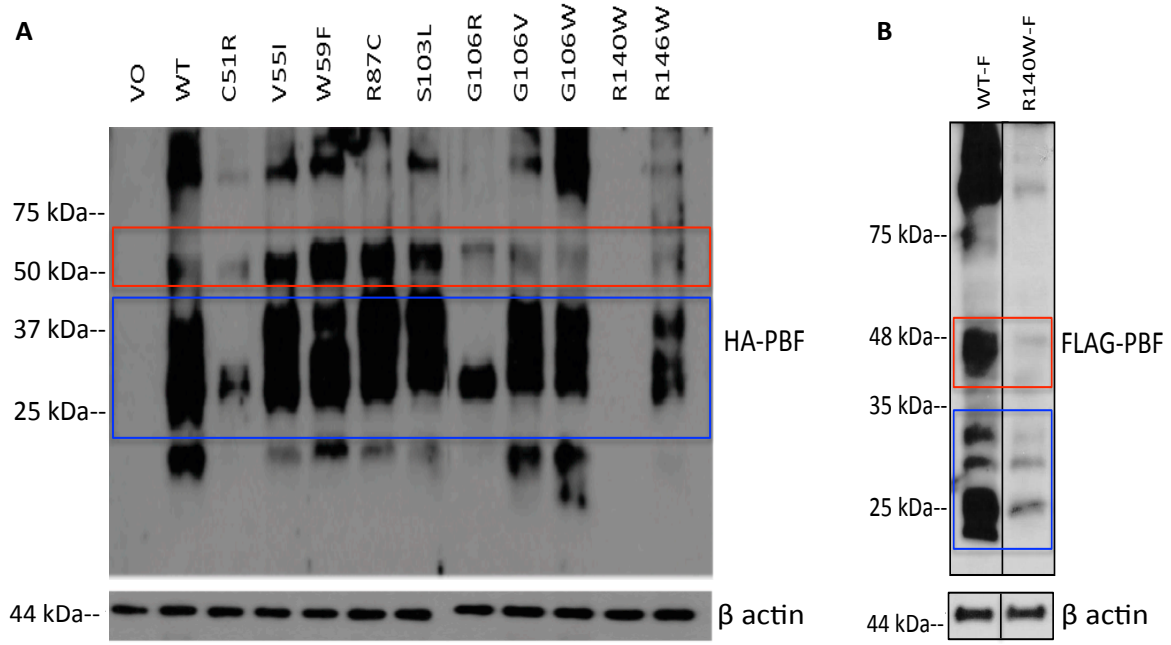

Figure 4.4: Influence of the genetic alterations on PBF glycosylation and dimerisation. *A, COS7 cells were transiently transfected with vector only (VO), wild-type (WT) PBF-HA and all HA tagged PBF mutants. PBF bands were detected by Western blotting with a mouse monoclonal anti-HA antibody (1:1000) and mouse monoclonal anti-β-actin (1:10000). B, COS-7 cells were transfected with FLAG-tagged WT-PBF and R140W-PBF mutant. PBF bands were detected by Western blotting with a mouse monoclonal anti-FLAG antibody (1:500) and mouse monoclonal anti-β-actin (1:10000). Red square denotes*

putative PBF dimers at ~50 kDa, while the blue square illustrates the predominant monomeric and glycosylated forms of the protein (~25-37 kDa).

Western blotting revealed that all mutations were broadly evident at the protein level and showed similar molecular weights to monomeric WT PBF (~25 kDa; Fig. 4.4). However, R140W could not be detected via HA-tagging through either Western blotting (Figure 4.4A) or IF (Figure 4.2). Putative dimers of PBF were also apparent at ~50 kDa, with mutants C51R and G106R showing reduced expression (Figure 4.4A). Interestingly, different amino acid substitutions at residue 106 illustrated very different biochemical properties of the protein, with G106R showing significantly reduced glycosylation and dimerisation, whereas G106V and G106W demonstrated wild type levels of PBF glycosylation and dimerisation (Figure 4.4A).

Since no PBF band was detected for R140W-HA, a FLAG tagged R140W plasmid was created. Although R140W-FLAG showed altered subcellular localisation (Figure 4.3), the Western blotting illustrated that this mutation still provided both monomeric and dimeric bands similar to wild-type PBF, albeit with significantly reduced protein expression (Figure 4.4B).

4.3.3 Amino Acid Substitutions Alter PBF Stability

We investigated the effect of all missense PBF substitutions on protein stability through half-life studies in MCF7 cells transfected with VO, HA tagged WT-PBF and all PBF mutations except R140W-HA. For this mutant, stability was determined through FLAG-tagged PBF in additional experiments, due to the difficulty in detecting the HA tag with this mutant.

Scanning densitometry of the monomeric form revealed that mutants C51R and V55I, both within the PSI domain of PBF, demonstrated similar protein stability to wild type, with a half-lives of around 22 hours (Figure 4.5A and 4.5B). Figure 4.6 illustrates that FLAG-tagged R140W was also relatively stable compared to FLAG-WT PBF, even though R140W-FLAG showed lower protein expression. Differences between levels of FLAG-tagged WT PBF protein (Figure 4.6) and HA-tagged WT PBF (Figure 4.5) suggest that either a FLAG-tag at the N-terminus of PBF might reduce protein stability or a C-terminal HA tag may increase PBF protein stability. In contrast, all other substitutions were markedly less stable than WT, ranging up to 12 hours (Figure 4.5A and 4.5B). In addition, the substitutions at the 'hot spot' 106 amino acid residue provided a range of the stability, with G106R carrying the least stability, while G106V had ~50% greater stability than G106R (Figure 4.5A and 4.5B). Indeed, the predicted 3D structure of G106R substitution demonstrated in Chapter 3 revealed a significant disruption of the long helix at the C-terminus of PBF (Figure 3.3), which may make mutant G106R particularly unstable, resulting in the complete disappearance of the protein by the 12-hour time point. It is possible that the half-life of G106R is only minutes which further decreases the likelihood of any sustained oncogenic activity.

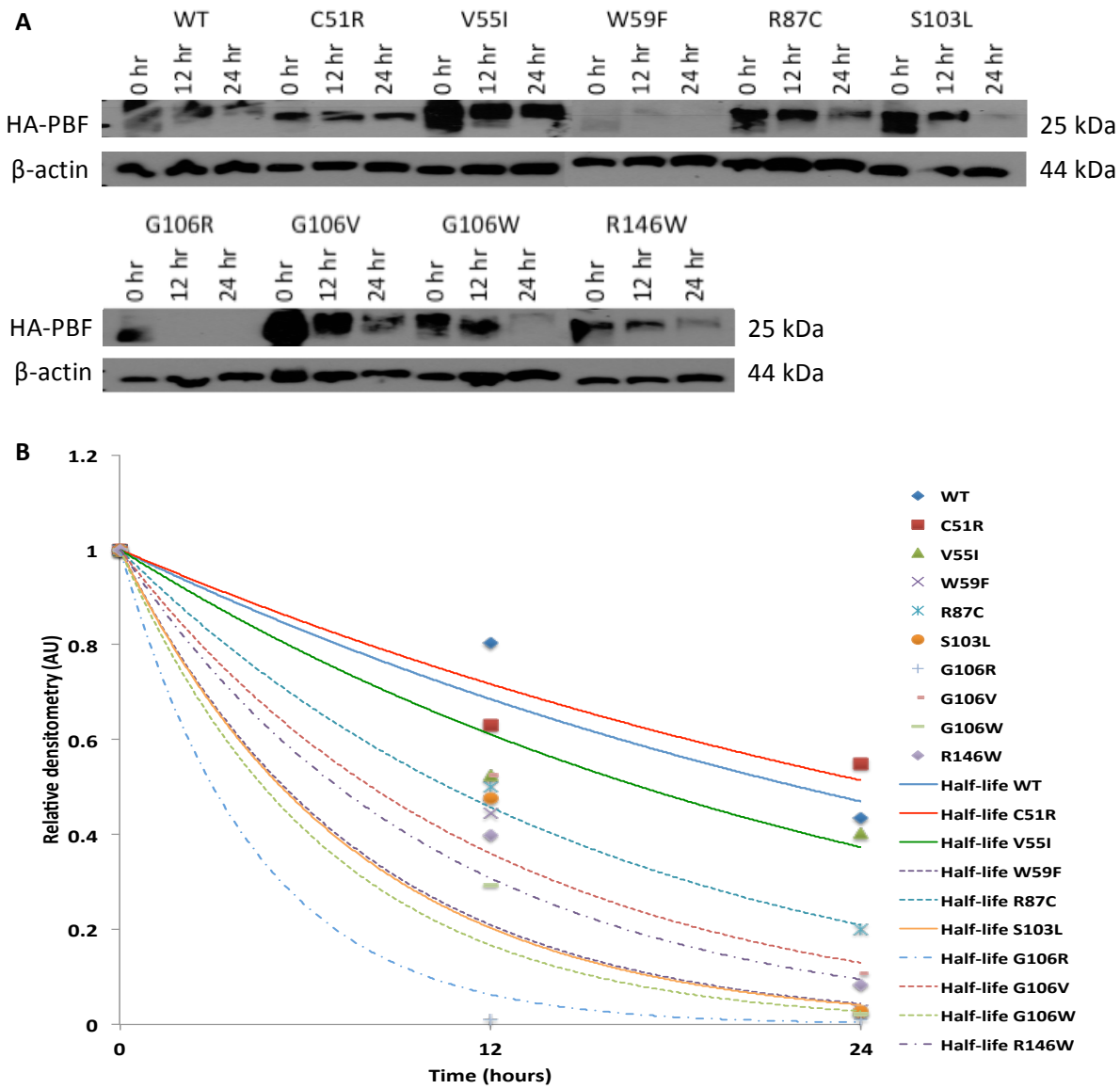

Figure 4.5: PBF substitutions modify protein stability. *A, representative Western blot analysis of Anisomycin half-life assays in MCF7 cells transfected with WT PBF-HA and all HA tagged PBF mutants, except the R140W substitution, at 0, 12 and 24 hours after adding Anisomycin. PBF bands were detected by Western blotting with a mouse monoclonal anti-HA antibody (1:1000) and mouse monoclonal anti-β-actin (1:10000). B, representative quantification of protein stability of the ~25 kDa isoform of PBF compared to β-actin from N=2 separate experiments, comparing WT PBF and all substitutions, except the R140W mutation.*

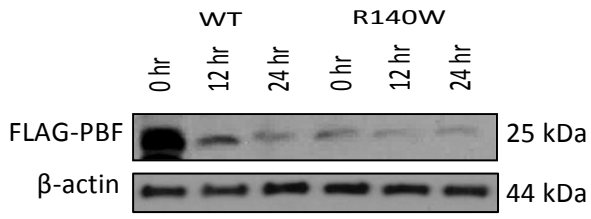

Figure 4.6: R140W-FLAG is relatively stable compared to WT-PBF. *Western blotting of half-life study in MCF7 cells transiently transfected with WT-FLAG and R140W-FLAG at 0, 12 and 24 hours after adding Anisomycin. PBF bands were detected by Western blotting with a mouse monoclonal anti-FLAG antibody (1:500) and mouse monoclonal anti-β-actin (1:10000).*

4.3.4 Amino Acid Substitutions Alter Cellular Proliferation

4.3.4.1 Hot Spot G106 Amino Acid Residue

To date, PBF function has been studied most extensively in thyroid and breast cancer cell models (Smith et al. 2012, Read et al. 2014, Read et al. 2011, Watkins et al. 2010). *In vivo*, PBF overexpression has a modest pro-proliferative influence, as evidenced by thyroid enlargement in transgenic mice (Read et al. 2011). We therefore sought to identify whether any of the described mutations conferred a growth advantage. Given that the G106 residue carried 3 mutations (G106R, G106V and G106W), initial proliferation assays were carried out in TPC1 and SW1736 thyroid cells transfected with WT and the G106 mutants at 48 hours after transfection.

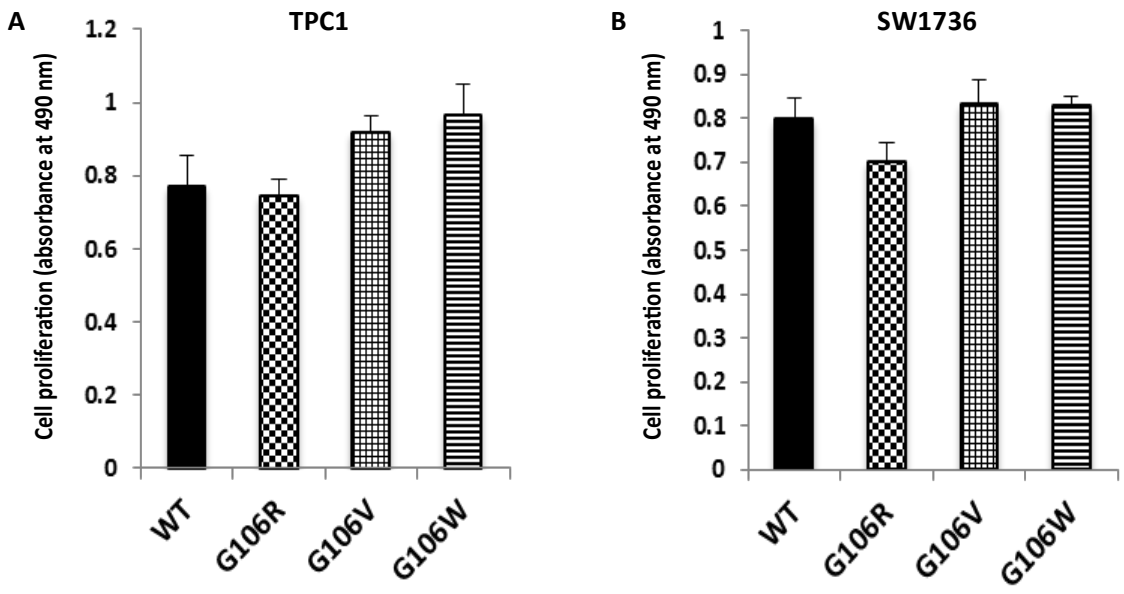

Figure 4.7: Substitutions at the G106 residue do not affect cellular proliferation compared to wild-type PBF. *MTS proliferation assays in TPC1 (A) and SW1736 (B) thyroid cancer cells transfected with WT-PBF, G106R, G106V and G106W. All 3 substitutions at residue G106 failed to significantly alter mitochondrial activity (cell proliferation (absorbance at 490 nm)), as a marker of cell number. Data presented as mean ± SEM. SEM = standard error of mean. N=3 individual experiments.*

As all 3 substitutions at the G106 amino acid residue failed to significantly modify proliferative capacity in MTS assays (Figure 4.7 A and 4.7B), residue G106 was subsequently considered not to be a hot-spot of functional mutational activation.

4.3.4.2 BrdU Assays

As most PBF mutations altered the PBF stability compared to WT-PBF, MTS proliferation assays of wild-type and all 10 PBF substitutions were conducted (data not shown). Most PBF substitutions had similar proliferative phenotypes to WT-PBF (data not shown). These preliminary results therefore enabled us to narrow down our

research to 2 mutations in the PSI domain (C51R and V55I), and 2 mutations close to nuclear localisation signal or NLS (R140W and R146W). Thus BrdU assays were conducted at 48 hours after cell transfection to investigate the consequence of these 4 substitutions on cellular proliferation, via the assessment of DNA replication as an indirect marker of cell division.

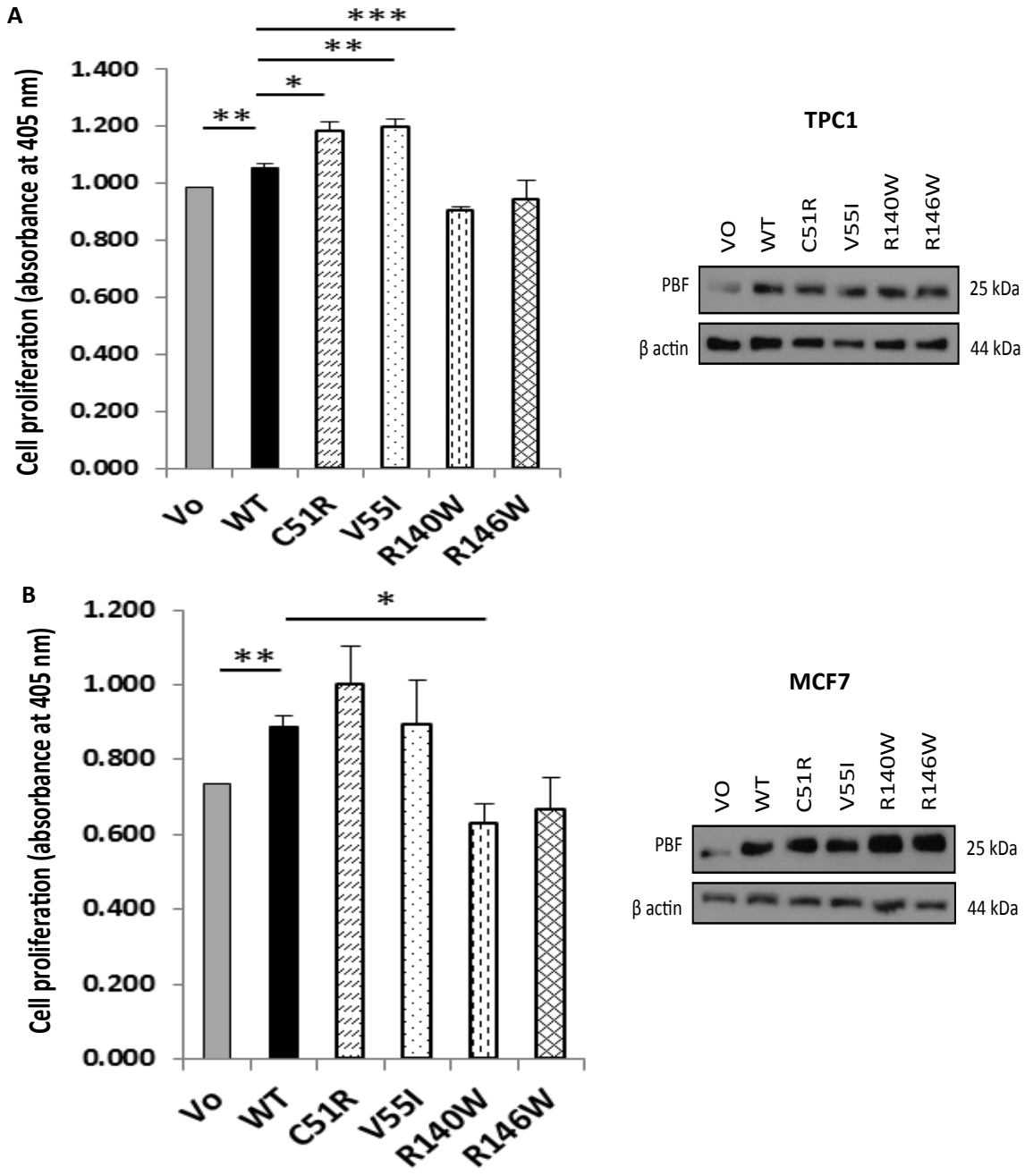

Figure 4.8: Mutations in the PSI domain are generally pro-proliferative, whereas mutants proximal to the NLS reduce cellular proliferation. *After transfection for 48*

*hours, BrdU cellular proliferation experiments were performed in TPC1 (A) and MCF7 (B) cells transfected with VO, WT-PBF, C51R, V55I, R140W and R146W mutants. Inset – Western blots demonstrate PBF expression relative to β-actin levels to assess transfection. Data presented as mean ± SEM. SEM = standard error of mean. *P<0.05, **P<0.01, ***P<0.001. N=3 separate experiments.*

Principally, three individual BrdU assays in TPC1 thyroid and MCF7 breast cancer cells suggested that C51R and V55I induced cell proliferation compared with WT, whilst R140W and R146W were broadly anti-proliferative (Figure 4.8).

4.3.4.3 MTS Assays

Following findings of the BrdU assays in the previous section, we performed MTS assays to validate the results of the consequence of PBF substitutions on a different marker of cell turnover. However, as mutant V55I showed inconsistent results between 2 cell lines and mutant R146W demonstrated less proliferative change than the other two substitutions, especially in MCF7 cells (Figure 4.8), we carried out these assays in TPC1 and MCF7 cell transfected with only VO, WT-PBF, C51R and R140W.

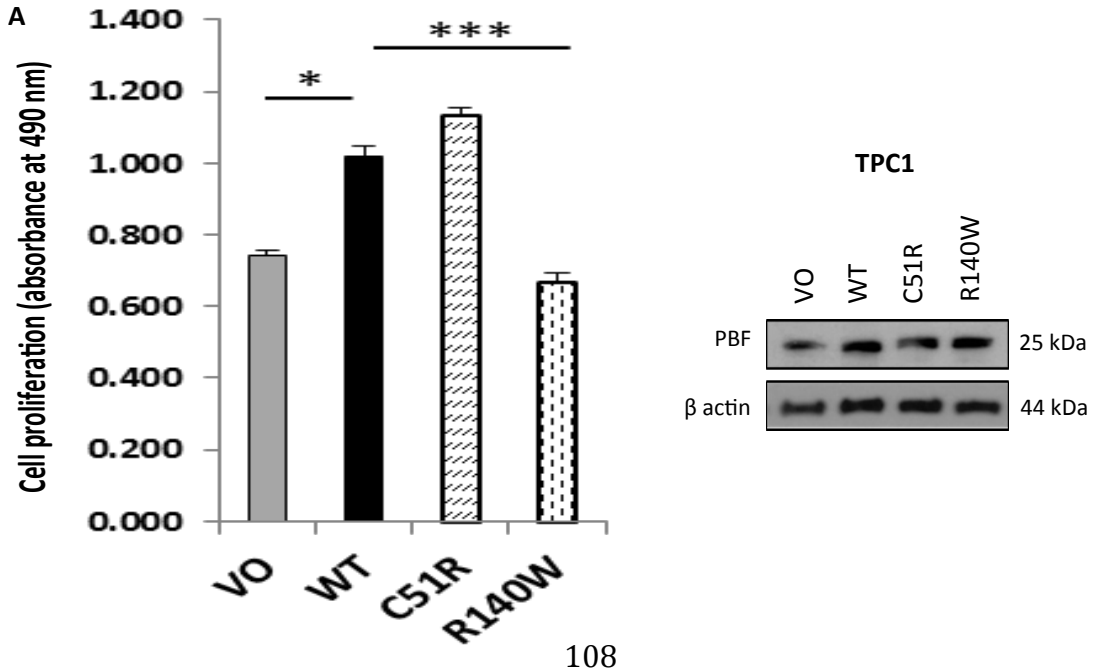

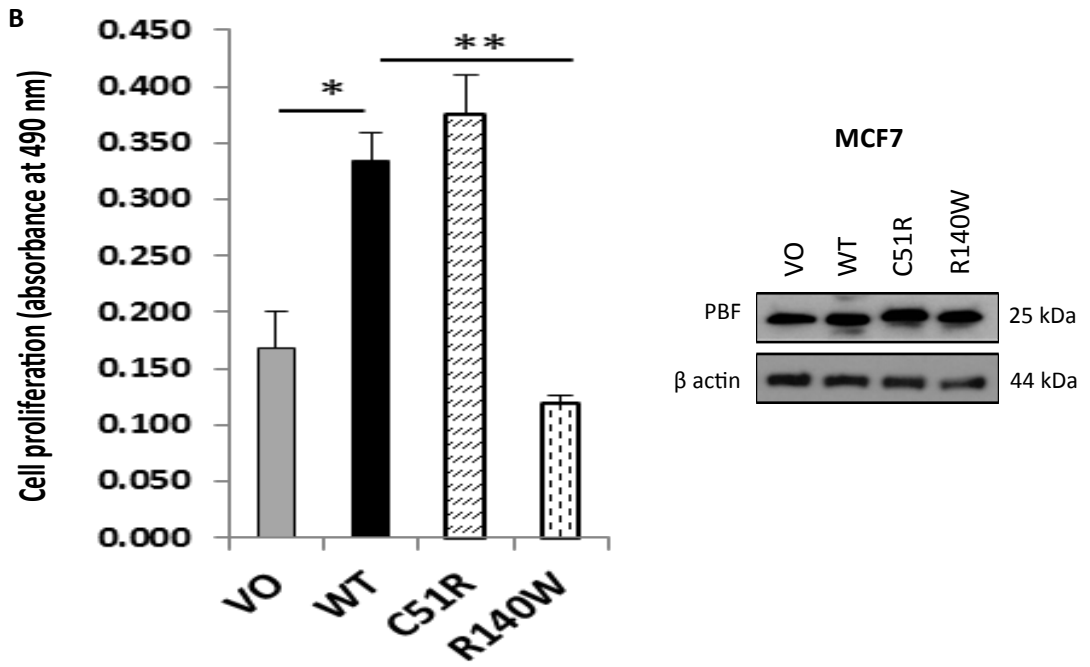

Figure 4.9: MTS assays in TPC1 (A) and MCF7 (B) cells. *48 hours post transfection with VO, WT-PBF, C51R and R140W cDNA constructs, MTS assays were performed. Inset – Western blots demonstrate PBF expression relative to β-actin levels to assess transfection. Data presented as mean ± SEM. SEM = standard error of mean. N=3 separate assays. *P<0.05, **P<0.01, ***P<0.001.*

The MTS assays at 48 hours after transfection revealed a small but non-significant increase in cell turnover for mutation C51R, but confirmed that R140W significantly repressed proliferation compared to WT-PBF (Figure 4.9).

4.3.4.4 Subcellular Localisation of C51R and R140W Substitutions

For subsequent investigations we therefore confined ourselves to the 2 mutations which (i) showed the most obvious differences in cellular proliferation compared with WT, (ii) were potentially damaging to the cell via SIFT, (iii) were apparent in the same tumour category (Table 3; colon cancer), (iv) showed altered

subcellular distribution compared to WT, (v) occurred at evolutionarily conserved sites, and (vi) were clearly expressed *in vitro*; C51R (N-terminal, within the PSI domain) and R140W (C-terminal, adjacent to the nuclear localisation signal). Therefore, immunofluorescence studies were applied to investigate in more detail the subcellular localisation of PBF caused by these two amino acid missense substitutions. Assays were carried out in HeLa cervical cancer and MCF7 breast cancer cells transfected with FLAG-tagged WT, C51R and R140W mutants, and then co-localisation with the endoplasmic reticulum (ER) marker or the Golgi apparatus marker assessed (Figure 4.10).

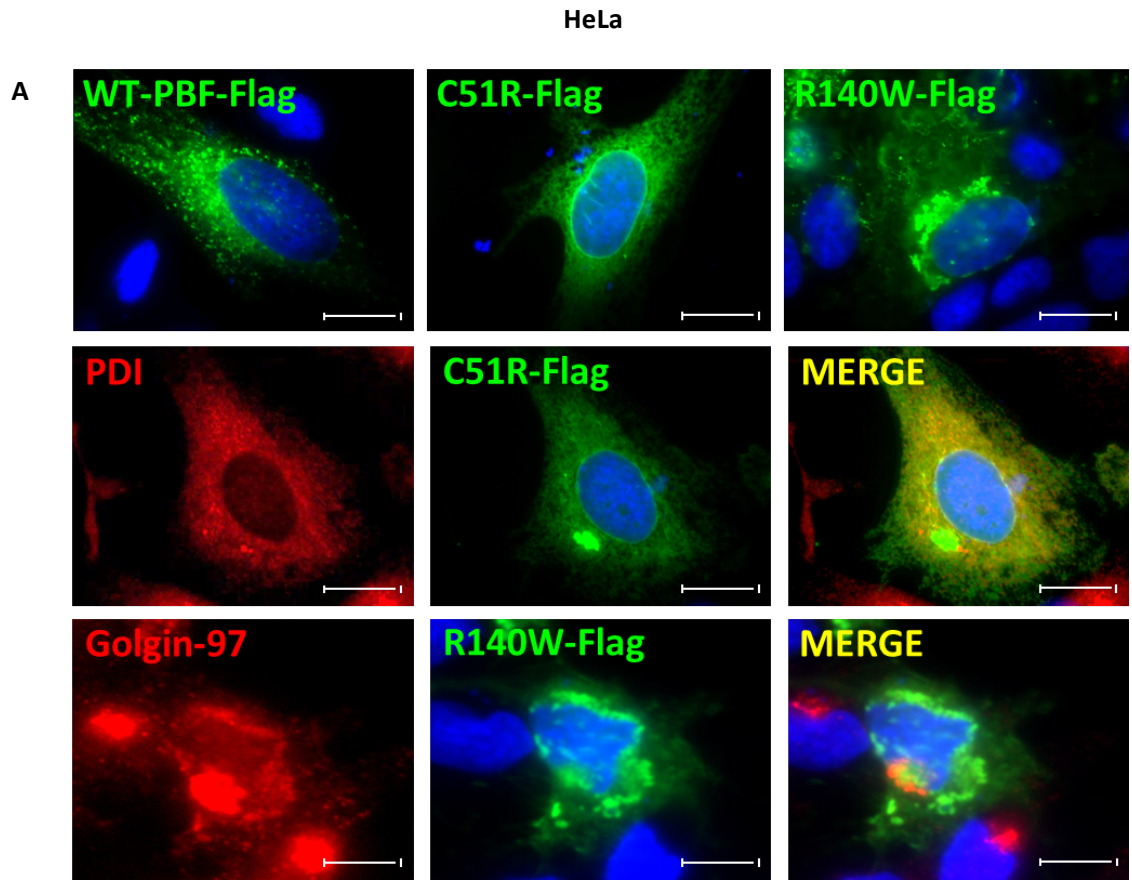

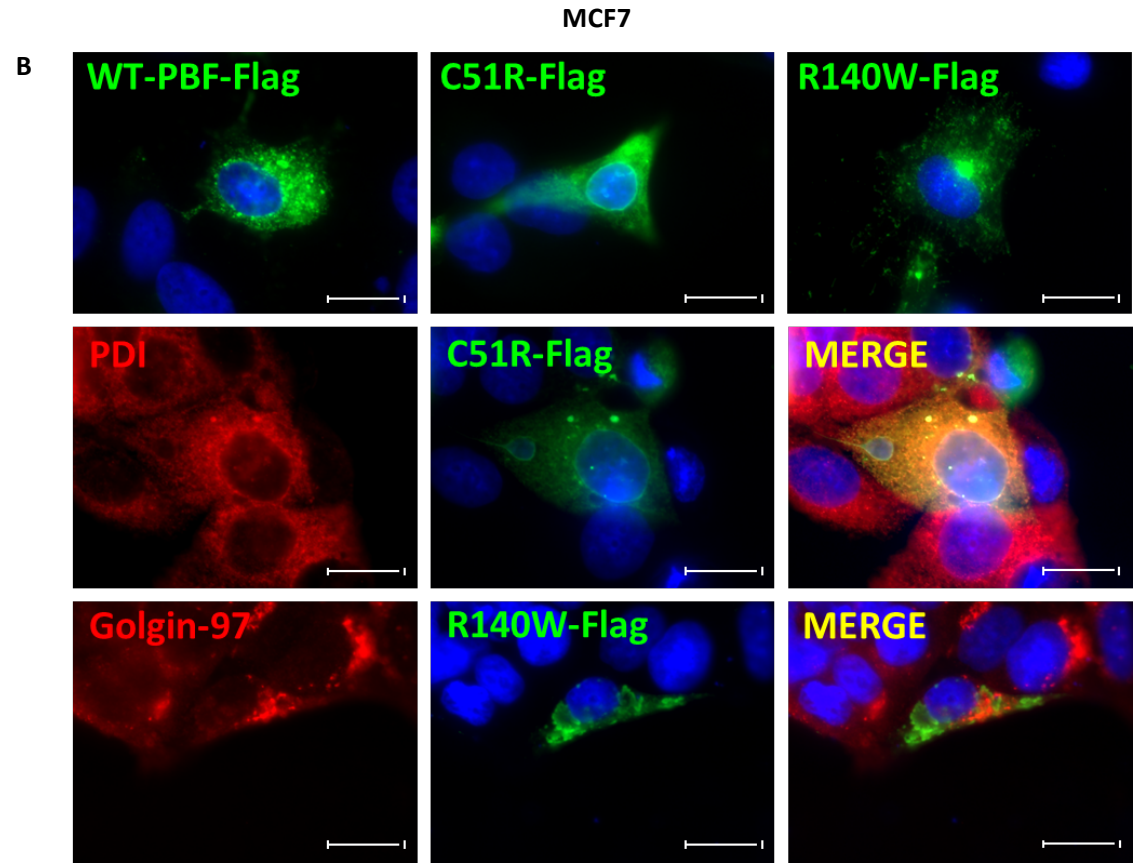

Figure 4.10: Mutant C51R is mostly located in the endoplasmic reticulum, while R140W is mainly observed in the Golgi apparatus. *Representative immunoflorescent microscopy of PBF-FLAG (green), endogenous PDI (ER marker; red), endogenous golgin-97 (Golgi marker; red), cell nuclei (DAPI; blue) and co-localisation (yellow) in HeLa (A) and MCF7 (B) cells transfected with WT-PBF-FLAG, C51R-FLAG and R140W-FLAG. Magnification = 100x. Scale bars = 20 µm.*

Figure 4.10A and 4.10B illustrate that whilst WT-PBF was mainly located in late endosomes and at the plasma membrane, as we have shown before (Smith et al. 2009), the C51R mutant was predominantly apparent in the endoplasmic reticulum, demonstrated by co-localisation with the anti-PDI antibody (ER marker), and R140W was mainly confined to the Golgi apparatus, with co-localisation between the mutant and anti-golgin-97 antibody (Golgi marker). Following the investigations of this

Chapter, mutations C51R and R140W were selected to explore in more functional depth in subsequent studies.

4.4 Discussion

It remains difficult to determine the actual functional consequences of mutations discovered in human cancers. Computational approaches do not as yet provide unequivocal evidence of whether DNA changes represent driver gene mutations, or are simply passenger mutations apparent in a given tumour. In this Chapter, we investigated the outcome of all of the first 10 non-synonymous mutations of PBF on subcellular localisation, glycosylation, dimerisation, protein stability and cellular proliferation as a way of assessing their likely basic biochemistry.

Since we know that changing the subcellular location of proteins generally causes protein functional modification, we started with immunofluorescence studies to determine the subcellular localisation of PBF. Figure 4.2 and Figure 4.3 illustrate that WT PBF and most missense substitutions were mainly confined to late endosomes and the plasma membrane as has been reported previously (Smith et al. 2009). Whilst endosomal and plasma membrane markers were not used specifically, no obvious deviation from WT localisation was evident. Mutants C51R, G106R and R140W, however, did show markedly different localisations to WT in HeLa cervical cancer cells. Indeed, the C51R mutant was predominantly located in the endoplasmic reticulum, whilst R140W-PBF was mainly localised in the Golgi apparatus (Figure 4.10). Although G106R was not examined for co-localisation with the ER marker PDI, its localisation was noticeably similar to C51R-PBF.

Most mutants identified *in vivo* failed to alter basic PBF biochemistry, as assessed via glycosylation and dimerisation, although mutations C51R and G106R exhibited reduced glycosylated and oligomerised forms of PBF. However, in Anisomycin half-life studies, mutants C51R and V55I in the PSI domain and R140W close to C-terminus showed unchanged PBF stability, while G106R had the least stability compared to WT-PBF. Indeed, all substitutions were less stable than wild-type PBF. Heterozygous mutations resulting in unstable proteins would ultimately lead to a reduction in the level of functional PBF protein. This is unlikely to drive oncogenesis and may even counter the overexpression of WT PBF thereby decreasing oncogenic activity. Therefore, amino acid substitutions resulting in modulation of PBF subcellular localisation might not be directly related to either glycosylation, dimerisation nor PBF stability, which differs from other proteins, such as receptor signalling proteins or hormones (DePristo, Weinreich & Hartl 2005, Ponnuswamy, Muthusamy & Manavalan 1982). Moreover, modifications of PBF glycosylation and dimerisation do not necessarily impact the protein stability. It is important to note, however, that the actual glycosylation patterns and oligomeric forms of the PBF protein have not been empirically determined in previous studies, and hence for the purpose of this thesis they must be considered putative.

PBF has a mild pro-proliferative characteristic *in vivo* (Read et al. 2011). When we examined the consequence of cell turnover caused by three substitutions at the G106R residue, MTS proliferation assays demonstrated that the G106 amino acid residue, which was mutated in 4 separate patients, was not associated with any significant change in cell turnover (Figure 4.7), and lacked any correlation with altered localisation, glycosylation, dimerisation or stability. Nevertheless, BrdU assays were

applied to determine whether other mutations altered cellular proliferation, and we interestingly found that mutants in PSI domain, C51R and V55I, generally induced proliferative ability compared to WT-PBF, whereas mutations close to C-terminal end, R140W and R146W, repressed proliferation down to the levels of VO control cells (Figure 4.8). We also re-assessed cellular proliferation using MTS assays to challenge the results through an alternative technical approach, which revealed that WT-PBF still significantly increased proliferative ability as we previously described before (Read et al. 2011). Moreover, the MTS results were broadly consistent with BrdU assays, with C51R showing a mild pro-proliferative effect, while R140W had anti-proliferative characteristic compared to WT-PBF (Figure 4.9).

Based on the basic biochemistry of the first 10 missense mutations reported in the COSMIC, we narrowed our subsequent functional studies to 2 potentially key substitutions: C51R and R140W. One criticism of this approach is that we may have missed genuinely oncogenic activities in the 8 other mutations which we did not pursue in depth. However, it was impractical to perform, for example, simultaneous 2D invasion assays for all 10 mutations, and initial proliferation data suggested no significant alterations in cell turnover. Our initial thought was that residue G106 might represent a hot-spot of mutational activation. Nevertheless, as discussed above, all 3 substitutions at G106 residue, G106V/R/W, failed to significantly enhance markers of cell proliferation compared to WT-PBF. It is possible that mutations of G106 may enhance other oncogenic properties of PBF, such as its pro-invasiveness. However, the G106 mutants were particularly unstable in half-life studies reducing their oncogenic potential. Thus, although this locus may be a mutation hot-spot, it is unlikely to result in increased oncogenic activity and induced tumour growth and development.

For our subsequent investigations we therefore confined ourselves to the 2 mutations which showed the most obvious differences in cellular proliferation compared with WT, were potentially damaging to the cell via SIFT, were apparent in patients within the same cancer subtype, and were clearly expressed *in vitro*; C51R (N-terminal, within the PSI domain) and R140W (C-terminal, adjacent to the nuclear localisation signal).

CHAPTER 5 - EFFECT OF PBF MUTATIONS C51R AND R140W ON CELL INVASION AND MIGRATION

5.1 Introduction

Our group initially characterised a potential role for PBF in breast and colon cell invasion and cell migration *in vitro* (Watkins et al. 2010, Read et al. 2016). Indeed, upregulation of PBF significantly promoted cell invasion in MCF7 breast cancer cells and induced cell migration in HCT116 colon cancer cells. Furthermore, recent evidence from three different studies in breast, colon and papillary thyroid cancers has circumstantially linked PBF to the process of tumour invasion, metastasis and poorer oncological outcomes *in vivo* (Xiang et al. 2012, Read et al. 2016, Hsueh et al. 2013). Firstly, overexpressed PBF significantly increases risk of breast cancer metastasis, and higher variable numbers of tandem repeats in the promoter of PBF also correlate with a significant rise in risk of ER positive breast cancer (Xiang et al. 2012). Secondly, the presence of extramural vascular invasion in colorectal tumours is significantly associated with higher PBF expression (Read et al. 2016). Thirdly, patients diagnosed with papillary thyroid cancer who have high PBF expression also harbour a higher risk of early locoregional recurrence and distant metastasis (Hsueh et al. 2013). Thus, it is possible that PBF is integral to tumour cell invasion *in vivo*.

One of the critical mechanisms in cell invasion concerns how actin congregates and forms protrusive structures at the leading edge of cancer cells (Friedl, Alexander 2011). There are various molecules in the Rho family of GTPases such as Rho (Ras homologous), Cdc42 (cell cycle division 42) and Rac (Ras-related C3 botulinum toxin substrate), which modulate regulation of actin and migration (Ridley 2011, Parsons, Horwitz & Schwartz 2010, Lee, Dominguez 2010, Etienne-Manneville, Hall 2002). However, the mechanistic impact of actin polymerisation in the tumour is still poorly understood.

Cortactin (CTTN) is a scaffold protein active predominantly at the periphery of cells which promotes actin polymerisation by binding and activating the Arp2/3 complex, as well as inhibiting debranching of actin networks (Weaver et al. 2001). In this way, CTTN is able to exert a potent influence upon cell movement and invasion (Figure 5.1) (MacGrath, Koleske 2012, Kirkbride et al. 2011, Pollard, Borisy 2003). Indeed, over-expression of CTTN is associated with increased cellular motility and invasiveness in multiple cancer settings (MacGrath, Koleske 2012, Kirkbride et al. 2011, Kowalski et al. 2005). CTTN function is however multifaceted and has been linked to numerous processes, including vesicular trafficking (Kirkbride et al. 2012, Kirkbride et al. 2011), focal adhesion dynamics (Tomar et al. 2012), extracellular matrix (ECM) secretion (Sung et al. 2011), cell-cycle progression (Croucher et al. 2010) and degradation of growth factor receptors (Timpson et al. 2005) (Figure 5.1). These studies emphasise the importance of CTTN as a key player in aggressive cancers (MacGrath, Koleske 2012), but indicate that further work is required to establish the precise role of CTTN in different tumour settings. Of key relevance to the current Chapter, our previous unpublished mass spectometry data suggested that cortactin is a potential binding partner of PBF (Sharma 2014). However, the mechanism of how PBF interacts with cortactin and the specific binding sites between the two proteins still remains elusive.

Given that PBF appears to have roles in multiple tumourigenic processes, including cell invasion and migration *in vitro* (Watkins et al. 2016, Manuscript under revision), the potential mechanism of PBF in cell invasion and migration was investigated, to determine how PBF interacts with cortactin and whether the C51R and R140W substitutions alter these properties.

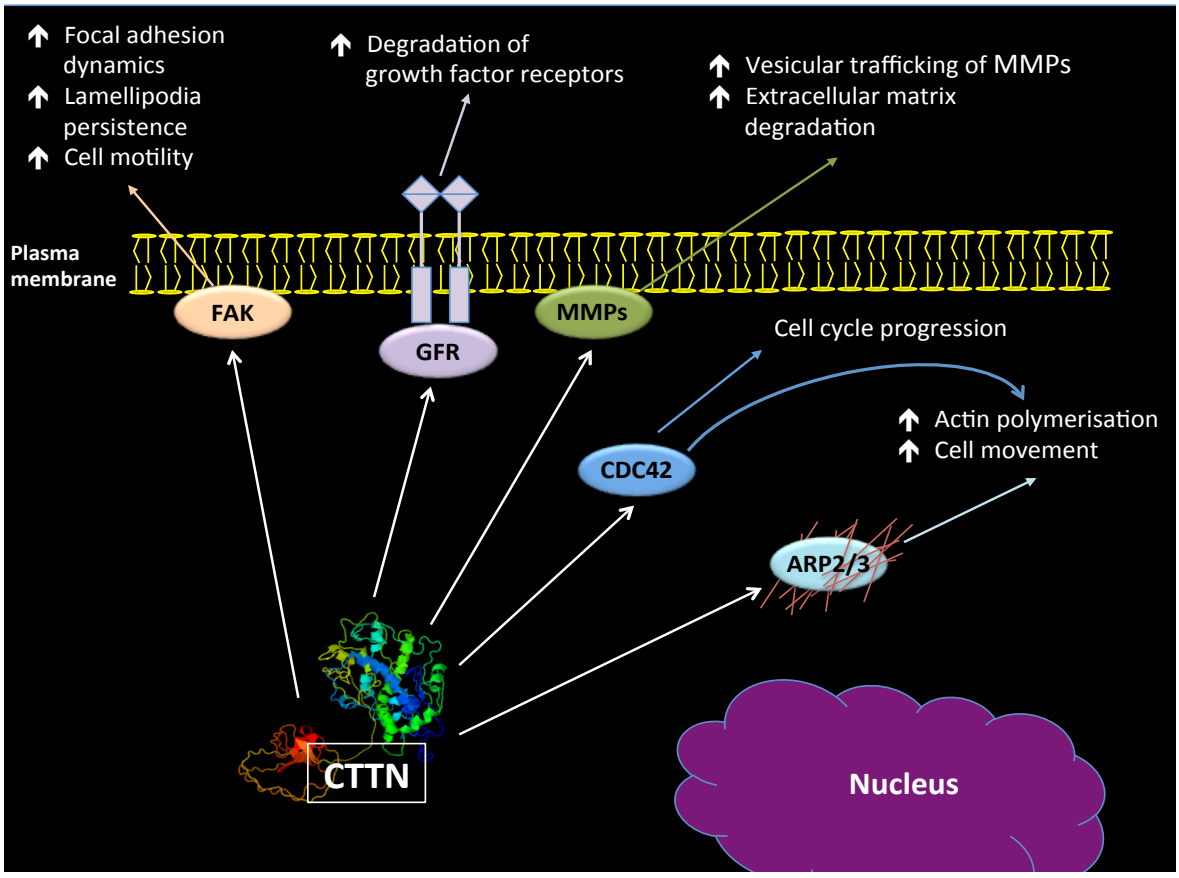

Figure 5.1: Schematic diagram of cortactin functions to induce cell motility and cell invasion. *Representative diagram illustrating potential binding partners and functions of cortactin. CTTN = cortactin, FAK = focal adhesion kinases, GFR = growth factor receptors, MMPs = matrix metalloproteinases, CDC42 = cell cycle division 42 and Arp 2/3 = actin - related proteins 2 and 3.*

5.2 Materials and Methods

5.2.1 Cell Culture and Transfection

TPC1, SW1736 thyroid and MCF7 breast cancer cells were supplemented with RPMI containing 10% FCS, whilst HCT116 colon cancer cells were cultivated in McCoy's 5a media consisting of 10% FCS, and HeLa cervical cancer cells were maintained in

DMEM containing 10% FCS as described in section 2.1.1. TPC1 cells were seeded at 75,000 cells per well of 6-well plates, while SW1736, MCF7, HCT116 and HeLa cells were seeded into 6 well plates at 150,000 cells each well. The cells were incubated at 37°C and 5% CO_2 condition for 24 hours before the transfection was carried out. SW1736, HCT116 and MCF7 cells were transfected with VO and HA-tagged WT-PBF in cell invasion assays used to explore the effect of cortactin knockdown. Moreover, VO, WT-PBF, C51R and R140W mutants were used in the transfection of TPC1 and MCF7 cells to investigate the effect of 2 PBF substitutions on cell invasion.

5.2.2 Short Interfering Ribonucleic Acid (siRNA) Transfection

After being seeded in 6-well plates for 24 hours as described in section 5.2.1, SW1736, HCT116 and MCF7 cells were transfected with silencer cortactin siRNAs 4666 and 4667 or negative control siRNA combined with siPORT™ NeoFX™ transfection reagent (Invitrogen, UK) as described in section 2.1.4. The cells were then incubated for 24 hours, before PBF overexpression was determined as previously described in section 2.1.3.

5.2.3 Cell Invasion Assays

SW1736 thyroid, MCF7 breast and HCT116 colon cancer cells were seeded in 6-well plates for 24 hours as described in section 5.2.1. Then, the cells were transfected with two silencing CTTN siRNAs to knockdown CTTN for 24 hours, followed by transfection with VO or PBF-HA for the next 24 hours, before actual cell invasion experiments were performed. However, for the modification of cell invasion caused by

PBF mutations, TPC1 thyroid and MCF7 breast cancer cells were transfected with VO, WT-PBF, C51R-PBF and R140W-PBF plasmids for 48 hours before starting the actual steps of cell invasion assays. The cells were transfected with duplicate samples in each separate experiment. Post transfection, the transfection reagent was then removed and replaced with complete medium containing 2% FCS to drive cell invasion. After 16-hour incubation, the cells were harvested and reseeded into 8 μm growth reducing invasive chambers (BD bioscience, UK) in triplicate fashion for each sample, and then incubated for 24 hours to let cells invade. Finally, membrane staining was performed as described in section 2.9. The experiments were individually replicated twice.

5.2.4 Cell Migration Assays

After clonal selection of NIH 3T3 cells stably overexpressing pCI-neo vectors containing VO, WT-PBF, C51R-PBF and R140W-PBF, cells were seeded into 6-well plates in triplicate. The stable cells were incubated until becoming 100% confluent, before one scratch wound in each well was created by standard scraping with a P10 pipette tip. The images were captured at 0, 4, 6, and 8 hours after creating the wounds, and taken for 3 different areas in each well. The area and percentages of wound closure were analysed using Image J software. The assays were carried out in 3 separate experiments.

5.2.5 Immunoflorescence Microscopy

HeLa and MCF7 cells were seeded at 150,000 cells per well of 6-well plates and incubated for 24 hours, before being transfected with VO, WT-PBF-HA, C51R-PBF-HA and CTTN-Myc as described in section 2.1.3. The cells were then used to examine co-

localisation between PBF or Y174 phospho-PBF and cortactin (CTTN) through immunofluorescence microscopy as explained in section 2.6. Primary antibodies were rabbit polyclonal anti-HA (1:200, Santa Cruz Biotechnology, UK), mouse monoclonal anti-Myc (9B11, 1:500, Cell Signaling, UK), mouse monoclonal anti-CTTN (1:100, Merck and Millipore, Germany), rabbit polyclonal anti-PBF (1:100, In-house) and rabbit polyclonal anti-phosphoPBF (Y174, 1:50, In-house). The cells were visualised using a Zeiss Axioplan fluorescence microscope (Zeiss, Germany) with 10x and 100x objectives. Subcellular co-localisation of PBF or Y174 phospho-PBF and cortactin (CTTN) was additionally investigated in HeLa and MCF7 cells using a LSM510 META confocal microscope with 63x and 100x objective lens (Zeiss, Germany).

5.2.6 Protein Extraction and Quantification (Bicinchoninic Acid Assay or BCA)

Protein samples were extracted to confirm overexpression or knockdown conditions, and BCA assays were performed as described in section 2.2. After measuring the absorbance, protein concentrations and volumes were determined to apply in further Western blotting analysis.

5.2.7 Co-immunoprecipitation (Co-IP)

The interaction between PBF and CTTN, including endogenous and exogenous circumstances, was analysed using co-IP experiments as defined in section 2.11. The antibodies used for pull down were mouse monoclonal anti-CTTN (Merck and Millipore,

Germany), mouse monoclonal anti-Myc (9B11, Cell Signaling, UK) and mouse monoclonal anti-HA (Covance, USA).

5.2.8 Proximity Ligation Assays (PLA)

To detect specific interaction between endogenous CTTN and PBF in single cells, we applied Proximity Ligation Assays (PLA) in HeLa and MCF7 cells. Protein interaction was determined using Duolink® In Situ reagents from Olink® Bioscience (Sigma, UK) and the primary antibodies for mouse monoclonal anti-CTTN (1:100, Merck and Millipore, Germany), rabbit polyclonal anti-PBF (1:100, In-house), and rabbit polyclonal anti-phospho-PBF (pY174, 1:50, In-house). The PLA probes (Sigma, UK) were Plus and Minus probes raised in different species depending on the required primary antibodies. A pair of the PLA probes, visualised as an individual fluorescent red spot in specific subcellular localisation, yields a signal only when the probes are held together in close proximity.

The cells were seeded at a density of 150,000 cells/well on a cover slip placed into a well in a 6-well plate and then leaving for 48 hours. After washing with PBS, the cells were fixed using fixing solution (0.1M phosphate buffer Na_2HPO_4 (pH 7.4), 2% paraformaldehyde (PFA), 2% glucose, 0.02% sodium azide) for 20 minutes at room temperature. Subsequently, cells were permeabilised with 100% chilled methanol and blocked in 10% NCS in PBS (Invitrogen, UK) as described in section 2.6. After the primary antibodies were diluted into 1% BSA (Jackson Immunoresearch, USA) in PBS, 80 µl of the solution were applied to the cells. After 1 hour incubation in humidified chambers, coverslips were washed with PBS for 5 minutes, two times, and next

incubated with 80 µl of diluted two PLA probes (1:5) in 1% NCS and 1% BSA in PBS at 37°C for one hour. The cells were then washed for 5 minutes twice with 1x Wash Buffer A (provided in the kit) under gentle agitation. In the meantime, the Ligase was added 1:40 in diluted Ligation Stock (1:5 in purified water) and mixed by vortexing, before the ligation-Ligase solution was aliquoted on to each cover slip. After incubation at 37°C for an hour, the sample was washed with 1x Wash Buffer A twice for 2 minutes under shaking condition. Subsequently, the Polymerase was immediately diluted 1 in 80 in diluted Amplification Stock (1:5 in purified water), before being applied to the cells and then incubated at 37°C for 100 minutes. The cover slip was then washed twice with 1x Wash Buffer B (provided in the kit) for 10 minutes, rinsed with 0.01x Wash Buffer B for 1 minute, and dried at room temperature in the dark. Finally, the cover slip was mounted using Duolink In Situ Mounting Medium with DAPI (Sigma, UK), and sealed with nail polish. The slide was analysed using confocal fluorescence microscopy and stored at -20 °C in the dark.

5.3 Results

5.3.1 Interaction between PBF and Cortactin

5.3.1.1 Endogenous PBF and CTTN

Our group recently performed extensive mass spectrometry in papillary thyroid K1 and TPC1 cells in order to identify possible binding partners of PBF with roles in cell motility. Potential proteins interacting with PBF-HA were isolated through co-immunoprecipitation (co-IP) using anti-HA (Covance, USA) and then separated by SDS-PAGE. Following destaining, proteins were reduced, alkylated and trypsinised before

undergoing tandem mass spectrometry (Bruker, USA). Mass spectrographs were analysed via the Mascot search engine (v2.2.06, Matrix Science, UK) and ProteinScape (v3.0.0.446, Bruker, USA). Multiple separate runs were performed to identify consistent protein interactors. We identified the cortical actin binding protein CTTN to be the top hit across all runs (12 peptide hits, average score per peptide = 40.0, n = 5 runs) (Sharma 2014). Given CTTN's pivotal role in cell migration and invasion, and since PBF is shown to induce 2D cell invasion in breast cancer cells (Watkins et al. 2010), we appraised the mass spectrometry data using co-IP assays (Figure 5.2), proximity ligation assays (Figure 5.3) and immunofluorescence studies (Figure 5.4) in HeLa, MCF7, SW1736 and HCT116 cells.

5.3.1.1.1 Co-IP Studies

The co-IP experiments were performed to evaluate a potential interaction between PBF and CTTN in HeLa cervical, MCF7 breast and HCT116 colon cancer cells. 10 µl anti-CTTN antibody were applied to pull down PBF or phosphorylated PBF in each positive condition, while the HA antibody, from the same IgG1 isotope as the CTTN antibody, was used as a negative control. Additionally, no antibody (Nab) controls were used as a second negative control. All co-IPs were performed on at least two separate occasions.

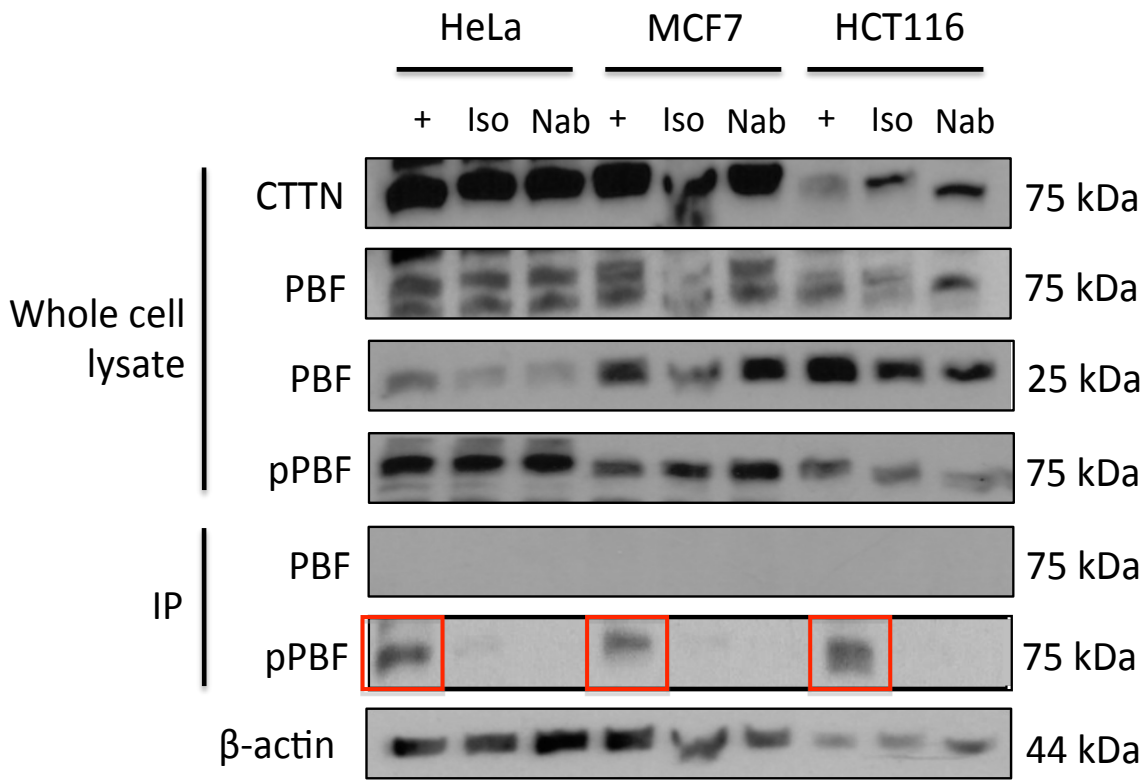

Figure 5.2: PBF and CTTN bind in vitro through co-IP assays. *Representative co-IP experiments between total PBF and CTTN or Y174 phospho-PBF (pPBF) and CTTN from HeLa, MCF7 and HCT116 cells. + indicates the co-IP condition where anti-CTTN antibody (ab) was used to pull down PBF or phospho-PBF, while Iso denotes HA ab applied to co-IP samples as a negative control. Nab = no antibodies used to pull down the protein. Red squares illustrate specific interaction between 2 proteins.*

The results showed that endogenous phosphorylated Y174 PBF specifically interacted with CTTN (Figure 5.2), whereas 'total' PBF failed to show specific interaction with CTTN. This is likely to reflect the fact that our in-house PBF antibody does not detect phosphorylated PBF (Smith et al. 2013, Smith et al. 2009). Further, the predominant interaction was with the putatively oligomeric form of pY174 at around 75 kDa, and not monomeric PBF, suggesting both that oligomeric PBF is phosphorylated, and that CTTN preferentially binds when PBF is an oligomer.

5.3.1.1.2 Proximity Ligation Assays (PLA)

We challenged our co-IP findings with the separate methodology of proximity ligation assays (PLA). The interaction between CTTN and PBF was confirmed in HeLa (Fig. 5.3A) and MCF7 (Fig. 5.3B) cells, through which binding is visualised as subcellular fluorescence (Figure 5.3).

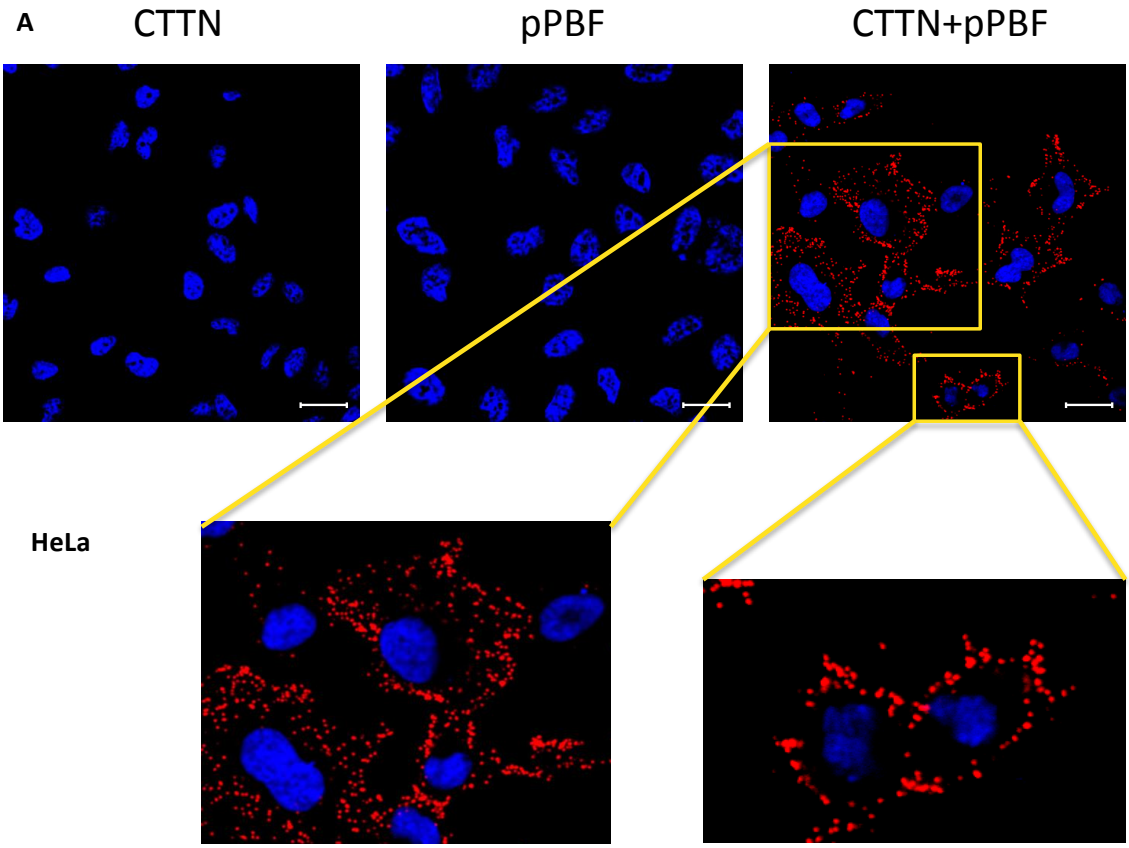

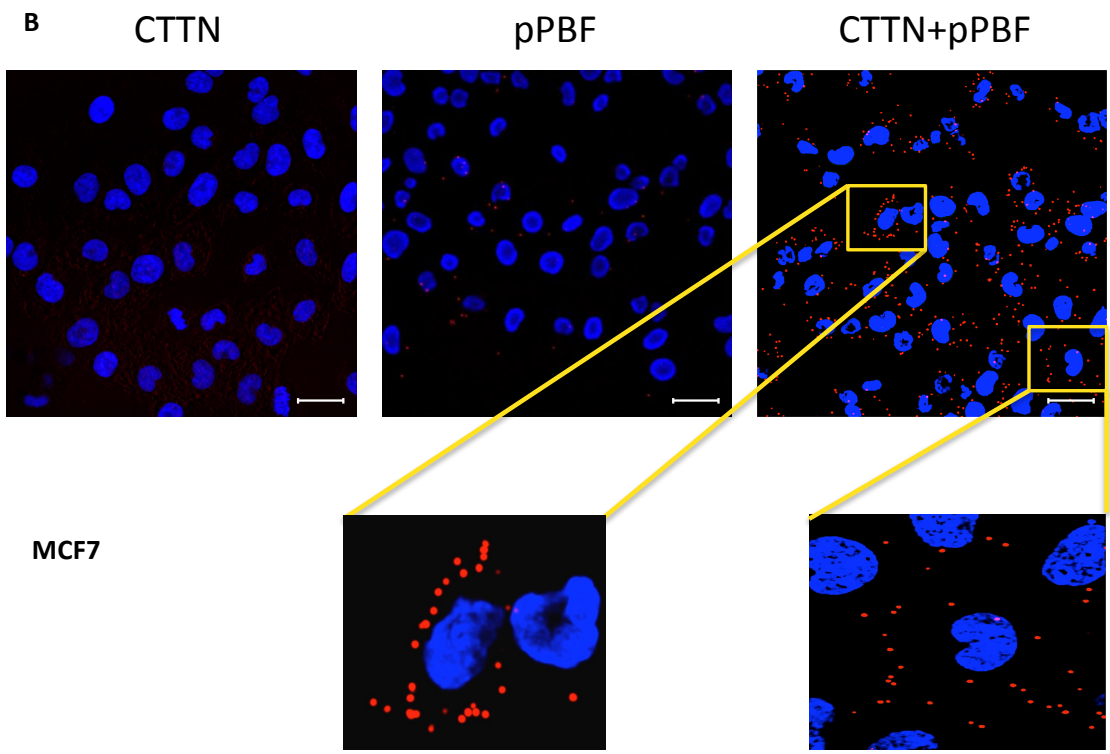

Figure 5.3: PBF and CTTN bind in vitro via PLA assays. *Representative immunofluorescent confocal microscopy of PLA experiments in HeLa (A) and MCF7 (B) cells. CTTN indicates the condition where only anti-CTTN ab was used, while pPBF denotes the condition where only anti-phosphoPBF (Y174) ab was applied. CTTN+pPBF illustrates the condition where both anti-CTTN and anti-phosphoPBF (Y174) antibodies were applied simultaneously. Red spots indicate specific interaction between 2 proteins. Zoomed image shows that Y174 phospho-PBF and CTTN interaction occurs predominantly at the cell periphery. Magnification = 100x. Scale bars = 20 µm.*

Specific interaction (red spots) occurred predominantly towards the cellular periphery of HeLa cervical (Figure 5.3A) and MCF7 breast (Figure 5.3B) cells when endogenous phosphorylated PBF and CTTN were co-expressed, which was not apparent in control PLA experiments. In addition, we could not detect any particular interaction between total PBF using our 'total' PBF antibody and CTTN (data not shown) in keeping with the co-IP results (Figure 5.2).

5.3.1.1.3 Immunofluorescence Confocal Microscopy

The interaction between PBF and CTTN was also investigated through immunofluorescence assays in HeLa and MCF7 cells. These results determined where CTTN and PBF were in the cells and where co-localisation occurred.

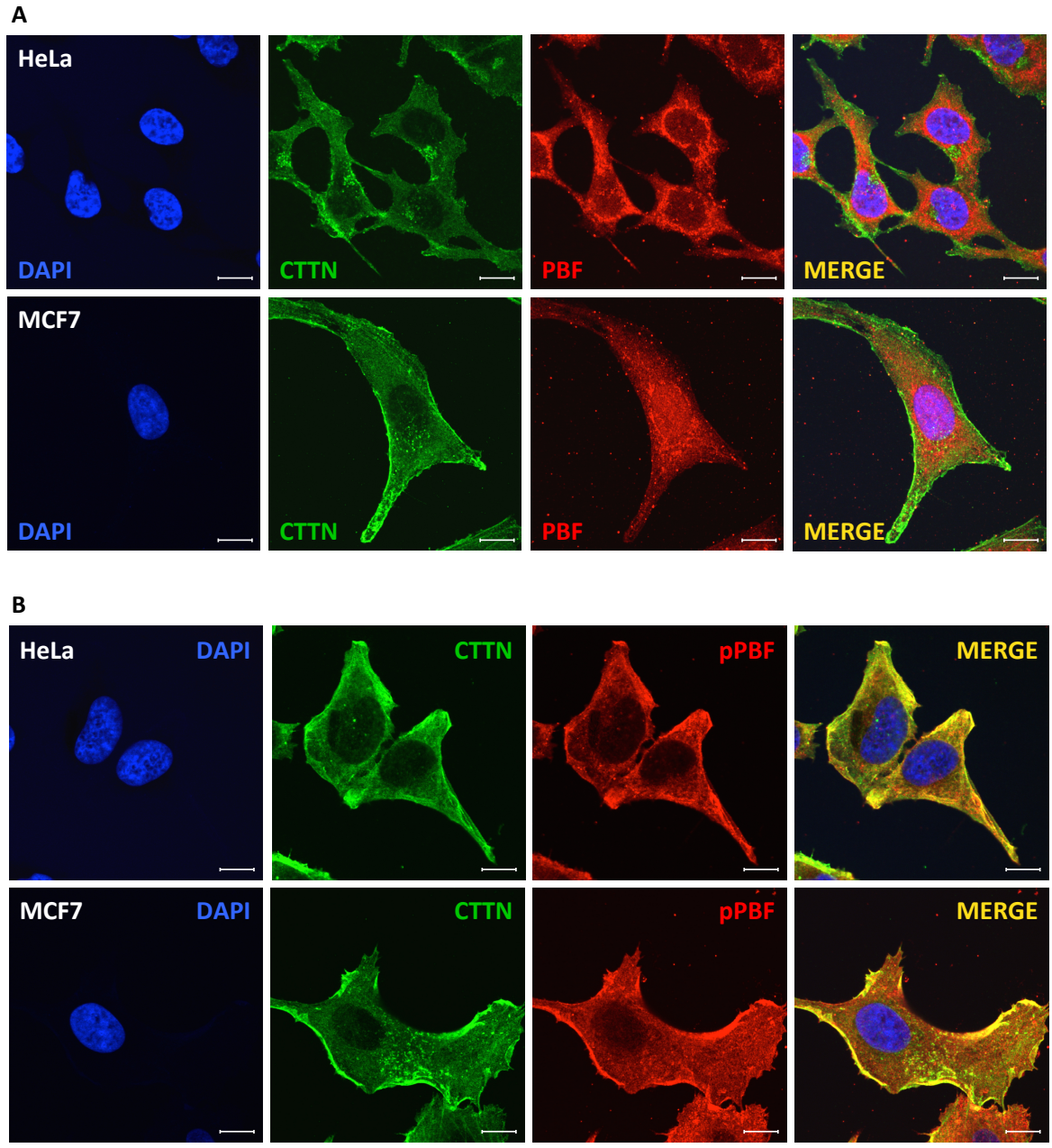

Figure 5.4: PBF and CTTN co-localise in vitro via immunofluorescence confocal microscopy. *Representative confocal images demonstrating co-localisation between PBF*

and CTTN (A) or Y174 phospho-PBF and CTTN (B). Representative figures showing CTTN (green), PBF (red), Y174 or phospho-PBF (red), DAPI (blue) and co-localisation (yellow) in HeLa and MCF7 cells. Magnification = 100X. Scale bars = 20 µm.

Immunofluorescence microscopy confirmed co-localisation between endogenous phosphorylated PBF and CTTN predominantly at the plasma membrane of cancer cell lines *in vitro* (Figure 5.4B).

5.3.1.2 Co-localisation between Exogenously Overexpressed PBF and CTTN

The experiments above revealed that endogenous phosphorylated PBF and CTTN interact *in vitro*. However, due to the fact that our in-house PBF antibody struggles to detect pY174 PBF (Smith et al. 2009), it was important to define the co-localisation between PBF and CTTN more thoroughly. Exogenous proteins tagged with HA (PBF) and Myc (CTTN) were therefore utilised in additional immunofluorescence microscopy experiments.

Immunofluorescence microscopy in HeLa and SW1736 cells was used to determine subcellular location and co-localisation between PBF-HA and CTTN-Myc. The cells were co-transfected with VO control or HA tagged WT-PBF and Myc tagged CTTN for 48 hours as described in section 2.1.3.

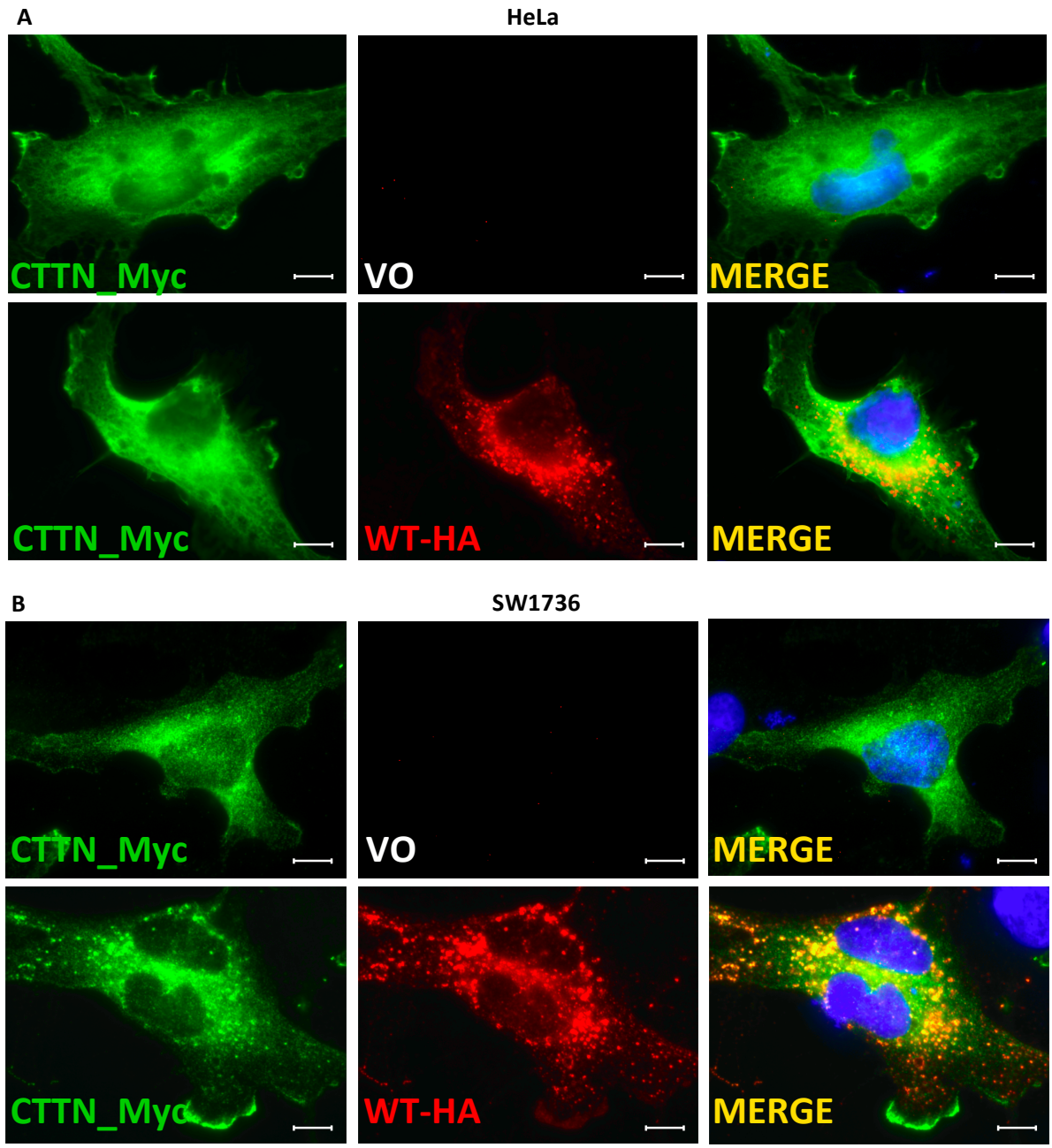

Figure 5.5: Overexpressed WT-PBF co-localises with CTTN-Myc in vitro via immunofluorescence assays. *Representative IF microscopy illustrating CTTN-Myc (mouse anti-Myc antibody, green), WT-PBF-HA (rabbit anti-HA antibody, red), DAPI (blue) and co-localisation (yellow) in HeLa (A) and SW1736 (B) cells. Magnification = 100X. Scale bars = 20 µm.*

Figure 5.5 shows that cortactin was located in intracellular vesicles and at the plasma membrane, while PBF was mostly noticeable in late endosomes within

cytoplasm, as reported previously (Smith et al. 2009). The co-localisation between the proteins in intracellular portions of both cell lines was also observed, with a small amount apparent at the plasma membrane (Figure 5.5). Together these IF results indicate that overexpressed CTTN, as well as endogenous CTTN, colocalises with PBF.

5.3.2 Alteration of Cell Invasion with Cortactin Knockdown

According to data published previously, either PBF or cortactin (CTTN) is capable of enhancing cellular motility and cell invasion (Watkins et al. 2010, MacGrath, Koleske 2012, Kirkbride et al. 2011, Pollard, Borisy 2003). Importantly, CTTN was the top hit for potential protein-binding partners of PBF identified through mass spectrometry (Sharma 2014). However, the precise mechanism how PBF and CTTN interact remains obscure.

Therefore, in this study, we investigated the capability of PBF to induce cell invasion when CTTN was depleted in a panel of cancer cell lines, including SW1736 thyroid, HCT116 colon and MCF7 breast cancer cells, using 2D Boyden cell invasion assays (Figure 5.6).

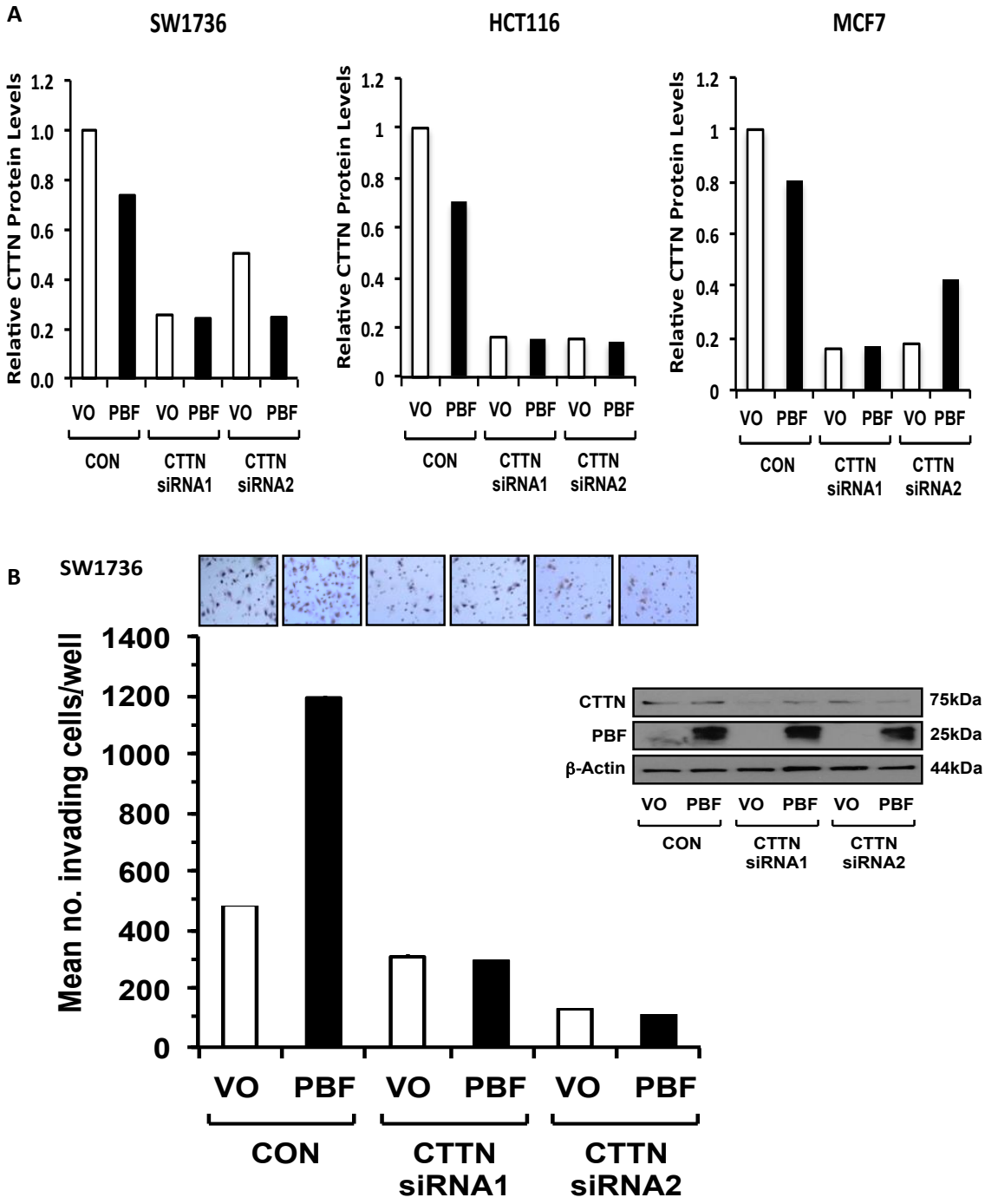
A
SW1736
HCT116
MCF7
Relative CTTN Protein Levels
1.2
1.0
0.8
0.6
0.4
0.2
0.0
VO PBF VO PBF VO PBF
CON
CTTN siRNA1
CTTN siRNA2
B
SW1736
Mean no. invading cells/well
1400
1200
1000
800
600
400
200
0
CTTN
PBF
β-Actin
75kDa
25kDa
44kDa

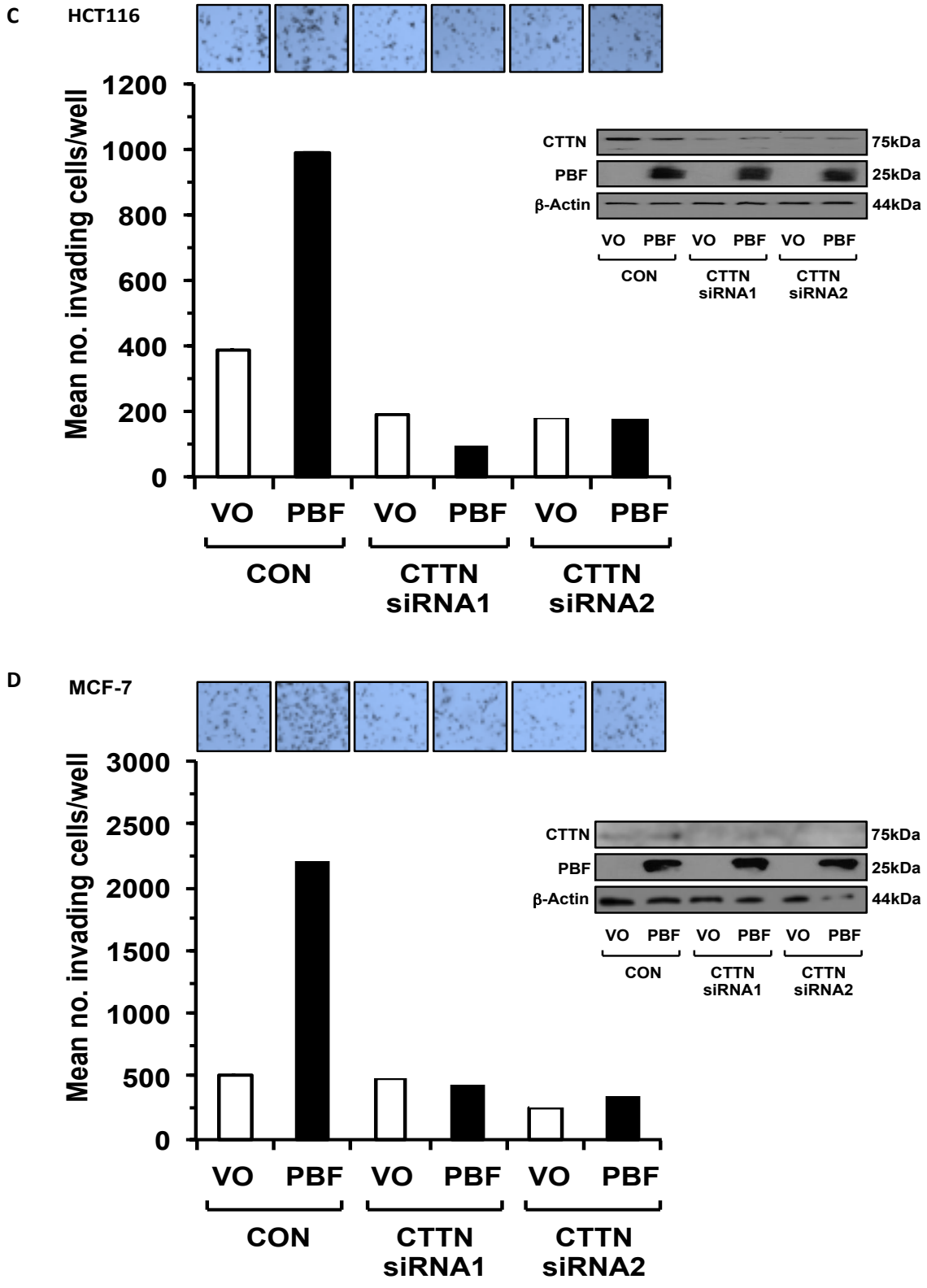

Figure 5.6: Depletion of CTTN blocks the ability of PBF to induce cellular invasion. *A, representative graph shows quantification of CTTN protein levels relative to β-actin from siRNA experiments in SW1736, HCT116 and MCF7 cells. B, C and D representative*

quantification of number of invading cells per well from 2D Boyden invasion assays in SW1736 (B), HCT116 (C) and MCF7 (D) cells treated with specific siRNAs for CTTN (siRNA 1 and 2) or control siRNA (CON) for 24 hours, and then transfected with VO or PBF-HA in duplicate. Graphs represent mean from two independent experiments, while above inset shows representative photomicrographs of 2D Boyden assay chamber cell invasion experiments. Inset - Western blots of CTTN and PBF expression for each cell line as above in response to siRNA treatments. PBF bands were detected with a mouse monoclonal anti-HA antibody (1:1000), while CTTN bands were demonstrated with a monoclonal anti-CTTN antibody (1:500) compared to β-actin. N=2.

The results revealed that knockdown of CTTN by two different CTTN siRNAs was associated with a significant reduction in the invasive capacity of SW1736 ($P<0.01$), HCT116 ($P<0.001$) and MCF7 cells ($P<0.05$) transfected with PBF (Figure 5.6). Of importance, the invasive capacity of CTTN-depleted cells transfected with PBF was equivalent (P=NS) or lower ($P<0.05$) than VO-control cells similarly depleted of CTTN (Figure 5.6). Together these results provide evidence that the potent induction of cell invasion by PBF is driven in its entirety via CTTN.

5.3.3 Alteration of Cell Invasion and Cell Migration due to C51R and R140W PBF Mutations

5.3.3.1 Effects of Mutants C51R and R140W on Cell Invasion

Chapter 4 narrowed down the PBF substitutions discovered *in vivo* to 2 mutants, C51R and R140W. In this section, having better defined the mechanism by which PBF and CTTN interact in the process of cell invasion, the impact of these 2 mutations on cell

invasion was examined through 2-dimensional cell invasion assays in TPC1 thyroid and MCF7 breast cancer cells transfected with VO, WT-PBF, C51R and R140W mutants (Figure 5.7).

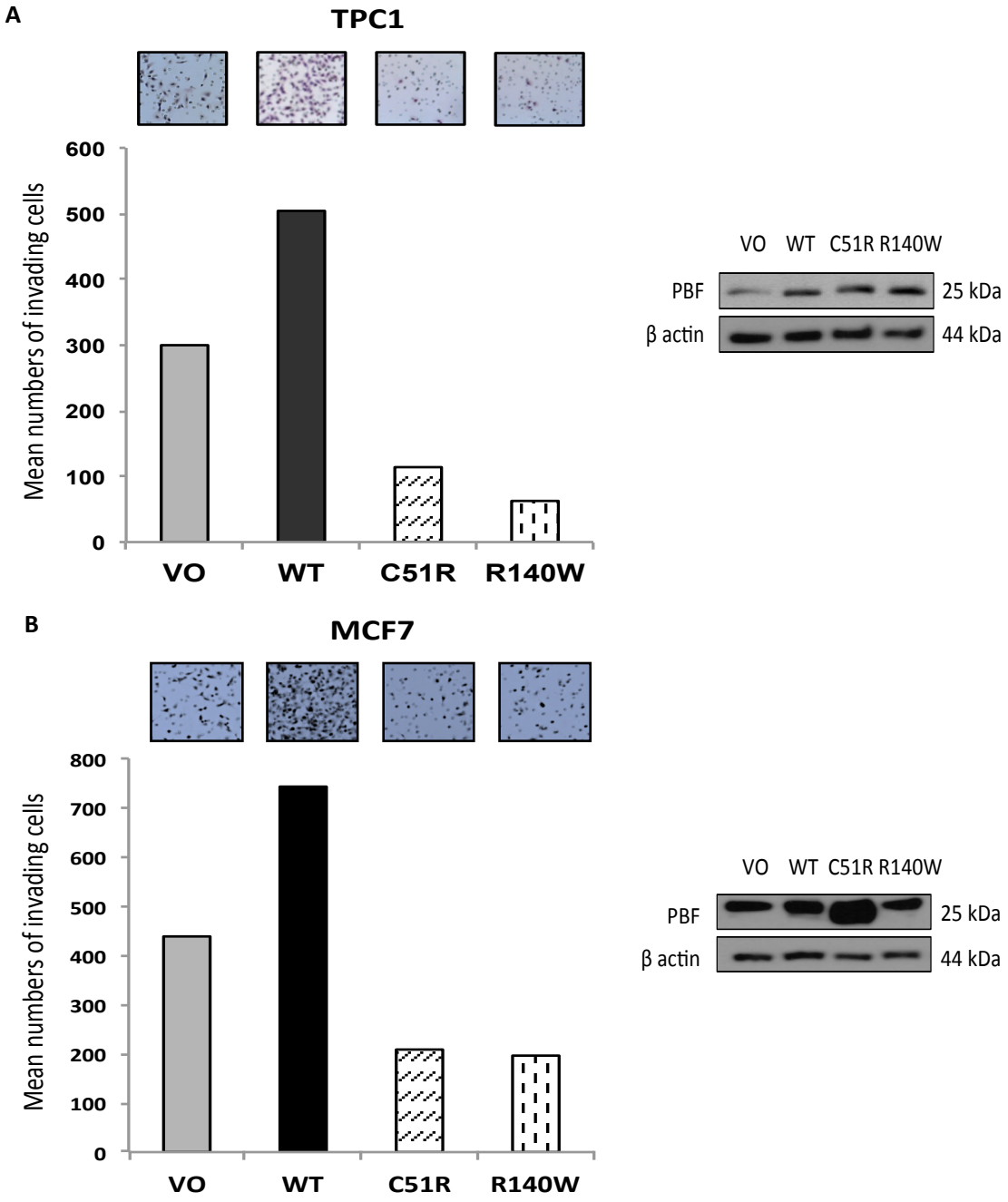

Figure 5.7: Invasive properties of C51R and R140W mutants. *Number of invading cells per well from 2D Boyden invasion assays in TPC1 (A) and MCF7 (B) cells transfected with VO, WT-PBF, C51R and R140W mutants in duplicate. Graphs represent mean from two independent experiments, with representative photomicrographs shown above. Inset -*

Western blots demonstrate PBF expression relative to β-actin levels to assess transfection. N=2.

As in Figure 5.6, wild-type PBF was markedly pro-invasive compared to VO, in TPC1 and MCF7 cells (Figure 5.7). However, both C51R and R140W substitutions entirely lost invasive capacity, and in fact had significantly repressed cellular invasion compared with VO-control cells (Figure 5.7).

5.3.3.2 Effects of Mutants C51R and R140W on Cell Migration

As cell invasion is related to and encompasses cell migration, cell migration was examined to determine whether oncogenic PBF over-expression is pro-migratory. Stable murine NIH3T3 cells over-expressing VO, WT-PBF, C51R-PBF and R140W-PBF were therefore used to determine the effect of the PBF substitutions on cell migration via classical scratch wound assays. Construction of these stable cell lines over-expressing PBF (>20-fold increase in PBF mRNA, data not shown) was performed as described in section 2.13. The scratch wounds were created when the cells became 100% confluent, and images of wound recovery were captured at 0, 4, 6 and 8 hours after creating the wounds.

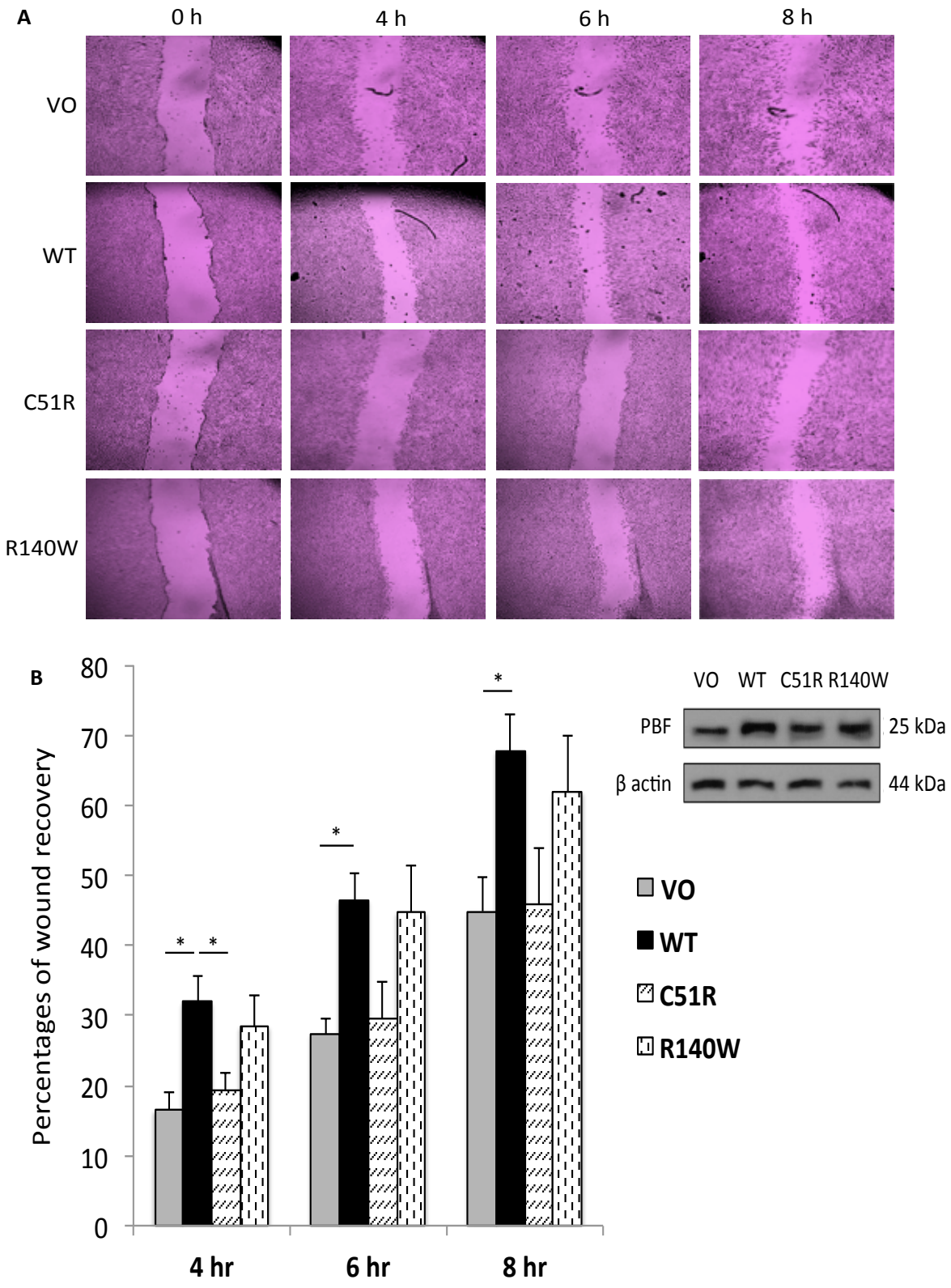

Figure 5.8: Migratory properties of C51R and R140W mutants. *A, representative classical scratch wound assays in NIH 3T3 cells stably transfected with VO, WT-PBF, C51R and R140W substitutions at 0, 4, 6 and 8 hours after creating the wounds. B, Calculated*

*percentages of wound recovery at 4, 6 and 8 hours. Graph represents mean ± SEM from three independent experiments. SEM = standard error of mean. Inset – Western blotting analysis of PBF expression levels relative to β-actin levels in response to transfection. *P<0.05. N=3.*

Figure 5.8A and 5.8B show that wild-type PBF had a significant pro-migratory capacity compared to VO controls at all 4, 6 and 8 hours (P<0.05) post recovery (Fig. 5.8). In contrast, mutant C51R failed to significantly induced wound healing compared to stable VO cells (Fig. 5.8), although mutant R140W appeared closer to retaining WT function in inducing wound recovery than C51R (Fig. 5.8). Therefore, 2 mutations of PBF discovered in colon cancer, one N-terminal and the other C-terminal, both lost the ability to induce cell invasion and also reduced capability to increase cell migration compared to WT-PBF.

Altogether these results demonstrate in thyroid, breast, colorectal and fibroblast cells that oncogenic expression of PBF exhibits a broad and consistent role in promoting cell invasion and migration, but the mutants C51R and R140W lose this ability.

5.3.3.3 *In Vitro* Binding between C51R and Cortactin

PBF specifically interacts and co-localises with CTTN *in vitro* in three cancer cell lines through co-IP, PLA and immunofluorescence, resulting in significantly induced cellular invasion and migration (Fig. 5.2-5.7). Further, C51R and R140W substitutions show significantly reduced cellular invasion in both thyroid and breast cancer cells (Figure 5.7), and lower migratory potential compared to WT-PBF (Figure 5.8). However, the effect of these substitutions, C51R and R140W, on the ability of PBF to interact with

cortactin remains ill-defined and was therefore investigated. However, R140W can only be detected via FLAG tagging, which caused technical issues in initial co-IPs (data not shown). Consequently, it was only possible to examine the interaction between C51R and CTTN.

HeLa cells were transfected with VO, WT-HA, C51R-HA and CTTN-Myc for 48 hours as described in section 2.1.3, before performing co-IP assays.

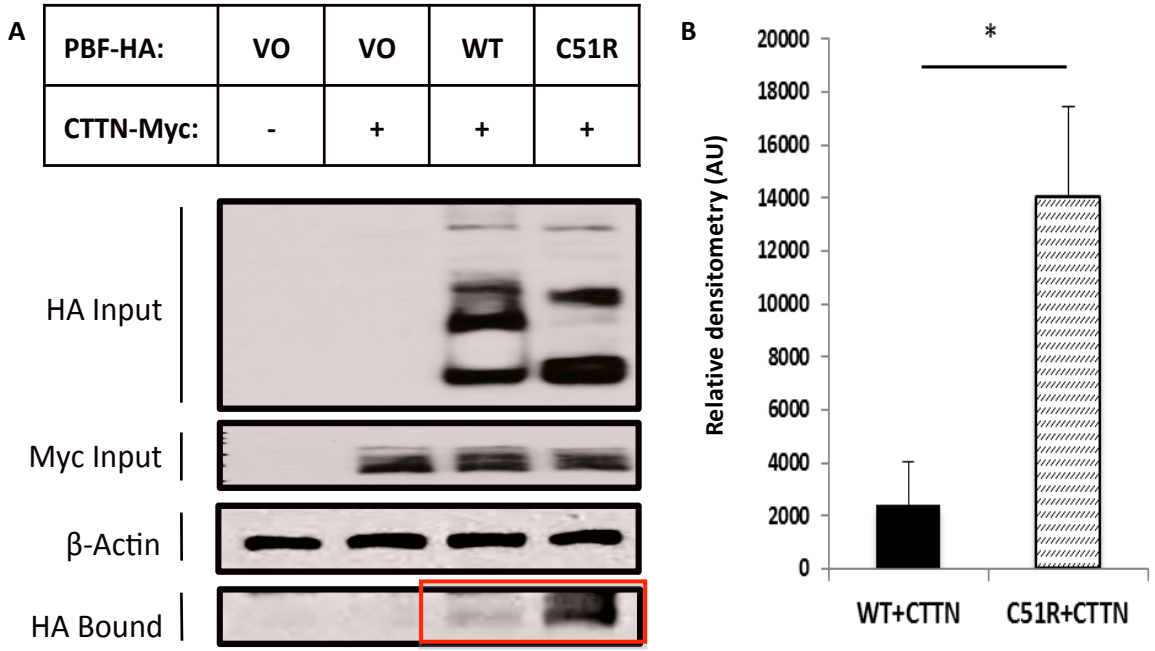

Figure 5.9: C51R substitution increases protein binding with cortactin compared to wild-type PBF. *A, representative co-IP assay illustrating specific interactions (red square) at ~25 kDa between CTTN-Myc and PBF-HA. B, quantification of protein interaction levels through scanning densitometry relative to β-actin from three independent experiments in HeLa cells. Data presented as PBF levels ± SEM. *P<0.05. N=3.*

The co-IP results revealed that arginine substitution at the C51 residue, C51R, was associated with a greatly increased binding affinity with CTTN compared to wild-type PBF (Fig. 5.9; >6-fold; $P<0.05$).

5.3.3.4 Subcellular Localisation of C51R-PBF and Cortactin

To investigate whether the C51R mutation impacts on subcellular location and co-localisation with CTTN further immunofluorescence studies were carried out. Again, R140W was difficult to investigate in this context due to our validated HA and FLAG antibodies both being murine in origin, and mutant R140W being difficult to detect via HA-tagging. We therefore determined only C51R-HA compared to WT-PBF-HA in this study.

After HeLa cervical and SW1736 thyroid cancer cells were transfected with VO, WT-HA, C51R-HA and CTTN-Myc for 48 hours, immunofluorescence assays were performed as described in section 2.6.

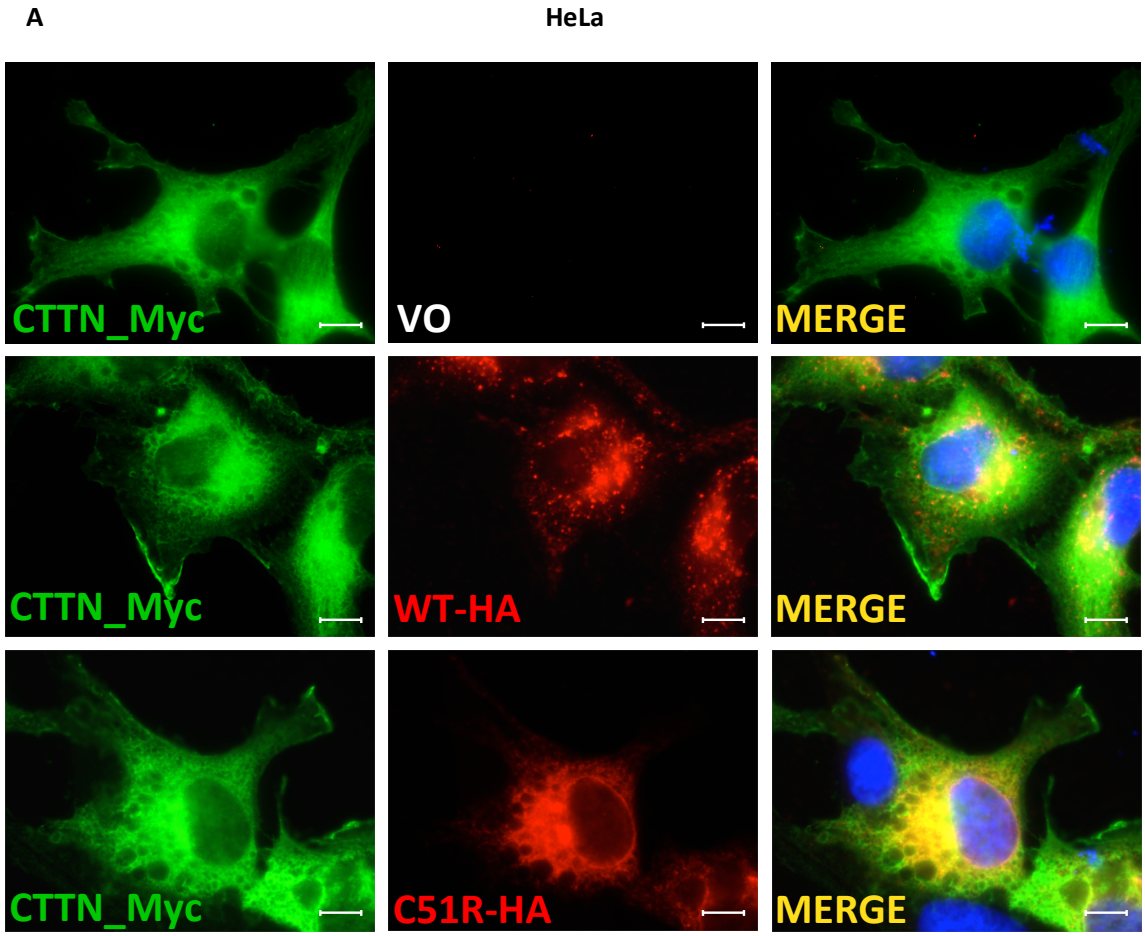

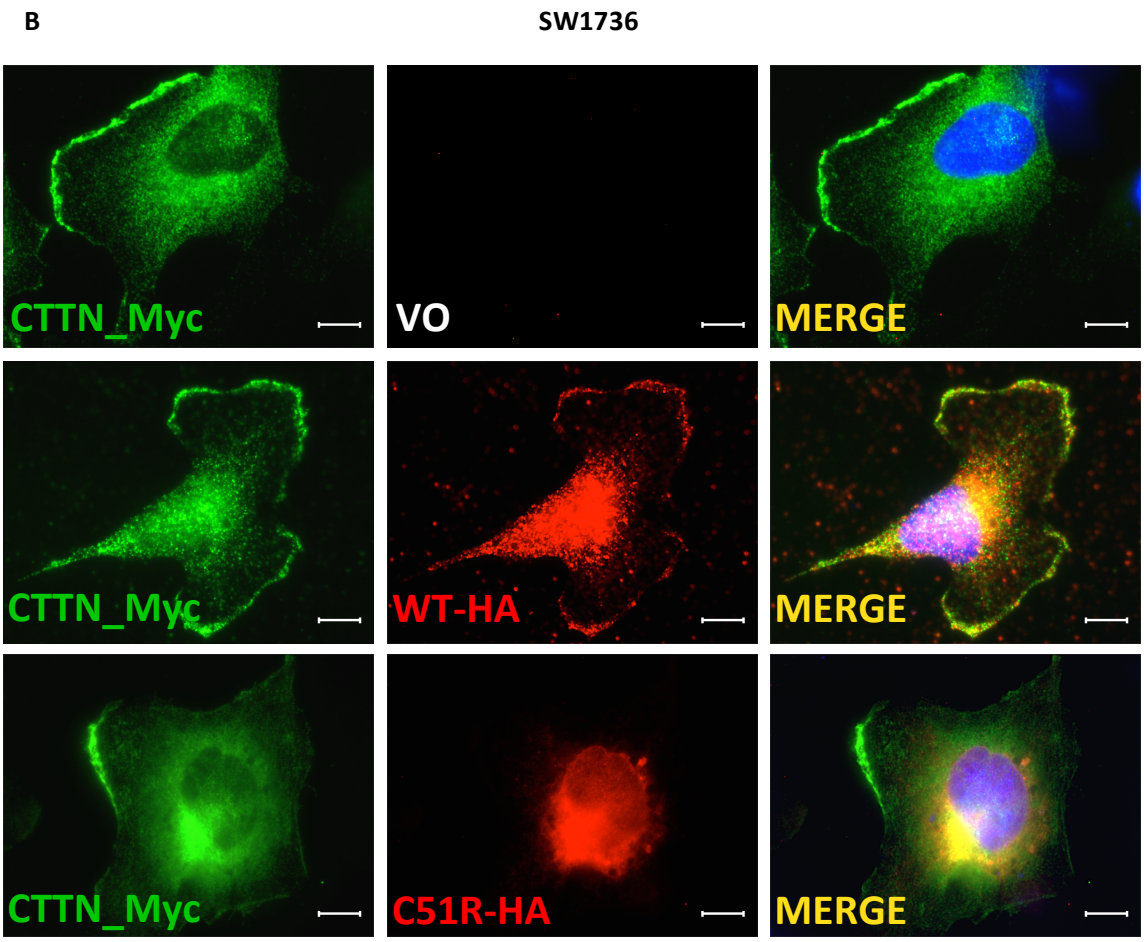

Figure 5.10: WT-PBF and mutant C51R co-localise with cortactin through immunofluorescence assays. *Representative immunofluorescence images showing co-localisation (merge, yellow) between CTTN-Myc (mouse anti-Myc, green) and either WT-PBF-HA (rabbit anti-HA, red) or C51R-PBF-HA (rabbit anti-HA, red) in HeLa (A) and SW1736 (B) cells. Blue indicates DAPI nuclear staining. Magnification = 100X. Scale bars = 20 μm.*

IF experiments in HeLa and SW1736 cells demonstrated that CTTN and WT-PBF were located in both the cytoplasm and the plasma membrane (Figure 5.10), whilst C51R-PBF was mainly apparent in the endoplasmic reticulum (ER) (Figure 5.10) as illustrated previously in Figure 4.10. Interestingly, when HeLa and SW1736 cells were co-transfected with C51R-PBF and CTTN, the location of CTTN seemed to shift away

from the plasma membrane to be more apparent in the intracellular compartment, and co-localised with mutant C51R at the endoplasmic reticulum (Figure 5.10).

Together, co-IP results suggest that C51R binds more strongly with cortactin compared to WT-PBF, and although not quantified, IF suggested that over-expression of C51R was associated with CTTN being localised less intensely at the plasma membrane, where CTTN it is functional. This apparent shift in CTTN localisation might be hypothesised to underlie the reduced ability of C51R to induce cell invasion and migration.

5.4 Discussion

Differentiated thyroid cancer has a 5-year survival rate of 97.7%, but this falls dramatically to 54% in patients with distant metastases (http://seer.cancer.gov/). The statistics are equally unpromising in metastatic breast and colorectal cancer, where patients have a 5-year survival rate of just 26% and 13%, respectively (http://seer.cancer.gov/). In general, as it is the metastasis that ultimately proves fatal, the metastatic pathway requires continued investigation to establish new therapeutic targets. The movement of cells within the metastatic pathway is contingent upon CTTN, which enables individual actin filaments to be assembled into branched structures predominantly at the periphery of cells. However, the cellular actions of CTTN are diverse and incompletely understood, especially as CTTN binds signalling, cytoskeletal, membrane phospholipids and trafficking proteins thereby linking them to dynamic actin networks (Mattila, Batista & Treanor 2016, Kirkbride et al. 2011).

Through extensive mass spectrometry a previous study in the McCabe lab identified CTTN as a potential binding partner of the proto-oncogene PBF. In this Chapter, a clear interaction between PBF and CTTN was demonstrated by co-IP and PLA. PBF phosphorylation at Y174 was of importance to this interaction, which occurred mainly within or close to the PM, as revealed by PLA analysis and immunofluorescent assays. However, the specific binding site between PBF and CTTN is not established in this thesis and should be therefore investigated through a GST pull-down assay to characterise the actual domain where PBF and CTTN interact. Critically, functional CTTN expression was needed in order for PBF to induce invasion. The oncogenic action of PBF would therefore appear to be contingent upon CTTN function.

Expression of PBF has been circumstantially associated with metastasis in patients with breast (Xiang et al. 2012) and thyroid cancer (Hsueh et al. 2013), and we recently reported that colorectal cancer patients who demonstrate extramural vascular invasion have significantly higher PBF expression (Read et al. 2016). However, these associations have not been appraised for causality, and the *in vitro* mechanisms by which PBF induces tumour cell invasion are unclear. For this section of work in the thesis, established thyroid, breast and colorectal models were used to address the mechanism by which PBF induces cellular invasion and migration. A robust finding was that PBF consistently induced pro-migratory and pro-invasive phenotypes across a panel of different cell types and across each of the assays used (Figure 5.5-5.7). These results therefore imply that PBF may represent a novel marker of the ability of cells to escape tumours and invade, which provides further insight for the recent identification of PBF as a central driver gene in human cancers across multiple tumour types including thyroid (Melloni et al. 2014).

Immunofluorescence (IF) assays in cervical HeLa and thyroid SW1736 cells demonstrated that CTTN is predominantly expressed within intracellular vesicles and at the PM (Figure 5.5). WT-PBF has previously been shown to be enriched within late endosomes (Smith et al. 2009). In both HeLa and SW1736 cells, PBF-HA expression was mainly vesicular, and partially overlapped with CTTN-Myc, although not consistently within the same vesicular structures. However, co-localisation was pronounced at discrete PM regions where CTTN-Myc expression was concentrated (Figure 5.5). Together these results indicate that CTTN, as well as binding to PBF, colocalises with PBF predominately at the PM.

As described in Chapter 4, C51R and R140W substitutions provided a significant alteration in both subcellular localisation of PBF itself and cellular proliferation. In this Chapter the impact of these two mutations on cell invasion and migration was determined *in vitro*. Mutants C51R and R140W lost invasive and migratory characteristics in thyroid and breast cancer cells. Co-IP and immunofluorescence assays demonstrated that when PBF was predominantly located in the endoplasmic reticulum by C51R mutation, the invasive capacity of TPC1 and MCF7 cells *in vitro* was lost, which was accompanied by significantly increased PBF:CTTN binding through co-IP experiments (Fig. 5.9), and enhanced co-localisation between the 2 proteins in the ER via IF microscopy (Fig. 5.10). A possible explanation is that C51R-PBF sequestered CTTN activity by pulling it away from its canonical site of action at the PM or by blocking critical interactions with one or more recognised CTTN binding partners such as Src (Sarcoma) and NCK1 (non-catalytic region of tyrosine kinase adaptor protein 1) (Kirkbride et al. 2011). Unfortunately, the precise mechanism of how the R140W mutant abrogates cellular invasion and migration compared to WT-PBF could not be

investigated due to detection problems via HA-tagging of this plasmid. The Biacore system represents another method to gain further insights into potential protein-protein interactions using purified recombinant proteins, including WT-PBF, C51R-PBF, R140W-PBF and CTTN. In these experiments, a sensor chip surface would first be labelled with CTTN and potential protein binding partners such as WT-PBF injected across the surface based on surface plasmon resonance (SPR) technique. This system would help to identify specific binding between two proteins by determining the affinity of their interaction (K_d/K_a values) in real time without the need for labelling. Assessment of the affinity of interaction between CTTN and PBF, as well as PBF mutants, would therefore help to validate the results of co-IP and PLA assays performed in this thesis.

To conclude, the proto-oncogene PBF is a novel interacting partner of the F-actin binding protein CTTN, which regulates the actin-nucleating Arp2/3 complex (Weaver et al. 2001). PBF potently and consistently induces cell invasion and migration, which is dependent upon the presence of functional CTTN. As PBF and CTTN are both induced in multiple tumour types, it is possible that PBF specifically interacts with CTTN to increase invasion and metastasis. Hypothetically, when CTTN is pulled away from the PM via PBF mutation, cell motility, invasion and metastatic mechanisms may be inhibited. Hence, therapeutic strategies to manipulate the interaction between PBF and CTTN by direct or indirect routes might represent promising new avenues in the treatment of tumour metastasis.

CHAPTER 6 - CORRELATION BETWEEN PBF AND CORTACTIN IN HUMAN THYROID CANCER SAMPLES

6.1 Introduction

PBF is a ubiquitously expressed glycoprotein that is induced in multiple endocrine neoplasias including pituitary and thyroid (McCabe et al. 2003, Smith, Franklyn & McCabe 2011, Smith, Franklyn & McCabe 2010). PBF is also associated with decreased specific survival and increased early recurrence and distant metastasis at the time of diagnosis in papillary thyroid cancer (Hsueh et al. 2013), while colon cancer having extramural invasion has higher PBF expression (Read et al. 2016). PBF is associated with vesicular trafficking, and interacts with multiple transport proteins such as MCT8 (Monocarboxylate transporter 8), modulating thyroid hormone action (Smith et al. 2013), NIS, modulating radioiodine uptake in thyroid cells (Smith, Franklyn & McCabe 2011, Smith et al. 2009), and p53, impacting its stability and ubiquitination (Read et al. 2016, Read et al. 2014). Extensive mass spectrometry from our group also showed that cortactin was a potential binding partner of PBF. Moreover, we already revealed in the previous Chapter 5 that overexpressed PBF significantly induced cellular invasion and cell migration in a panel of cell lines, including thyroid, colon and breast cancer cells, via a mechanism dependent upon the presence and subcellular localisation of cortactin. The C51R substitution increased binding affinity with CTTN predominantly within the endoplasmic reticulum, resulting in significantly reduced cellular invasion and cell migration.

Cortactin (CTTN) is a cytoskeleton protein that enhances actin polymerization and prohibits debranching of actin networks (Weaver et al. 2001), resulting in the promotion of cell motility and cellular invasion in a variety of cancer cells such as breast and head and neck squamous cell carcinoma (HNSCC) (Spring et al. 2015, Fantozzi et al. 2008). CTTN is also upregulated in a panel of human malignant tumours such as colon

cancer, oral squamous cell carcinoma (SCC) and esophageal cancer (Cai et al. 2010, Ni et al. 2015, Yamada et al. 2010, Lu et al. 2014). For example, Ni et al. reported upregulation of CTTN expression in colon cancer compared to normal tissue, and that overexpression was associated with tumour size, staging, lymphatic invasion and prognosis (Ni et al. 2015). In oral SCC, cortactin overexpression was found more commonly in high grade and aggressive carcinomas (Yamada et al. 2010). Xu et al. also found that there was a significant increase in CTTN expression levels in melanoma compared to normal nevi, with higher expression levels in metastatic compared to non-metastatic cancers (Xu et al. 2010). They also revealed that high CTTN levels were associated with poorer disease-specific survival compared to those who had low CTTN expression (Xu et al. 2010). Although there is a range of evidence addressing the influence of CTTN on cancer outcome, no studies to date have investigated CTTN expression in well-differentiated thyroid cancer.

In this Chapter, we therefore determined PBF and CTTN expression, including mRNA and protein levels, in differentiated thyroid cancer, and also investigated the correlations between the expression levels of these 2 genes in ex vivo human samples.

6.2 Materials and Methods

6.2.1 Protein Homogenisation and Quantification

After weighing normal and tumourous thyroid cancer samples (obtained via local ethical approval; LREC 05/Q2704/43), protein homogenisation, protein extraction and Bicinchoninic Acid (BCA) assays were performed as described in section 2.2 and section 2.3 to quantify and prepare the samples for Western blotting.

6.2.2 Western Blotting

Western blotting in this study was applied to quantify protein levels of cortactin in human thyroid samples. The procedure was carried out as described in Section 2.5. The primary antibodies used in this chapter were mouse monoclonal anti-CTTN (1:500, Merck and Millipore, Germany) and mouse monoclonal anti-β-actin AC-15 (1:10000, Sigma, USA).

6.2.3 Ribonucleic Acid (RNA) Extraction of Formalin-fixed, Paraffin-embedded (FFPE) Samples

After determining areas of normal and cancerous lesions of human thyroid FFPE samples under the microscope, samples were scraped using a sterile scalpel, transferred to a 1.5 ml Eppendorf, and then kept on ice. Changing blades and leaving a small area between normal and cancer tissue were vital to prevent cross-contamination between the samples. RNA was next extracted from the FFPE samples using RNeasy FFPE kit (Qiagen, USA) following the manufacturer's instructions. Firstly, paraffin coated tissue was removed by adding 160 µl Deparaffinization Solution (Qiagen, USA) to each sample, vortexing vigorously for 10 seconds, and centrifuging briefly to let the sample fall to the bottom of the Eppendorf. After the sample was incubated at 56°C for 3 minutes and left to cool at room temperature, 150 µl Buffer PKD or proteinase K digestion buffer (Qiagen, USA), an optimized lysis buffer containing proteinase K that was used to release RNA from the sections, were added and mixed by vortex. The sample was then centrifuged at 10,000 rpm for 1 min, before 10 µl proteinase K were added to the clear

lower phase of the tube and mixed by pipetting up and down. Next, the RNA was incubated at 56°C for 15 minutes, then at 80°C for the next 15 minutes. The clear content was transferred to a new Eppendorf and incubated on ice for 3 minutes, before being centrifuged at 13,500 rpm for 15 minutes. The supernatant was next transferred to a new microcentrifuge tube, and 16 µl of DNase Booster Buffer (Qiagen, USA) were added, before being mixed gently by inverting the Eppendorf and centrifuging briefly. After the RNA was incubated at room temperature for 15 min, 320 µl Red Blood Cell lysis solution (Qiagen, USA) was mixed thoroughly to optimise binding conditions. 720 µl 100% ethanol were applied to the sample, and mixed by pipetting, before the content was transferred to an RNeasy MinElute spin column placed in a 2 ml collection tube (supplied in the kit). The tube was centrifuged at 10,000 rpm for 15 seconds, and the flow-through was discarded. 500 µl Buffer RPE were added to the spin column, and centrifuged at 10,000 rpm for 15 seconds, before discarding the flow-through. Another 500 µl of Buffer RPE were placed into the spin column, and the tube was centrifuged at 10,000 rpm for 2 minutes to wash the column membrane. The old collection tube and the flow-through were discarded, and the spin column was placed into a new collection tube, before being centrifuged with the lid open at full speed for 5 minutes to get rid of all residual ethanol. After the RNeasy MinElute spin column was inserted into a new sterile collection tube, 14 µl RNase-free water were added directly to the membrane, and centrifuged at full speed for 1 minute to elute the RNA. The concentration of RNA samples were quantified using the NanoDrop Spectrometer (NanoDrop Products, USA) and the extracted RNA products were stored at -80°C.

6.2.4 One Step Reverse Transcription and Quantitative Real-time Polymerase Chain Reaction (One Step RT-PCR)

The one step RT-PCR assay is a technique allowing the process of reverse transcription and polymerase chain reaction to occur sequentially in the same tube using any RNA samples. The one step RT-PCR kit (Qiagen, UK) provides specific enzymes, including Sensiscript and Omniscript reverse transcriptases, having high affinity for RNA samples, and HotStarTaq DNA polymerase, yielding specific PCR amplification by stopping extension of nonspecific annealed primers when PCR cycle starts.

In this Chapter, the mRNA expression of genes including PBF and cortactin in matched normal and thyroid cancer samples was determined by using one step RT-PCR (Qiagen, UK) following the manufacturer's instructions, and compared with the internal controls PPIA (peptidylprolyl isomerase A (cyclophilin A)) and HPRT1 (hypoxanthine gaunine phosphoribosyltransferase 1). The TaqMan probes (Life technologies, UK) were oligonucleotides consisting of a 5'fluorophore, VIC for HPRT1 and FAM (6-carboxy-fluoresciein) for other genes, and a 3'quencher, which was TAMRA (6-carboxy-tetramethyl-rhodamine). Each sample consisted of 20 ng of RNA combined with 1 μl of each TaqMan gene set, 10 μl of 2x QuantiTect Probe RT-PCR Master Mix (Qiagen, UK), 0.2 μl of QuantiTect RT Mix (Qiagen, UK) and 6.8 μl of nuclease free water in a 96-well plate. Polymerase chain reaction (PCR) was performed to evaluate the cycle threshold (Ct) values using the ABI prism 7500 real-time PCR system. There were two steps consisting of reverse transcription and PCR cycles as follows: 50°C for 30 minutes; 95°C for 15 minutes; 45 cycles of 94°C for 15 seconds and 60°C for 60 seconds. Comparative cycle threshold (ΔCt) values were obtained from the Ct value of the gene of interest

deducted from the Ct value of internal controls, and then A ΔΔCt value was calculated, and used to ascertain a fold change to determine relative mRNA expression with an equation: $2^{-(\Delta Ct \text{ of an experimental group} - \Delta CT \text{ of a control group})}$ or $2^{-\Delta\Delta Ct}$.

6.2.5 Statistical Analysis

In this Chapter, Spearman's rank correlation coefficient was used to study the significance of the association between PBF and cortactin gene expression datasets. If two variables show the same tend, the coefficient or rho (r) is positive. However, if two variables have an inverse trend, the rho is negative. When two parameters correlate perfectly, the rho is closer to 1 or -1. A correlation of zero (0) implies that there is no association between them (http://www.biostathandbook.com/spearman.html). The non-parametric Kruskal-Wallis test was also used to compare statistical differences between median values in non-matched samples.

6.3 Results

6.3.1 mRNA Expression Levels of Pituitary Tumor Transforming Gene 1 - Binding Factor (PBF) and Cortactin in Normal and Matched Human Thyroid Cancer Samples

PBF expression has been documented in multiple tumours such as pituitary, breast, colon and thyroid (McCabe et al. 2003, Watkins et al. 2010, Read et al. 2016, Smith, Franklyn & McCabe 2010, Smith, Franklyn & McCabe 2011). Cortactin expression has also been investigated in a variety of human cancers, but has not been addressed in

well-differentiated thyroid cancer (DTC). In this study, we determined the mRNA levels of PBF and CTTN expression in a series of N=43 matched tumour and normal DTC formalin-fixed, paraffin-embedded (FFPE) specimens through one step RT-PCR.

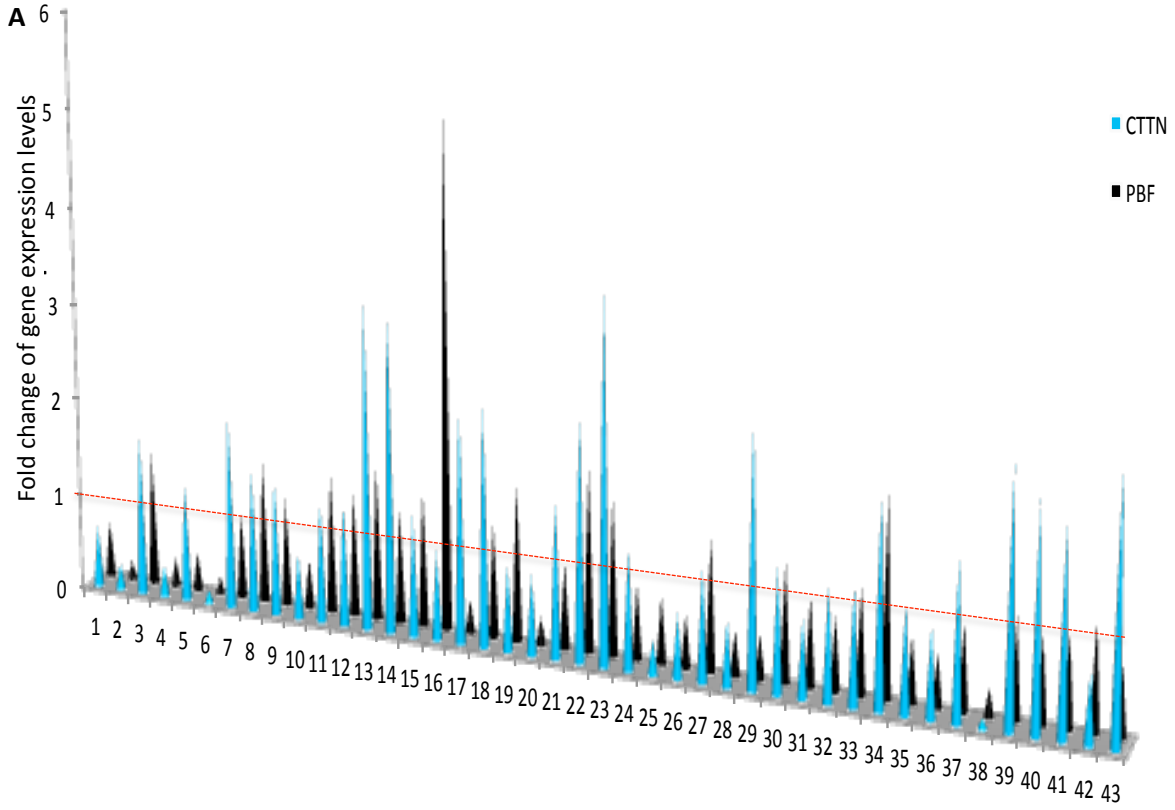

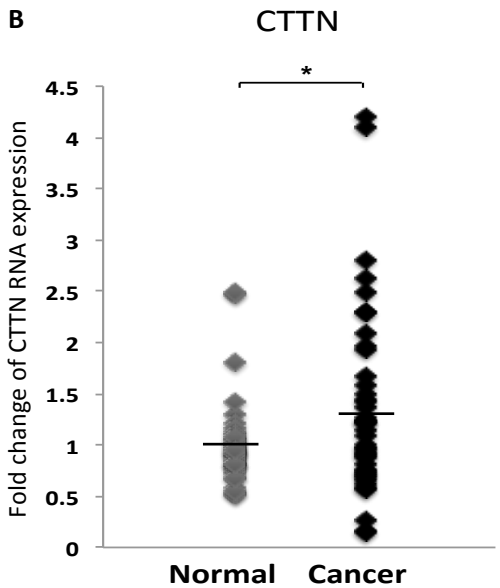

n	43	43
Mean±SE	1.0±0.1	1.35±0.1

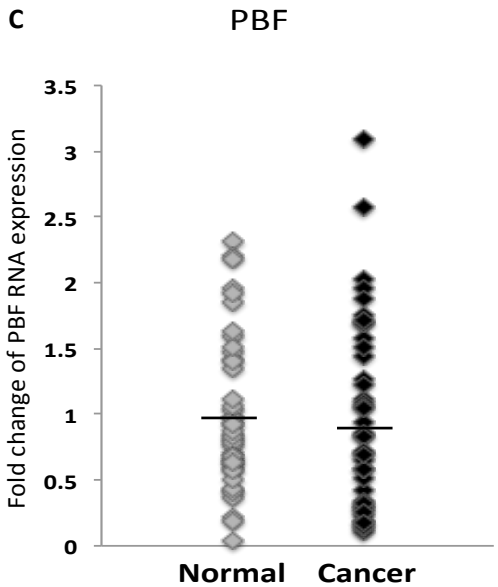

n	43	43
Mean±SE	1.0±0.1	0.95±0.1

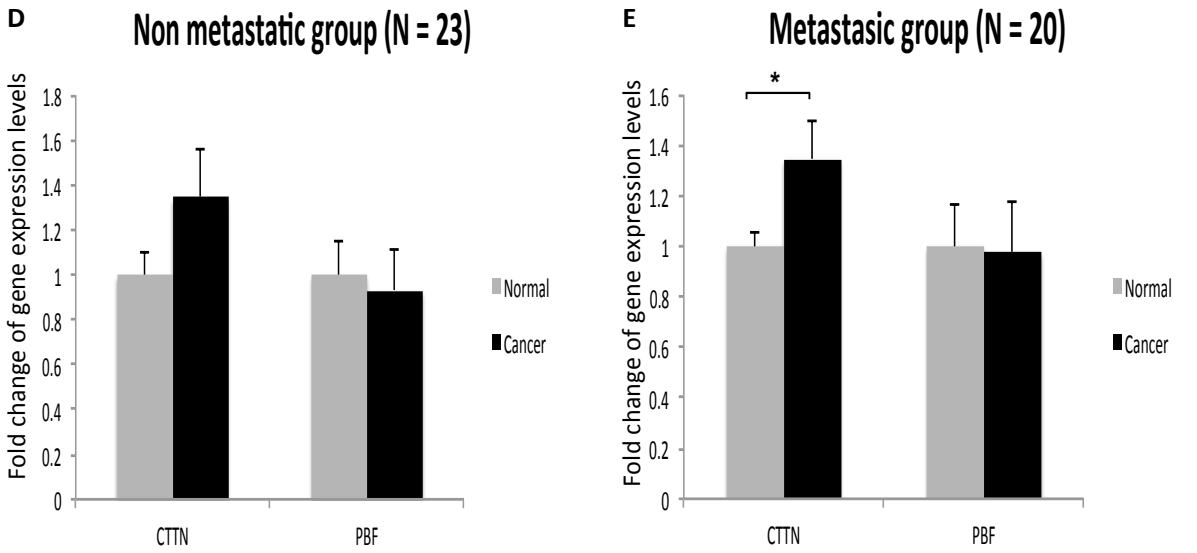

Figure 6.1: CTTN is over-expressed in thyroid cancer, especially in metastatic disease. *A, quantification of fold change of CTTN and PBF expressions in thyroid tumours relative to matched normal tissue (N=43). Red dashed line represents a relative fold change = 1.0. The value above the red dashed line (1) illustrates overexpression of CTTN or PBF in a thyroid cancer compared to matched normal tissue. B and C, quantification of fold change of RNA expressions of CTTN (B) and PBF (C) comparing between cancers and matched normal thyroid samples (N=43). Black lines show mean fold change of CTTN (B) and PBF (C) RNA expressions in each group. D, quantification of fold change of CTTN and PBF RNA expressions in thyroid cancers relative to matched normal tissue in non metastatic group (AnyT, N0, M0), N=23. E, quantification of fold change of CTTN and PBF RNA expressions in thyroid cancers relative to matched normal tissue in the metastatic group (AnyT, N1, AnyM), N=20. Results are mean ± SEM for B, C, D and E. *P<0.05 (Student's t-test).*

The results revealed CTTN RNA expression was variable, but showed a significant approximately 1.5-fold induction overall in N=43 tumours compared with matched normal thyroid tissue (Fig. 6.1A and 6.1B). In contrast to previous studies (Stratford et al. 2005) PBF RNA expression did not differ between tumours compared to

matched normal thyroid tissue (Fig 6.1A and 6.1C). Indeed, in Stratford et al. 2005, there was a 3-fold increase in PBF expression in thyroid cancer compared to normal tissue, and they used the tissue of contralateral lobe of thyroid glands to be normal samples (Stratford et al. 2005). In contrast, the matched normal tissue in this Chapter came from the normal area within the same FFPE slides having tumour, probably having higher tendency to contain non cancerous abnormality such as hyperplasia and resulting in more similar levels of PBF expression in both tumour and normal samples. A further consideration is that PBF expression is reported to be highly elevated in more aggressive and recurrent thyroid disease. In this study, a broad range of thyroid cancers with different TNM staging was used from T1 to T3, and the majority of samples were non-metastatic (N0). In contrast, the majority of samples used in the study by Stratford et al 2005 were from more aggressive cancers (i.e TNM staging of T3 and N1). Hence, differences in the size and aggressiveness of thyroid tumours examined in my study may have accounted for the disparate result.

When we classified patients into 2 groups, non-metastatic and nodal metastatic disease (Fig 6.1D and 6.1E), only the metastatic group had significant CTTN overexpression in tumours compared to normal tissue (Fig. 6.1E; $P<0.05$). However, PBF expression did not differ in either classification (Fig 6.1D and 6.1E).

6.3.2 Correlation of Genes of Interest

We first next determined the association between CTTN and PBF gene expression in human well-differentiated thyroid cancer (N=43).

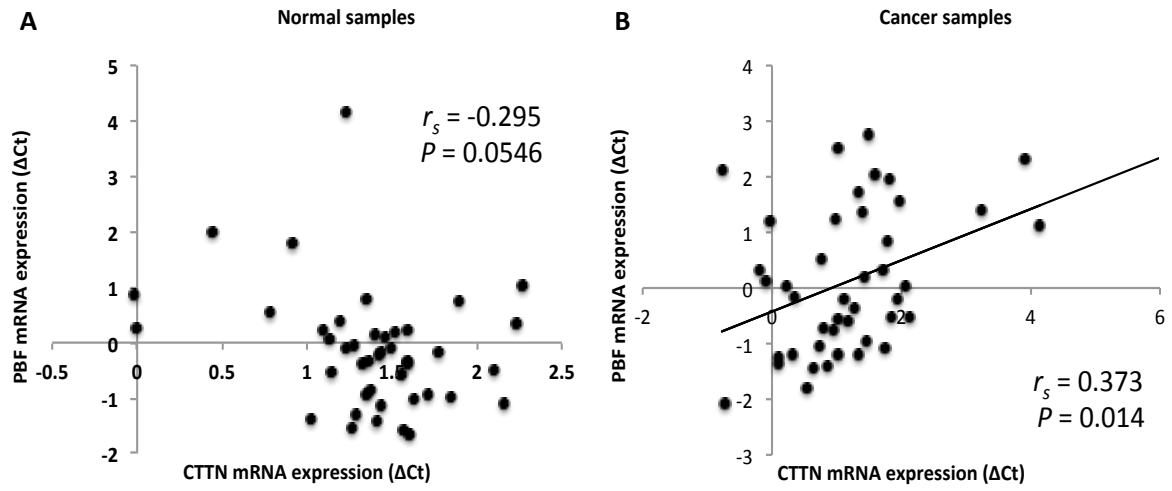

Figure 6.2: CTTN is correlated with PBF in thyroid cancer. *Scatterplot showing relationship between CTTN and PBF gene expression in normal thyroid tissue (A) and in human well-differentiated thyroid cancer (B). Data represented as ΔCt values of CTTN and PBF expressions, and a correlation was determined via Spearman's rank correlation. N=43.*

The result using the Spearman's rank correlation coefficient analysis showed a positive and significant correlation expression between CTTN and PBF genes in human DTC (P=0.014; r_s=0.373; N=43) (Figure 6.2B), while there was no any association between two genes in normal thyroid tissue (P=0.0546; r_s=-0.295; N=43) (Figure 6.2A).

6.3.3 Protein Expression Levels of Cortactin in Normal and Human Thyroid Cancer Samples

We next determined the protein expression levels of cortactin comparing human thyroid cancer and normal thyroid samples through Western blotting analysis. The protein samples were extracted from fresh thyroid tissues of a further 9 patients which did not belong to the 43 FFPE samples used in section 6.3.1 and 6.3.2.

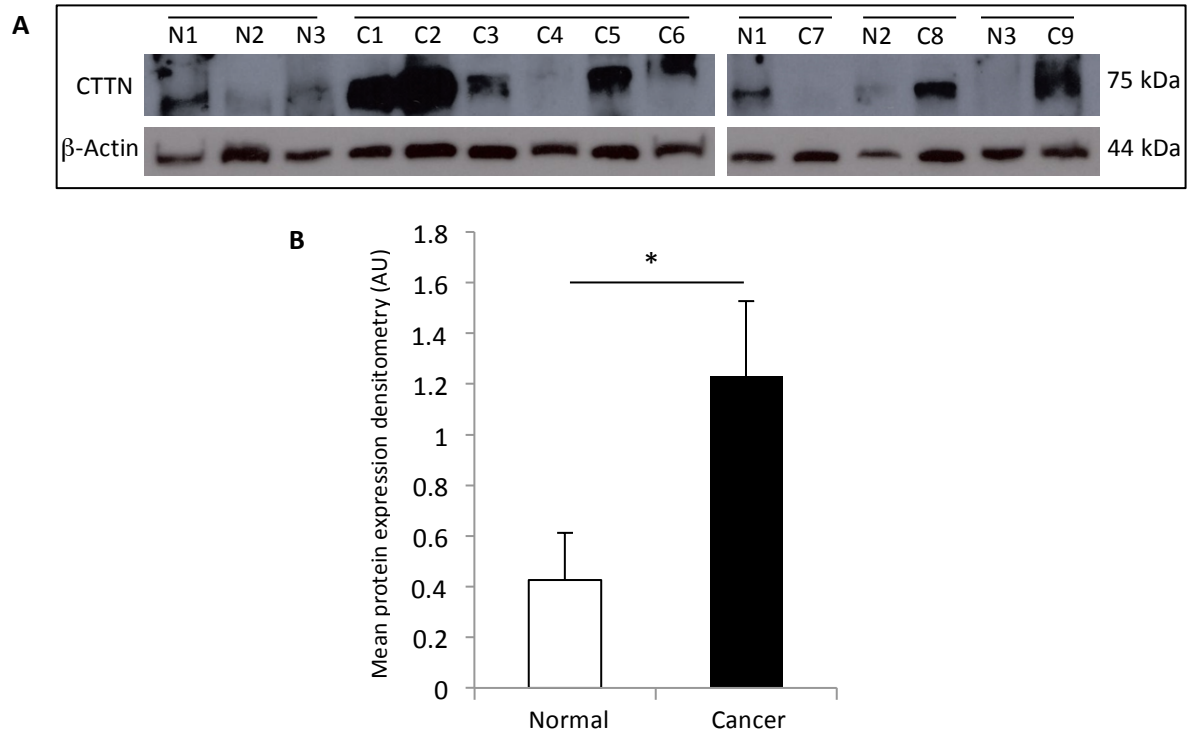

Figure 6.3: CTTN protein is over-expressed in thyroid cancer, determined through Western blotting. *A, detection of CTTN expression by Western blotting in thyroid tumours (C1-9) and normal tissue (N1-3), with quantification of relative protein levels shown in B. *P<0.05 (Student's t-test).*

CTTN expression was also increased in a small additional series of DTC specimens by Western blotting (Figure 6.3A). Again, CTTN expression was relatively variable, but scanning densitometry revealed a statistically significant ~3-fold induction in CTTN protein level in tumours compared to normal thyroid (Figure 6.3B).

6.3.4 Correlation between PBF and CTTN in Human Thyroid Cancers from the TCGA Database

We further evaluated mRNA levels of CTTN and PBF expression and their correlation in well-differentiated thyroid cancer as detected by RNA-seq, from the TCGA database, in which gene expression data for a large number of thyroid tumours (N=326), with complete clinical annotation, are available.

For TCGA database, the normalized gene expression data generated using the Illuminia RNA-seq platform and the clinical information from the cBioPortal were downloaded. Gene expression values based on RNA-seq data were transformed as $X = \log_2(X+1)$ where X represents the normalized fragments per kilobase transcript per million mapped reads (FPKM) values retrieved from the TCGA dataset. For matched normal (N) and tumour (C) pairs relative fold-changes (FC) were transformed as $\log_2 FC = \log_2(C) - \log_2(N)$ where C and N represent normalized FPKM values.

The error bars for the RNAseq data based on $\log_2$ FPKM values would be wide as they were plotted on a box-whisper plot in which the error bars show the full distribution of the data (i.e. from the third quartile to the maximum value), and the median value is shown instead on the mean value in the qPCR data. The non-parametric Kruskal-Wallis test however clearly showed a significant difference between datasets which is indicative of a difference in median values as well as in the overall distribution of the data.

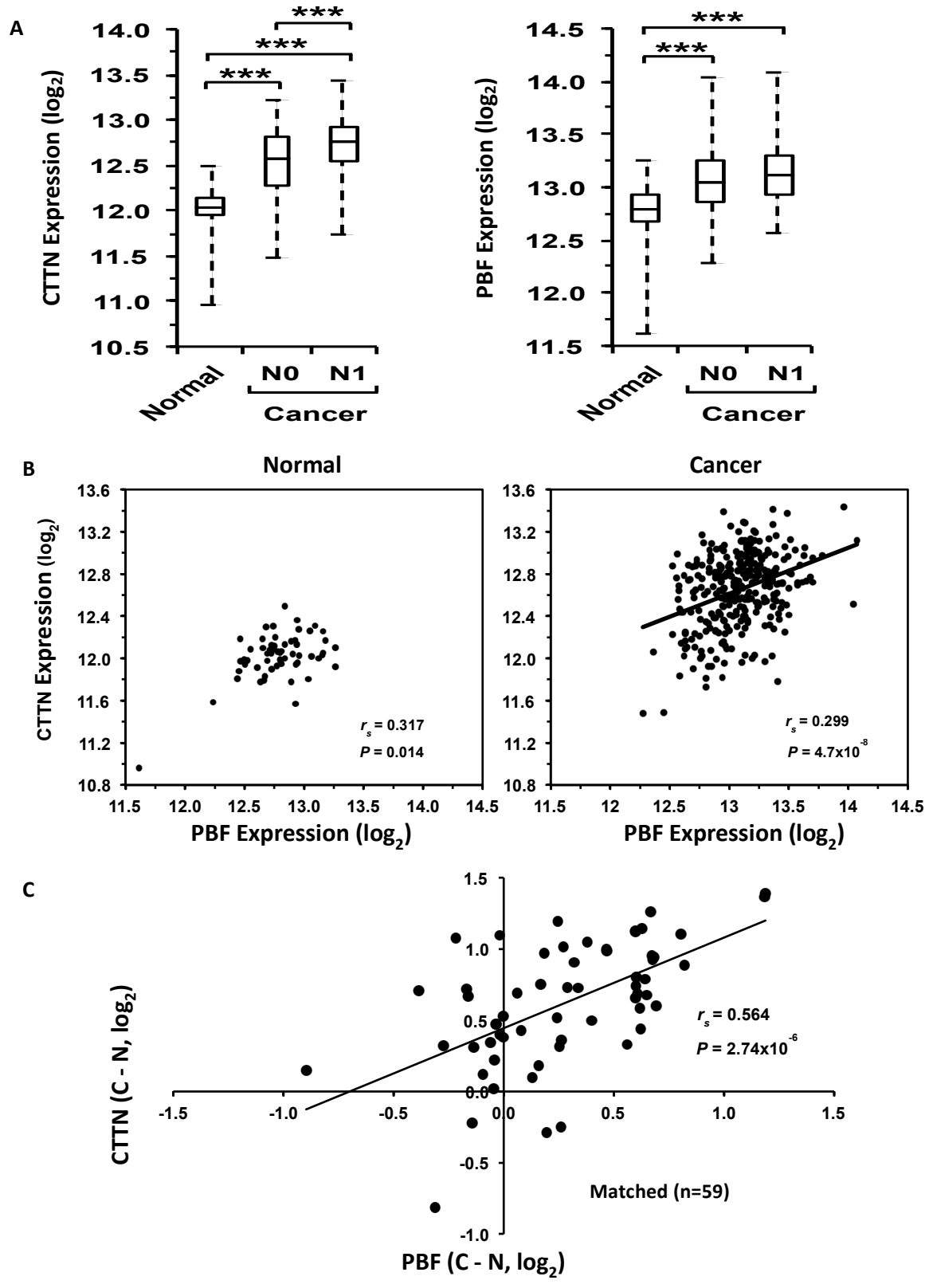

Figure 6.4: CTTN is upregulated in thyroid cancer and associated with PBF via the TCGA data. *A, CTTN and PBF gene expression levels are increased in non-metastatic (N0; N=121) and metastatic (N1, N=205) thyroid cancer versus normal thyroid (N=59). Data*

*represented in box plots. ***P<0.001 (Kruskal-Wallis test). B, scatterplots showing correlation between CTTN and PBF gene expression in normal and DTC samples. P=0.014; r_s=0.317; N=59 for normal tissue and P=4.7 x 10^{-8}; r_s=0.299; N=326 for thyroid cancer. C, scatterplot illustrating correlation in the fold-change in relative gene expression between CTTN and PBF in matched cancer and normal pairs (shown as log_2 values). P=2.74 x 10^{-6}; r_s=0.564; N=59. Data analysed by Spearman's rank correlation in B and C.*

Consistent with our initial observations in section 6.3.1, 6.3.2 and 6.3.3, we also found a significant increase in CTTN mRNA expression (Fig. 6.4A) in both non-metastatic (N0; *P*=5.6 x 10^{-17}; N=121) and nodal metastatic DTC (N1; *P*=7.5 x 10^{-27}; N=205) compared to normal thyroid tissue (N=59). Moreover, PBF expression from the TCGA database (Fig. 6.4A) was induced in both non-metastatic (N0; *P*=1.0 x 10^{-7}; N=121) and nodal metastatic DTC (N1; *P*=8.5 x 10^{-13}; N=205), in contrast to PBF mRNA expression being similar in our own samples of normal and tumourous tissue. Importantly, we again found a strong correlation between CTTN and PBF gene expression in both normal and DTC (Figure 6.4B; *P*=0.014; r_s=0.317; N=59 for normal thyroid and *P*=4.7 x 10^{-8}; r_s=0.299; N=326 for cancer). Examination of relative fold-changes in CTTN and PBF expression using matched tumour and normal samples (N = 59) in the TCGA dataset also showed a strong correlation (Fig. 6.4C; *P*=2.74 x 10^{-6}, r_s=0.564).

Together our results demonstrated that even being quite variable, CTTN was noticeably over-expressed in well-differentiated thyroid cancer, especially in patients carrying metastasis, and also significantly correlated with PBF expression. Of particular significance, CTTN gene expression (Figure 6.4A) was higher in invasive nodal metastatic DTC (N1; *P*=3.6 x 10^{-5}) than in non-metastatic DTC (N0). In addition, in the

larger TCGA dataset PBF was up-regulated in thyroid cancer compared to normal tissue, although there was no PBF induction when comparing nodal metastatic and non-metastatic thyroid cancer (Figure 6.4A).

6.4 Discussion

CTTN expression has not been determined before in human thyroid tumours. In this study analysis of human DTC specimens revealed that CTTN expression, whilst variable, was elevated in approximately two thirds of tumours, with an overall induction of around 1.5-fold at the mRNA level and 2.5-fold at the protein level. Importantly, analysis of a much larger clinically annotated genomic dataset (TCGA) for DTC confirmed that CTTN was significantly increased in DTC, especially in cases where regional lymph node metastasis (N1) was present. A significant positive association between PBF and CTTN mRNA expression was also evident in DTC specimens from our group, as well as in the TCGA dataset. This would not likely result from direct transcriptional regulation via either binding partner as recent *in vitro* experiments in our laboratory have shown that neither CTTN nor PBF were capable of upregulating the other (Watkins et al. 2016, Manuscript under revision). Previously, amplification of the gene that encodes CTTN has been reported in ~15% of primary metastatic breast carcinomas and ~30% of head and neck squamous cell carcinomas (Buday, Downward 2007). Thus the apparent induction of CTTN in DTC may be via gene amplification, or other gene regulatory mechanisms. Notwithstanding this, CTTN over-expression has been extensively linked to invasive cancers, including glioblastoma, melanoma and colorectal cancer (Kirkbride et al. 2011, Xu et al. 2010, Hirakawa, Shibata & Nakayama 2009).

PBF is upregulated in multiple types of human cancer, especially endocrine neoplasias, and has been associated with poor prognosis (McCabe et al. 2003, Watkins et al. 2010, Read et al. 2016, Smith, Franklyn & McCabe 2010, Smith, Franklyn & McCabe 2011). In this Chapter, the analysis of differentiated thyroid cancer in the TCGA dataset illustrated DTC harboured a significant increase in PBF mRNA expression levels compared to normal samples, although the mean levels were similar in both non-metastatic and nodal metastatic groups. In our smaller series (N=43) there was no difference in PBF mRNA expression comparing cancer and matched normal thyroid tissue. This may in part reflect the problem of how to define normal thyroid tissue on FFPE slides. Our samples for the normal category included either an area with no grossly abnormal histopathology, or an area having hyperplastic or macrofollicular structure. Importantly, Read et al. showed that human multinodular goitre or thyroid tissue demonstrating hyperplastic or macrofollicular structure had higher PBF expression compared to normal thyroid (Read et al. 2011). Thus the constraints of estimating that a histopathological region is 'normal' may underlie the reason that PBF expression in our group of 43 samples was similar in normal and cancer specimens.

In this study RNA was extracted from FFPE-fixed thyroid tissue which is known to be highly degraded. Instead I focused my efforts in developing techniques such as one-step RT-PCR that can be used to determine expression levels in degraded RNA samples. This was achieved by using specific targeted primers of PBF or CTTN to perform both reverse transcription and qPCR in a single step. In addition, the primers were chosen to produce only short amplicons in the PCR reaction (<100 bases) which helps the detection of gene expression in degraded RNA samples.

In conclusion, this is the first study to determine CTTN expression in well-differentiated thyroid cancer, and reveals a significant correlation between CTTN and PBF mRNA expression. As both genes promote cell migration, cell invasion and tumour metastasis, both cortactin and PBF might be specific targets in the treatment of thyroid cancer metastasis. However, further experiments are needed to address this hypothesis.

CHAPTER 7 - EFFECT OF PBF MUTATIONS C51R AND R140W ON RADIOIODINE UPTAKE

7.1 Introduction

In the previous Chapters, it was apparent that whilst wild-type PBF significantly induces cellular proliferation, cell invasion and cell migration, some PBF substitutions retain these properties whereas others do not. In addition, PBF is significantly upregulated in thyroid cancer, and patients diagnosed with papillary thyroid cancer who demonstrate overexpressed PBF are also more likely to have distant metastases at the time of diagnosis, and poorer disease specific survival compared to patients who have low PBF expression levels (Hsueh et al. 2013).

Successful radioactive iodine (RAI) treatment is a necessary step to destroy remaining thyroid cancer cells after surgery, and influences the prognosis of this particular cancer, by virtue of significantly reduced locoregional recurrence and distant metastasis (Sawka et al. 2004). RAI therapy also facilitates long term follow up and early detection of tumour recurrence or metastasis in patients who undergo total thyroidectomy by scheduled measurement of serum thyroglobulin (Tg) levels or RAI scanning. However, thyroid tumour tissues are able to take up only a small amount (around 0.1-27%) of administered ^{131}I, while the remaining ^{131}I is excreted via kidney (Maxon et al. 1983).

The data from our group previously demonstrated that overexpressed PBF significantly reduced radioiodine uptake by two mechanisms. Firstly, PBF upregulation significantly represses activity of the gene promoter of NIS, leading to decreased NIS expression (Boelaert et al. 2007). Secondly, PBF interacts with and modulates the subcellular localisation of NIS from the plasma membrane to intracellular late endosomes, where NIS co-localises with PBF and is non-functional, contributing to decreased functional activity of NIS *in vitro*, and resulting in reduced radioiodine uptake

(Smith et al. 2009). Transgenic mice with targeted thyroid specific PBF overexpression also showed reduced NIS expression and impaired radioiodine uptake (Read et al. 2011).

NIS, or solute carrier family 5 membrane 5 (SLC5A5), is encoded by the SLC5A5 gene. It is a transmembrane glycoprotein with 13 transmembrane domains and a molecular weight of around 90 kDa. NIS delivers two sodium cations for an iodide anion into thyroid cells and regulates iodine uptake into follicular cells. This process is positively influenced by thyroid-stimulating hormone (TSH) in thyroid cells via both transcriptional and posttranslational mechanisms (Kogai, Brent 2012, Kogai, Taki & Brent 2006). In contrast, transforming growth factor beta or TGFβ, which is induced by several factors including the $BRAF^{V600E}$ mutation, negatively regulates NIS expression and also inhibits NIS localising at the plasma membrane (Kogai, Brent 2012). Indeed, overexpression of TGFβ1 significantly repressed TSH-stimulated NIS mRNA and protein expression levels, reflecting reduced ability to uptake radioiodine in FRTL-5 rat thyroid cells (Kawaguchi et al. 1997). Importantly, a low level of NIS mRNA expression is associated with aggressive papillary thyroid carcinomas (Ward et al. 2003).

In this Chapter, the impact of the substitutions C51R and R140W identified *in vivo* on the well-described ability of PBF to repress the central thyroid cancer treatment of radioiodine uptake was appraised. The hypothesis was that alteration of subcellular localisation of PBF mutants might affect co-localisation with NIS, resulting in an altered ability to uptake radioiodine, which is critical for treatment of thyroid cancer.

7.2 Materials and Methods

7.2.1 Cell Culture and Transfection

TPC1 and MCF7 cells were maintained in RPMI containing 10% FCS as described in section 2.1.1.1. The cells were transfected with VO, WT-PBF, C51R-PBF, R140W-PBF and NIS-Myc as described in section 2.1.3.

7.2.2 Radioiodine Uptake Assays

Radioiodine uptake assays were performed in cells co-transfected with VO, wild-type PBF, mutated PBF and the sodium iodide symporter (NIS). After 48 hours of transfection, sodium perchlorate was added to block iodine uptake in control samples for 1 hour, before administration of 10^{-4}M sodium iodide (NaI) and 0.05 µl ^{125}I solution and incubation at 37°C for an hour. Next, Hank's balanced salt solution (HBSS) was used to wash away any excess radioiodine, ensuring that only iodine that was internalised into the cells was measured. Finally, cells were lysed twice with 2% sodium dodecyl sulfate (SDS) and the radioactivity was count using a LKB Wallac 1260 Multi gamma II gamma counter. All results of radioiodine uptake assays were normalized to control samples with sodium perchlorate. The control data demonstrated background radioiodine levels and all other data represent NIS-specific uptake of radioiodine into the cells.

7.2.3 Protein Quantification for Actual Radioiodine Counts (Bicinchoninic Acid Assay or BCA)

After measuring the radioiodine activity, protein concentration was measured using the bicinchoninic acid (BCA) assay kit as described in section 2.2, with cell lysates compared to bovine serum albumin (BSA) standards of 0, 0.125, 0.25, 0.5, 0.75, 1 and 2 mg/ml in 2% SDS solution. The standard curve produced from the BSA standard concentrations was then used to determine the protein concentration. Finally, the sample concentration and the relative radioiodine count measured with the Wallac gamma counter were used to calculate the actual radioiodine counts.

7.2.4 Western Blotting

Western Blotting was performed as described in Section 2.5. The primary antibodies used in this Chapter were mouse anti-Myc (1:1000, Cell Signaling, UK), rabbit anti-PBF (1:500, In-house) and mouse anti-β-actin AC-15 (1:10000, Sigma, USA).

7.2.5 Immunofluorescence Microscopy

HeLa, MCF7 and SW1736 cells were plated on coverslips and were then transfected with VO, FLAG-tagged WT-PBF, C51R-PBF, R140W-PBF and NIS-Myc as described in section 2.1.3. The cells were then processed as described in section 2.6. Primary antibodies were mouse monoclonal anti-FLAG (1:200, Sigma, UK) and rabbit polyclonal anti-NIS (1:500, Abcam, UK).

7.3 Results

7.3.1 Radioiodine Uptake Assays

^{125}I radioiodine uptake assays in TPC1 and MCF7 cells co-transfected with VO, WT-PBF, C51R-PBF, R140W-PBF and NIS-Myc confirmed that transient NIS transfection induced ^{125}I uptake compared to VO alone (Figure 7.1A and 7.1B) as previously described by our group (Smith et al. 2009). Western blotting demonstrated successful transfection of both PBF and NIS (Figure 7.1A and 7.1B). Co-transfection with WT-PBF resulted in significantly reduced uptake in TPC1 and MCF7 cells (Figure 7.1A and 7.1B). Interestingly, both PBF mutations retained the ability to repress radioiodine uptake in both cell lines (Figure 7.1A and 7.1B).

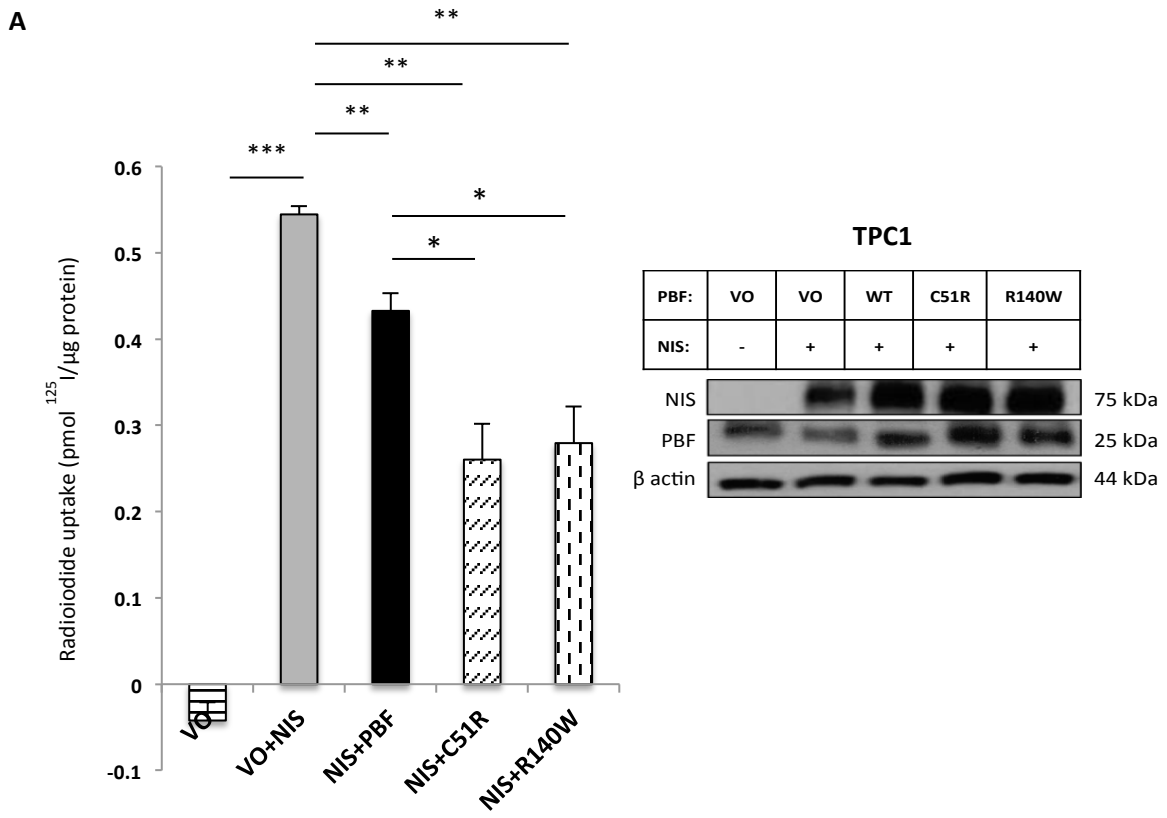

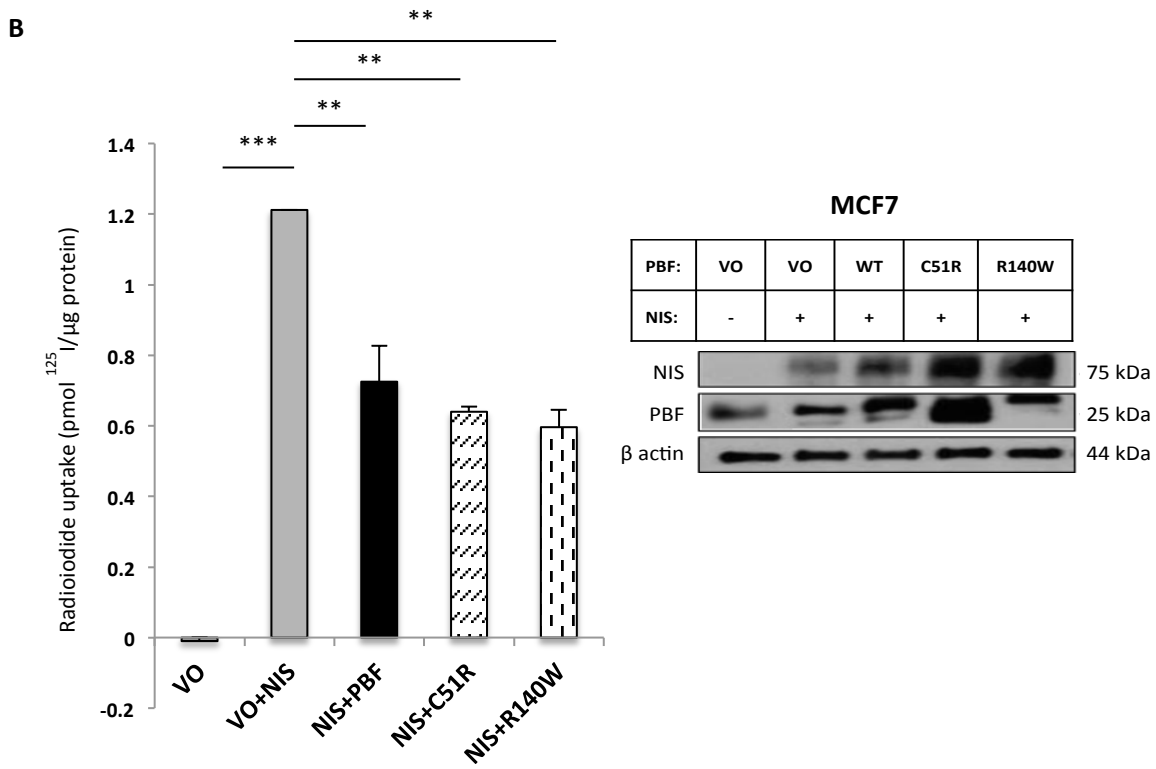

Figure 7.1: PBF mutations retain the capability to repress radioiodine uptake in vitro. *Representative graphical data of radioiodine uptake experiments in TPC1 (A) and MCF7 (B) cells transfected with VO, WT-PBF, C51R-PBF, R140W-PBF or NIS-Myc. Graphs represent mean ± SEM from three independent experiments. SEM = standard error of mean. Inset – Western blotting of PBF and NIS levels relative to β-actin levels for confirmation of transfection. PBF bands were detected with a polyclonal anti-PBF antibody (1:500), while NIS bands were demonstrated with a monoclonal anti-Myc antibody (1:1000). **P<0.01; ***P<0.001. N=3.*

7.3.2 Co-localisation between PBF and NIS

To determine the consequence of mutated PBF on the subcellular localisation of NIS, immunofluorescence microscopy was carried out in HeLa, MCF7 and SW1736 cells either transfected with VO alone or co-transfected with VO, WT PBF-FLAG, C51R-FLAG,

R140W-FLAG and NIS-Myc. Figure 7.2A shows that endogenous NIS (in red) in MCF-7 cells transfected with VO alone was located ubiquitously throughout the cells, with little evidence of plasma membrane staining. These findings explained the result of the low radioiodine uptake of transfected VO in MCF7 cells in Figure 7.1B. However, cells co-transfected with VO and NIS-Myc revealed distinct NIS staining at the plasma membrane, resulting in a definite outline of the cells (Figure 7.2B and 7.2C). Nevertheless, when the cells were co-transfected with WT or mutated PBF, NIS was increasingly intracellular (Figure 7.2B and 7.2C) compared to VO and NIS-Myc as our group has shown before (Smith et al. 2009). In addition, there was visible co-localisation (in yellow) between WT PBF and NIS-Myc in definite vesicles within the cells (Figure 7.2B and 7.2C), while the co-localisation of mutant C51R with NIS-Myc was apparent in the endoplasmic reticulum (Figure 7.2B and 7.2C), and the Golgi apparatus was the main structure where R140W mutant and NIS-Myc co-localised (Figure 7.2B and 7.2C).

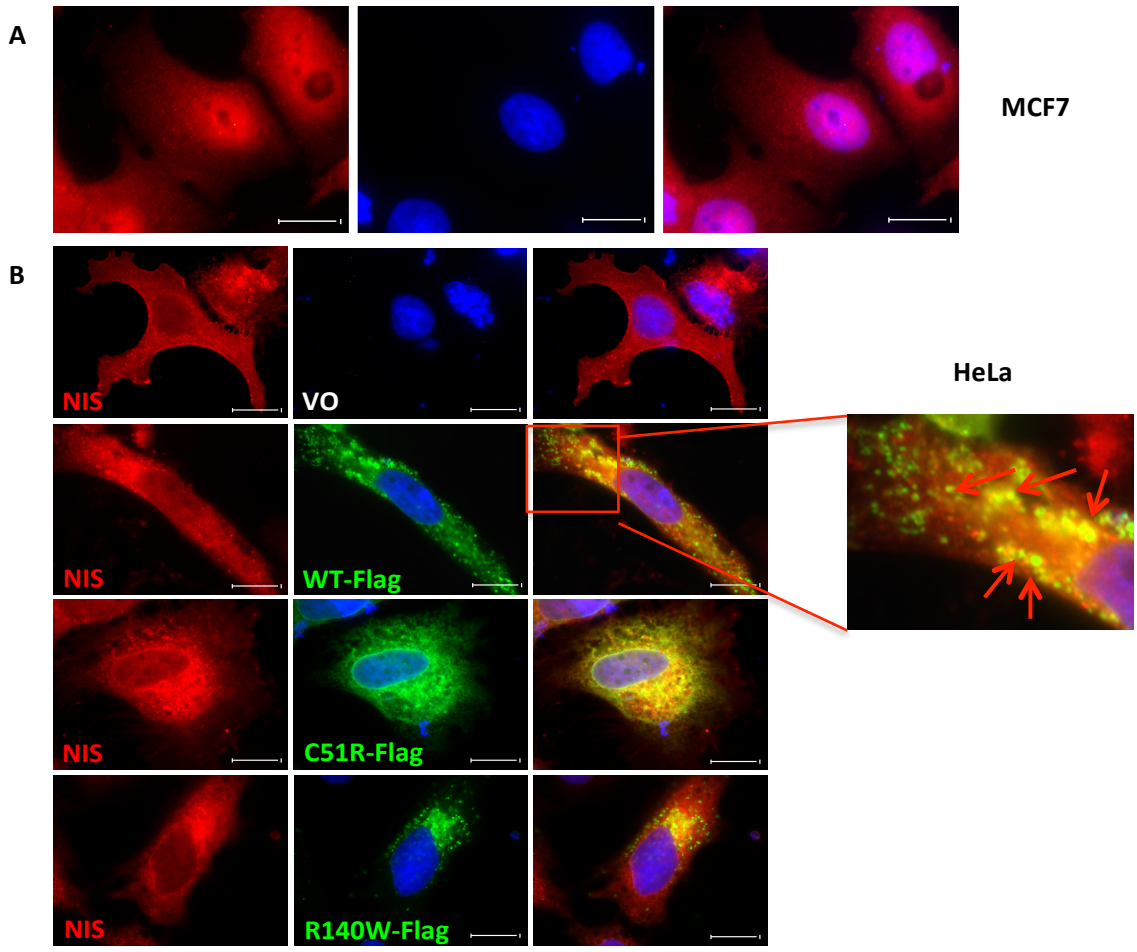

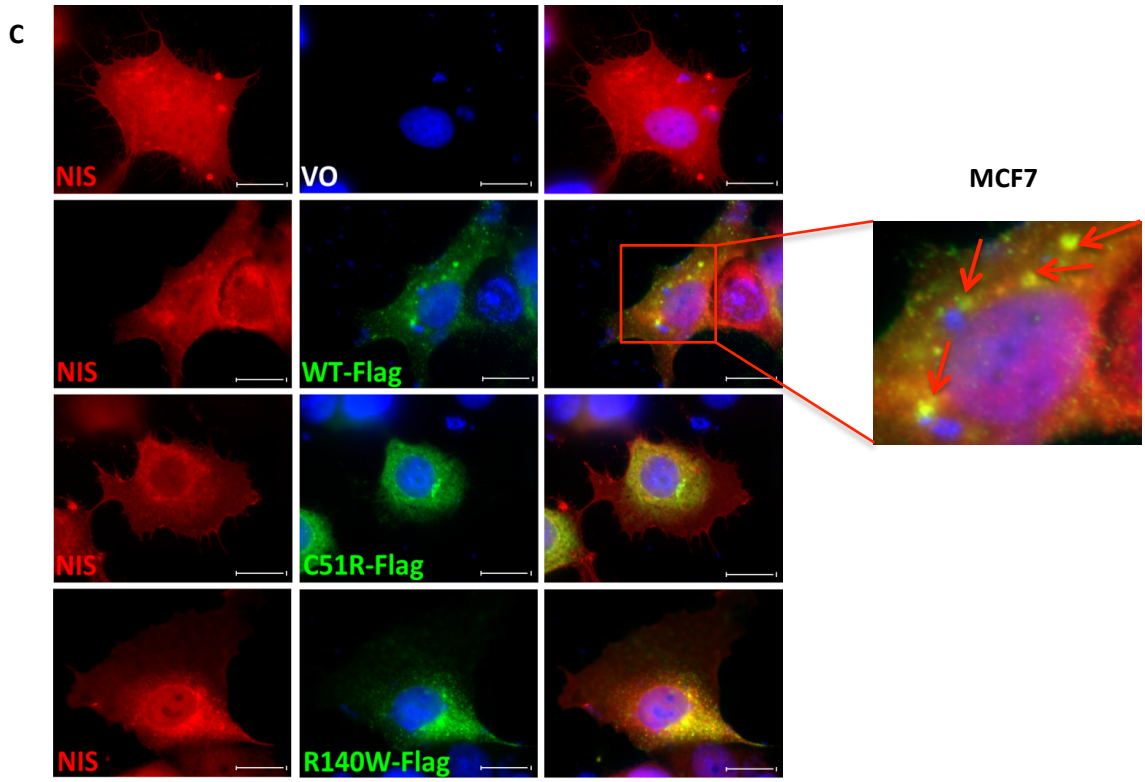

Figure 7.2: PBF mutations co-localise with NIS in vitro. *A, representative immunofluorescent microscopy of endogenous NIS (rabbit, anti-NIS, red) and DAPI (blue) in untransfected MCF7 cells. B and C, representative immunofluorescent images of NIS-Myc (rabbit, anti-NIS, red) and PBF-FLAG (mouse, anti-FLAG, green) co-localisation (yellow) in HeLa (B) and MCF7 (C) cells co-transfected with VO, WT-PBF-FLAG, C51R-FLAG, R140W-FLAG and NIS-Myc. Zoomed image shows NIS and WT-PBF co-localisation in specific vesicles within the cells. Arrows highlight regions of co-localisation (yellow). Magnification = 100x. Scale bars = 20 µm.*

Thus, mutants C51R and R140W retained the ability to repress radioiodine uptake *in vitro*, despite being mislocalised to the ER and the Golgi apparatus, respectively. This would imply for the first time that the well-documented interaction between PBF and NIS is able to occur in multiple compartments of the cell.

7.4 Discussion

PBF is significantly upregulated in thyroid cancer (Stratford et al. 2005), and radioiodine treatment is the necessary step for destroying residual cancer cells and improving oncological outcome. The best-characterised function of PBF lies in its repression of radioiodine uptake via the cellular redistribution of the sodium iodide symporter, NIS (Smith et al. 2013, Smith, Franklyn & McCabe 2011, Read et al. 2011, Smith et al. 2010, Smith et al. 2009). According to previous data from the McCabe group, the tyrosine phosphorylated residue Y174 is the critical amino acid regulating PBF trafficking (Smith et al. 2013). Artificial mutation of Y174 to Y174A resulted in PBF not internalising and being retained at the plasma membrane (Smith et al. 2013). This substitution significantly alters interaction between PBF and NIS, and then modifies the ability to uptake radioiodine *in vitro* (Smith et al. 2013). To further examine the impact of PBF mutations C51R and R140W, ^{125}I radioiodine uptake assays were conducted in thyroid and breast cancer cells. Interestingly, both PBF mutations retained the ability to repress radioiodine uptake even though they lost invasive and transforming properties in other studies within this thesis. To examine this more closely through immunofluorescent microscopy, PBF WT co-localised with NIS predominantly in late endosomes as we have reported previously (Smith et al. 2013). As IF results in Chapter 4 demonstrated that the C51R mutant was mainly located in the endoplasmic reticulum, shown by co-localisation with the ER marker (anti-PDI antibody), while R140W was mostly noticed in the Golgi apparatus, with co-localisation between the mutant and Golgi marker (anti-golgin-97 antibody) (Figure 4.10), and the use of three antibodies simultaneously in an immunofluorescence study is impractical and technically extremely difficult, in this Chapter IF microscopy therefore illustrated only co-

localisation between the C51R or R140W mutants and NIS. The results showed that co-localisation between C51R or R140W substitutions with NIS presumably appeared to occur in the endoplasmic reticulum, where C51R is observed, and in the Golgi apparatus, where R140W was detected, respectively (Figure 7.2). Hence although mutations C51R and R140W show significantly altered subcellular localisation, they retain NIS co-localisation, and preserve the ability to repress radioiodine uptake. We hypothesise therefore that PBF binds to NIS in multiple cellular compartments, and not solely in late endosomes as previously described (Smith et al. 2009).

The sodium iodide symporter NIS is known to be an intrinsic transmembrane glycoprotein that usually originates in the endoplasmic reticulum (ER), traffics through the Golgi apparatus, and then moves to cell surface membrane where it is functional (Beyer et al. 2011). NIS is also generally processed, phosphorylated and glycosylated during its cellular journey. Therefore, we hypothesise that while travelling through the ER and the Golgi apparatus, NIS interacts with mutants C51R-PBF and R140W-PBF, respectively, resulting in reduced NIS localisation at the plasma membrane and hence then repressed iodine uptake. This process is in contrast to the effects of overexpressed PBF on cellular invasion, migration, colony formation ability and anchorage independent growth, where appropriate subcellular localisation of PBF would appear to be critical given that mutants C51R and R140W lost wild-type function. Regarding cellular invasion and migration investigated in Chapter 5, WT-PBF interacted with CTTN predominantly at the PM where CTTN is functional, resulting in induced cell invasion and migration *in vitro*. However, mutant C51R altered the subcellular localisation of PBF from the late endosomes and the PM to the endoplasmic reticulum. The C51R mutant was able to bind and interact with cortactin more tightly than WT-PBF, leading to a shift

of CTTN from the PM, and reducing cellular invasion and migration. In contrast, the C51R and R140W mutants reduced NIS localisation to the plasma membrane, retaining the ability of WT-PBF to interfere with NIS trafficking, albeit by a different route, through preventing NIS moving to the plasma membrane from the ER and the Golgi compartments, respectively. Thus these 2 PBF mutants were able to function to reduce RAI *in vitro* to a similar degree as wild-type PBF. Accordingly, if C51R and R140W substitutions were discovered in thyroid cancer, they would be predicted to provide reduced radioiodine uptake and repressed ^{131}I treatment, in common with over-expressed wild-type PBF.

CHAPTER 8 - EFFECT OF PBF MUTATIONS C51R AND R140W ON CELL TRANSFORMATION ABILITY

8.1 Introduction

The critical hallmark of oncogenic mutation is the ability to render normal cells malignant, through the process of cell transformation. Driver mutation status can be confirmed by switching on or off expression or function of the oncogene *in vitro* to examine its contribution to the process of cell transformation. For instance, NRAS (neuroblastoma rat sarcoma viral oncogene homolog) overexpression transformed murine NIH 3T3 cells, resulting in a significant increase in anchorage independent cell growth in soft agar assays (Eisfeld et al. 2014). Alternatively, inhibition of BRAF (v-Raf murine sarcoma viral oncogene homolog B) levels in papillary thyroid cell lines using siRNA knockdown significantly reduced colony numbers in colony formation and soft agar assays, demonstrating that the BRAF gene is vital for transformation capability of these cells (Liu et al. 2007). Cells carrying stable BRAF knockdown also showed decreased tumourigenic ability in nude mice compared to controls (Liu et al. 2007). Thus, manipulating the expression and function of putative oncogenes *in vitro* and examining anchorage-independent growth remains a useful initial tool in assessing the potential oncogenic impact of a mutational change.

PBF has previously been reported to be transforming *in vitro* and tumourigenic *in vivo*. Stratford et al. demonstrated that thyroid cancer had significantly increased PBF mRNA expression compared to normal thyroid, and PBF mRNA expression in thyroid tumours which subsequently recurred was higher than those for cancers without recurrence (Stratford et al. 2005). In Chapter 6, PBF expression from the TCGA dataset was also significantly upregulated in thyroid tumour compared to normal tissue (Figure 6.4A). In addition, stably overexpressed PBF in murine NIH 3T3 fibroblast cells significantly induced colony formation in soft agar assays (Stratford et al. 2005).

In Chapter 4, the effect of C51R and R140W substitutions on cellular proliferation was investigated. Mutant C51R demonstrated increased proliferative function, while R140W had an anti-proliferative consequence. In this Chapter, we therefore performed colony formation and soft agar assays to investigate whether the mutants C51R and R140W retained colony formation capability and anchorage independent transforming ability.

8.2 Materials and Methods

8.2.1 Cell Culture and Transfection

Early passage TPC1 and NIH3T3 fibroblast cell lines were used to produce stable cell lines, and were stably transfected with VO, WT-PBF, C51R-PBF and R140W-PBF. These cell lines were selected and subcultured as described in section 2.13.

8.2.2 Western Blotting

Protein samples from stable clones were extracted and used to run Western blotting as described in section 2.5. The experiments were performed to determine PBF protein expression levels between PBF stable cells and VO control group. The primary antibodies were rabbit anti-PBF (1:500, In-house) and mouse anti-β-actin AC-15 (1:10000, Sigma, USA).

8.2.3 Stable Cell Line Generation

TPC1 and NIH 3T3 cell lines were selected to produce stable cell lines as described in section 2.13. These cells were transfected with VO, WT-PBF, C51R-PBF and R140W-PBF plasmids, with pcDNA3.1(+) vectors for TPC1 cells and pCI-neo vectors for NIH 3T3 cells as described in section 2.1.3. 1 mg/ml G418 was applied to both TPC1 and NIH 3T3 cells after 24 hours of transfection to select cells containing plasmids. Cells were supplemented with new fresh media with suitable antibiotics twice a week and cultured until they formed colonies as described in section 2.13. The expression levels of each clone were then determined before the cells were used in subsequent assays.

8.2.4 Colony Formation Assays

TPC1 stable cell lines overexpressing VO, WT-PBF, C51R and R140W mutants were used in colony formation assays. After validating PBF overexpression, the experiments were established in 6-well plates, and cells were seeded at 400 cells/well. The cells were supplemented with RPMI containing 10% FCS and G418 (1mg/ml) twice weekly. After 14 days of incubation, colonies were stained with 0.005% crystal violet and the numbers of colonies were counted. The assays were carried out in 3 individual experiments.

8.2.5 Soft Agar Assays

Stable NIH 3T3 colonies with elevated PBF expression compared to VO controls were selected to determine transforming capability through soft agar assays. Cells were resuspended in media, counted and seeded into 6-well plates, with two layers of agar: The bottom layer was made from 0.8% sterile agar, aliquoted into each well and

allowed to set at room temperature, whilst the upper layer was created from sterile 0.35% agarose and mixed with the single-cell suspension. Both layers were set and equilibrated at 40°C. The cells were fed with DMEM containing 10% calf serum and G418 (1mg/ml) twice a week. After 14 days of incubation, the colonies were counted. The assays were performed in 3 separate experiments.

8.3 Results

8.3.1 Confirmation of Stable Cell Line Expression

For each PBF genotype (wild-type, C51R and R140W), 3 stable clones were selected for determination of PBF expression compared to VO stable control cells, before using these cells in further assays.

Protein expression levels of PBF in selected TPC1 thyroid cancer and NIH 3T3 fibroblast clones were determined through Western blotting as described in section 8.2.2.

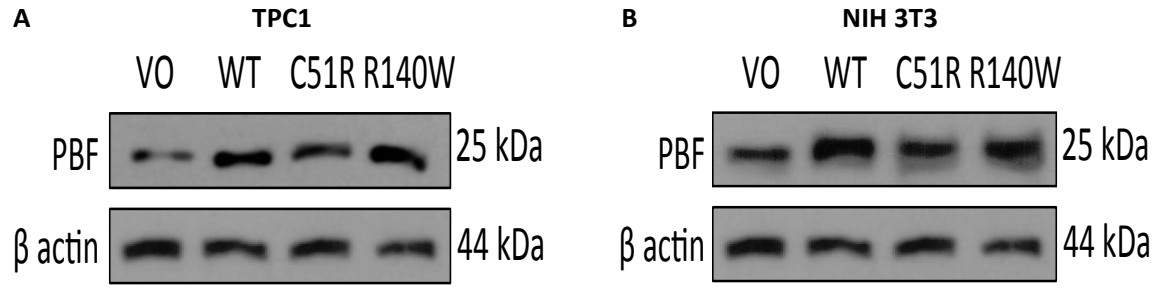

Figure 8.1: Overexpression of PBF in selected TPC1 and NIH 3T3 stable clones via Western blotting. *Western blots of PBF protein expression levels relative to β-actin levels in TPC1 (A) and NIH 3T3 (B) clones stably transfected with VO, WT-PBF, C51R and R140W mutants.*

Initial screening (data not shown) identified one clone from each stable cell line with similar levels of PBF protein over-expression from the 3 clones. Subsequent Western blotting confirmed that selected TPC1 and NIH 3T3 clones stably transfected with WT-PBF, C51R-PBF and R140W-PBF carried similarly induced PBF protein expression compared to VO controls (Figure 8.1). These cell lines were subsequently utilised in colony formation and soft agar assays.

It is difficult to determine the relative proportion of endogenous WT-PBF and exogenous PBF within each stable cell line through Western blotting, although significant levels of overexpression of both WT and mutants PBF are clearly seen. Some effects of the mutants may be under- or over-estimated due to the presence of endogenous WT protein. However, the level of endogenous protein is likely to have been comparable across each cell line, including the WT line to which each mutant was compared.

8.3.2 Effect of PBF Mutations C51R and R140W on Cell Transformation Ability

8.3.2.1 Colony Formation Assays

Previous data from our group revealed that up-regulation of PBF significantly induces cell transformation *in vitro* (Stratford et al. 2005). To determine whether PBF mutations C51R and R140W retain this capability, colony formation assays were firstly utilised in TPC1 cells stably transfected with VO, WT-PBF and both PBF mutants (Figure 8.2).

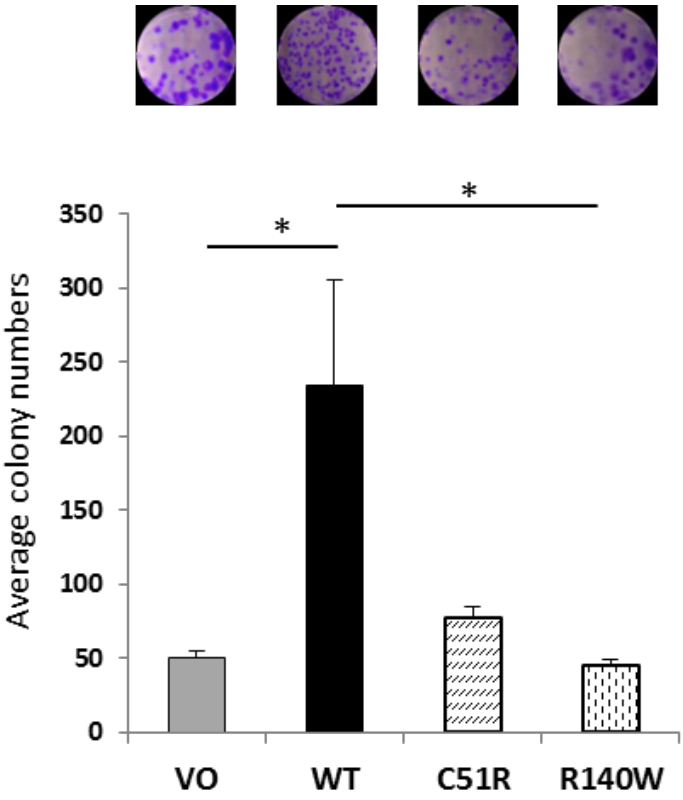

Figure 8.2: C51R and R140W substitutions lose colony formation ability compared to WT-PBF. *Colony formation assays in TPC1 cells stably transfected with VO, WT-PBF and 2 mutants; representative photomicrographs shown above. Data showed as mean ± SEM. SEM = standard error of mean. N=3 experiments, each with 3 replicates. *P<0.05.*

Wild-type PBF significantly enhanced the ability of TPC1 cells to form colonies, whereas both C51R and R140W mutants failed to induce colony formation compared to WT in stably transfected TPC1 cells (Figure 8.2).

8.3.3.2 Soft Agar Assays

To further assess whether the mutants C51R and R140W preserved an ability to transform cells *in vitro* compared to WT-PBF, soft agar experiments were conducted in NIH 3T3 cells stably transfected with VO, WT-PBF, C51R and R140W mutants to examine anchorage-independent growth.

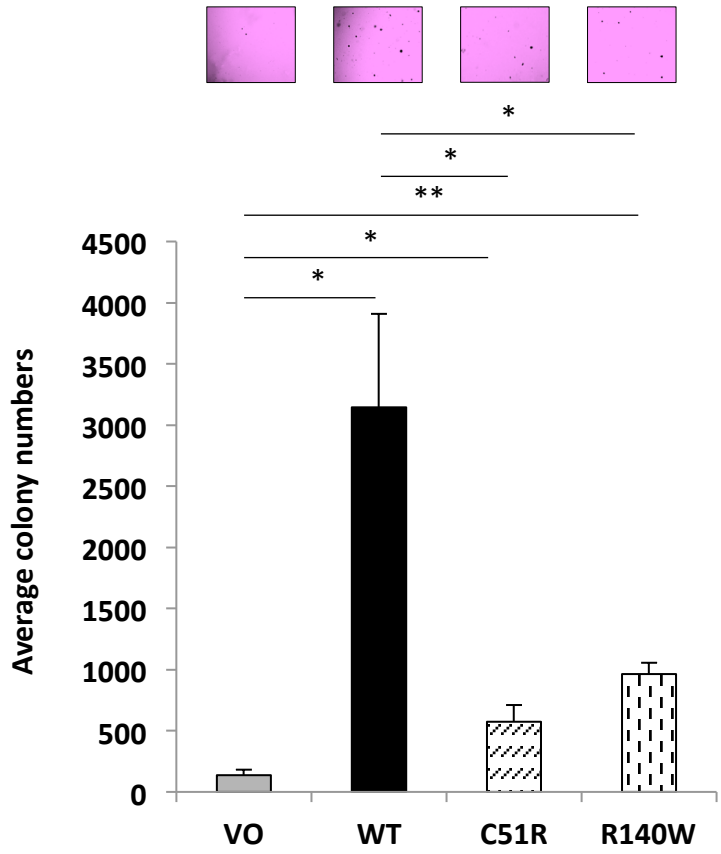

Figure 8.3: C51R and R140W substitutions show reduced cell transformation ability in vitro compared to WT-PBF. *Soft agar assays in NIH 3T3 cells stably transfected with VO, WT-PBF, C51R and R140W mutants. Colonies of over ~50 cells in size were counted. N = 3 experiments, each with 3 replicates. Microscopic figures illustrate relative numbers of colonies as demonstrated above. Graph represents mean ± SEM. SEM = standard error of mean. *P<0.05.*

Figure 8.3 illustrates that all 3 genotypes of PBF, including WT, C51R and R140W mutants, showed a variably significant increase in transforming ability compared to stable VO controls (Figure 8.3). However, mutants C51R and R140W markedly lost the ability to elicit anchorage-independent growth in soft agar assays compared to wild-type PBF (Figure 8.3).

Taken together, even though the PBF mutations C51R and R140W still had an ability to transform the cells in soft agar assays, a critical hallmark of malignant cells, both substitutions significantly reduced transforming capability compared to WT-PBF. Therefore, although some canonical PBF functionality is retained, these two PBF mutants are unlikely to be driver mutations.

8.4 Discussion

Soft agar assays in this Chapter were applied to assess whether C51R and R140W substitutions carried an ability to transform cells compared to VO and wild-type PBF. Generally, normal cells have an anchorage-dependent cell growth, and require solid surfaces such as a plate or a flask to grow and divide. They usually grow in a monolayer pattern and when reaching confluency, the cells stop dividing and enter into G_0 phase, via contact inhibition. By contrast, when normal cells transform into malignant cells, they gain the ability to grow in semi-solid agar, named an anchorage-independent ability. This characteristic is associated with tumourigenicity *in vivo* and invasiveness of cancer (Carney, Gazdar & Minna 1980).

A soft agar assay remains the best *in vitro* method to identify an ability of cells to grow independently without solid surface, suggesting transforming ability *in vitro*. In comparison, colony formation assays, whilst easily performed and a good screening tool, do not directly evaluate malignant characteristics, because the cells still grow and form colonies on solid surfaces such as culture plates. Although the results of the colony formation assays were consistent in 3 experiments, the TPC1 papillary thyroid cancer cell line is not ideal to demonstrate transforming ability *in vitro* because these cancer cells are already transformed. Therefore, the stably overexpressed NIH 3T3 cell lines

were constructed and applied in this Chapter. As fibroblast cell lines such as NIH 3T3 cells are essentially untransformed, these cells are suitable for estimating the capability of genes or mutations to transform normal to malignant cells in soft agar assays.

In this Chapter, we found that WT-PBF had a significant increase in the ability to transform cells compared to VO stable clones, as assessed through colony formation and soft agar assays. However, mutants C51R and R140W almost entirely lost this property compared to WT-PBF as shown in both experiments. Should these mutants have demonstrated strong *in vitro* oncogenic activity, *in vivo* studies would be needed to confirm that these mutations drive tumourigenesis. The stable cell lines could have been employed in a xenograft model. However, as C51R and R140W demonstrated reduced cell invasion, migration and transforming ability compared with WT-PBF, and in line with the 3Rs (replacement, reduction and refinement) principle used in animal research to minimise animal numbers and suffering, such studies are not warranted.

We therefore conclude that, in contrast to bioinformative prediction (Melloni et al. 2014), rare mutations in PBF are unlikely to be driver events in human cancer. Although some canonical PBF functionality is retained, we propose that PBF over-expression in human tumours, rather than sequence alteration, is the more important cellular mechanism. Over-expression of the wild type protein, which has been associated with tumour induction in xenograft models (Stratford et al. 2005), hyperplasia and follicular lesions in thyroid glands of transgenic mice (Read et al. 2011), extramural vascular invasion in human colorectal tumours (Read et al. 2016) and reduced disease-specific survival in patients with papillary thyroid cancer (Hsueh et al. 2013), is a more pertinent driver event. However, why PBF is upregulated in tumours, and exactly how this induction drives hyperplastic and neoplastic progression, remains ill-defined.

CHAPTER 9 - FINAL CONCLUSIONS AND FUTURE DIRECTIONS

Recently, there has been a dramatic increase in the number of genetic mutations reported in human cancer, which has come as a result of improvements in next generation sequencing, and have been collated via the COSMIC and the TCGA initiatives. Nevertheless, cell biology has not kept pace with sequencing technology: quick and effective methods to discern those genes eliciting a tumour growth benefit (driver mutations) from the majority of gene changes which do not drive clonal expansion (passenger mutations) still remain elusive. Computational statistical approaches based on protein function, frequency of mutation, pathway and pattern are widely used for the prediction of rare driver gene changes. However, the results are not guaranteed. For instance, $BRAF^{V600E}$ is prominent in a variety of human tumours such as melanoma, breast, thyroid and colon cancer through the COSMIC and the TCGA databases (http://cancer.sanger.ac.uk/, http://www.cbioportal.org/), and is the most common mutation found in BRAF gene. Mutation of $BRAF^{V600E}$ also retains transforming ability *in vitro* (Liu et al. 2007) and tumourigenicity *in vivo* (Knauf et al. 2005), suggesting that $BRAF^{V600E}$ is a driver mutation. However, $BRAF^{V600E}$ is predicted to be a non-functional mutation through the Mutation Assessor server, which is a computational programme based on conservation of the mutated amino acid residue in protein homologs (http://mutationassessor.org/). Therefore, a range of standard assays applied to determine the impact of discovered mutations on cell biology is still needed to the confirm status of these genes.

The studies in this thesis were established to investigate whether PBF amino acid substitutions discovered in the COSMIC database influenced important PBF functions and impacted on routine cellular measures of cell behaviour, to estimate whether these PBF mutations might be driver mutations. This notion was supported by

recent bioinformatic data which predicted that PBF may be a driver gene in thyroid cancer (Melloni et al. 2014).

PBF is a ubiquitously expressed glycoprotein upregulated in a variety of human tumours, especially endocrine neoplasias such as pituitary, breast and thyroid (McCabe et al. 2003, Xiang et al. 2012, Watkins et al. 2010, Smith, Franklyn & McCabe 2010, Stratford et al. 2005). PBF overexpression also correlates with poorer clinical outcome in various human cancers. To illustrate this, colorectal samples containing extramural vascular invasion showed significantly higher PBF expression levels (Read et al. 2016), while high PBF mRNA expression in patients diagnosed with papillary thyroid cancer was also associated with early local recurrence and tumour metastasis at the time of diagnosis and significantly reduced disease-specific survival (Hsueh et al. 2013). Additionally, high PBF promoter activity influences metastatic incidence in breast cancer (Xiang et al. 2012). PBF expression is higher in human multinodular goiter and inversely correlates with NIS expression, resulting in decreased radioiodine uptake (Read et al. 2011).

PBF modulates the intracellular signaling and trafficking of a variety of proteins, resulting in an alteration of their functions. For instance, when binding and interacting with monocarboxylate transporter 8 (MCT8), PBF alters the subcellular location of MCT8 from the plasma membrane to intracellular vesicles, resulting in a significant increase in thyroid hormone accumulation in the thyroid gland, and a marked reduction in thyroid hormone secretion in a murine model with thyroid specific PBF overexpression (Smith et al. 2012, Smith et al. 2010). Upregulated PBF also reduces activity of the basal promoter and hNUE (human NIS upstream enhancer element) of the sodium iodide symporter (NIS) promoter, leading to repression of ability to uptake

radioiodine (Boelaert et al. 2007). Furthermore, PBF binds NIS, and pulls NIS away from the plasma membrane (PM) where NIS is functional, leading to decreased radioiodine uptake (Read et al. 2011, Smith et al. 2010, Smith et al. 2009), which is critical for radioiodine treatment and prognosis in thyroid cancer. Src kinase also interacts and co-localises with PBF, and phosphorylates PBF at tyrosine 174 residue, regulating its influence on radioiodine uptake activity (Smith et al. 2013). Additionally, PBF reduces p53 stability and induces p53 ubiquitination, dysregulating p53 function (Read et al. 2016, Read et al. 2014). PBF has a moderate pro-proliferative property in various cell lines such as breast, colon and thyroid (Watkins et al. 2010, Read et al. 2016, Read et al. 2011), and is transforming *in vitro* and tumourigenic *in vivo* (Stratford et al. 2005). Taken together, therefore, there was a broad rationale to predict that patient mutations in PBF might relate to tumour behaviour or outcome. The work presented in this thesis sought to examine whether, rather than simple overexpression of PBF, these sequence changes might alter tumour cell behaviour.

Currently, the incidence of discovered PBF mutations continues to increase in the COSMIC and the TCGA databases as more tumours are sequenced. However, when this thesis started in 2013, the COSMIC database reported the first ten missense PBF substitutions found in multiple types of cancer such as colon, prostate and ovary. Seven out of 10 PBF mutations were found in colon cancer. At the beginning of this study, the I-TASSER (Iterative Threading Assembly Refinement) and the SIFT (Sorting Intolerant From Tolerant) databases were used to predict 3D protein structures and risk of alteration in protein function for all 10 mutations, respectively. The results in Chapter 3 revealed that most missense amino acid substitutions were likely to elicit protein damage, and be potentially oncogenic.

The effects of all 10 PBF substitutions were first characterised through immunofluorescence microscopy to determine potential alterations in subcellular localisation compared to WT-PBF. Wild-type PBF localised to late endosomes and at the plasma membrane as previously shown (Smith et al. 2009). Interestingly, most mutations retained this WT subcellular localisation pattern, with only C51R, G106R and R140W mutants showing noticeably different localisations. Indeed, mutants C51R and G106R were mainly noticed in the endoplasmic reticulum, and R140W was predominantly observed in the Golgi apparatus. As the precise status of cellular PBF glycosylation, dimerisation and stability have not been definitively established in previous studies, they were investigated through Western blotting in Chapter 4. Most amino acid substitutions showed both glycosylated (~25-37 kDa) and dimeric (~50 kDa) forms in keeping WT-PBF. Interestingly, reductions in apparent glycosylation and oligomerisation patterns were most obvious in C51R and G106R mutants, which were located in the ER. Regarding PBF stability, the results showed for the first time that wild-type PBF has a half-life around 24 hours, which was preserved for the C51R and V55I mutations in the PSI domain, and R140W close to C-terminal end. However, all remaining mutations had considerably less protein stability than WT, with G106R most unstable.

WT-PBF significantly increased cell turnover in breast and colon (Read et al. 2016, Watkins et al. 2010). In Chapter 4, the impact of these PBF mutations identified *in vivo* on cellular proliferation was determined using BrdU and MTS assays. Whilst substitutions at the G106 residue (G106R/V/W) failed to alter this proliferative characteristic, mutants C51R and V55I in the PSI domain increased cellular proliferation compared to WT-PBF. In contrast, R140W and R146W mutations proximal to C-

terminus provided broadly anti-proliferative phenotypes. Together, these data reveal no consistent effect of amino acid substitutions on glycosylation, dimerisation, stability, subcellular localisation and cellular proliferation. However, as PBF generally traffics through the ER and the Golgi to be processed and some glycosylation and dimerisation processes occur in the ER (Lodish et al. 2000), protein synthesised from mutants C51R and G106R, located in the ER, might not be correctly processed, resulting in decreased glycosylation and oligomerisation. Nevertheless, even though C51R had the same stability as WT-PBF and induced cellular proliferation, the G106R mutant, observed in the same subcellular location as C51R, harboured the least stability and failed to alter proliferation compared to wild-type PBF. Therefore, it is difficult to correlate ER localisation of both substitutions with PBF stability and proliferation ability.

Following the investigations of Chapters 3 and 4, we narrowed further experiments from 10 mutations down to 2 potentially functional mutations, C51R and R140W. However, curtailing our subsequent approaches was a potential drawback in this study because oncogenic functions of the remaining 8 PBF substitutions may have been missed. Nevertheless, this approach provided the advantage of focusing in depth in complicated assays such as 2D cell invasion assays and proximity ligation assays, improving accuracy of those approaches unsuited to large scale studies.

Other cellular mechanisms involved in cancer progression include cell invasion and migration as precursors to tumour metastasis. Generally, distant metastasis in human cancers such as breast, colon and thyroid is associated with a marked reduction in overall survival rate (http://seer.cancer.gov/), and may eventually become fatal. Understanding of the metastatic pathway is therefore needed to appraise targeted treatments. Previous mass spectrometry in our group demonstrated cortactin to be one

of the top potential protein binding partners of PBF (Sharma 2014). While PBF significantly increases cell invasion and migration in a panel of cancer cells, including breast and colon (Watkins et al. 2010, Read et al. 2016), CTTN also induces assembly of actin filaments mainly at the cell periphery, and inhibits debranching of actin fibres (Weaver et al. 2001) leading cell to migrate and invade (MacGrath, Koleske 2012, Kirkbride et al. 2011, Pollard, Borisy 2003). However, the precise mechanism of how PBF and CTTN promote cell invasion and migration still remains ill-defined.

In Chapter 5, the specific interaction between PBF and CTTN was confirmed through co-IP, PLA and immunofluorescence, especially at the plasma membrane (PM). The ability of PBF to induce cell invasion was also entirely dependent on the presence of cortactin function. IF assays showed endogenous CTTN co-localised with PBF within intracellular vesicles and at the PM. However, the specific in-house antibody, PBF8, used in the detection of PBF was not able to detect all forms of PBF, especially phosphorylated PBF at the PM (Smith et al. 2009). HA-tagged PBF and Myc-tagged CTTN plasmids were applied in subsequent co-IP and IF microscopy assays to appraise the interaction between 2 proteins. Additionally, co-IP experiments in cells transfected with WT-PBF-HA and CTTN-Myc confirmed exogenous wild-type PBF and CTTN had a specific interaction in keeping with the untransfected conditions. The immunofluorescence results affirmed that WT-PBF-HA co-localised with CTTN-Myc in definite vesicles within the cells and at the PM. In addition, wild-type PBF demonstrated pro-invasive and pro-migratory characteristics in different cell lines such as thyroid, colon, breast and fibroblast cells. However, mutants C51R and R140W had entirely lost invasive and migratory phenotypes in thyroid and breast cancer cells compared to WT-PBF. The results of IF experiments illustrated that the C51R-HA mutant of PBF was

mainly located, and co-localised with, CTTN-Myc in the endoplasmic reticulum (ER). Co-IP assays demonstrated that C51R-PBF bound CTTN more avidly than WT-PBF. C51R specifically interacted with CTTN and appeared to 'lock' it in the ER, pulling CTTN away from the plasma membrane where it binds proteins such as Src kinase, Arp2/3 complex and NCK1 (Kirkbride et al. 2011, Weaver et al. 2001), resulting in significantly reduced cell invasion compared to VO and WT-PBF. However, mutant R140W was not investigated in Chapter 5 because of detection problems of HA-tagged R140W. Therefore, C51R showed altered subcellular localisation, from late endosomes and the plasma membrane to the ER, but was still able to bind CTTN, albeit in a different subcellular location. One hypothesis is thus that by holding CTTN away from the PM, C51R prevented its interaction with proteins involved in actin polymerisation, hence abrogating cell invasion.

Although CTTN is up-regulated in various cancers such as colon, melanoma and esophagus, and influences their prognosis (Ni et al. 2015, Cai et al. 2010, Xu et al. 2010, Lu et al. 2014), it has not been investigated in thyroid tumours. The studies in Chapter 6 revealed a significant upregulation of cortactin mRNA and protein expression in our small series of 43 human well-differentiated thyroid cancers (DTC) compared to normal thyroid tissue as demonstrated through PCR and Western blotting. The data from 326 thyroid cancers and 59 normal thyroid samples in the TCGA database importantly confirmed that CTTN and PBF were significantly over-expressed in thyroid tumours compared to normal tissue, and CTTN expression in tumours with nodal metastasis had a significantly higher level compared to those which had no nodal metastasis. Interestingly, the results in both sample groups demonstrated a significant correlation between PBF and CTTN mRNA expression in human DTC. Taken together, the data of

Chapters 5 and 6 imply that PBF and CTTN may play important roles in thyroid tumour development and progression, and may represent future prognostic markers and therapeutic targets in the treatment of thyroid cancer metastasis.

As PBF is vital for modulating radioiodine uptake in thyroid cells, the assays in Chapter 7 investigated the outcome of the C51R and R140W substitutions on radioiodine uptake, which is critical for thyroid cancer treatment. Co-expressed WT-PBF and NIS again significantly reduced radioiodine activity compared to NIS transfection alone as previously shown (Smith et al. 2013, Smith et al. 2009). Moreover, both mutants C51R and R140W still maintained a significant reduction in radioiodine activity. IF results showed that WT-PBF co-localised with NIS in late endosomes (Smith et al. 2009), while co-localisation between NIS and C51R and R140W took place in the ER and the Golgi apparatus, respectively. This implies that even though the subcellular locations of the two PBF mutants were significantly altered, C51R and R140W still interacted with NIS and pulled it away from the plasma membrane where is functional, leading to repressed radioiodine uptake similarly to WT-PBF. Further evidence for this proposed mechanism could come from performing co-IP assays on ER and Golgi extracts from transfected cells, although this would be technically challenging. However, given the effects of the C51R and R140W substitutions on cell invasion, migration and radioiodine uptake ability, it is interesting to note that despite marked changes in subcellular localisation, these mutations retain the ability to interact with critical proteins such as CTTN and NIS, suggesting that the avidity of binding is presumably high.

Although both C51R and R140W mutations altered proliferative characteristics and retained radioiodine uptake repression, the ability of these 2 mutants to transform

normal cells to malignant was needed to determine whether the changes might be aetiological. This was evaluated through colony formation and soft agar assays in Chapter 8. Soft agar assays are used for evaluating the capability of anchorage-independent cell growth, reflecting transformation ability *in vitro*, and tumourigenicity and tumour cell aggressiveness *in vivo* (Mori et al. 2009, Carney, Gazdar & Minna 1980, Shin et al. 1975, Freedman, Shin 1974). Unfortunately, although WT-PBF retained the anchorage-independent growth pattern, with significantly increased colony numbers in both assays, C51R and R140W stably transfected cells lost transforming ability compared to WT-PBF suggesting that these 2 substitutions are unlikely to be directly oncogenic.

Given that PBF impacts on the progression of several cancers, interacts with multiple important proteins and has multiple point mutations, the studies in this thesis aimed to determine the functional characteristics, including the stability, cellular proliferation, cellular invasion, cell migration and radioiodine uptake, of the first ten non-synonymous substitutions, and to shed new light onto the precise molecular mechanisms of PBF biology in tumourigenesis. Extensive data delineated in this thesis indicate that even though the mutations still preserve some canonical PBF functions, its up-regulation in cancer may be more critical in terms of tumour development and progression than sequence changes per se.

Moreover, although there are a lot of novel genetic substitutions discovered through next generation sequencing in the COSMIC and the TCGA databases, cell biological experiments to investigate exactly how the mutations function are still the most important steps to identify driver genes that may further influence specific targets for treatment in human cancer.

Regarding future directions, there are currently 27 PBF mutations discovered in the COSMIC database, the vast majority (18/27) being single amino acid missense substitutions. Some of these mutations are found in both the COSMIC and the TCGA databases, including Q42E, C121del, E153K, R140Q and R144Q in different human tumour types. Several of them are highly predicted to cause protein damage using Mutation assessor or PolyPhen score. Future work may therefore use further cell biological assays to determine whether these new PBF mutations are driver events. Furthermore, even though CTTN and PBF are up-regulated in differentiated thyroid cancer, and significantly induce cellular invasion and migration as shown in Chapters 5 and 6, the precise mechanism of how PBF and CTTN interact still remains elusive. Other future directions could focus on treatments to specifically abolish CTTN or PBF expression, or drug targets to increase binding between PBF and CTTN and to prevent CTTN trafficking to the plasma membrane and interacting with other important proteins related to cell motility, resulting in decreased cell invasion and metastasis.

REFERENCES

Andreyev, H.J., Norman, A.R., Cunningham, D., Oates, J.R. & Clarke, P.A. 1998, "Kirsten ras mutations in patients with colorectal cancer: the multicenter "RASCAL" study", *Journal of the National Cancer Institute,* vol. 90, no. 9, pp. 675-684.

Arey, B.J. 2012, "The role of glycosylation in receptor signaling", *INTECH*.

Ascierto, P.A., Kirkwood, J.M., Grob, J., Simeone, E., Grimaldi, A.M., Maio, M., Palmieri, G., Testori, A., Marincola, F.M. & Mozzillo, N. 2012, "The role of BRAF V600 mutation in melanoma", *J Transl Med,* vol. 10, no. 85, pp. 10.1186.

Beyer, S., Lakshmanan, A., Liu, Y., Zhang, X., Wapnir, I., Smolenski, A. & Jhiang, S. 2011, "KT5823 differentially modulates sodium iodide symporter expression, activity, and glycosylation between thyroid and breast cancer cells", *Endocrinology,* vol. 152, no. 3, pp. 782-792.

Boelaert, K., Smith, V., Stratford, A., Kogai, T., Tannahill, L., Watkinson, J., Eggo, M., Franklyn, J. & McCabe, C. 2007, "PTTG and PBF repress the human sodium iodide symporter", *Oncogene,* vol. 26, no. 30, pp. 4344-4356.

Bork, P., Doerks, T., Springer, T.A. & Snel, B. 1999, "Domains in plexins: links to integrins and transcription factors", *Trends in biochemical sciences,* vol. 24, no. 7, pp. 261-263.

Brennan, C.W., Verhaak, R.G., McKenna, A., Campos, B., Noushmehr, H., Salama, S.R., Zheng, S., Chakravarty, D., Sanborn, J.Z. & Berman, S.H. 2013, "The somatic genomic landscape of glioblastoma", *Cell,* vol. 155, no. 2, pp. 462-477.

Bromberg, Y. & Rost, B. 2009, "Correlating protein function and stability through the analysis of single amino acid substitutions", *BMC bioinformatics,* vol. 10, no. 8, pp. 1.

Buday, L. & Downward, J. 2007, "Roles of cortactin in tumor pathogenesis", *Biochimica et Biophysica Acta (BBA)-Reviews on Cancer,* vol. 1775, no. 2, pp. 263-273.

Cai, J., Zhao, R., Zhu, J., Jin, X., Wan, F., Liu, K., Ji, X., Zhu, Y. & Zhu, Z. 2010, "Expression of cortactin correlates with a poor prognosis in patients with stages II–III colorectal adenocarcinoma", *Journal of Gastrointestinal Surgery,* vol. 14, no. 8, pp. 1248-1257.

Carina, V., Zito, G., Pizzolanti, G., Richiusa, P., Criscimanna, A., Rodolico, V., Tomasello, L., Pitrone, M., Arancio, W. & Giordano, C. 2013, "Multiple pluripotent stem cell markers in human anaplastic thyroid cancer: the putative upstream role of SOX2", *Thyroid,* vol. 23, no. 7, pp. 829-837.

Carney, D.N., Gazdar, A.F. & Minna, J.D. 1980, "Positive correlation between histological tumor involvement and generation of tumor cell colonies in agarose in specimens taken directly from patients with small-cell carcinoma of the lung", *Cancer research,* vol. 40, no. 6, pp. 1820-1823.

Castro, M.R., Bergert, E.R., Goellner, J.R., Hay, I.D. & Morris, J.C. 2001, "Immunohistochemical analysis of sodium iodide symporter expression in metastatic differentiated thyroid cancer: correlation with radioiodine uptake", *Journal of Clinical Endocrinology & Metabolism,* vol. 86, no. 11, pp. 5627-5632.

Chapman, P.B., Hauschild, A., Robert, C., Haanen, J.B., Ascierto, P., Larkin, J., Dummer, R., Garbe, C., Testori, A. & Maio, M. 2011, "Improved survival with vemurafenib in melanoma with BRAF V600E mutation", *New England Journal of Medicine,* vol. 364, no. 26, pp. 2507-2516.

Chien, W. & Pei, L. 2000, "A novel binding factor facilitates nuclear translocation and transcriptional activation function of the pituitary tumor-transforming gene product", *The Journal of biological chemistry,* vol. 275, no. 25, pp. 19422-19427.

Cifola, I., Lionetti, M., Pinatel, E., Todoerti, K., Mangano, E., Pietrelli, A., Fabris, S., Mosca, L., Simeon, V., Petrucci, M.T., Morabito, F., Offidani, M., Di Raimondo, F., Falcone, A., Caravita, T., Battaglia, C., De Bellis, G., Palumbo, A., Musto, P. & Neri, A. 2015, "Whole-exome sequencing of primary plasma cell leukemia discloses heterogeneous mutational patterns", *Oncotarget,* vol. 6, no. 19, pp. 17543-17558.

Cline, M.S., Craft, B., Swatloski, T., Goldman, M., Ma, S., Haussler, D. & Zhu, J. 2013, "Exploring TCGA pan-cancer data at the UCSC cancer genomics browser", *Scientific reports,* vol. 3.

Croucher, D.R., Rickwood, D., Tactacan, C.M., Musgrove, E.A. & Daly, R.J. 2010, "Cortactin modulates RhoA activation and expression of Cip/Kip cyclin-dependent kinase inhibitors to promote cell cycle progression in 11q13-amplified head and neck squamous cell carcinoma cells", *Molecular and cellular biology,* vol. 30, no. 21, pp. 5057-5070.

Davies, H., Bignell, G.R., Cox, C., Stephens, P., Edkins, S., Clegg, S., Teague, J., Woffendin, H., Garnett, M.J. & Bottomley, W. 2002, "Mutations of the BRAF gene in human cancer", *Nature,* vol. 417, no. 6892, pp. 949-954.

DePristo, M.A., Weinreich, D.M. & Hartl, D.L. 2005, "Missense meanderings in sequence space: a biophysical view of protein evolution", *Nature Reviews Genetics,* vol. 6, no. 9, pp. 678-687.

Desforges, J.F. & Mazzaferri, E.L. 1993, "Management of a solitary thyroid nodule", *New England Journal of Medicine,* vol. 328, no. 8, pp. 553-559.

Eisfeld, A.K., Schwind, S., Hoag, K.W., Walker, C.J., Liyanarachchi, S., Patel, R., Huang, X., Markowitz, J., Duan, W., Otterson, G.A., Carson, W.E.,3rd, Marcucci, G., Bloomfield, C.D. & de la Chapelle, A. 2014, "NRAS isoforms differentially affect downstream pathways, cell growth, and cell transformation", *Proceedings of the National Academy of Sciences of the United States of America,* vol. 111, no. 11, pp. 4179-4184.

Etienne-Manneville, S. & Hall, A. 2002, "Rho GTPases in cell biology", *Nature,* vol. 420, no. 6916, pp. 629-635.

Fantozzi, I., Grall, D., Cagnol, S., Stanchi, F., Sudaka, A., Brunstein, M., Bozec, A., Fischel, J., Milano, G. & Van Obberghen-Schilling, E. 2008, "Overexpression of cortactin in head and neck squamous cell carcinomas can be uncoupled from augmented EGF receptor expression", *Acta Oncologica,* vol. 47, no. 8, pp. 1502-1512.

Fearon, E.R. 2011, "Molecular genetics of colorectal cancer", *Annual Review of Pathology: Mechanisms of Disease,* vol. 6, pp. 479-507.

Flaherty, K.T., Hodi, F.S. & Fisher, D.E. 2012, "From genes to drugs: targeted strategies for melanoma", *Nature Reviews Cancer,* vol. 12, no. 5, pp. 349-361.

Forbes, S., Bhamra, G., Bamford, S., Dawson, E., Kok, C., Clements, J., Menzies, A., Teague, J., Futreal, P. & Stratton, M. 2008, "The catalogue of somatic mutations in cancer (COSMIC)", *Current protocols in human genetics,* , pp. 10.11. 1-10.11. 26.

Forbes, S.A., Beare, D., Gunasekaran, P., Leung, K., Bindal, N., Boutselakis, H., Ding, M., Bamford, S., Cole, C., Ward, S., Kok, C.Y., Jia, M., De, T., Teague, J.W., Stratton, M.R., McDermott, U. & Campbell, P.J. 2015, "COSMIC: exploring the world's knowledge of somatic mutations in human cancer", *Nucleic acids research,* vol. 43, no. Database issue, pp. D805-11.

Forbes, S.A., Bindal, N., Bamford, S., Cole, C., Kok, C.Y., Beare, D., Jia, M., Shepherd, R., Leung, K., Menzies, A., Teague, J.W., Campbell, P.J., Stratton, M.R. & Futreal, P.A. 2011, "COSMIC: mining complete cancer genomes in the Catalogue of Somatic Mutations in Cancer", *Nucleic acids research,* vol. 39, no. Database issue, pp. D945-50.

Freedman, V.H. & Shin, S. 1974, "Cellular tumorigenicity in nude mice: correlation with cell growth in semi-solid medium", *Cell,* vol. 3, no. 4, pp. 355-359.

Friedl, P. & Alexander, S. 2011, "Cancer invasion and the microenvironment: plasticity and reciprocity", *Cell,* vol. 147, no. 5, pp. 992-1009.

Friesema, E.C., Ganguly, S., Abdalla, A., Manning Fox, J.E., Halestrap, A.P. & Visser, T.J. 2003, "Identification of monocarboxylate transporter 8 as a specific thyroid hormone transporter", *The Journal of biological chemistry,* vol. 278, no. 41, pp. 40128-40135.

Garnett, M.J. & Marais, R. 2004, "Guilty as charged: B-RAF is a human oncogene", *Cancer cell,* vol. 6, no. 4, pp. 313-319.

Greenman, C., Stephens, P., Smith, R., Dalgliesh, G.L., Hunter, C., Bignell, G., Davies, H., Teague, J., Butler, A. & Stevens, C. 2007, "Patterns of somatic mutation in human cancer genomes", *Nature,* vol. 446, no. 7132, pp. 153-158.

Gromiha, M.M. 2003, "Factors influencing the thermal stability of buried protein mutants", *Polymer,* vol. 44, no. 14, pp. 4061-4066.

Guo, Y., Sheng, Q., Li, J., Ye, F., Samuels, D.C. & Shyr, Y. 2013, "Large scale comparison of gene expression levels by microarrays and RNAseq using TCGA data", *PloS one,* vol. 8, no. 8, pp. e71462.

Haber, D.A. & Settleman, J. 2007, "Cancer: drivers and passengers", *Nature,* vol. 446, no. 7132, pp. 145-146.

Hanahan, D. & Weinberg, R.A. 2011, "Hallmarks of cancer: the next generation", *Cell,* vol. 144, no. 5, pp. 646-674.

Hanahan, D. & Weinberg, R.A. 2000, "The hallmarks of cancer", *Cell,* vol. 100, no. 1, pp. 57-70.

Heaney, A.P., Singson, R., McCabe, C.J., Nelson, V., Nakashima, M. & Melmed, S. 2000, "Expression of pituitary-tumour transforming gene in colorectal tumours", *The Lancet,* vol. 355, no. 9205, pp. 716-719.

Hirakawa, H., Shibata, K. & Nakayama, T. 2009, "Localization of cortactin is associated with colorectal cancer development", *International journal of oncology,* vol. 35, no. 6, pp. 1271-1276.

Hornbeck, P.V., Zhang, B., Murray, B., Kornhauser, J.M., Latham, V. & Skrzypek, E. 2015, "PhosphoSitePlus, 2014: mutations, PTMs and recalibrations", *Nucleic acids research,* vol. 43, no. Database issue, pp. D512-20.

Hsueh, C., Lin, J., Chang, Y., Hsueh, S., Chao, T., Yu, J., Jung, S., Tseng, N., Sun, J. & Kuo, S. 2013, "Prognostic significance of pituitary tumour-transforming gene-binding factor (PBF) expression in papillary thyroid carcinoma", *Clinical endocrinology,* vol. 78, no. 2, pp. 303-309.

Imanaka, T., Shibazaki, M. & Takagi, M. 1986, "A new way of enhancing the thermostability of proteases", .

James, S., Franklyn, J., Reaves, B.J., Smith, V., Chan, S., Barrett, T., Kilby, M. & McCabe, C. 2009, "Monocarboxylate transporter 8 in neuronal cell growth", *Endocrinology,* vol. 150, no. 4, pp. 1961-1969.

Jonklaas, J., Sarlis, N.J., Litofsky, D., Ain, K.B., Bigos, S.T., Brierley, J.D., Cooper, D.S., Haugen, B.R., Ladenson, P.W. & Magner, J. 2006, "Outcomes of patients with differentiated thyroid carcinoma following initial therapy", *Thyroid,* vol. 16, no. 12, pp. 1229-1242.

Kawaguchi, A., Ikeda, M., Endo, T., Kogai, T., Miyazaki, A. & Onaya, T. 1997, "Transforming growth factor-β1 suppresses thyrotropin-induced Na /I-symporter messenger RNA and protein levels in FRTL-5 rat thyroid cells", *Thyroid,* vol. 7, no. 5, pp. 789-794.

Kebebew, E., Weng, J., Bauer, J., Ranvier, G., Clark, O.H., Duh, Q.Y., Shibru, D., Bastian, B. & Griffin, A. 2007, "The prevalence and prognostic value of BRAF mutation in thyroid cancer", *Annals of Surgery,* vol. 246, no. 3, pp. 466-70; discussion 470-1.

Kim, D., Fong, J., Read, M. & McCabe, C. 2007, "The emerging role of pituitary tumour transforming gene (PTTG) in endocrine tumourigenesis", *Molecular and cellular endocrinology,* vol. 278, no. 1, pp. 1-6.

Kirkbride, K.C., Hong, N.H., French, C.L., Clark, E.S., Jerome, W.G. & Weaver, A.M. 2012, "Regulation of late endosomal/lysosomal maturation and trafficking by cortactin affects Golgi morphology", *Cytoskeleton,* vol. 69, no. 9, pp. 625-643.

Kirkbride, K.C., Sung, B.H., Sinha, S. & Weaver, A.M. 2011, "Cortactin: a multifunctional regulator of cellular invasiveness", *Cell adhesion & migration,* vol. 5, no. 2, pp. 187-198.

Knauf, J.A., Ma, X., Smith, E.P., Zhang, L., Mitsutake, N., Liao, X.H., Refetoff, S., Nikiforov, Y.E. & Fagin, J.A. 2005, "Targeted expression of BRAFV600E in thyroid cells of transgenic mice results in papillary thyroid cancers that undergo dedifferentiation", *Cancer research,* vol. 65, no. 10, pp. 4238-4245.

Kogai, T. & Brent, G.A. 2012, "The sodium iodide symporter (NIS): regulation and approaches to targeting for cancer therapeutics", *Pharmacology & therapeutics,* vol. 135, no. 3, pp. 355-370.

Kogai, T., Taki, K. & Brent, G.A. 2006, "Enhancement of sodium/iodide symporter expression in thyroid and breast cancer", *Endocrine-related cancer,* vol. 13, no. 3, pp. 797-826.

Kowalski, J.R., Egile, C., Gil, S., Snapper, S.B., Li, R. & Thomas, S.M. 2005, "Cortactin regulates cell migration through activation of N-WASP", *Journal of cell science,* vol. 118, no. Pt 1, pp. 79-87.

Kozlov, G., Perreault, A., Schrag, J.D., Park, M., Cygler, M., Gehring, K. & Ekiel, I. 2004, "Insights into function of PSI domains from structure of the Met receptor PSI domain", *Biochemical and biophysical research communications,* vol. 321, no. 1, pp. 234-240.

Lakshmanan, A., Wojcicka, A., Kotlarek, M., Zhang, X., Jazdzewski, K. & Jhiang, S.M. 2015, "microRNA-339-5p modulates Na+/I- symporter-mediated radioiodide uptake", *Endocrine-related cancer,* vol. 22, no. 1, pp. 11-21.

Lee, S.H. & Dominguez, R. 2010, "Regulation of actin cytoskeleton dynamics in cells", *Molecules and cells,* vol. 29, no. 4, pp. 311-325.

Leiserson, M.D., Blokh, D., Sharan, R. & Raphael, B.J. 2013, "Simultaneous identification of multiple driver pathways in cancer", *PLoS Comput Biol,* vol. 9, no. 5, pp. e1003054.

Lin, H., Dai, T., Xiong, H., Zhao, X., Chen, X., Yu, C., Li, J., Wang, X. and Song, L., 2010, "Unregulated miR-96 induces cell proliferation in human breast cancer by downregulating transcriptional factor FOXO3a", *PloS one*, *5*(12), p.e15797.

Lisowska, E. & Jaskiewicz, E. 2012, "Protein glycosylation, an overview", *eLS,* .

Liu, D., Liu, Z., Condouris, S. & Xing, M. 2007, "BRAF V600E maintains proliferation, transformation, and tumorigenicity of BRAF-mutant papillary thyroid cancer cells", *The Journal of Clinical Endocrinology & Metabolism,* vol. 92, no. 6, pp. 2264-2271.

Lodish, H., Berk, A., Zipursky, S.L., Matsudaira, P., Baltimore, D. & Darnell, J. 2000, "Protein glycosylation in the ER and Golgi complex", .

Loi, S., Michiels, S., Lambrechts, D., Fumagalli, D., Claes, B., Kellokumpu-Lehtinen, P.L., Bono, P., Kataja, V., Piccart, M.J., Joensuu, H. & Sotiriou, C. 2013, "Somatic mutation profiling and associations with prognosis and trastuzumab benefit in early breast cancer", *Journal of the National Cancer Institute,* vol. 105, no. 13, pp. 960-967.

Lu, P., Qiao, J., He, W., Wang, J., Jia, Y., Sun, Y., Tang, S., Fu, L. & Qin, Y. 2014, "Genome-wide gene expression profile analyses identify CTTN as a potential prognostic marker in esophageal cancer", *PloS one,* vol. 9, no. 2, pp. e88918.

MacGrath, S.M. & Koleske, A.J. 2012, "Cortactin in cell migration and cancer at a glance", *Journal of cell science,* vol. 125, no. Pt 7, pp. 1621-1626.

Mattila, P.K., Batista, F.D. & Treanor, B. 2016, "Dynamics of the actin cytoskeleton mediates receptor cross talk: An emerging concept in tuning receptor signaling", *The Journal of cell biology,* vol. 212, no. 3, pp. 267-280.

Maxon, H.R., Thomas, S.R., Hertzberg, V.S., Kereiakes, J.G., Chen, I., Sperling, M.I. & Saenger, E.L. 1983, "Relation between effective radiation dose and outcome of radioiodine therapy for thyroid cancer", *New England Journal of Medicine,* vol. 309, no. 16, pp. 937-941.

McCabe, C., Khaira, J., Boelaert, K., Heaney, A., Tannahill, L., Hussain, S., Mitchell, R., Olliff, J., Sheppard, M. & Franklyn, J. 2003, "Expression of pituitary tumour transforming gene (PTTG) and fibroblast growth factor-2 (FGF-2) in human pituitary adenomas: relationships to clinical tumour behaviour", *Clinical endocrinology,* vol. 58, no. 2, pp. 141-150.

McMahon, M., Ayllon, V., Panov, K.I. & O'Connor, R. 2010, "Ribosomal 18 S RNA processing by the IGF-I-responsive WDR3 protein is integrated with p53 function in cancer cell proliferation", *The Journal of biological chemistry,* vol. 285, no. 24, pp. 18309-18318.

Mei, G., Di Venere, A., Rosato, N. & Finazzi-Agrò, A. 2005, "The importance of being dimeric", *FEBS journal,* vol. 272, no. 1, pp. 16-27.

Melloni, G.E., Ogier, A.G., de Pretis, S., Mazzarella, L., Pelizzola, M., Pelicci, P.G. & Riva, L. 2014, "DOTS-Finder: a comprehensive tool for assessing driver genes in cancer genomes", *Genome medicine,* vol. 6, no. 6, pp. 44.

Menéndez-Arias, L. & Argosf, P. 1989, "Engineering protein thermal stability: sequence statistics point to residue substitutions in α-helices", *Journal of Molecular Biology,* vol. 206, no. 2, pp. 397-406.

Monod, J., Wyman, J. & Changeux, J. 1965, "On the nature of allosteric transitions: a plausible model", *Journal of Molecular Biology,* vol. 12, no. 1, pp. 88-118.

Mori, S., Chang, J.T., Andrechek, E.R., Matsumura, N., Baba, T., Yao, G., Kim, J.W., Gatza, M., Murphy, S. & Nevins, J.R. 2009, "Anchorage-independent cell growth signature identifies tumors with metastatic potential", *Oncogene,* vol. 28, no. 31, pp. 2796-2805.

Ng, P.C. & Henikoff, S. 2006, "Predicting the effects of amino acid substitutions on protein function", *Annu.Rev.Genomics Hum.Genet.,* vol. 7, pp. 61-80.

Ng, P.C. & Henikoff, S. 2003, "SIFT: Predicting amino acid changes that affect protein function", *Nucleic acids research,* vol. 31, no. 13, pp. 3812-3814.

Ni, Q., Yu, J., Qian, F., Sun, N., Xiao, J. & Zhu, J. 2015, "Cortactin promotes colon cancer progression by regulating ERK pathway", *International journal of oncology,* vol. 47, no. 3, pp. 1034-1042.

Oikonomou, E., Makrodouli, E., Evagelidou, M., Joyce, T., Probert, L. & Pintzas, A. 2009, "BRAF V600E efficient transformation and induction of microsatellite instability versus KRAS G12V induction of senescence markers in human colon cancer cells", *Neoplasia,* vol. 11, no. 11, pp. 1116-IN2.

Parsons, J.T., Horwitz, A.R. & Schwartz, M.A. 2010, "Cell adhesion: integrating cytoskeletal dynamics and cellular tension", *Nature reviews Molecular cell biology,* vol. 11, no. 9, pp. 633-643.

Pollard, T.D. & Borisy, G.G. 2003, "Cellular motility driven by assembly and disassembly of actin filaments", *Cell,* vol. 112, no. 4, pp. 453-465.

Ponnuswamy, P., Muthusamy, R. & Manavalan, P. 1982, "Amino acid composition and thermal stability of proteins", *International journal of biological macromolecules,* vol. 4, no. 3, pp. 186-190.

Ravnan, M.C. & Matalka, M.S. 2012, "Vemurafenib in Patients With BRAF V600E Mutation–Positive Advanced Melanoma", *Clinical therapeutics,* vol. 34, no. 7, pp. 1474-1486.

Read, M.L., Seed, R.I., Fong, J.C., Modasia, B., Ryan, G.A., Watkins, R.J., Gagliano, T., Smith, V.E., Stratford, A.L. & Kwan, P.K. 2014, "The PTTG1-Binding Factor (PBF/PTTG1IP) regulates p53 activity in thyroid cells", *Endocrinology,* .

Read, M.L., Seed, R.I., Modasia, B., Kwan, P.P., Sharma, N., Smith, V.E., Watkins, R.J., Bansal, S., Gagliano, T. & Stratford, A.L. 2016, "The proto-oncogene PBF binds p53 and is associated with prognostic features in colorectal cancer", *Molecular carcinogenesis,* vol. 55, no. 1, pp. 15-26.

Read, M.L., Lewy, G.D., Fong, J.C., Sharma, N., Seed, R.I., Smith, V.E., Gentilin, E., Warfield, A., Eggo, M.C., Knauf, J.A., Leadbeater, W.E., Watkinson, J.C., Franklyn, J.A., Boelaert, K. & McCabe, C.J. 2011, "Proto-oncogene PBF/PTTG1IP regulates thyroid cell growth and represses radioiodide treatment", *Cancer research,* vol. 71, no. 19, pp. 6153-6164.

Reva, B., Antipin, Y. & Sander, C. 2011, "Predicting the functional impact of protein mutations: application to cancer genomics", *Nucleic acids research,* vol. 39, no. 17, pp. e118.

Ribeiro, F.R., Meireles, A.M., Rocha, A.S. & Teixeira, M.R. 2008, "Conventional and molecular cytogenetics of human non-medullary thyroid carcinoma: characterization of eight cell line models and review of the literature on clinical samples", *BMC cancer,* vol. 8, pp. 371-2407-8-371.

Ridley, A.J. 2011, "Life at the leading edge", *Cell,* vol. 145, no. 7, pp. 1012-1022.

Ross, D.T. & Perou, C.M. 2001, "A comparison of gene expression signatures from breast tumors and breast tissue derived cell lines", *Disease markers,* vol. 17, no. 2, pp. 99-109.

Russo, A., Bazan, V., Iacopetta, B., Kerr, D., Soussi, T., Gebbia, N. & TP53-CRC Collaborative Study Group 2005, "The TP53 colorectal cancer international collaborative study on the prognostic and predictive significance of p53 mutation: influence of tumor site, type of mutation, and adjuvant treatment", *Journal of clinical oncology : official journal of the American Society of Clinical Oncology,* vol. 23, no. 30, pp. 7518-7528.

Saiselet, M., Floor, S., Tarabichi, M., Dom, G., Hébrant, A., van Staveren, W.C. & Maenhaut, C. 2012, "Thyroid cancer cell lines: an overview", *Frontiers in endocrinology,* vol. 3.

Sakoparnig, T., Fried, P. & Beerenwinkel, N. 2015, "Identification of Constrained Cancer Driver Genes Based on Mutation Timing", *PLoS Comput Biol,* vol. 11, no. 1, pp. e1004027.

Sawka, A.M., Thephamongkhol, K., Brouwers, M., Thabane, L., Browman, G. & Gerstein, H.C. 2004, "A systematic review and metaanalysis of the effectiveness of radioactive iodine remnant ablation for well-differentiated thyroid cancer", *The Journal of Clinical Endocrinology & Metabolism,* vol. 89, no. 8, pp. 3668-3676.

Scherer, W.F., Syverton, J.T. & Gey, G.O. 1953, "Studies on the propagation in vitro of poliomyelitis viruses. IV. Viral multiplication in a stable strain of human malignant epithelial cells (strain HeLa) derived from an epidermoid carcinoma of the cervix", *The Journal of experimental medicine,* vol. 97, no. 5, pp. 695-710.

Sharma, N. 2014, *Novel binding partners of PBF in thyroid tumourigenesis,* .

Shental-Bechor, D. & Levy, Y. 2008, "Effect of glycosylation on protein folding: a close look at thermodynamic stabilization", *Proceedings of the National Academy of Sciences of the United States of America,* vol. 105, no. 24, pp. 8256-8261.

Shin, S.I., Freedman, V.H., Risser, R. & Pollack, R. 1975, "Tumorigenicity of virus-transformed cells in nude mice is correlated specifically with anchorage

independent growth in vitro", *Proceedings of the National Academy of Sciences of the United States of America,* vol. 72, no. 11, pp. 4435-4439.

Smith, N., Barbachano, Y., Norman, A., Swift, R., Abulafi, A. & Brown, G. 2008, "Prognostic significance of magnetic resonance imaging-detected extramural vascular invasion in rectal cancer", *British Journal of Surgery,* vol. 95, no. 2, pp. 229-236.

Smith, V., Read, M., Turnell, A., Sharma, N., Lewy, G., Fong, J., Seed, R., Kwan, P., Ryan, G. & Mehanna, H. 2012, "PTTG-binding factor (PBF) is a novel regulator of the thyroid hormone transporter MCT8", *Endocrinology,* vol. 153, no. 7, pp. 3526-3536.

Smith, V., Sharma, N., Watkins, R., Read, M., Ryan, G., Kwan, P., Martin, A., Watkinson, J., Boelaert, K. & Franklyn, J. 2013, "Manipulation of PBF/PTTG1IP phosphorylation status; a potential new therapeutic strategy for improving radioiodine uptake in thyroid and other tumors", *The Journal of Clinical Endocrinology & Metabolism,* vol. 98, no. 7, pp. 2876-2886.

Smith, V.E., Franklyn, J.A. & McCabe, C.J. 2010, "Pituitary tumor-transforming gene and its binding factor in endocrine cancer", *Expert Rev Mol Med,* vol. 12, pp. e38.

Smith, V., Read, M., Watkins, R., Lewy, G., Fong, J., Seed, R., Sharma, N., Ryan, G., Boelaert, K. & Franklyn, J. 2010, "The role of PBF in NIS and MCT8 cellular trafficking", .

Smith, V.E., Franklyn, J.A. & McCabe, C.J. 2011, "Expression and function of the novel proto-oncogene PBF in thyroid cancer: a new target for augmenting radioiodine uptake", *The Journal of endocrinology,* vol. 210, no. 2, pp. 157-163.

Smith, V.E., Read, M.L., Turnell, A.S., Watkins, R.J., Watkinson, J.C., Lewy, G.D., Fong, J.C., James, S.R., Eggo, M.C., Boelaert, K., Franklyn, J.A. & McCabe, C.J. 2009, "A novel mechanism of sodium iodide symporter repression in differentiated thyroid cancer", *Journal of cell science,* vol. 122, no. Pt 18, pp. 3393-3402.

Solbach, C., Roller, M., Fellbaum, C., Nicoletti, M. & Kaufmann, M. 2004, "PTTG mRNA expression in primary breast cancer: a prognostic marker for lymph node invasion and tumor recurrence", *The Breast,* vol. 13, no. 1, pp. 80-81.

Soule, H.D., Vazguez, J., Long, A., Albert, S. & Brennan, M. 1973, "A human cell line from a pleural effusion derived from a breast carcinoma", *Journal of the National Cancer Institute,* vol. 51, no. 5, pp. 1409-1416.

Spring, K., Fournier, P., Lapointe, L., Chabot, C., Roussy, J., Pommey, S., Stagg, J. & Royal, I. 2015, "The protein tyrosine phosphatase DEP-1/PTPRJ promotes breast cancer cell invasion and metastasis", *Oncogene,* .

Stratford, A.L., Boelaert, K., Tannahill, L.A., Kim, D.S., Warfield, A., Eggo, M.C., Gittoes, N.J., Young, L.S., Franklyn, J.A. & McCabe, C.J. 2005, "Pituitary tumor transforming gene binding factor: a novel transforming gene in thyroid tumorigenesis", *Journal of Clinical Endocrinology & Metabolism,* vol. 90, no. 7, pp. 4341-4349.

Stratton, M.R., Campbell, P.J. & Futreal, P.A. 2009, "The cancer genome", *Nature,* vol. 458, no. 7239, pp. 719-724.

Sung, B.H., Zhu, X., Kaverina, I. & Weaver, A.M. 2011, "Cortactin controls cell motility and lamellipodial dynamics by regulating ECM secretion", *Current Biology,* vol. 21, no. 17, pp. 1460-1469.

Tamborero, D., Gonzalez-Perez, A. & Lopez-Bigas, N. 2013, "OncodriveCLUST: exploiting the positional clustering of somatic mutations to identify cancer genes", *Bioinformatics (Oxford, England),* vol. 29, no. 18, pp. 2238-2244.

Timpson, P., Lynch, D.K., Schramek, D., Walker, F. & Daly, R.J. 2005, "Cortactin overexpression inhibits ligand-induced down-regulation of the epidermal growth factor receptor", *Cancer research,* vol. 65, no. 8, pp. 3273-3280.

Tomar, A., Lawson, C., Ghassemian, M. & Schlaepfer, D.D. 2012, "Cortactin as a target for FAK in the regulation of focal adhesion dynamics", *PloS one,* vol. 7, no. 8, pp. e44041.

Tomczak, K., Czerwińska, P. & Wiznerowicz, M. 2015, "The Cancer Genome Atlas (TCGA): an immeasurable source of knowledge", *Contemporary oncology,* vol. 19, no. 1A, pp. A68.

Torkamani, A. & Schork, N.J. 2008, "Prediction of cancer driver mutations in protein kinases", *Cancer research,* vol. 68, no. 6, pp. 1675-1682.

Verkman, A., Hara-Chikuma, M. & Papadopoulos, M.C. 2008, "Aquaporins—new players in cancer biology", *Journal of Molecular Medicine,* vol. 86, no. 5, pp. 523-529.

Vogelstein, B., Papadopoulos, N., Velculescu, V.E., Zhou, S., Diaz, L.A.,Jr & Kinzler, K.W. 2013, "Cancer genome landscapes", *Science (New York, N.Y.),* vol. 339, no. 6127, pp. 1546-1558.

Vogt, G., Woell, S. & Argos, P. 1997, "Protein thermal stability, hydrogen bonds, and ion pairs", *Journal of Molecular Biology,* vol. 269, no. 4, pp. 631-643.

Wang, Y., Rathinam, R., Walch, A. and Alahari, S.K., 2009, "ST14 (suppression of tumorigenicity 14) gene is a target for miR-27b, and the inhibitory effect of ST14 on cell growth is independent of miR-27b regulation", *Journal of Biological Chemistry*, *284*(34), pp.23094-23106.

Ward, L.S., Santarosa, P.L., Granja, F., da Assumpção, L.V., Savoldi, M. & Goldman, G.H. 2003, "Low expression of sodium iodide symporter identifies aggressive thyroid tumors", *Cancer letters,* vol. 200, no. 1, pp. 85-91.

Watkins, R.J., Read, M.L., Smith, V.E., Sharma, N., Reynolds, G.M., Buckley, L., Doig, C., Campbell, M.J., Lewy, G., Eggo, M.C., Loubiere, L.S., Franklyn, J.A., Boelaert, K. & McCabe, C.J. 2010, "Pituitary tumor transforming gene binding factor: a new gene in breast cancer", *Cancer research,* vol. 70, no. 9, pp. 3739-3749.

Weaver, A.M., Karginov, A.V., Kinley, A.W., Weed, S.A., Li, Y., Parsons, J.T. & Cooper, J.A. 2001, "Cortactin promotes and stabilizes Arp2/3-induced actin filament network formation", *Current Biology,* vol. 11, no. 5, pp. 370-374.

Xiang, C., Gao, H., Meng, L., Qin, Z., Ma, R., Liu, Y., Jiang, Y., Dang, C., Jin, L. & He, F. 2012, "Functional variable number of tandem repeats variation in the promoter of proto-oncogene PTTG1IP is associated with risk of estrogen receptor-positive breast cancer", *Cancer science,* vol. 103, no. 6, pp. 1121-1128.

Xing, M., Westra, W.H., Tufano, R.P., Cohen, Y., Rosenbaum, E., Rhoden, K.J., Carson, K.A., Vasko, V., Larin, A. & Tallini, G. 2005, "BRAF mutation predicts a poorer clinical prognosis for papillary thyroid cancer", *Journal of Clinical Endocrinology & Metabolism,* vol. 90, no. 12, pp. 6373-6379.

Xu, X., Garcia, M.V., Li, T., Khor, L., Gajapathy, R.S., Spittle, C., Weed, S., Lessin, S.R. & Wu, H. 2010, "Cytoskeleton alterations in melanoma: aberrant expression of cortactin, an actin-binding adapter protein, correlates with melanocytic tumor progression", *Modern Pathology,* vol. 23, no. 2, pp. 187-196.

Yamada, S., Yanamoto, S., Kawasaki, G., Mizuno, A. & Nemoto, T.K. 2010, "Overexpression of cortactin increases invasion potential in oral squamous cell carcinoma", *Pathology & Oncology Research,* vol. 16, no. 4, pp. 523-531.

Yang, J. & Zhang, Y. 2015, "I-TASSER server: new development for protein structure and function predictions", *Nucleic acids research,* vol. 43, no. W1, pp. W174-81.

Yaspo, M., Aaltonen, J., Horelli-Kuitunen, N., Peltonen, L. & Lehrach, H. 1998, "Cloning of a novel human putative type Ia integral membrane protein mapping to 21q22. 3", *Genomics,* vol. 49, no. 1, pp. 133-136.

Zhang, Y. 2008, "I-TASSER server for protein 3D structure prediction", *BMC bioinformatics,* vol. 9, pp. 40-2105-9-40.

Zou, H., McGarry, T.J., Bernal, T. & Kirschner, M.W. 1999, "Identification of a vertebrate sister-chromatid separation inhibitor involved in transformation and tumorigenesis", *Science (New York, N.Y.),* vol. 285, no. 5426, pp. 418-422.

BIBLIOGRAPHY

Publications Relating to Thesis

*Rachel J. Watkins, *Waraporn Imruetaicharoenchoke, *Martin L. Read, Neil Sharma, Vikki L. Poole, Erica Gentillin, Sukhchain Bansal, Emy Bosseboeuf, Rachel Fletcher, Hannah R. Nieto, Ujjal Mallick, Allan Hackshaw, Hisham Mehanna, Kristien Boelaert, Vicki E. Smith, Christopher J. McCabe. Pro-invasive effect of proto-oncogene PBF is modulated by a targetable interaction with cortactin in endocrine cells. Manuscript under minor revision at J Clin Endo Metab.

*Imruetaicharoenchoke W, Watkins RJ, Modasia B, Poole VL, Nieto HR, Sharma N, Fletcher A, Thompson R, Boelaert K, Read ML, Smith VE, McCabe CJ. Functional consequences of the first reported mutations of the proto-oncogene PTTG1IP/PBF. Manuscript under submission.

*These authors are the first authors and contributed equally to this work.

Presentations

Oral presentation at Society for Endocrinology BES 2016, Scotland

Poster presentation at Society for Endocrinology BES 2016, Scotland

Short oral communication at 15th International Thyroid Conference 2015, USA

Poster presentation at 15th International Thyroid Conference 2015, USA

Oral presentation at 63th Annual meeting of the British Thyroid Association 2014, UK

Oral presentation at European Thyroid Association 2014, Spain

Poster presentation at Society for Endocrinology BES 2014, UK

Poster presentation at 62th Annual meeting of the British Thyroid Association 2013, UK